UNIVERSITY OF NOTTINGHAM

DEPARTMENT OF CIVIL ENGINEERING

SATELLITE LASER RANGING AND THE

DETERMINATION OF EARTH ROTATION PARAMETERS

by

Terry Moore, B.Sc

Thesis submitted to the University of Nottingham for

the degree of Doctor of Philosophy

October 1986

TABLE OF CONTENTS

# SATELLITE LASER RANGING AND THE
# DETERMINATION OF EARTH ROTATION PARAMETERS

## ABSTRACT

Over recent years considerable advances have taken place in the field of space geodesy, resulting in a number of highly precise global positioning techniques. The increased resolution of many of the scientific products from the new observational techniques has stimulated the interest of not only geodesists but also geophysicists. Furthermore, their potential to determine the orientation of the earth's axis of rotation (polar motion) and the variations of the rate of rotation of the earth about that axis, was recognised by the scientific community. The result was the establishment of Project MERIT, to intercompare these new observational techniques.

Satellite Laser Ranging, a method of measuring the distance from a point on the earth's surface to an artificial satellite by means of timing the flight of a short pulse of laser light, is currently the most accurate available means of tracking near earth satellites. However, in order to reach the accuracy requirements of current geodetic applications dedicated satellites, such as the NASA LAser GEOdynamic Satellite (LAGEOS), must be tracked and specialised processing software must be used.

This Thesis describes the basic theory behind the analysis of Satellite Laser Ranging Observations, with a special emphasis on the determination of earth rotation parameters (the polar motion and the variations in the rate of rotation). The development and testing, at Nottingham, of the Satellite Orbit Determination and Analysis Package Of Programs, SODAPOP, for the processing of laser range data, is described. The thesis also presents and discusses the results of the analysis of laser range observations to the LAGEOS satellite, from the short and main campaigns of project MERIT.

## <u>ACKNOWLEDGEMENTS</u>

Although the three years of research concluded by this thesis involved considerable personal labour, it would not have been possible without the guidance, help and encouragement of several people.

Most importantly was the continued support and encouragement of my parents and close family and in particular my wife, Ingrid, to whom I express my sincere thanks for her invaluable patience and help.

The work was carried out in the Department of Civil Engineering at the University of Nottingham, with the support of the Head of Department Professor P. S. Pell. The research was funded under the co-operative awards scheme by the Science and Engineering Research Council and the Ordnance Survey.

Of equal importance was the encouragement and advice of my supervisor, Professor Vidal Ashkenazi; for whose continued support I am sincerely indebted.

The data and other documentation vital for this research project were kindly provided by the Royal Greenwich Observatory and by the Center for Space Research of the University of Texas at Austin. Sincere thanks are extended to the staff at both these establishments and especially to Dr. Andrew Sinclair, Mr. Graham Appleby and Professor B. E. Schutz.

To be able to work in a stimulating and friendly environment is both a pleasurable and profitable experience, and I would like to thank all past and

LIST OF FIGURES

CHAPTER   ONE

INTRODUCTION

# 1.    INTRODUCTION

During the last thirty years significant scientific advances have led to the development of completely new observational techniques, which have changed the face of geodesy. Traditionally, the science of measuring and mapping the surface and gravity field of the earth depended on measurements of terrestrial angles and distances combined with astro-geodetic and gravimetric observations. In contrast, the new techniques of 'space geodesy' are based on observations to both real (the moon) and artificial satellites, and extra galactic radio sources (such as quasars). However, the accuracy of the measurements and products has not only challenged the traditional methods of triangulation and trilateration, but has led to many new and diverse applications of space geodesy in the fields of geophysics and geodynamics.

Over recent years the greatest impact of the new observational techniques has been their contribution to the monitoring of both the orientation to the earth and the global and local movements of the crust. In order to stimulate the development of the techniques and promote the exploitation of the scientific products several major international collaborative scientific projects have been established. Notable amongst these are the Crustal Dynamics Project (US National Aeronautics and Space Administration) and Project MERIT (joint IAU/IUGG working group on the rotation of the earth).

Satellite geodesy was born in 1957 following the launch of the first Sputnik spacecraft. Since then many other artificial satellites have been launched, including several with dedicated geodetic missions. The majority of satellite geodetic techniques consists of tracking a particular satellite from a number of tracking stations distributed around the world. These observations may be subsequently used to determine the satellite's orbit, the three dimensional positions of the tracking stations and many other geodetic and geophysical parameters. Generally, the techniques are based on the precise timing of the propagation of either radio (microwave) or visible light (laser) signals between the ground tracking station and the satellite.

Laser ranging is currently the most precise method of tracking both near earth satellites and the moon. The development of Satellite Laser Ranging Systems started in the early 1960's and the first measurements were achieved in 1964 at the NASA Goddard Space Flight Center. Although the first measurements were only accurate to a few metres the last decade has seen considerable advances in the instrumentation, which has resulted in current state-of-the-art systems which are capable of accuracies of the order of 2-5cm. In principle, the technique consists of a ground based laser which transmits a series of intense short pulses of laser light to the satellite. These are reflected

back by the satellite and the time of flight of each pulse forms the raw 'range' observations. To ensure the transmitted laser pulses are reflected back to the ground tracking stations, the satellites must carry corner cube retro-reflectors. Of the many hundreds of spacecraft launched into earth orbit only a very small number are suitably equipped for laser tracking. However, two satellites, LAGEOS and STARLETTE, which are dedicated passive laser ranging targets, have been launched, and are regularly tracked by the global network of ranging systems.

Clearly, a set of 'raw' distance (range) measurements between a tracking station and a satellite is of little scientific interest to a geodesist or geophysicist, and the data must be processed in order to yield the necessary products. The most common approach to this analysis (the dynamical method) is based on an orbit determination process which computes, simultaneously, both the satellite orbit and a number of other geodetic parameters, depending on the particular application. The basis of the orbit determination process is a model of all the forces acting on the satellite, which may include both gravitational and surface forces. The vector sum of all these forces gives the resultant acceleration of the satellite as a function of it's position and velocity. By numerically integrating this acceleration twice the position and velocity of the satellite, as a function

of time, are obtained. In order for the process to begin the initial position and velocity vectors must be known; however, to begin with these need not be known precisely as they may be subsequently improved. The second stage of the procedure combines this 'computed' orbit with the range observations from a number of tracking stations and performs a least squares solution for a series of unknowns. These may include the initial satellite position (and velocity), the coordinates of all the tracking stations and a number of other parameters.

The movement of the earth's axis of rotation with respect to it's surface and the variations of the rate of rotation of the earth about this axis, have been predicted for many years. Indeed, 'polar motion' has been determined from astrometric observations since 1899, when the International Latitude Service was formed. More recently the monitoring of these phenomena has been the task of the International Polar Motion Service and the Bureau International de l'Heure. Over the last decade, however, several of the new space geodetic technniques have demonstrated their potential to determine the polar motion and the variations in the rate of rotation to a far higher resolution than had been previously possible. As a result, in 1978 a working group was formed to study the future of the international monitoring services and to encourage the development and exploitation of these new techniques.

A 'special programme of international collaboration to Monitor Earth Rotation and Intercompare the Techniques of observation and analysis' to be known as Project MERIT was the resulting initial proposal of the working group. The project was based around two observational campaigns in 1980 (3 months) and in 1983/84 (14 months), with subsequent periods for the analysis of the observations.

Of the six different observational techniques which contributed to project MERIT, it became evident that Satellite Laser Ranging (SLR) and Very Long Baseline Interferometry (VLBI) would provide the most precise results, and form the basis of any future monitoring service. The Geodesy Group at Nottingham has been involved with Project MERIT as an Associate Analysis Centre since the 2nd MERIT workshop held at the Royal Greenwich Observatory in 1983 (Wilkins, 1984). In particular the Group has concentratted on the processing and analysis of both SLR and VLBI data observed during the short and main MERIT campaigns.

This thesis is the result of research at Nottingham to develop orbit determination software and to subsequently process Satellite Laser Ranging observations. A Satellite Orbit Determination and Analysis Package Of Programs, SODAPOP, has been developed in order to analyse laser range observations to LAGEOS. Despite the specific purpose of the software suite, it has been structured so as to enable its

extension, at a later date, to include other satellite systems. In view of Project MERIT, the aim of the analysis was to establish a reliable method of determining earth rotation parameters (i.e. the polar motion and the variations in the rate of rotation of the earth) from SLR observations. In addition, a further aim was the computation of a precise, and repeatable, set of coordinates of the tracking stations. The software was initially tested using laser range data observed during 1980, around the time of the Short MERIT Campaign. Following the validation and testing period, SODAPOP was subsequently used to process data from the first four months of the Main MERIT Campaign. The development and testing of the software and the results of the anlyses are reported in this thesis.

The observational technique of Satellite Laser Ranging is discussed in Chapter 2 and the basic theory behind the dynamical analysis of SLR observations is described in Chapter 3. The determination of earth rotation parameters and Project MERIT, with a special emphasis on the application of Satellite Laser Ranging, are outlined in Chapter 4. Chapter 5 describes the software package, SODAPOP, developed at Nottingham and outlines the specifications and testing of the programs. The results of the analysis of LAGEOS laser ranging data are presented and discussed in Chapter 6. The thesis is concluded in Chapter 7.

CHAPTER   TWO

SATELLITE LASER RANGING

## 2.1    INTRODUCTION

The development of a laser system for precise satellite tracking started in 1961 at the NASA Goddard Space Flight Center (GSFC), and in 1964 the first range measurements were obtained. Basically the technique of Satellite Laser Ranging consists of a ground based tracking station which transmits a series of intense short pulses of laser light towards an artificial satellite capable of reflecting some of these back to the receiving optics of the tracking station. By accurately timing the time of flight of an individual pulse, one obtains a precise measure of the double range to the satellite. The simple schematic, fig 2.I, illustrates the principle of the laser ranging measurement.

The first measurements, in the early 1960's, were to Beacon Explorer B (Explorer 22) which was the first satellite to be equipped for laser ranging. Although the observed ranges had a precision of a few metres, the last 20 years have seen an improvement in accuracy of almost two orders of magnitude. Current state-of-the-art systems are demonstrating the capability of ranging with a precision of around 3cm.

For a satellite to be suitably equipped for Satellite Laser Ranging it must carry corner cube optical retro-reflectors. Since Beacon Explorer B, a total of 16 other suitable satellites have been launched, as described in § 2.2.3. Notable is the LAser

GEOdynamic Sateliite, LAGEOS, launched by NASA in 1976, which was designed specifically to support geodetic and geophysical research. Consequently, LAGEOS has become the primary laser ranging target.

Very similar in concept to Satellite Laser Ranging is the techinique of laser ranging to the moon (Lunar Laser Ranging, LLR). Several Satellite Laser Ranging systems are also used to monitor the distance to arrays of planer retro-reflector placed on the surface of the moon. There are currently 5 such arrays; three were placed by the astronauts of the Apollo 11,14 and 15 missions, and two were carried by the Soviet Lunakod 1 and Lunakod 2 spacecraft. Lunar Laser Ranging has provided a wealth of information on the dynamics of the earth-moon system as well as the determination of geophysical parameters and general relativity.

Over the last few years a global network of precise, fixed and mobile, tracking stations have routinely tracked LAGEOS and a number of other satellites, producing a large quantity of very precise data. Analysis of these data sets have demonstrated the potential of the current, centimetre accuracy, laser ranging systems to make significant contributions to geodesy, geophysics and crustal mechanics. The applications of Satellite Laser Ranging are discussed in more detail in § 2.2.4.

## 2.2   GENERAL SYSTEM DESCRIPTION

### 2.2.1 Basic Technique

As described in § 2.1 Satellite Laser Ranging consists of accurately measuring the time of flight of a short pulse of laser light, as illustrated in fig. 2.I. As the laser fires, a small fraction of the pulse is diverted to the range receiver which triggers the timing system. The remainder of the pulse is directed through the transmitting telescope and from there propagates through the atmosphere to be reflected by the satellite retro-reflectors. The returning pulse again propagates through the atmosphere back to the receiving telescope, which focuses on to the detector package. The latter instrument produces a signal which stops the timing mechanism. The 'time of firing' and 'time of return' of the pulse combine to form the basic observable, the 'time of flight'. This leads to the range measurement, using the simple model,

$$R = c(t_r - t_f)/2 \qquad (2.1)$$

where  R  :   range from the laser reference point to
                the average satellite retro-reflector
                position

       c  :   speed of light in a vacuum

     $t_r$ :   epoch corresponding to the return of the
                laser pulse

     $t_f$ :   epoch corresponding to the firing of the
                laser pulse.

Satellite
carrying retro-
reflectors

Returning
Pulse

Transmitted
Pulse

Receiving
Telescope

Transmitting Telescope

Telescope Pointing
System

(Satellite Orbit
Prediction)

Timing System

Data Storage
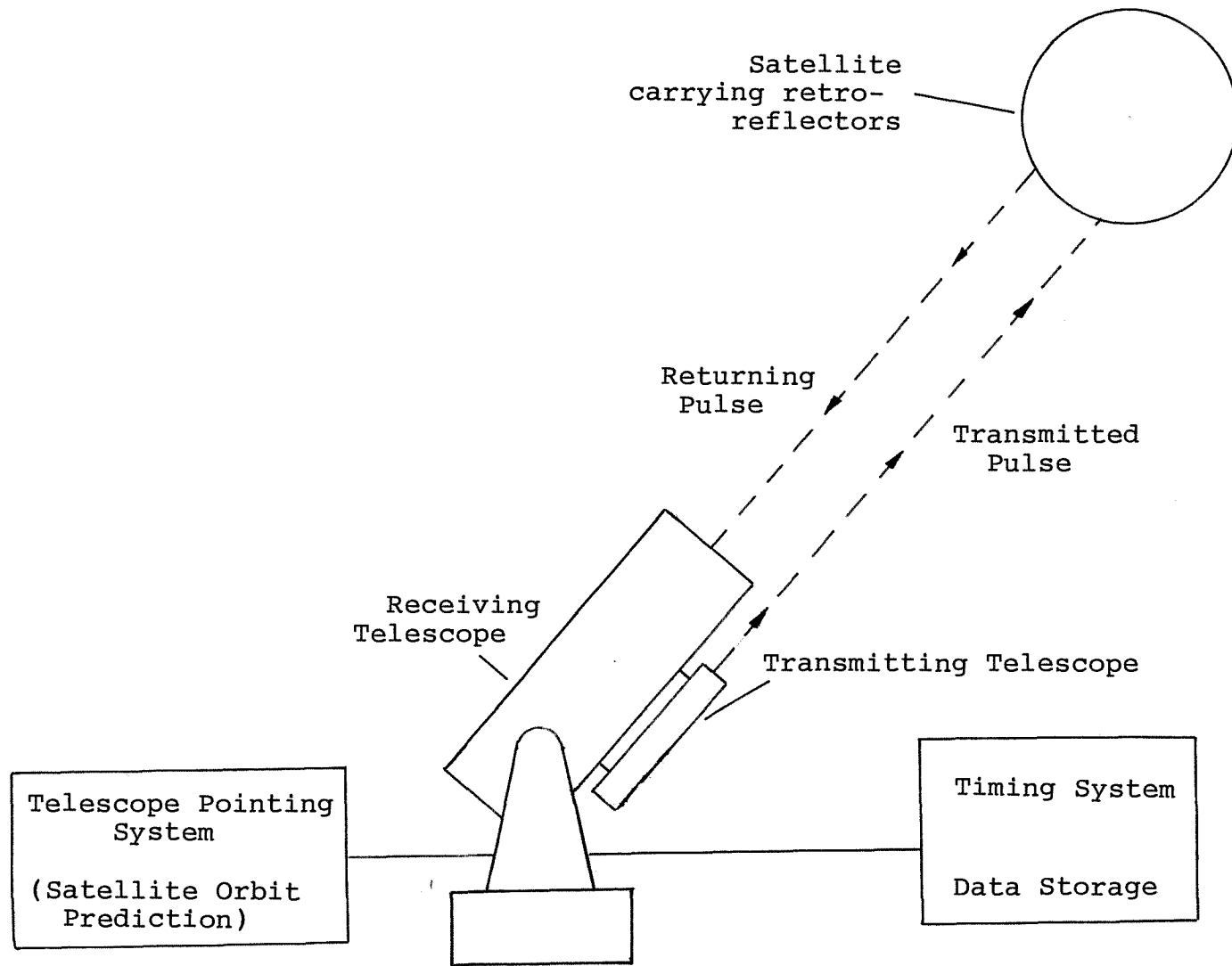
Fig 2.I Principles of Satellite Laser Ranging

However, this model is clearly not realistic, as no delays, biases or errors, such as the delay due to atmospheric refraction and delays in the firing and timing systems, are accounted for. The modelling of error sources and the calibration of biases from laser ranging systems are discussed in § 2.4. Equation (2.1) may be re-written, to allow for possible error sources, as,

$$R = c \, \Delta t/2 - \varepsilon_R - \varepsilon_B - \varepsilon_C - \varepsilon \qquad (2.2)$$

where  $\varepsilon_R$ :  atmospheric refraction correction

$\varepsilon_B$ :  system delays, determined by calibration

$\varepsilon_C$ :  centre of mass correction (see § 2.3.1)

$\varepsilon$ :  remaining systematic and random errors

$\Delta t$ :  $t_r - t_f$ , time of flight.

Both equations (2.1) and (2.2) calculate a 'one way' range to the satellite by assuming that the time of flight of the pulse to the satellite and the time of flight back from the satellite are identical, and equal to half the total flight time of the laser pulse. This is the procedure adopted by most centres currently processing laser ranging observations (Tapley, Schutz and Eanes, 1982). Furthermore, the raw range measurements are transmitted to analysis centres in the form of one-way ranges, determined in this way. However, for reasons to be discussed in § 5.5.1, the Nottingham suite of programs processes the data as 'two-way' ranges, as would be obtained directly from the time of flight.

An observed laser range is a measure of the distance (one-way or two-way) between some reference point of the tracking system (determined by calibration) to the retro-reflectors on the satellite. The processing of laser range observations involves the computation of the satellite's orbit (see Chapter 3), which is expressed as the 3 dimensional cartesian coordinates of the centre of mass of the satellite. Consequently, a small correction (determined before the launch of the satellite) is applied to the observed ranges to refer them to the centre of mass rather than the outer surface of the satellite (see § 2.3.1).

Clearly, a single measurement of the range can yield very little useful information and, therefore, the usual practice is to track a satellite during many 'passes' over a laser ranging station, taking range measurements up to 10 times per second. These ranges, possibly combined with ranges from other tracking stations as well, may be input into a least squares 'variation of coordinates' analysis procedure. This processing of laser ranges allows analysts to determine, for example, the satellite's orbit, the coordinates of the tracking stations and several other geophysical and orbital parameters. The analysis of Satellite Laser Ranging data is outlined in § 2.5 and discussed in more detail in Chapter 3.

The principal components of a tracking station may be discussed under five headings: the telescopes

and mounts, the control computers and software, the laser, the detection system and the timing system. Clearly, when tracking a satellite there is a need to direct the 'out going' laser pulse towards the satellite and also point the telescope so it will receive the returning pulse. For this purpose the transmitting and receiving telescopes (which may in some cases be a single telescope) are generally attached to the same gimbal mount, which may be directed either manually or automatically. In an automated system the pointing of the telescopes would be controlled by a computer system using a prediction of the satellite's orbit. The computer may also be used to control the timing system and the flow of data between the other systems (for example, the storage of the range observations).

Probably the most important of the hardware devices is the system of laser oscillators and amplifiers which produces the short pulse of high intensity light transmitted through the telescope. Detailed descriptions of the 'Light Amplification by the Stimulated Emission of Radiation, LASER' devices used in laser ranging systems is clearly beyond the scope of this thesis, however a general description of the characteristics of typical lasers is included. Traditionally, all laser tracking stations used Ruby laser which produced coherent light with a wavelength of 694.3nm, an energy of a few Joules and a pulse width

(duration of an individual pulse) of the order of 10ns.
Current, state-of-the-art, tracking systems utilise
Nd:YAG lasers with a wavelength of 532.0nm, an energy
of less than a Joule and a very short pulse width of
around 150-200 ps. Details of operational lasers used
in satellite tracking, and other aspects of hardware,
may be found in a recent paper by Dr. J Degnan of the
Goddard Space Flight Center (Degnan, 1985).

A typical detection package could operate as
follows. The receiving telescope focuses the returning
pulse on the cathode of a photomultiplier, after
passing through timing and spectral filters (the latter
only allow a very narrow bandwidth of light to pass
through). The output of the photomultiplier is
amplified (if necessary) and sent to a device which
produces the necessary logic signal to either stop or
start the timing system. Two types of timer are in
general use, namely, 'interval' and 'event' timers. An
interval timer operates rather like a precise
stop-watch which is started when the pulse is fired and
stopped when it returns, the elapsed time giving the
time of flight. In comparison, an event timer reads the
epoch at which particular events occur, such the the
firing or return of a pulse, off a 'clock' which
operates continously. Lunar Laser Ranging systems
generally use event timers as they allow more than one
pulse to be in flight at any time. Details of a typical
'third generation' Satellite Laser Ranging' facility

are given in a technical note of the Royal Greenwich
Observatory (Sharman, 1982).

## 2.2.2 Satellite Laser Ranging Tracking Stations

Laser ranging systems have developed in a number
of different countries over the past two decades. As
would be expected, this diversity of development has
led to a wide variety of different systems and
specifications ranging from fixed satellite and lunar
tracking systems to highly mobile systems specifically
designed for monitoring crustal movements. As
development has progressed laser tracking systems have
been catagorised into three generations which can be
loosely defined by their single shot root mean square
precisions (the average precision of a one way range
measurement) as,

|                   |   |                     |
|-------------------|---|---------------------|
| first generation  | : | greater than 50cm   |
| second generation | : | between 10 and 50 cm |
| third generation  | : | better than 10cm    |

Differences in instrumentation and approach also
differentiate between the three generations, and where
applicable these will be discussed in later sections.
Tracking systems in all these catagories are still
operational in various parts of the world, but many are
in the process of upgrading to the 3rd generation
specifications, in order to meet the stringent
precision requirements being set by current geodynamic
and geophysical applications.

As already stated, soon after the launch of Beacon Explorer B in October 1964, the first laser system was operational at the Goddard Space Flight Center (GSFC) and had an accuracy of 1 to 2 metres. During 1970 a preliminary three month polar motion experiment was conducted by the GSFC using two 50cm precision ranging systems. Soon after, in 1972, tracking stations at either end of a 900km baseline in California observed the initial measurements of the San Andreas Fault Experiment (SAFE). By the early 1970's several experimental tracking stations were operational in Europe as well as the systems already commisioned by the GSFC and the Smithsonian Astrophysical Observatory (SAO). Since then numerous laser tracking systems have been developed and operated throughout the world.

The currently operational satellite laser tracking stations can be, generally, divided into three different types. Firstly, there are a number (in Europe particularly) of 'fixed' systems at satellite and astronomical observatories, which are designed to operate at one location and not move from one site to another. However, movement of some of these stations is possible, as demonstrated by the recent move of one of the SAO systems from Natal in Brazil to Matera in Italy, but not without considerable disassembly. Between 1972 and 1978 the GSFC commissioned eight mobile laser ranging systems, MOBLAS 1 to 8, to form the basis of the Goddard Laser Tracking Network (GLTN).

The telescopes, laser and other instrumentation are mounted in a number of large vans, allowing the whole system to be moved from one global location to another. Although the eight systems have been deployed around 50 times at over 20 different locations, they are not highly mobile and tend to stay at one site for a number of years.

The need for highly mobile systems, for the study of crustal dynamics on a regional and global basis, became evident a number of years ago. Currently four highly transportable laser tracking stations are operational. Two Transportable Laser Ranging Stations, TLRS-1 and TLRS-2, have been developed by the University of Texas and the GSFC respectively. They have been operated at many locations of the past few years and have clearly demonstrated their ability to start observing soon after occupying a new site. Two additional TLRS systems are planned by the GSFC, the first TLRS-3 is expected to be operational in 1986, to meet the needs of the Crustal Dynamics Project in studying regional deformations. Since 1984, two European Modular Transportable Laser Ranging Systems, MTLRS-1 and MTLRS-2, have been operated by the Institut für Angewandte Geodäsie (IfAG) and the Observatory for Satellite Geodesy of the Delft University of Technology (DUT/OSG), respectively. These tracking systems are modular in construction and are designed to be highly mobile.

The global network of operational tracking stations can be considered as three seperate, but cooperating, groups. The first of these, the Goddard Laser Tracking Network consists of the eight MOBLAS systems, the Transportable Laser Ranging Stations (TLRS), four Smithsonian Astrophysical Observatory (SAO) fixed stations. In addition a further three fixed satellite and lunar laser ranging facilities, at Hawaii, Texas and Orroral Valley, Australia, are also operated by the GLTN. The second group, the Intercosmos INSATLAS network, comprises around fifteen fixed stations around the world. These tracking stations are mainly first generation, however some systems (notably Potsdam in East Germany) have been upgraded and regularly contribute data to the global data set. Unlike the two previous groups, the third is not operated by a central agency but consists of the various European, Japanese and Chinese tracking systems operated by scientific institutions of the host country. These stations do, however, cooperate closely with the Goddard Laser Tracking Network for observational campaigns and projects (notably the NASA Crustal Dynamics Project, see § 2.2.4).

The operational status and even the location of satellite laser tracking stations are constantly changing, consequently making the task of producing a definitive list of the 'current' network almost impossible. Therefore, in order to provide an

illustration of the distribution of the tracking
stations those contributing data during the 14 months
of the main campaign of Project MERIT (see § 2.2.4)
have been listed in fig 2.II. As described in § 4.4.3
two data sets were compiled from the data observed
during the campaign, namely the Standard Data Sets of
compressed filtered data and the Full Rate set of raw
observations. The first half of fig 2.II details the
thirty stations which contributed data to the Standard
Data Sets and the second half the remaining eight
stations which contributed data to the Full Rate but
not to the Standard Data Sets. The flexibility of the
TLRS transportable systems is clearly illustrated, and
indeed TLRS-1 contributed data observed at six
different sites in North America and Chile. Fig 2.III
illustrates the global locations of the stations
described in fig 2.II.

### 2.2.3 Laser Ranging Satellites

Since the launch of Explorer 22 (Beacon B), on
the $9^{th}$ October 1964, a further 16 satellites equipped
with retro-reflectors have been launched by a number of
countries. The purpose of the retro-reflectors is to
ensure a strong return of a fraction of the transmitted
laser pulse by the satellite. This is achieved by using
an array of 'corner-cubes'. As the name suggests a
corner-cube retro-reflector is basically a glass
tetrahedron, of which three sides are mutually

| ID No. | System | Location |
|--------|--------|----------|
| 1181 | POTSDM | ZIPE, Potsdam, GDR |
| 7086 | MLRS | Ft. Davis, Texas |
| 7090 | MOBLAS-5 | Yarragadee, Australia |
| 7105 | MOBLAS-7 | GSFC, Greenbelt, Md |
| 7109 | MOBLAS-8 | Quincy, Ca |
| 7110 | MOBLAS-4 | Monument Peak, Ca |
| 7112 | MOBLAS-2 | Platteville, Co |
| 7121 | MOBLAS-1 | Huanhine, French Pol. |
| 7122 | MOBLAS-6 | Mazatlan, Mexico |
| 7210 | HOLLAS | Haleakala, Maui, Hawaii |
| 7265 | TLRS-1 | Mojave, Barstow, Ca |
| 7400 | TLRS-1 | Santiago, Chile |
| 7401 | TLRS-1 | Cerro-Tololo, Chile |
| 7805 | METFIN | Metsahovi, Finland |
| 7810 | ZIMMER | Zimmerwald, Switzerland |
| 7831 | HELWAN | HIAG and TUP, Helwan, Egypt |
| 7833 | KOOTWK | Kootwijk Obs., Netherlands |
| 7834 | WETZEL | IfAG, Wetzell, FRG |
| 7835 | GRASSE | GRGS/CERGA, Grasse, France |
| 7837 | CHILAS | Shanghai, China |
| 7838 | SHO | Simosato Hydrographic Obs., Japan |
| 7839 | GRAZ | Obs. Graz-Lustbuehel, Austria |
| 7840 | RGO | Royal Greenwich Obs., UK |
| 7843 | ORRLAS | Orroral Val., Australia |
| 7882 | TLRS-2 | Cabo San Lucas, Mexico |
| 7886 | TLRS-1 | Quincy, Ca |
| 7907 | ARELAS | Arequipa, Peru |
| 7939 | MATERA | PSN, Matera, Italy |
| 7940 | DIONYS | Dionysis, Athens, Greece |
| 8843 | MTLRS-1 | Kootwijk, Netherlands |
| 1072 | ZVENIG | Zvienigorod, USSR |
| 1837 | SIMIEZ | Simiez, Crimea, USSR |
| 7062 | TLRS-2 | Otay Mountain, Ca |
| 7082 | TLRS-1 | Bear Lake, Utah |
| 7106 | GORF | Greenbelt, Md |
| 7220 | TLRS-1 | Monument Peak, Ca |
| 7824 | SANFAN | San Fernando, Spain |
| 7935 | DODAIR | Dodair, Tokyo, Japan |

Fig 2.II Details of MERIT Tracking Stations (1983/84)
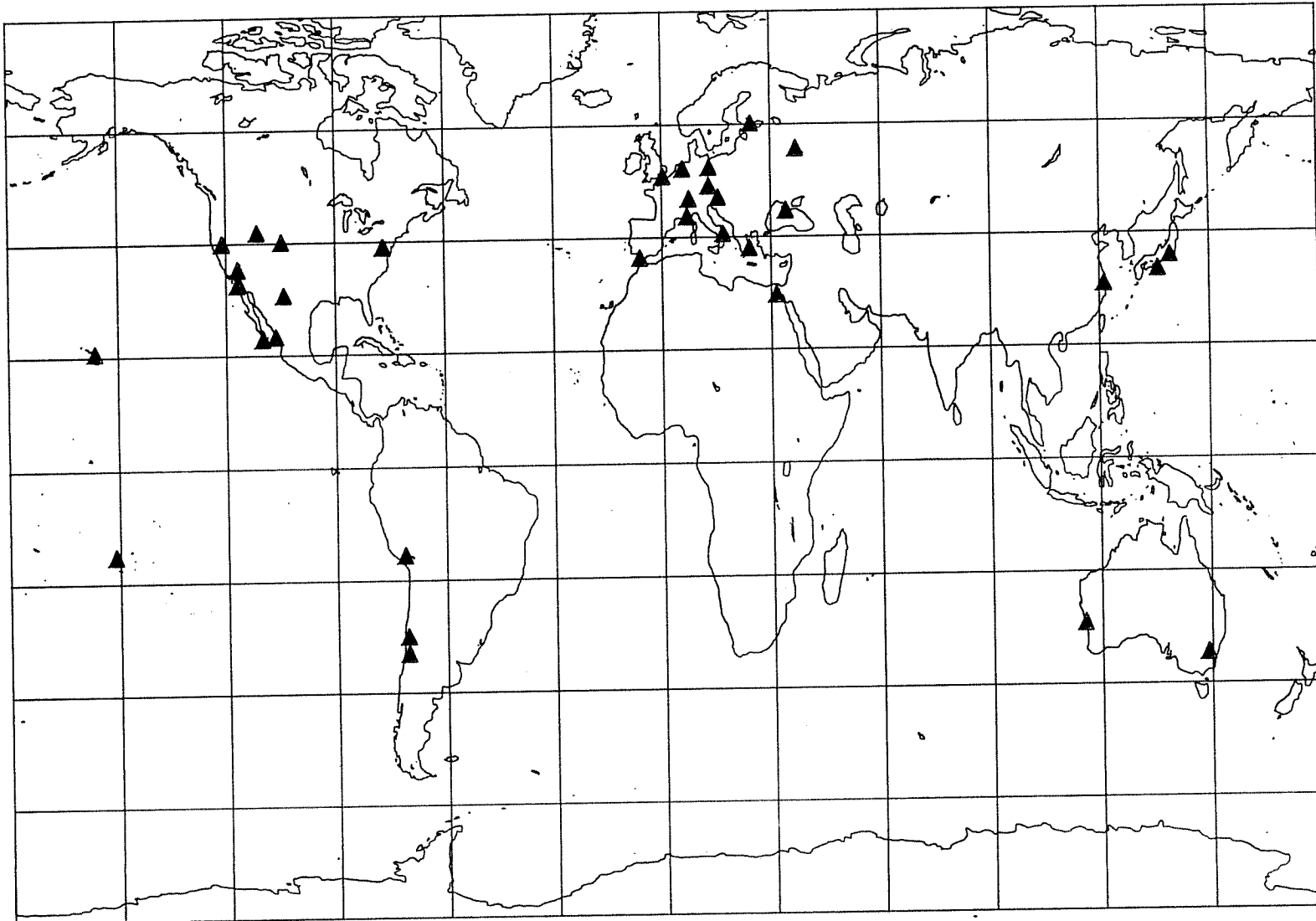
Fig 2.III Locations of tracking stations (1983)

perpendicular and silvered, obtained by diagonally slicing the corner of a cube of glass. Any light incident with the remaining face will be reflected, in turn, by each of the back faces and will emerge from the corner-cube parallel to the incoming light. Clearly, therefore, regardless of the direction of the incoming light incident on the front face it will be reflected back in a parallel direction. Typically, these optical retro-reflectors are made of fused silica, and operate throughout the visible and near infra-red portions of the spectrum.

Apart from the optical retro-reflectors no further payload is required on an artificial satellite to enable it to be tracked by a laser ranging station. However, the objectives of the particular missions of the various satellites, and consequently the structure and payloads, are extremly varied. The details of the 17 satellites are presented in fig 2.IV. Notable is the range of the 'nominal heights' of the orbits, ranging from 300km to 20,000km. Clearly, the choice of satellite to be tracked will be determined by the application being considered, as certain applications will be best realised by using observations to a particular satellite (and orbit). For example, if one aims to determine precise tracking station coordinates and earth rotation parameters, then a satellite in a high (above the earth's upper atmosphere), extremely stable, well known orbit is most suitable. Whearas, if

| Satellite | ID No. | Launch Date | Height (km) | Eccentricity | Inclination |
|---|---|---|---|---|---|
| Explorer 22 (Beacon B) | 1964-64A | 13 Oct 1964 | 890-1080 | 0.013 | 79.7 |
| Explorer 27 (Beacon C) | 1965-32A | 29 Apr 1965 | 940-1320 | 0.025 | 41.2 |
| Explorer 29, Geos 1 | 1965-89A | 6 Nov 1965 | 1110-2280 | 0.072 | 59.4 |
| Diademe 1 | 1967-11A | 28 Feb 1967 | 570-1350 | 0.053 | 40.0 |
| Diademe 2 | 1967-14A | 15 Apr 1967 | 590-1880 | 0.085 | 39.5 |
| Explorer 36, Geos 2 | 1968-02A | 12 Jan 1968 | 1080-1580 | 0.032 | 105.8 |
| Peole 1 | 1970-109A | 12 Dec 1970 | 520-750 | 0.016 | 15.0 |
| NTS 1 (Timation 3) | 1974-54A | 22 Jul 1974 | 13400-13800 | 0.008 | 125.1 |
| Starlette | 1975-10A | 6 Feb 1975 | 810-1110 | 0.021 | 49.8 |
| Geos 3 | 1975-27A | 10 Apr 1975 | 840-850 | 0.001 | 115.5 |
| Castor - D5B | 1975-39A | 19 May 1975 | 270-1270 | 0.070 | 30.0 |
| Lageos | 1976-39A | 4 May 1976 | 5800-5900 | 0.004 | 109.9 |
| NTS 2 | 1977-53A | 23 Jun 1977 | 19500-20200 | 0.012 | 62.3 |
| Intercosmos 17 | 1977-96A | 24 Sep 1977 | 460-510 | 0.004 | 82.9 |
| Seasat | 1978-64A | 27 Jun 1978 | 776-800 | 0.002 | 108.0 |
| Tansei 4 | 1980-15A | 17 Feb 1980 | 517-602 | 0.006 | 38.7 |
| Intercosmos 22 | 1981-75A | 7 Aug 1981 | 800-895 | 0.007 | 81.2 |

Fig 2.IV Laser Ranging Satellites

the aim is to study, for example, the fine details of the earth's gravity field, tidal effects or the upper atmosphere, then a satellite in a lower orbit (i.e. less than 1000km) would be required. Satellite Laser Ranging may also provide supportive role to other missions, such as Satellite Altimetry, in order to determine the orbit of the particular satellite. For this reason altimetry satellites, such as GEOS-3 and SEASAT, also carry retro-reflectors together with their principle payloads. Applications of laser ranging to satellites are discussed in more detail in § 2.2.4.

Although many of the early observations were to Beacon C and later the GEOS satellite, the majority of tracking stations currently concentrate on two dedicated laser ranging satellites, LAGEOS and STARLETTE, the former being the principle target for geodetic and geophysical research. STARLETTE was launched on 6 February 1975 by the French Centre Nationale d'Etudes Spatiale (CNES), into an orbit of eccentricity 0.021, perigee 806km and inclination $49.82^{\circ}$. The satellite is a small sphere of radius 12cm, which is covered with 60 corner-cube retro-reflectors. The shell, in which the corner-cubes are embedded, is constructed from aluminium alloy sheets around a Uranium 238 core, resulting in a mass of 47.295kg. STARLETTE is completely passive and was developed exclusively for laser ranging, the shape and low 'area/mass' ratio (see § 3.3.5) designed to minimise

the effects of non-gravitational forces. The orbit of STARLETTE was chosen to be highly suitable for tidal analysis (see § 3.3.4) and over the last decade analyses have demonstrated the ability to precisely determine tidal and other geodetic parameters from STARLETTE laser ranging data (Williamson and Marsh, 1985).

The LAser GEOdynamic Satellite (LAGEOS) was launched by NASA on the 4$^{th}$ May 1976. Similar in appearance and design to STARLETTE, LAGEOS is a spherical passive satellite (60cm diameter) with a brass core and an aluminium shell, and a mass of 407kg. Embedded in the outer shell are 426 corner-cube retro-reflectors of which 422 are made of fused silica (operative throughout the visible and near infra-red portions of the spectrum) and four of germanium (effective in the middle infra-red region).

LAGEOS was launched into a near circular orbit having an altitude of about 5800km, an inclination of 109.9$^0$ and an eccentricity of 0.004. The orbital characteristics were selected so that the effects of atmospheric drag and short wavelength uncertainties in the gravity field, would be minimised. Hovever, the satellite also had to be at a low enough altitude to ensure a strong return of the laser pulses. As with STARLETTE, the high density and spherical shape are designed to reduce the effects of solar radiation on the satellite. The use of state-of-the-art precise

laser ranging systems with LAGEOS over the past few years has clearly demonstrated the enormous potential of this combination for the investigation of geodynamic and geophysical phenomena and maintaining a global geodetic reference frame.

The list shown in fig 2.IV gives the current status of laser ranging satellites, although at present a metrological balloon, METEOR-3, is also carrying retro-reflectors. There are also firm plans for the launch of EGP, a Japanese dedicated laser ranging satellite, in October 1986. This satellite will be a 2m diameter sphere carrying mirrors as well as retro-reflectors to allow optical tracking.

Three other missions, ERS-1 (ESA Remote Sensing Satellite), POPSAT (Precise Positioning Satellite) and TOPEX (Ocean Topography Experiment) are currently being planned by the European Space agency (ESA) and (the latter) by NASA. All three will carry laser retro-reflectors as part of the payload. POPSAT is designed as a geodetic satellite for determining the positions of points on the earth's surface for earthquake prediction and monitoring (Wintzer and de Villiers, 1982). At present no launch has been date proposed for POPSAT, although it is planned for the 1990's. ERS-1 and TOPEX are proposed remote sensing satellites which will carry several different payloads for a variety of experiments. Both, however, will have radar altimeters to monitor the surface of the oceans.

ERS-1 (Haskell, 1983) is currently scheduled for launch
in 1991 and the earliest possible launch for TOPEX is
1990, although the future of this mission is uncertain
at present.

To complement and enhance the dramatic effect
LAGEOS has had on the earth sciences over the last few
years, NASA and the Piano Spaziale Nazionale (PSN) of
the National Research Council of Italy have agreed to
develop and launch a second LAser GEOdynamic Satellite,
LAGEOS II (Christodoulidis and Zerbini, 1985). The
satellite will have the same physical size and
construction as LAGEOS I and very similar orbital
characteristics, with the exception of the inclination
of $51^0$-$53^0$, in comparison with $109.8^0$ for LAGEOS I. The
current proposal is to launch the satellite using
NASA's Space Shuttle during November 1988.


## 2.2.4 Applications of Satellite Laser Ranging

During recent years the analysis of laser range
observations to artificial satellites has led to a
significant improvement of our knowledge of several
aspects of the earth's science and of the forces acting
on satellites. A review of some of the recent
applications of Satellite Laser Ranging is presented in
this section and where applicable an estimate of the
precision currently achievable is given.

A product of the analysis of laser range
obervations is the three dimensional position of the

tracking stations. If a dynamical approach of analysis is used, as discussed in § 2.5, then there is a requirement to fix the longitude of one of the tracking stations. It has been demonstrated (Christodoulidis and Smith, 1983a), that laser ranging to satellites has the potential to define a vertical datum to approximately 1cm and a horizontal datum to an accuracy of better than 2cm. Clearly, positioning to this precision leads to the possibility of studying the movements of tectonic plates on a regional and global scale, and so to assist in the prediction of earthquakes.

The Crustal Dynamics Project (CDP) was initiated in 1979 as part of the NASA Geodynamics Program. The aim of the project are to determine regional deformations in regions of the US (and tectonically similar regions), global tectonic plate movements and internal deformations of the North American and Pacific plates. The San Andreas Fault Experiment (SAFE), which is now a part of the CDP, has used laser ranging to satellites to monitor a baseline in California for the last fourteen years, resulting in a rate of around -6.5±0.7 cm/yr (Christodoulidis and Smith, 1983b). On a global scale laser ranging measurements of the rate of movement of major tectonic plates have been compared with a model of the motions derived by Minster and Jordan (1978) and show a good general agreement. The CDP is cooperating with the WEGENER (Working group of European Geoscientists for the Establishment of

Networks for Earthquake Research) consortium, with the objective of monitoring regional deformations around the tectonically active region of the Eastern Mediterranean. Transportable laser ranging systems, in addition to fixed systems , will range to LAGEOS from a number of sites around the area during 1986, and again in 1988 and 1990 (Reinhart et al, 1985).

Satellite Laser Ranging has also proven to be one of the most accurate methods of orientating the earth within an inertial reference system. Laser range measurements have been used to determine, since 1976, the two components of the earth's polar motion ($x_p$ and $y_p$) and the excess length of day (see § 3.2.4). The resulting series are now regularly included in the Bureau International de l'Heure (BIH) determination of the earth's orientation. Currently attainable accuracies are of the order of 0.002 arc seconds in $x_p$ and $y_p$ (around 6 cm on the earth's surface) and 0.2 ms in length of day (Smith et al, 1985). Laser ranging to satellites is also one of the principal techniques of project MERIT (as discussed in Chapter 4).

In addition, laser tracking of satellites is the most precise means available of determining the orbital motion of artificial satellites. The principal force acting on a satellite is that of the earth's gravity field, and over recent years laser range measurements have contributed to a number of geopotential models. Notable is the GEM-L2 model for LAGEOS (Lerch et al,

1982), which included a contribution from around two and a half years of LAGEOS tracking data. During the development of the PGS-1331 'tailored' gravity for STARLETTE tidal parameters were also determined (Marsh, Lerch and Williamson, 1985). The tidal model obtained showed a close agreement with the ocean tidal model of Schwiderski (ocean tides are discussed in § 3.3.4.2) and confirmed the frequency dependent love numbers of the Wahr model.

Precise orbit monitoring also allows for the improvement of constituents of the force model acting on the satellite. For example, atmospheric drag models, and solar radiation pressure (see § 3.3.5), and also other geophysical effects inferred from the orbital parameters. The study of the evolution of the node of LAGEOS's orbit has enable geophysicists to gain important knowledge regarding the earth's rheology. A change in the earth's oblateness has been inferred, and attributed to the 'post glacial rebound', leading to an estimate of the viscosity of the lower mantle (Rubincam, 1984).

During the next few years a slight improvement of the single shot precision of laser ranging systems is predicted (5-10mm)and by maintaining a global network of tracking stations it is anticipated that Satellite Laser Ranging will make further significant contributions to the geosciences (Christodoulidis and Smith, 1983b).

2.3  LASER RANGE MEASUREMENT ERRORS

2.3.1 Classification of Error Sources

As previously stated in § 2.2 a measurement of a
range to a satellite is corrupted by a series of errors
from a variety of sources. These may be classified as
instrument errors and modelling errors, the former
directly affecting the recorded measurement while the
latter refers to corrections applied to the data due to
modelled effects, such as atmospheric refraction. The
'error budget' (or more commonly, the single shot range
precision) of a tracking system is evaluated as the sum
of the best estimates of the effects of all the error
sources. A standard method of asssessing the magnitude
and effect of errors in laser ranging systems has been
proposed (Pearlman, 1984). This model attempts to
standardise the tests, models and calibration
procedures used by the various laser ranging stations
and to classify the possible error sources and the
nature of the errors. Clearly, by the laser ranging
community adopting a standard such as this, a
quantitative comparison of the relative performances of
different tracking systems may be obtained. A
consistent estimate of the error budget could also be
provided to the analysts of laser ranging data to allow
representative weighting to be applied to the range
measurements during the processing.

Typically, the major component of the instrument
errors is due to the combined effect of the delays

within the systems, which are usually determined by
internal calibration. Details of the calibration of
system delays are given in § 2.3.2. In contrast, the
delay of the laser pulse as it propagates through the
atmosphere is the principal model error source. This
may not be removed by calibration but must be accounted
for by means of a model based on measurements of
surface temperature and pressure. Atmospheric
refraction and the models adopted for corrections to
laser ranging measurements is discussed in § 2.3.3.1,
together with other sources of model errors which
corrupt laser range data.

## 2.3.2 Instrument Errors

The range measurements to a satellite are
referred to a fixed reference point within the
telescope system, usually the intersection of the two
axes of rotation of the telescope mount. However, it is
not practical, or generally possible, to mount all the
instrumentation at this 'point'. Therefore some delay
is introduced into the range measurements due to the,
often varying, optical and cable path lengths to the
detecton system and timer. Clearly, these errors must
be removed from the raw range measurements. The
magnitude of this error is usually determined by a
process of calibrating the tracking system, by
measuring over a fixed path length from the laser
reference point. This may be achieved by ranging to

ground targets (retro-reflectors) at known distances from the reference point. However, some tracking stations have internal calibration devices, where the laser pulse follows a known optical path (of fixed length) between transmitting and receiving telescopes. Clearly, if the distance is known precisely then the residual errors will be due to delays within the system. Typically, however, these errors often vary with time and consequently it is common practice for laser ranging stations to be calibrated for system delays before and after each pass. The method of calibration using ground targets is not, however, error free and may be corrupted by uncertainties in the measurement of the distance to the ground target, the varaible and uncertain refraction effects at low elevation angles, and by the effect of using different signal strengths during calibration to those used during satellite ranging.

The 'fixed' reference point is assumed to be invariant, but any eccentricity in the mount may introduce errors into the measurement, which will vary according to the direction in which the telescope is pointing. This error will not only affect the range measurements to satellites but also any ground target calibration ranges. Mount eccentricities are typically measured and modelled with periodic re-measurement to ensure there is no change in the modelled variations.

Errors in the time standards, used during the measuring of the time of flight of the laser pulses and for the 'time tagging' of the ranges in the database, must also be monitored and corrections applied where necessary. Clock errors may be separated into a bias term (relative to UTC, for example), a drift term and also any discontinuous behaviour of the time standard. Such errors are usually monitored by means of a comparison with time transfer services, such as LORAN or GPS, or with other broadcast sources. The interpretation of the time of reception of a pulse may also lead to errors in the range measurements if the returning pulse is non-Gaussian in from. Several third generation stations currently use a system based on the detection of a single photon of the returned pulse, and consequently this error source is eliminated. However, for tracking systems receiving a laser pulse of many photons, corrections must be made to the range measurements depending on whether a 'leading edge' or 'centroid' detection system is used.

The determination of systematic and random instrument errors of laser ranging systems is generally performed by the operators of the tracking stations and range measurements are corrected before their release to the laser ranging community. However, no correction is usually applied for model errors until the data is processed.

2.3.3   <u>Modelling</u> <u>Errors</u>

2.3.3.1 <u>Atmospheric</u> <u>Refraction</u> <u>Correction</u>

As a laser pulse propagates through the atmosphere, both on its journey to and from the satellite, it experiences a delay (and a bending of the path) due to troposheric refraction (Abshire and Gardner, 1985). This has the effect of an increase in the apparent range to the satellite, varying between approximately 13.5m at an elevation angle of $10^0$ to 2.4m at the zenith (Sinclair, 1982). Clearly, with current ranging accuracies, of the order of a few centimetres, a model is required which can determine the correction for atmospheric refraction with sufficient accuracy (say, better than 1cm).

The model recommended (Schutz, 1983b and Pearlman, 1984) is that of Marini and Murray, in which the correction is based on the computated index of refraction at the tracking station (Marini and Murray, 1973). The only additional measurements required to compute the corrections are those of the temperature, the pressure and the relative humidity at the laser tracking station. Preliminary comparisons with ray trace experiments indicated this model to be accurate to better than 5mm for elevation angles of greater than $10^0$. However, this was subsequently not considered representative (Bufton, 1978) and it has been estimated that the effect of horizontal variations of metrological conditions (horizontal gradients in

atmospheric density) could cause this model to be in error by up to 2cm at elevation angles of around $20^0$ (Bufton 1978 and Gardner, 1976). The correction to a one way range measurement is given by

$$\Delta R = \frac{f(\lambda)}{g(\phi,H)} \cdot \frac{A + B}{\sin E + \dfrac{B / (A+B)}{\sin E + 0.01}} \quad (2.3)$$

where $\quad A = 0.002357\ P + 0.000141\ e \quad\quad\quad (2.4)$

$$B = (1.084 \times 10^{-8})PTK + (4.734 \times 10^{-8})\frac{2P^2}{T(3-1/K)} \quad (2.5)$$

$$K = 1.163 - 0.00968\ \cos 2\phi - 0.00104\ T \quad (2.6)$$

$$+\ 0.00001435\ P$$

$$f(\lambda) = 0.965 + \frac{0.0164}{\lambda^2} + \frac{0.000228}{\lambda^4} \quad (2.7)$$

$$f(\lambda) = 1.0 \quad\quad \text{for } \lambda = 0.6943\ \mu m \text{ (Ruby Laser)}$$

$$f(\lambda) = 1.02579 \text{ for } \lambda = 0.5320\ \mu m \text{ (Nd:YAG Laser)}$$

$$g(\phi,H) = 1 - 0.0026\ \cos 2\phi - 0.00031\ H \quad (2.8)$$

$$e = R_h/100 \cdot 6.11 \times 10^S \quad\quad\quad (2.9)$$

$$s = \frac{7.5\ (T - 273.15)}{237.3 + (T - 273.15)} \quad\quad (2.10)$$

and $\quad \Delta R \ :\quad$ correction in metres

$\quad\quad\quad E \ \ :\quad$ true elevation angle of satellite

$\quad\quad\quad\quad\quad$ (see Appendix B)

$\quad\quad\quad P \ \ :\quad$ atmospheric pressure at tracking station

$\quad\quad\quad\quad\quad$ (in millibars)

$\quad\quad\quad T \ \ :\quad$ atmospheric temperature at tracking

$\quad\quad\quad\quad\quad$ station (in Kelvin)

$R_h$ : relative humidity at tracking station (percent)

$\lambda$ : laser wavelength in microns ($\mu$m)

$\phi$ : latitude of tracking station

H : height of the tracking station above mean sea level (km).

From equation (2.4) it is clear that the most significant term of equation (2.3) is dependent on the pressure at the tracking station and inversely proportional to the elevation angle, (Pearlman, 1984) as given by

$$\partial \Delta R = \frac{0.0024}{\sin E} \partial P \qquad (2.11)$$

where   $\partial \Delta R$ : change in the range correction $\Delta R$, in mm

$\partial P$ : change in atmospheric pressure in mb.

To quantify this expression, a measurement error of 1mb in the pressure will introduce an error of about 7mm in the correction to the range, whereas small errors in the elevation angle will have very little effect. The dependence of the model on the temperature measurement at the tracking station is given by

$$\partial \Delta R = \frac{1 \times 10^{-5}}{\sin^3 E} \partial T \qquad (2.12)$$

where   $\partial T$ : change in temperature T in Kelvin.

A error of 1K in the measurment of temperature at the tracking station results in an error of 0.3mm in the range correction. Clearly, in order that the

effects of atmospheric refraction may be removed with the precision predicted by the model, the barometers and thermometers at the tracking sites must be calibrated to ensure that errors in the pressure and temperature measurements do not corrupt the atmospheric delay correction.

### 2.3.3.2 Other Modelling Errors

For all laser ranging satellites the array of corner-cubes, which reflect the transmitted laser signal back to the tracking station, are displaced from the centre-of-mass of the spacecraft. Furthermore, the orbit determination is referred to this reference point (the centre-of-mass) and so the observed ranges must be corrected accordingly. However, the pulse is not reflected from a single point but is a combination of reflections from all the reflectors facing the station. For spherical satellites (such as LAGEOS and STARLETTE) this correction is a simple constant offset, however, for others the satellite attitude and consequently the position of the reflector array must be considered, resulting in more complex correction formulae.

For LAGEOS the centre-of-mass correction has been determined both analytically (Fitzmaurice et al, 1978 and Arnold, 1978) and by pre-launch calibration (Fitzmaurice et al, 1978). A constant value of 24.0 cm has been generally adopted by the laser ranging community and indeed is the value recommended by the

MERIT standards (Melbourne, 1983). For STARLETTE the correction is conventionally adopted as 7.5cm. It was shown during the analytical determination of the centre-of-mass correction for LAGEOS, that there was a dependence of the correction on the pulse width of the laser and on the detection system. It is estimated (Pearlman, 1984) that an error as large as 1cm could be introduced as a result of using a different pulse width or detection system, to that assumed during the determination of the correction. This range error would appear as a long term fixed bias in the observed ranges.

As previously discussed, in § 2.3.2, the laser ranges are referred to some 'fixed' reference point within the tracking system. However, particularly for mobile and transportable laser ranging stations, the offset to some local geodetic reference benchmark must be surveyed. This allows the transformation of the determined tracking station coordinates to this geodetic reference point from the laser reference point. Clearly, when a site is re-occupied, the tracking station cannot be placed in exactly the same position and so the laser reference point will also be in a different position. However, a local survey permits the connection to the same fixed geodetic (ground) reference point. Small errors may be introduced to the resulting coordinates from any errors in the surveyed transformation vector or from any local

movements of the laser ranging station with respect to the ground point. This is equally true for both fixed or mobile laser tracking systems.

Although corrections for model errors are generally applied by the analysts of laser ranging data during the processing, the atmospheric refraction correction and the ground survey of the laser position depend on measurements taken at the tracking stations. Consequently, as with instrument errors, the monitoring of modelling error sources and the process of calibration depend on measurements carried out by the field operators of the laser ranging stations.

## 2.4    Processing of Satellite Laser Ranging Data

### 2.4.1    Pre-processing of Observed Laser Ranges

#### 2.4.1.1 General Description

The processing of laser ranging observations can be divided into two distinct stages. The aim of the first of these stages, pre-processing, is to produce from the 'raw' observed data a 'clean' data set free from erroneous observations, and corrected for any known anomalies of the raw data. The data may also be compressed so as to produce a quantity of data suitable for the main stage of the analysis. The second stage takes the 'clean' data and computes the required unknowns, as described briefly in § 2.4.2 and in more detail in Chapter 3. This section is concerned with the process of producing the 'clean' data ready for analysis, from the raw data set of observed ranges.

Pre-processing of laser ranging data, for the purpose of this thesis, may be defined as any process concerning the observed ranges which is carried out by the analyst after the data has been received (at the analysis centres) and before the main computational stage. This definition clearly excludes any corrections which are applied at the tracking stations or data collection centres, to account for systematic and random errors discussed in § 2.4.2.

Some form of pre-processing is usually found necessary for a number of possible reasons. Firstly,

the raw data may contain spurious or 'bad' observations which must be removed, otherwise they would corrupt the final analysis. These may be the result of the incorrect detection of the returning laser pulse, particularly with systems operating at the single photon level, when background photons of light may pass through the spectral and time filters of the detection system. Other effects, such as timing errors, may also introduce 'noisy' observations into the data set. The recording and transmission (usually on magnetic tapes) of the observed ranges may possibly introduce some data corruption, although this would normally lead to gross errors rather than noise and so may be detected easily. Secondly, any known anomalies of the data set must be corrected. These usually occur as a result of incorrect 'flagging' when the data was recorded at the tracking stations. Within the standard data formats, a number of information flags indicate which corrections have been applied, which constants have been used and with reference to which time scale the observations were logged. Blunders of this nature are usually detected and publicised by the data collection centres before the general release of the data.

Lastly, the current trend in Satellite Laser Ranging is towards tracking systems operating at very high repetition rates, up to 10 pulses per second (Pearlman, 1984). This has resulted in immense quantities of data being collected, sometimes in the

region of several thousand ranges per pass (around 40 minutes for LAGEOS). Clearly, this is a considerable problem for analysts who may be presented with excessive volumes of data, which it may not be practical to handle. Rather than disregarding the majority of this data the current practice is to adopt some form of averaging or compression technique, with the aim of producing a reasonable volume of data which is representative of the larger data set. Various techniques of data compression to produce 'normal points' have been proposed over the last few years and are discussed in § 2.4.1.3.

Clearly, when adopting pre-processing procedures it is important that only the poor observations are removed and the data is averaged without introducing trends or biases in to the resulting data set. Two pre-processing strategies that have been tested at Nottingham are presented in § 2.4.1.4 and § 2.4.1.5 and their relative merits discussed.

## 2.4.1.2 Filtering of Raw Laser Ranging Data

After the initial correction of the observations for any known anomalies the purpose of filtering is to remove any 'bad' observations from the data set. The detection outliers from a series of data points is a very common, and well documented, concept not only in geodesy and surveying but all scientific disciplines. Consequently, there are many available approaches, but

the problem is to select, or develop, the most appropriate screening technique for Satellite Laser Ranging observations.

To illustrate the nature of the data, the range residuals from a single 'good' 30 minute pass are plotted in fig 2.V. The 'residuals' are simply the 'observed - predicted' ranges, the predicted range calculated from a approximate orbit determination. The details of this procedure are given in § 2.4.1.5; the figure is only included in this section as an illustration. Clearly, there is a need for the adopted method to adequately model the motion of the satellite over whatever period is required (usually one complete pass), to ensure that only outlying points are rejected and good observations are not 'trimmed' from the data set. Although not shown in fig 2.V, laser range observations are rarely continuous over a whole pass and breaks of a few minutes may occur, due to cloud cover or other problems. It is important that an adopted filtering algorithm is able to cope with such discontinuities, without loss of precision.

Several different techniques have been suggested for the screening of laser ranging observations, which primarily differ in the model chosen to represent the satellites orbit. However there are two major different approaches. Firstly, by using all the available data, prior to the period of the observations being filtered, a very stable long arc (orbit) may be computed and
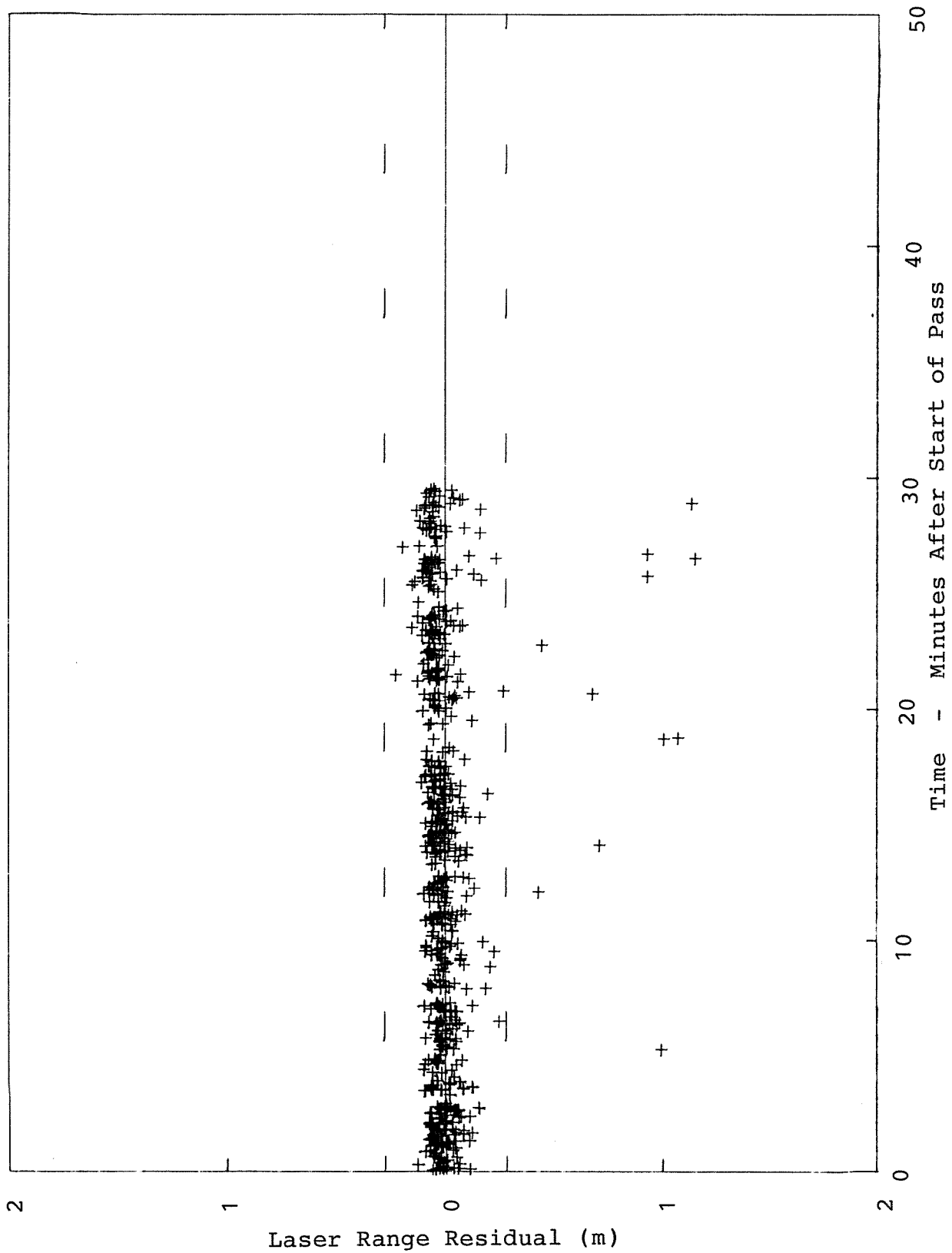
Fig 2.V Raw laser range residuals

extrapolated to include the relevant period of data
(Tapley et al, 1982). Residuals are calculated as the
'observed - predicted' range and any gross errors
detected and the corresponding observations rejected.
The residuals are subjected to either polynomial or
'bias' parameter fitting, to remove any remaining
systematic trends, before spurious observations are
detected by some rejection criteria. Clearly, not all
analysis centres possess the facility to compute very
long orbital arcs and so a 'short arc' version of the
same principle has been adopted by several groups, in
which simple Keplerian orbital elements (Ashkenazi and
Moore, 1986) are adjusted after the removal of gross
outliers.

A simpler approach is to represent the orbital
motion (over, say, the duration of a single pass) by an
$n^{th}$ order regression polynomial of the form

$$R_i = a_0 + a_1(t_i-t_0) + \ldots + a_n(t_i-t_0)^n \qquad (2.13)$$

where  $R_i$    :  observed range at epoch $t_i$

$t_i-t_0$  :  interval from reference epoch $t_0$

$a_0,,a_n$  :  coefficients.

By including a residual term in (2.13) this model may
be 'fitted' to a pass of observations, with the
coefficients determined by least squares. The
linearised model and least squares procedure are
described in Appendix C. The polynomial may be fitted
to the observed ranges, R, or the square of the ranges,
$R^2$ (Sinclair, 1985) and the order of the polynomial

selected to adequately model the orbital motion.
The advantage of such techniques is the simplicity with
which a polynomial representation of an orbit may be
evaluated, However, care must be taken if the residuals
are to be used at a later stage (for example during the
compression of the data) as high frequency trends may
be introduced by the model. This may result if the
polynomial model does not sufficiently represent the
orbital motion.

It has been shown (Masters et al, 1983) that
ranges to LAGEOS vary quadratically (approximately)
over short periods of time (up to 5 minutes).
Therefore, the second derivative of the ranges with
respect to time should be constant, or vary smoothly.
Consequently, by comparing successive differences of
the derivatives, outliers may be detected, as these
result in erratic changes of the derivative.

Having obtained the range residuals, by whatever
means, a criteria must be adopted in order to reject
the bad observations. A first criterion, to detect
gross errors, may be to use a fixed 'window' (say ±50m)
and reject any ranges with residuals outside this
window. The root-mean-square residual, $\sigma_r$, is the basic
parameter used by most filtering criteria, where

$$\sigma_r^2 = \frac{\sum_{i=1}^{n} v_i^2}{n} \qquad (2.14)$$

and $v_i$ : $i^{th}$ residual (observed - predicted)

n : number of residuals (of observed ranges)

Typically, data is filtered by rejecting all observations with residuals greater than 2σ or 3σ. The entire screening process would usually be repeated a number of times until no more observations are rejected.

## 2.4.1.3 Compression of Laser Range Observations

As previously mentioned, many laser ranging stations are currently producing data at the rate of several thousand ranges per pass (up to about 40 minutes for LAGEOS) and when tracking data from a number of stations are combined the resulting quantity of data cannot be handled economically or easily. A means of 'data compression' is necessary which will maintain (or even enhance) the quality of the observations and the contribution of the entire data set but greatly reduce the quantity of data that must be processed. The technique of producing 'normal points' has been employed by analysts of Lunar Laser Ranging data for many years, in order to compress observations over 10 minute intervals into single representative observations. For the analysis of LAGEOS laser ranging data intervals, or 'bins', of one to three minutes are suitable, while for STARLETTE bins of 30 seconds of data are typical.

As with data filtering techniques, many different approaches have been proposed. These are generally based on either range residuals from a predicted orbit or on some form of polynomial (fitted by least squares, see Appendix C) to the filtered ranges. Clearly, it is important, whichever approach is employed, that no systematic trends are introduced, either from the range residuals or from the fitting of a polynomial, as these may corrupt the resulting normal point ranges. A further variation between the different approaches concerns the choice of epoch, within the interval of data, at which the normal point range should be determined.

One method of producing normal points is based on the averaging of range residuals over short periods of time. By using a computed orbit range residuals may be obtained as the difference between the observed range and the range computed from the predicted orbit (see § 2.4.1.2). Over a single pass any remaining systematic trends in the residuals may be removed, for example, by fitting a low order polynomial. After splitting the data into short bins, the residuals are averaged over these periods. The normal point range is evaluated at the observation epoch nearest the mean epoch of the observations within the bin, as follows

$$R_{Njt} = R_t - v_t + v_j \qquad (2.15)$$

where     $v_j$     :   mean range residual for the $j^{th}$ 'bin'

          $v_t$     :   range residual at normal point epoch t

$R_t$   :   observed range at normal point epoch t

$R_{Njt}$  :   normal point range at epoch t within

the $j^{th}$ bin.

This technique has been recommended as a standard procedure for the generation of normal points, and was adopted by the laser ranging community during the $5^{th}$ International Workshop on Laser Ranging Instrumentation (Gaignebet, 1985). However, this procedure does require a knowledge of the satellite's orbit, and consequently 'simpler' models have also been proposed.

The satellite's orbital motion over the short periods of the normal point bins (say 3 minutes for LAGEOS) may be accurately represented by low order time polynomials (or Chebyshev polynomials) fitted to the filtered ranges. The normal points may be subsequently generated by evaluating the polynomial at the required epoch within the particular bin. This epoch may be either the mid epoch, the mean epoch, or the epoch of an observed range nearest to the mean epoch of the bin. The latter is generally accepted as the most suitable epoch at which normal points should be generated.

### 2.4.1.4 Simple Polynomial Pre-Processing Strategy

The aim of this section is to describe a polynomial pre-processing technique developed, tested and employed during the initial analyses of LAGEOS data at Nottingham. Subsequently a different method, based

on range residuals from a computed orbit, was adopted and the formalisation of this approach are discussed in the following section (§ 2.4.1.5). A polynomial approach to filtering and the generation of normal points was used because of its ease of programming and the relatively fast rate at which raw observations could be pre-processed. The initial tests were conducted using LAGEOS data which was generally of '2$^{nd}$ generation' accuracy and nature, and with this data set the model performed well. However, later attempts to pre-process '3$^{rd}$ generation' LAGEOS observations indicated certain limitations of the simple approach. The first stage of the procedure involves the filtering of any spurious ranges from the data set.

(i)   A 10$^{th}$ order polynomial is fitted by least squares (see Appendix C) to each pass of data and the root-mean-square residual of the fit, $\sigma_r$, is calculated.

(ii)  All the observed ranges with residuals greater than 2$\sigma_r$ are rejected and steps (i) and (ii) repeated up to four times, or until no more ranges are rejected.

This method successfully filters all spurious ranges from most passes of LAGEOS data. However, when a pass of data consists principally of 'noise' and very little 'signal' the method fails and most of the 'bad' observations pass through the filter. Consequently, a second filter is included during the formation of

normal points in order to trap any remaining bad observations which have passed through the main filtering procedure. The method of formation of normal points is as follows

(i)   The observations are divided into short periods (bins) of data, spanning one to three minutes.

(ii)  A $7^{th}$ order polynomial is fitted through each bin, by least squares, and the root-mean-square residual calculated.

(iii) If this rms residual exceeds some preset value, indicating 'bad' observations may still be included in the data, the whole bin of data is rejected.

(iv)  The epoch of the observation closest to the mid epoch of each bin is identified.

(v)   The normal points are generated by evaluating the polynomial for each bin at the corresponding epoch.

By evaluating the polynomial at the epoch of the 'real' observation, closest to the mid interval epoch, the corrections and other data contained within the data record, for that epoch, may also be used for the normal point range.

Various orders of polynomial were tested for both the filtering and generation of normal points, and $10^{th}$ and $7^{th}$ orders (respectively) were found to be the

most efficient. This procedure was used throughout all the initial trials of the Satellite Laser Ranging analysis software (see Chapter 5) and solutions obtained using the normal points were shown to be practically identical to those obtained using the full set of filtered data. However, the benefit of using normal points was the considerable decrease in both the quantity of data to be processed and the time this processing took.

Although this procedure proved to be efficient, it was not 'fool proof' and occasionally 'bad' observations would pass through the filters undetected. This was because trends in the residuals introduced by the polynomial, which was not always able to adequately fit all passes of data, were greater than the residuals of the 'bad' observations. Similarly, any similar trends introduced at the normal point stage would lead to a 'bias' in the normal point range. Finally, any breaks (of a few minutes) in the data, during a pass, may cause problems when fitting a polynomial. This could subsequently result in either of the two previous problems. After considering modifying the model to improve it's overall efficiency, it was decided that a completely revised strategy may be more suitable.

## 2.4.1.5 Orbit Residual Pre-Processing Strategy

The principal difference between this approach to pre-processing of LAGEOS range data and the method

described in § 2.4.1.4, concerns the modelling of the orbital motion of the satellite. In preference to a simple polynomial model, a computed orbit of the satellite is determined based on a model of the forces acting on the satellite. This technique of orbit determination (see Chapter 3) forms the basis of the majority of analysis procedures for laser ranging observations (see § 2.4.2). However, for pre-processing purposes the orbital parameters do not need to be known as precisely. The residuals from this computed orbit (observed - predicted range) are used to filter the raw LAGEOS observations as follows:

(i) The data is sampled at 2 or 3 minute intervals to produce a reduced raw data set.

(ii) The orbital parameters are fitted to this data (see Chapter 3), using the best available tracking station coordinates.

(iii) Any observations with very large residuals (gross errors) are rejected from this sampled data set and stage (ii) repeated if necessary.

(iv) The residuals of all the observations are calculated and, for each pass, any systematic trends in the range residuals are removed by fitting a $1^{st}$ order (for up to 20 minutes data) or $2^{nd}$ order (for over

20 minutes of data) polynomial, by least squares. The rms residual, $\sigma_r$, is calculated.

(v)    If $\sigma_r$ is greater than 0.5m then all the observations with residuals greater than $2\sigma$ are rejected. If $\sigma_r$ is less than 0.5m then all observations with residuals greater than $3\sigma$ are rejected.

(vi)    Steps (iv) and (v) are repeated until no more ranges are rejected.

This procedure assumes no previous knowledge of the orbit (steps (i),(ii) and (iii)), however, if a previous orbit is known this may be extraploated to produce a predicted orbit, spanning the interval of raw data. Consequently, the first three steps of the procedure may not be required. Step (iv) ensures that no systematic trends remain and the residuals are distributed about a zero mean. This is efficiently achieved by using low order polynomials. The first of the rejection criterion (step (v)) ensures an initial fast removal of gross outliers, while the second avoids 'trimming' good observations from the set once any gross errors have beeen removed. The filtered residuals are subsequently split into short bins (1 to 3 minutes) and normal points are generated using the procedure outlined in § 2.4.1.3.

Although this procedure is more time consuming, and requires a sophisticated model of the satellite's motion, it has proven to be very efficient with no evident problems or limitations. However both the polynomial and orbital pre-processing procedures are currently included in the Nottingham software suite (see Chapter 5).

## 2.4.2 Analysis of Satellite Laser Range Data

The observational technique of laser ranging to satellites results in batches of range measurements from ground tracking stations to a particular satellite. These observations are of very little use without some form of post-observational analysis. The aim of such analyses is to use these precise measurements to obtain estimates of many geodetic and geophysical parameters, and consequently a better understanding of the phenomena. The wide range of the applications to which processed laser ranging observations have contributed, or may contribute in the near future, has already been discussed in § 2.2.4.

For many years the analysis of Satellite Laser Ranging, and other geodetic satellite, observations has been dominated by two distinct approaches, namely dynamical methods and geometrical methods. Between these two extremes several techniques have evolved which bridge the gap, resulting in short-arc semi dynamic techniques. Many of the early experiments in

satellite geodesy used geometric analysis to determine inter-station baselines. However, over the years models of the orbital motion of satellites have improved and as a result dynamical methods of analysis have become the dominant techniques for the analysis of laser ranging data.

The fundamental component of a dynamical approach is a precise model of the orbital dynamics of the satellite, which is used to determine the satellite's orbit. This model consists of many components representing all the forces acting on the satellite. Clearly, imperfections in these models impose a limitation on the accuracy attainable from the analysis of laser ranging data. Indeed with the current trend towards tracking systems operating at the 2-5cm (single shot precision) level, certain force model components are becoming the dominant error sources, particularly for low satellites such as STARLETTE. Despite these apparent limitations, long arc dynamical solutions using observations spanning several years (Smith et al, 1985 and Tapley et al, 1985) have provided very stable geodetic reference systems, which define not only the coordinates of the globally distributed tracking stations but also the motion of the pole and fundamental constants (such the geocentric constant of gravitation, GM). These reference systems form a framework within which the analysis for other geophysical parameters may be based.

In contrast to the dynamical approach, geometric solutions do not rely on a precise knowledge of the dynamics of the satellite's orbit and consequently are not affected by imperfections in the force models. However, such solutions do require near simultaneous observations (usually co-observed passes, the observations of which are interpolated to produce quasi-simultaneous ranges) from a number of tracking station. In addition, the spatial geometry of the tracking stations and the distribution of the data is critical. The approach was severely restricted in the early years because of the poor geometry obtainable using low satellites (such as Beacon Explorer C), however, the launch of LAGEOS improved the situation considerably. Nevertheless, the dependence on accurate syncronisation of the clocks, at the tracking stations, and the dependence on the weather conditions make the use of a purely geometrical mode of analysis unlikely.

The use of semi-dynamic approaches has been studied by various groups over recent years. A method of using simultaneous range differences between two co-observing sites to determine the inter-station baseline has been proposed (Pavlis, 1982 and 1985). Studies concerning the use of short and medium arcs of STARLETTE data (Moore, 1985) have shown that, over short arcs (say up to 10 minutes) the dependence on the dynamical orbital model is greatly reduced and the precision of the fit of the orbit to the observations

is determined by the precision of the data and not by that of the models. However, the distribution of data and the geometry of the tracking stations become much more important.

In summary, despite the dependence on the models representing the orbital motion of the satellite, dynamical methods dominate the analysis of Satellite Laser Ranging data. This is a result of the ability of dynamical techniques to process laser ranging data with no requirement of co-observation and very little dependence on the geometry of the tracking stations, and in addition, to determine a wide variety of unknown parameters. Consequently, nearly all the software packages developed for the analysis of laser ranging data are based on dynamical approaches.

The principle of the dynamical analysis of laser range observations are presented in Chapter 3 and details of the software package, SODAPOP, developed at Nottingham, based on these principles, are given in Chapter 5.

CHAPTER   THREE

PRINCIPLES OF THE DYNAMICAL ANALYSIS

OF SATELLITE LASER RANGING DATA

3.1   BASIC CONCEPTS

The determination of a satellite's orbit is an important component of the dynamical analysis of Satellite Laser Ranging observations. Furthermore, by processing laser ranging data to altimetry satellites the determination of the satellite's orbit is the principal aim of the analysis. However, generally the orbit of the satellite provides a stable framework against which other parameters are derived. Orbit determination is basically the computation of the ephemeris of the satellite from a set of tacking data, usually from a global network of tracking stations. The principles are not, however, dedicated to laser ranging and other navigation and positioning systems have used the technique for many years. Both the Navy Navigation Satellite System (TRANSIT Doppler), which has been used for navigation and positioning since 1967, and the more recent NAVSTAR Global Positioning System, use the CELEST (O'Toole, 1976) orbit determination program to compute the satellite ephemerides which are subsequently broadcast to the satellites (Ashkenazi and Moore, 1986).

The process of orbit determination involves the use of an accurate model which describes the various forces acting on the satellite. This force model may include components due to gravitational, surface and other forces (see § 3.3). The vector sum of all the

components gives the resultant force acting on the satellite, and consequently the resultant acceleration of the satellite. This acceleration (which is a function of the position or, in the case of drag components, the velocity of the satellite) is numerically integrated, once to obtain the velocity and twice ot obtain the position of the satellite as a function of time.

For this 'orbit integration' to commence the satellite's state vector (consisting of the position and velocity vectors of the satellite) must be known at some initial epoch $t_0$. However, to begin with these starting elements need not be known accurately because observations, in this case laser range measurements, from a network of tracking stations may be used in a least squares solution to obtain better a estimate of the initial state vector. Depending on the particular objective of the processing, various other parameters may also be determined as unknowns in the least square solution. If the aim of the analysis is simply the determination of the orbit of a satellite then the coordinates of the tracking stations would be fixed and the starting elements (and possibly polar motion values) would be the principal unknowns. In contrast, for geophysical research the objective may be the determination of the tracking station coordinates (for crustal dynamics), the tidal Love numbers or geopotential coefficients.

In addition to the satellite coordinates, the orbit integration process also generates a series of partial differential terms of position and velocity with respect to the components of the initial state vector and other model unknowns. These are required so as to enable the coefficients of the observation equations (see § 3.4.4) to be computed during the least squares analysis. A general outline of the principles of orbit determination is illustrated in fig 3.I.

Although the coordinates of the tracking stations and various other force model components (particularly the geopotential model) are given in an 'earth fixed' reference frame, the numerical orbit integration must be carried out in an inertial (i.e. non-rotating) coordinate reference system. The various coordinate reference frames and the transformations between them are described in the following section (§ 3.2), and the components of the force model and the integration and adjustment procedures are discussed in § 3.3 and § 3.4 respectively.

Starting Elements

$\underset{\sim}{r}_0$, $\underset{\sim}{\dot{r}}_0$ at t = t$_0$

FORCE MODEL

$\underset{\sim}{\ddot{r}}$ = $f(\underset{\sim}{\dot{r}},\underset{\sim}{r})$

$\underset{\sim}{\ddot{r}}$ = $\dfrac{(\underset{\sim}{G} + \underset{\sim}{S} + \underset{\sim}{O})}{m}$

m : satellite mass
G : gravitational forces
S : surface forces
O : other forces

Numerical
Integrator

Improved
Starting
Elements

Expanded Ephemeris
and Partials

Least Squares
Solution

Laser Ranging
Observations

Final Solution
Inertial/Terrestrial
Frame

Corrected Starting Elements
Satellite Ephemeris
Tracking Station Coordinates
Force Model Components
Earth Rotation Parameters

Fig 3.I Principles of Orbit Determination

3.2     COORDINATE REFERENCE SYSTEMS

## 3.2.1   Earth Fixed Coordinate Systems

### 3.2.1.1 Geocentric Cartesian Coordinate System

In order to describe a three dimensional coordinate system it is necessary to define a number of properties. Firstly the location of the origin and the orientation of the axes must be specified (in addition, for a cartesian representation this would also include a definition of whether the axes form a 'right handed' or a 'left handed' system). The parameters, i.e. cartesian, polar or spheroidal, which define the position of a point relative to the coordinate system must also be specified. Finally, the scale of the system must be defined. Consequently, in order to adequately define a three dimensional reference frame a minimum of seven parameters must be specified. For a cartesian representation these are the position of the origin (3 parameters), the direction of the three axes (3 parameters) and the scale of the system (1 parameter).

The geocentric earth fixed coordinate reference frame is a right handed cartesian system with its origin at the geocentre (the earth's centre of mass) The Z-axis is directed towards the CIO pole as currently maintained by the Bureau International de l'Heure (BIH) and the X-axis towards the BIH zero meridian (see § 4.2) The Y-axis is mutually

perpendicular to the other two so as to form a right handed system. The scale is defined by the adopted standard. The position of a point, P, as shown in fig 3.II, is defined by three displacements, $X_p$, $Y_p$ and $Z_p$, along the three axes X, Y and Z from the geocentric origin. The resulting position vector is given by

$$\underline{P} = (X_p, Y_p, Z_p). \qquad (3.1)$$

Clearly, this definition of the position vector is also true for other geocentric cartesian coordinate systems, such as the inertial reference frame defined in § 3.2.2. The coordinates of laser ranging stations are generally given in the geocentric earth fixed system with either cartesian or spheroidal (see § 3.2.1.3) components. Similarly, the geopotential field is also given in terms of the earth fixed system but in this case a spherical polar representation is used.

### 3.2.1.2 Spherical Polar Representation

The position of a point, P, in a cartesian reference frame is usually expressed in terms of the three perpendicular components. However, a polar representation may also be used in which the position is expressed in terms of a distance and two angles, as illustrated in fig 3.II. The position vector of the point P is then given by

$$\underline{P} = (R_p, \lambda_p, \phi_p) \qquad (3.2)$$
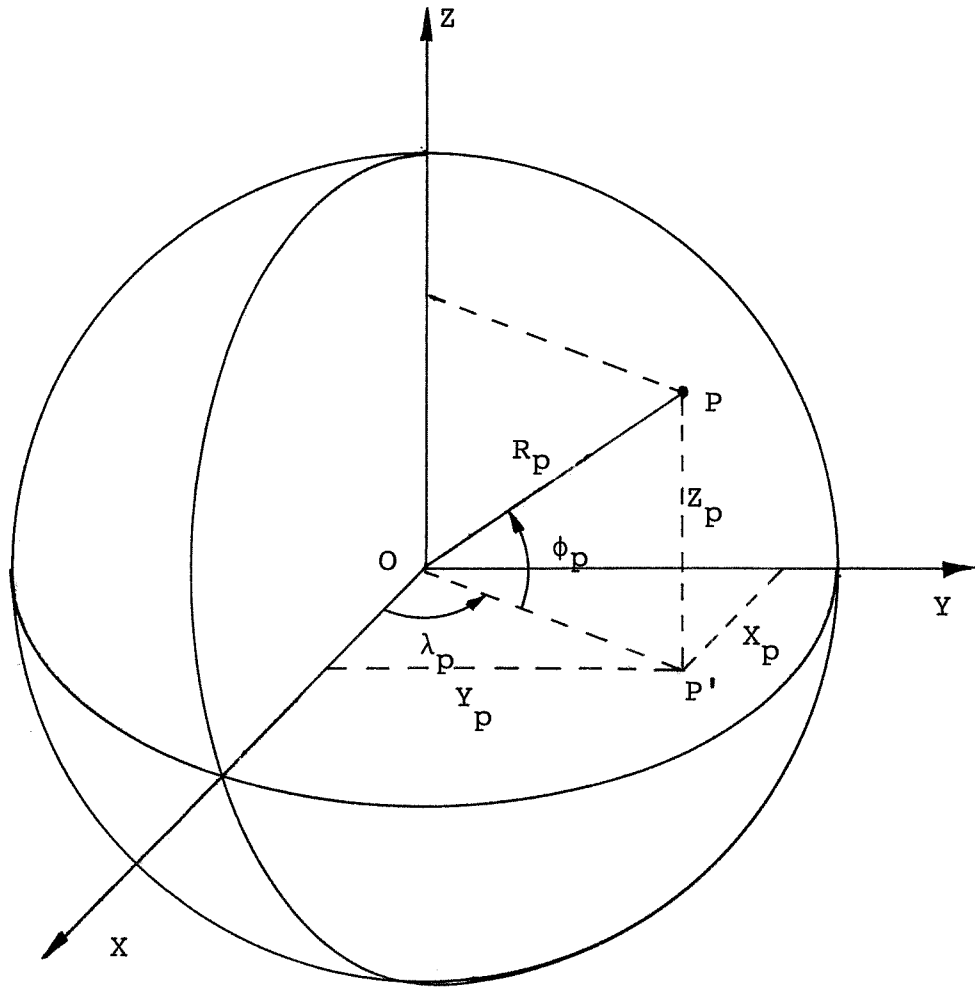
Fig 3.II <u>Geocentric Coordinate System</u>

where $R_p$ : distance of point P from origin O

$\lambda_p$ : spherical longitude, the anti-clockwise angle from the X-axis to OP' (the projection of OP in the X-Y plane)

$\phi_p$ : spherical latitude, the anti-clockwise angle from OP' (i.e. the X-Y plane) to OP.

The spherical and cartesian coordinates are related by

$$X_p = R_p \cos \phi_p \cos \lambda_p \qquad (3.3)$$

$$Y_p = R_p \cos \phi_p \sin \lambda_p \qquad (3.4)$$

$$Z_p = R_p \sin \phi_p \qquad (3.5)$$

and conversely

$$R_p = (X_p^2 + Y_p^2 + Z_p^2)^{\frac{1}{2}} \qquad (3.6)$$

$$\lambda_p = \tan^{-1}\left(\frac{Y_p}{X_p}\right) \qquad (3.7)$$

$$\phi_p = \sin^{-1}\left(\frac{Z_p}{R_p}\right) \qquad (3.8)$$

$$\phi_p = \tan^{-1}\left(\frac{Z_p}{\sqrt{(X_p^2 + Y_p^2)}}\right) \qquad (3.9)$$

### 3.2.1.3 Spheroidal Coordinate Representation

Traditionally, geodetic computations have separated the three dimensional coordinates of a point into horizontal and vertical components. This is usually achieved by adopting a reference surface closely resembling the figure of the earth and

expressing a points position by its height above this
surface and the position of the projection of the point
onto the surface. A convenient surface on which to
carry out such computations is an oblate spheroid (the
surface described by rotating an ellipse about its
minor axis). Clearly, to define a ellipsoidal
coordinate system it is necessary to specify two
parameters of the ellipsoid in addition to the usual
seven parameters. Typically, a spheroid is adopted
which closely fits the specific area of a local survey.
However, for global studies, such as the analysis of
laser ranging data, a geocentric mean ellipsoid is
defined, such that its minor axis is coincident with
the Z-axis of the geocentric cartesian system.

In order to specify the parameters which
describe the position of a point, it is first necessary
to define various properties of the ellipsoid. Firstly,
the equatorial plane is defined as the plane containing
the major axis of the ellipsoid, the X-Y plane shown in
fig 3.III. Secondly, the meridional plane through point
P is defined as the plane containing both the minor
axis (the Z-axis) and the point, and is illustrated in
the lower half of fig 3.III. The 'normal' at point P is
defined as the line ($P_1 P_2$ in fig 3.III) through point P
which is perpendicular to the ellipsoid at point $P_1$
(the projection of point P onto the spheroid). The
equation of any point on the surface of the spheroid,
in terms of the geocentric cartesian coordinates is
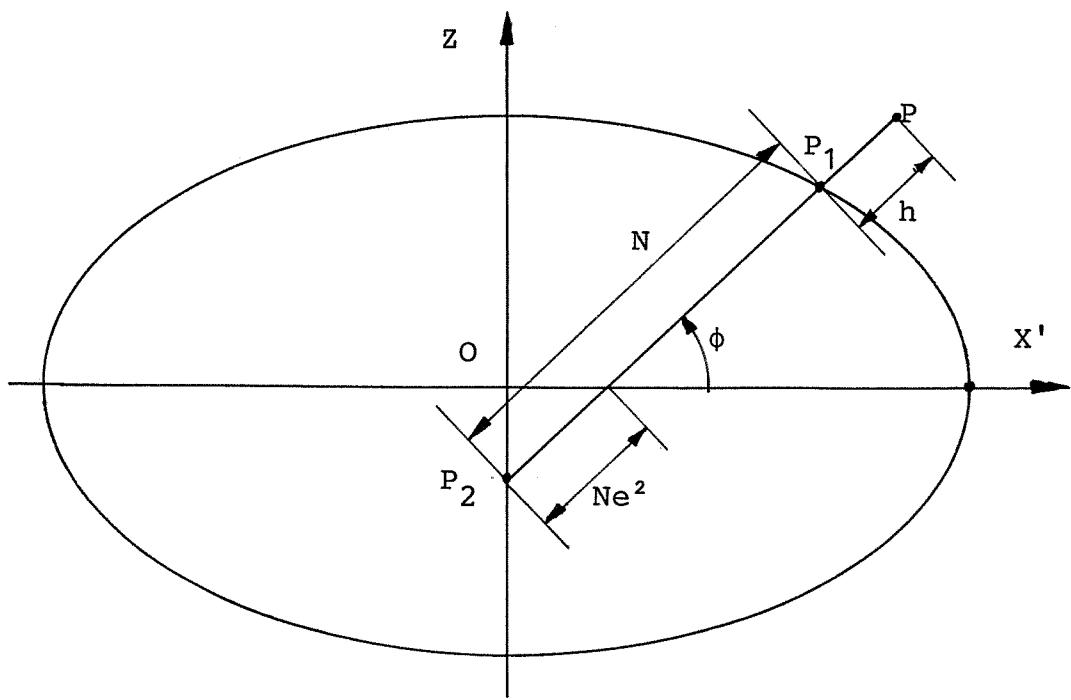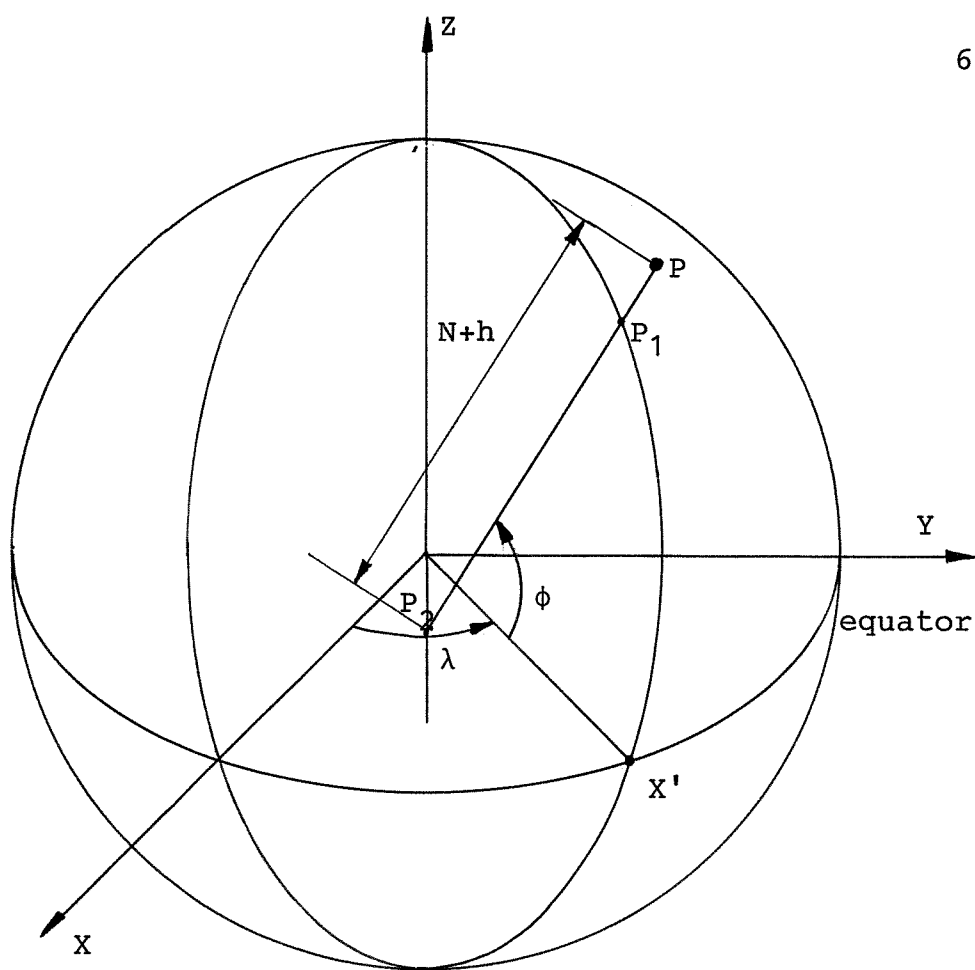
Meridional Section

Fig 3.III Spheroidal Coordinates

given by,

$$\frac{X^2}{a^2} + \frac{Y^2}{a^2} + \frac{Z^2}{b^2} = 1 \qquad (3.10)$$

where   a  :  semi-major axis

        b  :  semi-minor axis

The spheroidal representation of the position vector
of a point, P, is given by,

$$\underline{P} = (\phi, \lambda, h) \qquad (3.11)$$

where  $\phi$  :  geodetic latitude, the anti-clockwise

           angle between the normal at P (line $P_1P_2$)

           and the equatorial plane,

     $\lambda$  :  geodetic longitude, the anti-clockwise

           angle from the meridional plane which

           includes the X-axis (ie the Greenwich

           Meridian) to the meridional plane through

           the point P,

     h  :  height of the point P above the reference

           ellipsoid, along the normal at P (distance

           $PP_1$ in fig 3.III).

The transformation from geodetic (i.e. spheroidal) to
cartesian coordinates is given by,

$$X = (N + h) \cos \phi \cos \lambda \qquad (3.12)$$

$$Y = (N + h) \cos \phi \sin \lambda \qquad (3.13)$$

$$Z = ((N + h) - Ne^2) \sin \phi$$

$$= ((1 - e^2)N + h) \sin \phi \qquad (3.14)$$

where  e  :  eccentricity of the ellipsoid, given by,

$$e^2 = \frac{a^2 - b^2}{a^2} \qquad (3.15)$$

or $\qquad e^2 = 2f - f^2 \qquad (3.16)$

f  :  flattening of the ellipsoid, as given by

$$f = \frac{a - b}{a} \qquad (3.17)$$

N  :  radius of curvature in the plane

perpendicular to the meridional plane,

the prime vertical, which is given by

(Bomford, 1980),

$$N = \frac{a}{\sqrt{(1 - e^2 \sin^2\phi)}}. \qquad (3.18)$$

The reverse transformation, from cartesian to geodetic spheroidal coordinates is given by,

$$\lambda = \tan^{-1}\left(\frac{Y}{X}\right) \qquad (3.19)$$

$$\phi = \frac{\tan^{-1}(Z + Ne^2 \sin \phi)}{\sqrt{(X^2 + Y^2)}} \qquad (3.20)$$

$$h = \frac{X}{\cos \phi \cos \lambda} - N \qquad (3.21)$$

Equation (3.20) must be evaluated iteratively, starting with an initial assumption of the value of $\phi$. The geocentric latitude, as given by equation (3.8) may be used as a first approximation for the geodetic latitude, $\phi$. An alternative to this iterative procedure is given by Vincenty (1979). This approach allows the direct conversion from cartesian to geodetic

coordinates, without the need for any iteration, as follows,

$$P = \sqrt{(X^2 + Y^2)} \qquad (3.22)$$

$$\theta = \tan^{-1} \left( \frac{Z}{P} \cdot \frac{a}{b} \right) \qquad (3.23)$$

$$\phi = \tan^{-1} \left( \frac{Z + \varepsilon \, b \, \sin^3 \theta}{P - e^2 \, a \, \cos^3 \theta} \right) \qquad (3.24)$$

$$\lambda = \tan^{-1} \left( \frac{Y}{X} \right) \qquad (3.25)$$

$$u = \tan^{-1} \left( \frac{b}{a} \cdot \tan \phi \right) \qquad (3.26)$$

$$h = \sqrt{(P - a \cos u)^2 + (Z - b \sin u)^2} \qquad (3.27)$$

$$\varepsilon = \frac{a^2 - b^2}{b^2} \qquad (3.28)$$

and $\theta$, P and u are intermediate parameters. The sign of h is the same as the sign of (p - a cos u).

### 3.2.1.4 Topocentric Coordinate Systems

The topocentric coordinate system is a cartesian coordinate system with its origin at some point on the earth's surface. The Z-axis is in the direction of the perpendicular to the plane which is tangential to the surface of the earth, at the origin. The X-axis, which lies in the tangential plane, is directed towards the CIO pole. The Y-axis is perpendicular to both these axes, so as to form a left-handed system, as illustrated in fig 3.IV. Clearly, this system is of little use for expressing the positions of the tracking
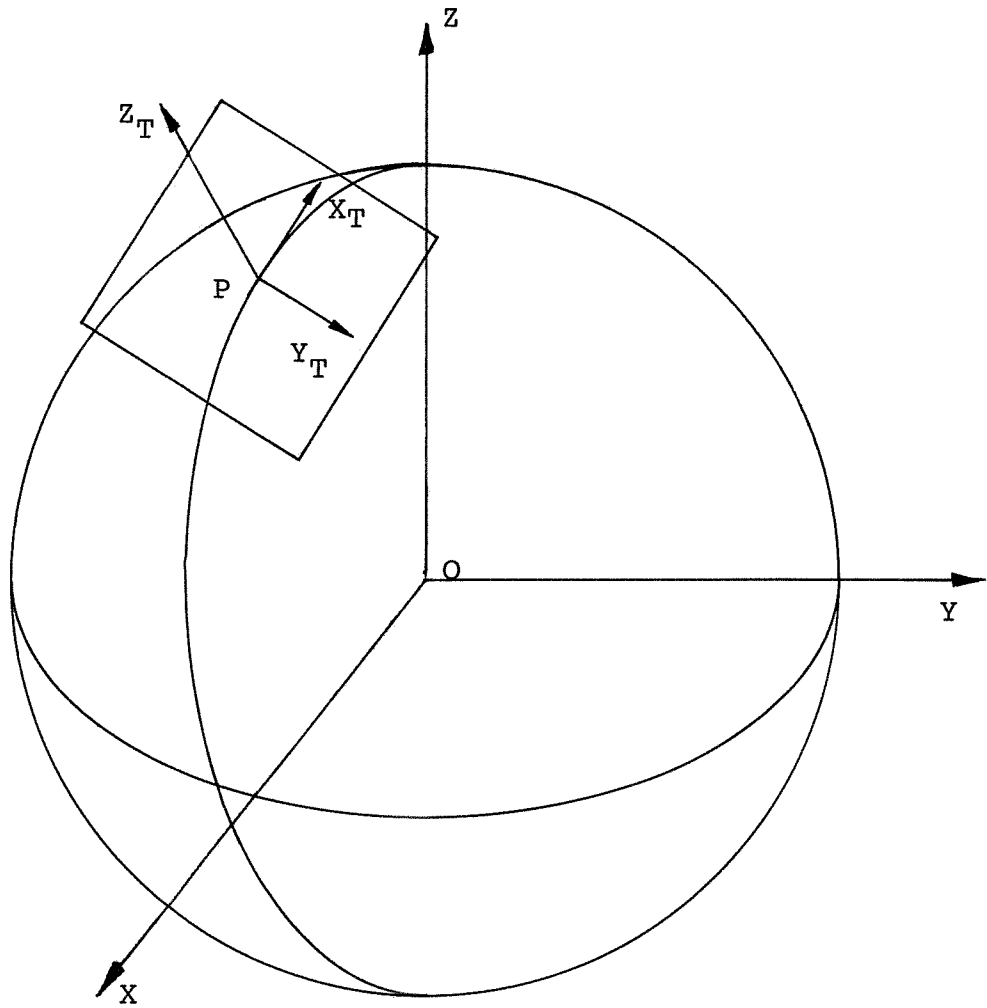
Fig 3.IV Topocentric Coordinates

stations of a global network. However, it is used in
the analysis of laser ranging observations as a
convenient system in which to determine the elevation
angle from the tracking station to the satellite. The
elevation angle of the satellite (see Appendix B) is
required in order to compute the correction for the
effects of atmospheric refraction (see § 2.3.3.1). In
this particular case all that is required is the
coordinate difference between the tracking station and
the satellite. The transformation between coordinate
differences in the geocentric cartesian frame and the
corresponding coordinate differences in the topocentric
system are given by (Vincenty, 1979),

$$
\begin{bmatrix} \Delta X_T \\ \Delta Y_T \\ \Delta Z_T \end{bmatrix} = R \begin{bmatrix} \Delta X \\ \Delta Y \\ \Delta Z \end{bmatrix}
\qquad (3.29)
$$

and the inverse transformation is given by,

$$
\begin{bmatrix} \Delta X \\ \Delta Y \\ \Delta Z \end{bmatrix} = R^\tau \begin{bmatrix} \Delta X_T \\ \Delta Y_T \\ \Delta Z_T \end{bmatrix}
\qquad (3.30)
$$

where

$$
R = \begin{bmatrix} -\sin \phi \cos \lambda & -\sin \phi \sin \lambda & \cos \phi \\ -\sin \lambda & \cos \lambda & 0 \\ \cos \phi \cos \lambda & \cos \phi \sin \lambda & \sin \phi \end{bmatrix}
\qquad (3.31)
$$

and

$\Delta X_T$, $\Delta Y_T$, $\Delta Z_T$ : coordinate differences in the
topocentric system,

$\Delta X, \Delta Y, \Delta Z$ : coordinate differences in the geocentric cartesian system,

$\phi, \lambda$ : geodetic latitude and longitude of the origin of the topocentric system.

### 3.2.1.5 Coordinate Transformations

The relationships between the geocentric cartesian coordinate system and the spherical and spheroidal representations have been given in § 3.2.1.3 and § 3.2.1.4, respectively. However, when comparing coordinates derived by different observational techniques, such as TRANSIT Doppler or VLBI, with those derived from the analysis of laser ranging data, it is necessary to account for any systematic differences resulting from the particular definition of the 'geocentric' reference frame (Mueller et al, 1982). This situation may also arise when comparing two sets of coordinates derived from laser ranging observations, as a result of different analytical procedures or models. The transformation from one earth fixed reference frame to another may be expressed by specifying three translations of the origin, three rotation angles and a scale correction (Vincenty, 1979). The resulting transformation is given by,

$$\begin{bmatrix} X_2 \\ Y_2 \\ Z_2 \end{bmatrix} = \begin{bmatrix} X_1 \\ Y_1 \\ Z_1 \end{bmatrix} + \begin{bmatrix} \delta x \\ \delta y \\ \delta z \end{bmatrix} + \begin{bmatrix} 0 & \theta_z & -\theta_y \\ -\theta_z & 0 & \theta_x \\ \theta_y & -\theta_x & 0 \end{bmatrix} \begin{bmatrix} X_1 \\ Y_1 \\ Z_1 \end{bmatrix} + c \begin{bmatrix} X_1 \\ Y_1 \\ Z_1 \end{bmatrix} \quad (3.32)$$

where

$X_1$, $Y_1$, $Z_1$ : coordinates in reference frame 1, $\underset{\sim}{x}_1$

$X_2$, $Y_2$, $Z_2$ : coordinates in reference frame 2, $\underset{\sim}{x}_2$

$\delta x$, $\delta y$, $\delta x$ : translations of the origin, $\underset{\sim}{\delta}x$

c : scale difference between the two systems

$\theta_x$, $\theta_y$, $\theta_z$ : small rotation angles about the X, Y and Z axes, respectively, elements of rotation matrix R.

Clearly, if these seven parameters are known it is possible to transform coordinates from one reference system to another. However, in the first instance this is generally not the case. Given two sets of coordinates, of corresponding points, in two different earth fixed reference frames, the initial task is to determine the seven parameters relating the two reference frames. This is achieved by setting up an 'observation equation' for each pair of matching coordinates, as follows,

$$\underset{\sim}{X}_2 - \underset{\sim}{X}_1 = \underset{\sim}{\delta}x + R \underset{\sim}{X}_1 + c \underset{\sim}{X}_1. \qquad (3.33)$$

With a minimum of three pairs of coordinates it is possible to solve, by least squares, for the seven unknown parameters. In order to compare the reference frames defined by two different observation techniques, such as laser ranging and VLBI, the coordinates of a number of 'colocated' points must be determined by both techniques (Mueller et al, 1982).

3.2.2 <u>Inertial</u> <u>Reference</u> <u>Frame</u>

A new fundamental astronomical reference system, FK5, was introduced on the 1$^{st}$ of January 1984, in accordance with the resolutions of the International Astronomical Union (IAU) in 1976 and 1979 (Kaplan, 1981). A series of constants and time scales were also introduced, including a new relationship between Greenwich Mean Sidereal Time (GMST) and Universal Time (see § 3.2.3), and new precession and nutation models (§ 3.2.4). The reference system also adopted the new standard epoch of J2000.0 (or January 1.5 of the year 2000) to replace the standard epoch 1950.0 of the previous FK4 system.

As mentioned previously, in § 3.1, the numerical integration to determine the orbit of a satelite must be carried out in an inertial reference frame. The generally adopted (and recommended by the MERIT Standards) inertial reference frame is a geocentric cartesian system defined by the mean equator and equinox of J2000.0. The X-axis of this system is directed towards the mean equinox of J2000.0 and the Z-axis is normal to the mean equatorial plane (of J2000.0). The Y axis is perpendicular to both the X and Z axes so as to form a right handed system. This inertial reference system is also used for a new lunar and planetary ephemeris, known as the Development Ephemeris Number DE200/LE200, computed in accordance with the resolutions of the IAU. However, the reference

frame of this ephemeris is heliocentric, as opposed to geocentric.

As outlined in § 3.1, the satellite's ephemeris is computed in the inertial J2000.0 reference frame and the tracking station coordinates and geopotential models are given in an earth fixed reference system. In order to transform the coordinates of a point from one of these geocentric reference frames to the other the position vector of a point must be subjected to a number of rotations, as given by,

$$\underset{\sim}{R} = P \; E \; N \; Q \; \underset{\sim}{r} \qquad (3.34)$$

where   $\underset{\sim}{r}$   :   inertial frame coordinates $(x, y, z)$,

       $\underset{\sim}{R}$   :   earth fixed coordinates, at UTC time $t_{UTC}$ $(X, Y, Z)$,

       $P$   :   polar motion matrix (see § 3.2.5),

       $E$   :   earth rotation matrix (see § 3.2.5),

       $N$   :   nutation matrix (see § 3.2.4),

       $Q$   :   precession matrix (see § 3.2.4).

and the inverse transformation is given by,

$$\underset{\sim}{r} = Q^{T} \; N^{T} \; E^{T} \; P^{T} \; \underset{\sim}{R} \qquad (3.35)$$

Details of the procedure and the particular expressions required to transform coordinates from one reference frame to another are given in the following sections.

3.2.3 <u>Time</u> <u>Scales</u>

This section aims to define the various time scales used during the dynamical analysis of laser ranging observations, and the relationships between these time scales. The reasons for using a particular time scale are also discussed.

Greenwich Apparent Sidereal Time (GAST) is defined as the hour angle (measured in units of time) between the Greenwich Meridian and the true equinox of date. Similarly, Local Apparent Sidereal Time (LAST) is defined as the hour angle between the meridian which includes the point of observation (the local meridian) and the true equinox of date. These two time scales are related by,

$$LAST = GAST + \lambda \qquad (3.36)$$

where $\lambda$ :  astronomical longitude (in units of time) of the local meridian from the Greenwich meridian (measured positive eastwards).

Greenwich Mean Sidereal Time (GMST) is the hour angle between the Greenwich meridian and the mean equinox of date. The true equinox of date differs from the mean equinox of date because of the effects of nutation (see § 3.2.4). Similary, the mean equinox of date is obtained from the mean equinox at the reference epoch (i.e. J2000.0) by correcting for the effects of precession.

From observations of the transits of stars, a number of observatories around the world (see § 4.2) determine their own LAST. These are combined by the Bureau International de l'Heure (in Paris) and result in a number of time scales which are known collectively as Universal Time (UT) and are closely related to the diurnal rotation of the earth. There are four Universal Time scales referred to as, UT0, UT1, UT2 and UTC, the first of which, UT0, is derived directly from the determinations of LAST. However, this time scale has periodic and irregular variations due to the polar motion and variations in the rate of rotation of the earth (see § 3.2.5). Subsequently, each determination of UT0 is corrected for the effects of polar motion and a weighted mean of these values (from all the participating observatories) leads to the time scale known as UT1. Both UT1 and GMST represent a determination of the rotation of the earth either with respect to a mean sun (in the case of UT1) or the fixed stars (for GMST). The two time scales are related by the following expressions (Kaplan, 1981),

$$t_{GMST} = t_{GMST(0)} + \Delta t_{GMST} \qquad (3.37)$$

where

$$t_{GMST(0)} = 24110^S.54841 + 8640184^S.812866 \; T_U \qquad (3.38)$$
$$+ \; 0^S.093104 \; T_U{}^2 - 6^S.2 \times 10^{-6} \; T_U{}^3$$

$$\Delta t_{GMST} = (1.002737909350795 + 5.9006 \times 10^{-11} \; T_U \qquad (3.39)$$
$$- \; 5.9 \times 10^{-15} \; T_U{}^2) \; t_{UT1}$$

and $t_{UT1}$ : UT1 time elapsed since 0.0hrs UT1 of the particular day,

$t_{GMST(0)}$ : GMST at 0.0hrs UT1 of the particular day,

$T_U$ : number of Julian centuries of 36525 days of UT elapsed since 2000 January 1.5 $12^h$ UT1 (Julian day No. 2451545.0).

The Greemwich hour angle of the true equinox of date (GAST) may be computed from GMST using the expression,

$$t_{GAST} = t_{GMSt} + \Delta\psi \cos \varepsilon \qquad (3.40)$$

where $\Delta\psi$ : nutation in longitude,

$\varepsilon$ : obliquity of the eclpitic (see § 3.2.4).

The Universal time scale, UT2, which is also maintained by the BIH, is determined by correcting the UT1 time scale for predicted values of the seasonal variations in the earth's rotation rate.

Traditionally the unit of time, the second, was defined initially by the mean solar day and later by the orbit of the earth. However, with the development of precise atomic clocks the second was redefined as the fundamental unit of time, by the International System (SI) of units. This definition is based on the resonance of the ceasium atom, which is monitored by many different atomic clocks around the world. The weighted mean of the readings of these atomic clocks

leads to a time scale based exclusively on the
SI second, International Atomic Time (TAI). Clearly,
this time scale bears no relation to Universal Time
(UT1 or UT2) and changes in the rate of rotation of the
earth. The requirement for a time scale which although
based on the SI second would keep pace with any changes
in the rate of rotation was recognised and led to the
establishment of Coordinated Universal Time, UTC. This
time scale differs from TAI by an integer number of
seconds. This difference is changed occasionally, by
the introduction of leap seconds, to keep UTC within
0.9s of UT1. The last adjustment was made on the $30^{th}$
June 1985, resulting in the current difference,
TAI-UTC, of 23.0 seconds. Both TAI and UTC are
maintained by the BIH and the differences from UTC,
i.e. UT1-UTC and UT1-TAI, are published monthly in the
BIH Circular D and yearly in the BIH Annual Report
(BIH, 1984).

Most of the standard time signals broadcast by
radio, television and satellites are based on UTC, and
consequently Coordinated Universal Time (UTC) is the
most readily available time scale around the world. As
a result, the epoch of satellite laser range
observations from the global network of tracking
stations are refered (directly or indirectly) to BIH
UTC. Consequently, UTC is very well suited for use as
the reference time scale for the analysis of laser
ranging data, provided the occasional leap seconds are

accounted for. Because of the constant time intervals
of UTC (except for the leap seconds) it is also used
for the numerical integration procedure to generate the
satellite orbit.

The IAU resolutions (Kaplan, 1981) recommended
the use of new models for both precession and nutation
(see § 3.2.4). Both of these models are given in terms
of a new time scale Barycentric Dynamical Time (TDB),
which together with the Terrestrial Dynamical Time
(TDT) scale is also defined in the resolutions.
Terrestrial Dynamical Time is the time scale for an
apparent geocentric ephemeris and replaces Ephemeris
Time. Continuity was maintained between TDT and
Ephemeris Time by adopting a suitable relationship
(i.e. offset) between TDT and TAI,

$$t_{TDT} = t_{TAI} + 32^S.184 \tag{3.41}$$

Barycentric Dynamical Time (TDB) is the time scale for
the equations of motion relative to the solar system's
barycentre, and differs from TDT by periodic
relativistic terms, as given by,

$$t_{TDB} = t_{TDT} + 0^S.001658 \sin (g + 0.0167\sin g) \tag{3.42}$$

where g : mean anomaly of the earth in its orbit,

$$g = (357^0.528 + 35999^0.05 \ T) . \frac{2 \pi}{360} \tag{3.43}$$

T : the interval, in Julian centuries of
  TDB, between J2000.0 and the epoch,

$$T = \frac{(J - 2451545.0)}{36525} \qquad (3.44)$$

J : the TDB Julian date of the epoch.

The applications of the various time scales during the process of orbit determination and the analysis of laser ranging observations are discussed, where applicable, in the following sections.

### 3.2.4 Precession and Nutation

The earth is not perfectly spherical but has an equatorial bulge. The attraction of the sun and planets on the earth causes the equator and the ecliptic (the plane of the earth's orbit) to be in a state of constant motion, with respect to an inertial reference frame. As a result of the motion of the equator and the ecliptic, the equinox (the point at which the ecliptic and equatorial planes intersect) also moves. The geocentric celestial sphere is illustrated in fig 3.V, together with the traces on the sphere of the mean equator (EQ) and the ecliptic (ec) at the J2000.0 reference epoch. The axes of the J2000.0 inertial reference frame (as described in § 2.2.2) are also shown. The angle $\varepsilon$ between the ecliptic and the equatorial planes is the obliquity of the ecliptic (an angle of about $23.5^{\circ}$).

The attraction of the moon and sun on the earth's equatorial bulge causes the celestial pole (normal to the earth's equator) to rotate in a westerly
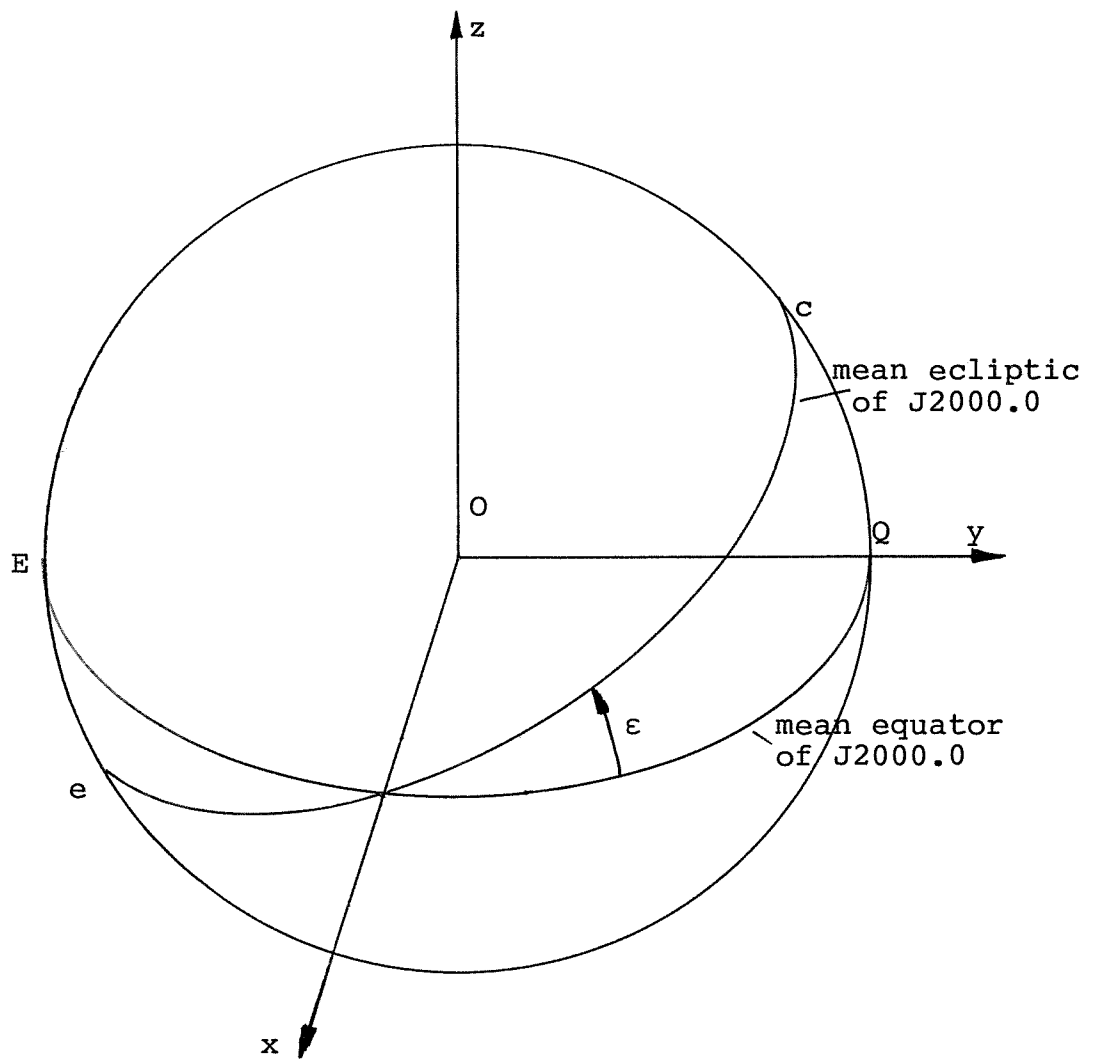
Fig 3.V Celestial Sphere

motion around the pole of the ecliptic, with a period of about 25800 years and an amplitude of about $23.5^0$ (the obliquity of the ecliptic). This effect is known as 'luni-solar precession'. Due to the changing configuarations of the planets, their action on the earth, as a whole, results in a motion of the ecliptic plane, known as 'planetary precession'. This has the effect of an eastward motion of the equinox of about 12" per century and a decrease in the obliquity of about 47" per century. The combined effect of luni-solar and planetary precession is known as 'general precession' and is described by three angles, the equatorial precession parameters, $\zeta_A$, $z_A$ and $\theta_A$ (Kaplan, 1981). These parameters relate the inertial frame (i.e. mean of J2000.0) to the 'mean-of-date' frame, as illustrated in fig 3.VI. The transformation from cordinates referred to J2000.0 to the mean-of-date coordinates, at an epoch of TDB, is given by,

$$\underline{r}_M = Q \underline{r} \qquad (3.45)$$

where $\underline{r}$ : $(x, y, z)^T$, inertial frame coordinates,

$\underline{r}_M$ : $(x_M, y_M, z_M)^T$, mean-of-date (at $t_{TDB}$) coordinates,

Q : precession matrix, as given by,

$$Q = R_3(-z_A) \ R_2(\theta_A) \ R_3(-\zeta_A) \qquad (3.46)$$

$R_3$, $R_2$ : rotation matrices about the z and y axes respectively (see Appendix A).
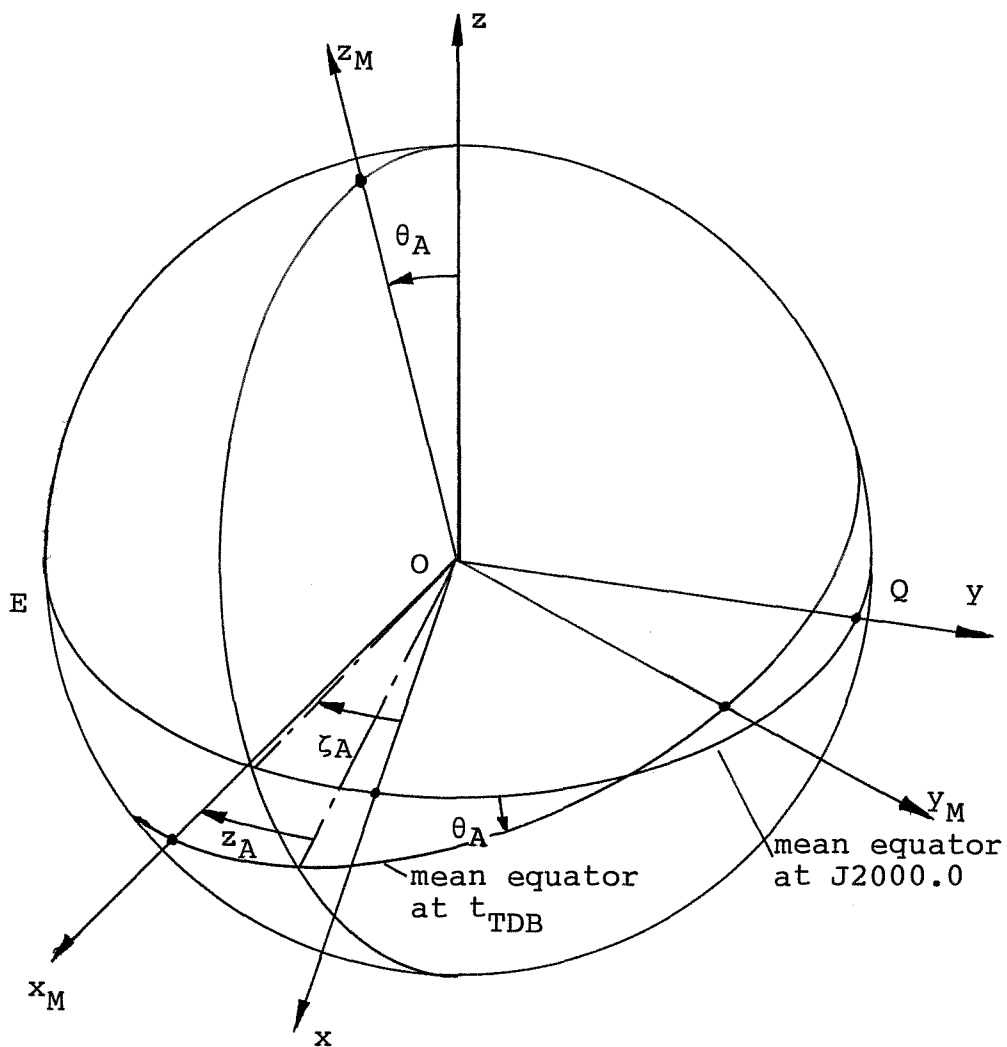
Fig 3.VI Precession Parameters

New expressions for the equatorial precession parameters were adopted by the IAU in 1976 and are given by (Kaplan, 1981),

$$\zeta_A = 2306".2181T + 0".30188T^2 + 0".017998T^3 \quad (3.47)$$

$$z_A = 2306".2181T + 1".09468T^2 + 0".018203T^3 \quad (3.48)$$

$$\theta_A = 2004".3109T - 0".42665T^2 - 0".041833T^3 \quad (3.49)$$

where T is given by equation (3.44).

Because the earth's orbit is not circular, and the moon's orbit does not lie in the ecliptic plane and is also not circular, the luni-solr precession is not a regular motion. As the configuration of the earth, moon and the sun changes this 'nutation' causes the true pole to rotate around the mean celestial pole, with a relatively short period. The principal componentof nutation has a period of 18.6 years and an amplitude of about 9", and depends on the longitude (in the plane of the ecliptic) of the ascending node of the mean lunar orbit ($\Omega$) measured from the mean equinox of date. Components of nutation also exist with varying periods and amplitudes, depending on the fundamental arguments of the earth-moon-sun system (fig 3.VII).

A new nutation model was adopted by the IAU in 1980 (Kaplan, 1981) which was developed by J. Wahr (Wahr, 1981), based on the work of H. Kinoshita and on the geophysical model 1066A of F. Gilbert and A. Dziewonski (Melbourne, 1983). The model includes the effects of a solid inner core and liquid outer core.

The new theory also uses a new reference pole, the 'Celestial Ephemeris Pole' which has no diurnal motion with respect to earth fixed and space fixed reference frames, as these motions are included implicitly in the model.

Nutation is described in terms of two angles, the nutation in longitude $\Delta\psi$, and the nutation in obliquity $\Delta\varepsilon$, which connect the mean-of-date system to the true-of-date reference system, as illustrated in fig 3.VIII. The mean-of-date system $(x_M, y_M, z_m)$ was described with reference to precession. The true-of-date system $(x_T, y_T, z_T)$ is defined by the true equator and equinox of date (i.e. at the particular epoch). The transformation of coordinates between these two coordinate systems is given by,

$$\underline{r}_T = N \underline{r}_M \qquad (3.50)$$

where the nutation matrix N is given by,

$$N = R_1(-\varepsilon-\Delta\varepsilon) R_3(-\Delta\psi) R_1(\varepsilon) \qquad (3.51)$$

and $\underline{r}_M$ : $(x_M, y_M, z_M)$, mean-of-date coordinates,

$\underline{r}_T$ : $(x_T, y_T, z_T)$, true-of-date coordinates,

$R_1, R_3$ : rotation matrices about the x and z axes respectively (see Appendix A),

and the obliquity of the ecliptic ($\varepsilon$) is given by,

$$\varepsilon = 84381''.448 - 46''.8150T - 0''.00059T^2 \qquad (3.51)$$

$$+ 0''.001813T^3$$

Plane of mean
lunar orbit

Ecliptic
Plane

perigee
of moon's
orbit

$\ell$

F

earth

$\ell'$

sun

$\omega'$

Perihelion

$\Omega$

moon's
ascending node

$x_M$
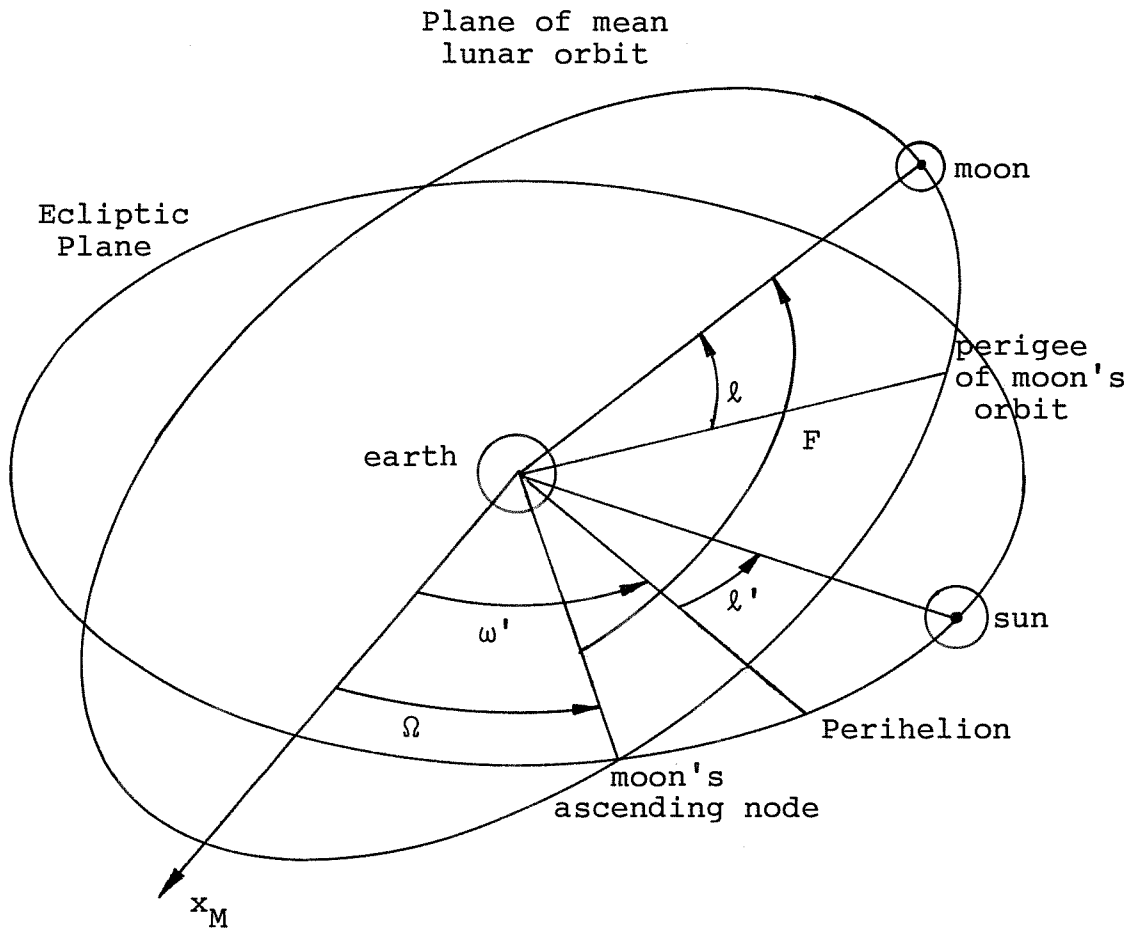
moon

L   :   moon's longitude (= $\Omega$ + F)

$\omega'$   :   longitude of perihelion

L'   :   sun's longitude ( = $\omega'$ + $\ell'$)

D   :   moon's mean elongation from sun (= L - L')

Fig 3.VII  Fundamental Arguments
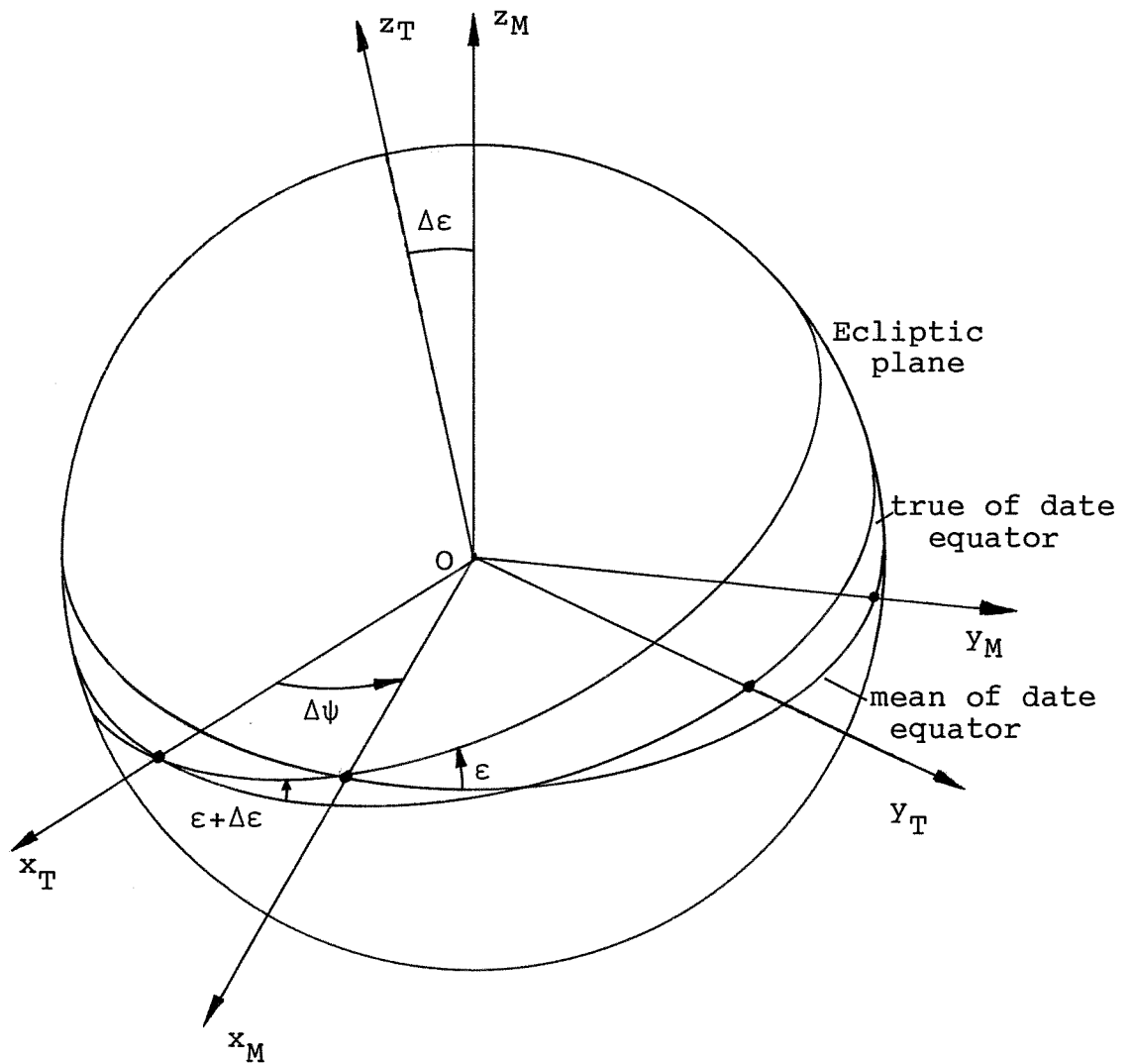
Fig 3.VIII Nutation Angles

The nutation in longitude ($\Delta\psi$) and in obliquity ($\Delta\varepsilon$) are given by the summation of a series of 106 terms,

$$\Delta\psi = \sum_{i=1}^{106} (p_i + q_i T)'' \sin(a_i \ell + b_i \ell' + c_i F + d_i D + e_i \Omega) \quad (3.53)$$

$$\Delta\varepsilon = \sum_{i=1}^{106} (r_i + s_i T)'' \cos(a_i \ell + b_i \ell' + c_i F + d_i D + e_i \Omega) \quad (3.54)$$

where T is given by equation (3.44) and,

$a_i$, $b_i$, $c_i$, $d_i$, $e_i$ : integer multiples of the fundamental arguments,

$(p_i + q_i T)''$ : coefficient of sine argument,

$(r_i + s_i T)''$ : coefficient of cosine argument,

and $\ell$, $\ell'$, $F$, $D$ and $\Omega$ are the fundamental arguments (fig 3.VII) as given by,

$$\ell = 134^\circ\ 57'\ 46'' + (1325^r + 198^\circ\ 52'\ 2''.633)T$$
$$+ 31''.310T^2 + 0''.064T^3 \quad (3.55)$$

$$\ell' = 357^\circ\ 31'\ 39''.804 + (99^r + 359^\circ\ 3'\ 1''.224)T$$
$$- 0''.577T^2 - 0''.012T^3 \quad (3.56)$$

$$F = 93^\circ\ 16'\ 18''.877 + (1342^r + 82^\circ\ 1'\ 3''.137)T$$
$$-13''.257T^2 + 0''.011T^3 \quad (3.57)$$

$$D = 297^\circ\ 51'\ 1''.307 + (1236^r + 307^\circ\ 6'\ 41''.328)T$$
$$- 6''.891T^2 + 0''.019T^3 \quad (3.58)$$

$$\Omega = 125^\circ\ 2'\ 40''.280 - (5^r + 134^\circ\ 8'\ 10''.539)T$$
$$+ 7''.455T^2 + 0''.008T^3 \quad (3.59)$$

where $1^r = 360^\circ$ .

The integer multiples, $a_i$, $b_i$, $c_i$, $d_i$, $e_i$, and the coefficients $p_i$, $q_i$, $r_i$, $s_i$, of equations (3.52) and (3.53) for the 1980 IAU nutation model are given in Kaplan (1981) and in the MERIT Standards (Melbourne, 1983).

## 3.2.5 <u>Earth</u> <u>Rotation</u> <u>and</u> <u>Polar</u> <u>Motion</u>

The rate of rotation of the earth is not constant but has secular, irregular and seasonal variations. Although predicted much earlier, the existence of these variations was not verified until about 50 years ago, in order to explain errors in the position of the moon and planets. With the advent of atomic clocks, the comparison of Universal Time (UT1) with atomic time scales (i.e. UTC or TAI) confirmed the variations. The principles of determining these fluctuations in the rate of rotation of the earth are discussed in detail in Chapter 4.

When transferring coordinates from a space fixed reference frame to an earth fixed system it is necessary to rotate from the true equinox of date to the Greenwich Meridian. This is equivalent to a rotation about the $z_T$-axiz of the true-of-date coordinate system through an angle equivalent to Greenwich Apparent Sidereal Time (GAST), the Greenwich hour angle of the true equinox of date. The resulting coordinate system is known as the instantaneous-terrestrial reference frame ($X_I$, $Y_I$, $Z_I$), as illustrated in fig 3.IX. The formulae for determining GAST at an epoch of UT1 are given in equations (3.37) to (3.40). The transformation between the true-of-date and the instantaneous-terrestrial coordinates is given by,

$$\underline{R}_I = E \; \underline{r}_T \qquad\qquad (3.60)$$

where the earth rotation matrix, E, is given by,

$$E = R_3(\text{GAST}) \qquad\qquad (3.61)$$

and $\quad \underline{r}_T \quad : \quad (x_T, \; y_T, \; z_T)$, true-of-date coordinates,

$\qquad \underline{R}_I \quad : \quad (X_I, \; Y_I, \; Z_I)$, instantaneous-terrestrial

coordinates,

$\qquad R_3 \quad : \quad$ rotation matrix about the x-axis

(see Appendix A).

The true pole (instantaneous spin axis) of the instantaneous-terrestrial system is not, however, fixed with respect to the body of the earth, but is in a state of constant motion, known as 'polar motion'. Although this effect was predicted by Euler in 1765, it was not observed until about a hundred yaers ago. Polar motion consists principally of a free Eulerian nutation (or 'Chandler Wobble') with a period of about 428 days, which results from the non-coincidence of the earth's axis of rotation and its principal axis of inertia. There is also a seasonal variation and evidence of a long term (or secular) drift of the mean position of the pole of about 0".25 over the last 75 years (Bomford, 1980). The motion of the true pole is described by two small angles, $x_p$ and $y_p$, between the instantaneous spin axis and the mean axis of rotation of the earth. The latter is known as the Conventional International Origin (CIO) and is defined in § 4.1. The monitoring and determination of the two components of
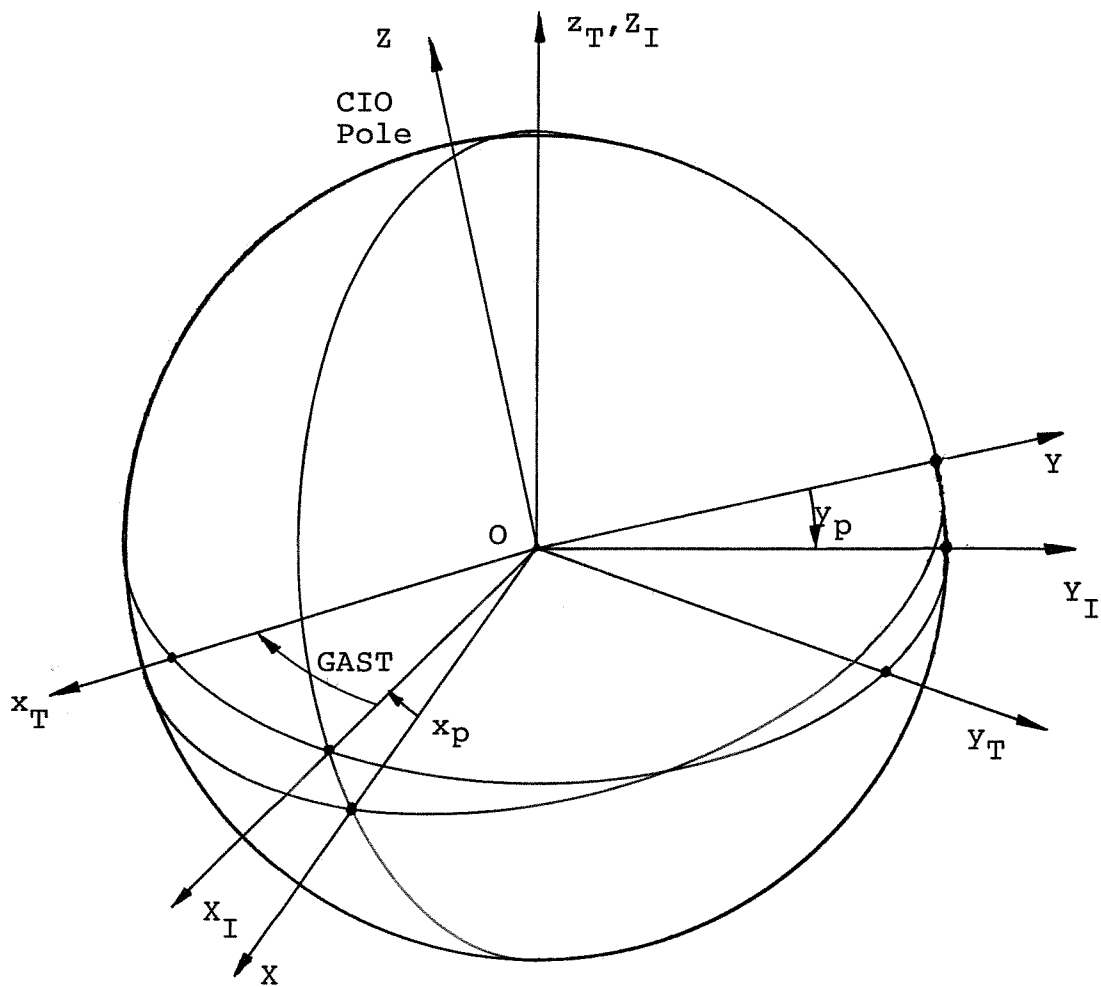
Fig 3.IX Earth Rotation and Polar Motion

polar motion are also discussed in Chapter 4.

The transformation of the coordinates of a point from the instantaneous-terrestrial reference frame $(X_I, Y_I, Z_I)$ to the earth fixed frame $(X, Y, Z)$ is also illustrated in fig 3.IX and is given by,

$$\underline{R} = P \underline{R}_I \qquad (3.62)$$

where the polar motion matrix P is given by,

$$P = R_2(-x_p) \, R_1(-y_p) \qquad (3.63)$$

and $\underline{R}_T$ : $(X_T, Y_T, Z_T)$, instantaneous-terrestrial coordinates,

$\underline{R}$ : $(X, Y, Z)$, earth fixed coordinates,

$R_1, R_2$ : rotation matrices about the x and y axes respectively (see Appendix A).

The complete transformation of coordinates from the J2000.0 inertial reference frame to the earth fixed frame (at some epoch of UTC, $t_{UTC}$) is given by equation (3.34) i.e.

$$\underline{R} = P \ E \ N \ Q \ \underline{r} \qquad (3.34)$$

where the rotation matrices P, E, N, Q are as defined in equations (3.63), (3.61), (3.51) and (3.46) respectively.

3.3   FORCE MODEL COMPONENTS

3.3.1 Introduction

As previously mentioned in § 3.1, the determination of the orbit of a satellite, by numerical integration, requires a model of the forces which govern the motion of the satellite. These may be categorised as gravitational forces, surface forces and any propulsion, the latter resulting from, for example, occasional thrusts used to manoeuvre the spacecraft. The sum of the individual components, which are evaluated independently, gives the resultant force acting on the satellite, and consequently the instantaneous acceleration vector. As the numerical integration must be performed in an inertial reference frame (i.e. the mean of J2000.0 system) then the resultant force model must also be evaluated in the same inertial coordinate system.

The gravity field of the earth is the principal component of the force model, however, in addition the gravitational attractions of the moon, sun and the planets are also accounted for. Due to the tidal effect of the moon and sun on the earth, the model of the gravitational field must be corrected for the effects of both ocean and solid earth tides. Surface forces depend on the cross-sectional area, mass, shape and attitude of the satellite and account for the effects of solar radiation pressure (and earth albedo radiation), atmospheric drag and photonic thrust.

The design of the satellite and choice of altitude can both minimise the effects of surface forces, for example LAGEOS, which is a small, dense and spherical satellite at a high altitude free from the effects of atmospheric drag.

The principal gravitational, surface (and other) forces which significantly contribute to the motion of a satellite are discussed, individually, in the remainder of this section. Where applicable particular references to the LAGEOS satellite are included.

### 3.3.2 Gravitational Attraction of the Earth

As mentioned in § 3.3.1 the attraction due to the gravitational field of the earth is the principal component of all the forces acting on an earth satellite. This force is a function of the position of the satellite in an earth fixed reference frame. The earth's gravity field is normally described by a geopotential expansion in terms of spherical harmonics. The potential, U, at all points external to the earth is given as a function of their spherical polar (earth fixed) coordinates by,

$$U = \frac{GM}{R_p} \left[ 1 + \sum_{n=2}^{\infty} \sum_{m=0}^{n} \left( \frac{a}{R_p} \right)^n P_n^m(\sin \phi_p) \right. \tag{3.64}$$
$$\left. \times (C_n^m \cos m\lambda_p + S_n^m \sin m\lambda_p) \right]$$

where G      :   universal gravitational constant,

M      :   mass of the earth,

a                    : earth's equatorial radius,

$R_p$, $\lambda_p$, $\phi_p$    : earth fixed spherical polar

coordinates of the point,

n, m                 : degree and order of the spherical

harmonic expansion,

$P_n^m(\sin \phi_p)$    : Legendre polynomial,

$C_n^m$, $S_n^m$    : Spherical harmonic coefficients.

Theoretically, the expansion given in equation (3.64)

is an infinite series, however, in practice all the

geopotential models truncate this series after a finite

number of terms. The $P_n^m(\sin \phi_p)$ terms are known as the

associated Legendre polynomials, which are functions of

$\sin \phi_p$, and are usually abbreviated to just $P_n^m$ , as

given by,

$$P_n^m = \cos^m \phi_p \cdot \frac{d^{n+m}(p^2 - 1)^n}{(2^n) \, n! \quad d \, p^{n+m}} \qquad (3.65)$$

where                $p = \sin \phi_p$                (3.66)

These Legendre functions are known as 'tesseral'

harmonics, except when the order m=0, they are referred

to as the zonal harmonics and when the degree and order

are equal (m=n) they are known as the sectorial

harmonics. These may be easily computed by simple

recurrence relations, which in the case of the zonal

harmonics is given by,

$$P_n^0 = \frac{1}{n} \left( (2n - 1) \sin \phi_p \, P_{n-1}^0 - (n - 1) \, P_{n-2}^0 \right) \qquad (3.67)$$

where    $P_1^0 = 1$    and    $P_1^0 = \sin \phi_p$.        (3.68, 3.69)

For the tesseral harmonics the recursion formula is given by,

$$P_n^m = P_{n-2}^m + (2n - 1) \cos \phi_p \, P_{n-1}^{m-1} \qquad (3.70)$$

and for the sectorials by,

$$P_n^m = (2n - 1) \cos \phi_p \, P_{n-1}^{m-1} \qquad (3.71)$$

with the initial value for both given by,

$$P_1^1 = \cos \phi_p \qquad (3.72)$$

The instantaneous acceleration vector of the satellite, in an earth fixed system, is given by the gradient of the potential field at the satellite,

$$\ddot{\underset{\sim}{R}} = \nabla U \qquad (3.73)$$

where $\ddot{\underset{\sim}{R}}$ : satellite acceleration vector $(\ddot{X}, \ddot{Y}, \ddot{Z})$
in an earth fixed reference system.

As the potential field, U, is expressed in terms of spherical polar coordinates the components of $\ddot{\underset{\sim}{R}}$ are evaluated as,

$$\ddot{R}_i = \frac{\partial U}{\partial R_i} = \frac{\partial U}{\partial R_p} \frac{\partial R_p}{\partial R_i} + \frac{\partial U}{\partial \lambda_p} \frac{\partial \lambda_p}{\partial R_i} + \frac{\partial U}{\partial \phi_p} \frac{\partial \phi_p}{\partial R_i} \qquad (3.74)$$

where $R_i$ : component (X, Y, Z) of the earth fixed coordinate of the satellite,

$\ddot{R}_i$ : corresponding component $(\ddot{X}, \ddot{Y}, \ddot{Z})$ of the acceleration vector.

The partial derivatives of equation (3.74) are given in Appendix F. This acceleration vector must then be transformed into the inertial reference frame, in which

the integration is performed, using,

$$\ddot{\underset{\sim}{r}} = Q^T N^T E^T P^T \ddot{\underset{\sim}{R}}$$ (3.75)

where $\ddot{\underset{\sim}{r}}$       : acceleration vector $(\ddot{x}, \ddot{y}, \ddot{z})$ in

the inertial reference frame,

P, E, N, Q : polar motion, earth rotation,

nutation, and precession matrices,

as given in § 3.2.4 and § 3.2.5.

Clearly, it is not possible to determine the acceleration of the satellite without a model describing the geopotential field. Various models are available which are derived from both satellite observations and terrestrial gravity measurements. The geopotential is described by a set of spherical harmonic coefficients, $C_n^m$ and $S_n^m$. These are usually expressed as the normalized forms, $\bar{C}_n^m$ amd $\bar{S}_n^m$, which are related to true cofficients by the expression,

$$C_n^m = N_n^m \bar{C}_n^m$$ (3.76)

and

$$S_n^m = N_n^m \bar{S}_n^m$$ (3.77)

where

$$N_n^m = \left[ \frac{(n - m)! \ (2n + 1) \ (2 - \delta_{om})}{(n + m)!} \right]^{\frac{1}{2}}$$ (3.78)

and $\delta_{om}$ : Kronecker delta, defined as,

$$\delta_{om} = 1 \ \text{for} \ m = 0, \quad \delta_{om} = 0 \ \text{for} \ m \neq 0$$ (3.79)

Over the last 10 or 15 years the accuarcy of the models of the earth's gravity field have shown a great improvement, brought about      mainly by the introduction of observations to a number of satellites.

The European GRIM models (Reigber et al, 1985) and the NASA Goddard Earth Models (GEM) have included progressively more laser ranging (and also radar range and doppler) measurements together with surface gravimetry and satellite altimetery data. (Lerch et al, 1985). Specially 'tailored' gravity models have also been developed such as the GEM-L2 model for LAGEOS and PGS-1331 for STARLETTE. GEM-L2 (Lerch et al, 1983) combined all the data from the previous 'satellite only' GEM-9 model with two and a half years of LAGEOS laser ranging data. Similary, PGS-1331 (Marsh et al, 1985) combined four years of STARLETTE observations with the data from the GEM-10B model and also included SEASAT satellite altimetry data and LAGEOS laser ranges (although the LAGEOS data only contributed to the tracking station coordinates, and not to the gravity field solution).

### 3.3.3 Moon, Sun and Planetary Attractions

In the same way the earth exerts a gravitational attraction on a satellite, the moon, the sun and the other planets also exert a similar attraction. This results in an acceleration vector $\ddot{\underline{r}}_s$ of the satellite towards the 'third body', $P_j$, as given by,

$$\ddot{\underline{r}}_s = \nabla U_s \qquad (3.80)$$

where the potential, $U_s$, at the satellite due to the third body $P_j$ is,

$$U_s = \frac{G\,M_j}{|\,\underline{r} - \underline{r}_j\,|} \qquad\qquad (3.81)$$

where  $M_j$  :  the mass of the third body, $P_j$,

$G$  :  universal gravitational constant,

$\underline{r}$  :  satellite position vector (inertial),

$\underline{r}_j$  :  position vector of third body (inertial)

resulting in,

$$\ddot{\underline{r}}_s = \frac{-\,G\,M_j}{(\,|\underline{r} - \underline{r}_j|\,)^3}\,(\underline{r} - \underline{r}_j) \qquad\qquad (3.82)$$

However, the earth is similarly attracted towards the third body $P_j$. Consequently, there is also an acceleration, $\ddot{\underline{r}}_e$, of the earth towards the $P_j$, as a result of the potential, $U_e$, at the earth due to the third body, as given by,

$$\ddot{\underline{r}}_e = \frac{-\,G\,M_j}{(\,|\underline{r}_e - \underline{r}_j|\,)^3}\,(\underline{r}_e - \underline{r}_j) \qquad\qquad (3.83)$$

where $\underline{r}_e$ is the inertial frame position vector of the earth. However, since the inertial reference frame is geocentric, this is a zero vector, and so equation (3.83) becomes,

$$\ddot{\underline{r}}_e = -\,\frac{G\,M_j}{r_j{}^3}\,\underline{r}_j \qquad\qquad (3.84)$$

where $r_j$ is the distance of $P_j$ from the geocentre. Consequently, the resultant acceleration of the satellite, $\ddot{\underline{r}}$, with respect to the earth (in the

inertial frame) is given by,

$$\ddot{\underset{\sim}{r}} = \ddot{\underset{\sim}{r}}_s - \ddot{\underset{\sim}{r}}_e \qquad (3.85)$$

and so,

$$\ddot{\underset{\sim}{r}} = - G M_j \left( \frac{\underset{\sim}{r} - \underset{\sim}{r}_j}{( | \underset{\sim}{r} - \underset{\sim}{r}_j | )^3} + \frac{\underset{\sim}{r}_j}{r_j^3} \right) \qquad (3.86)$$

Clearly, in order to evaluate this acceleration the positions (in the inertial reference frame) and the masses of the moon, sun and planets must be known. The new planetary and lunar ephemeris, adopted by the IAU in 1984 (Kaplan, 1981), is Development Ephemeris Number DE200/LE200. This gives the positions of the moon and planets in a heliocentric (J2000.0) inertial frame at 0.0hrs TDB of each day, together with the masses of the planets and the constants associated with the ephemeris. In order to use these positions they must first be converted to the geocentric inertial frame, by subtracting the coordinates of the earth from those of the other planets and the moon. The geocentric position vector of the sun is obtained by multiplying the heliocentric position vector of the earth by -1. The position vectors of moon, sun and planets at a specific epoch (for example, the epoch of an observation or orbit integration step) may be subsequnetly computed by interplation (see Appendix D) between the daily vectors.

## 3.3.4   Solid Earth and Ocean Tides

## 3.3.4.1 Solid Earth Tides

As the earth is not entirely rigid, its
anelastic deformation under the influence of the
gravitational attractions of the moon and sun changes
the acceleration of a satellite due to the 'fixed'
geopotential field of the earth. The principal effect
is due to the solid earth (or body) tides, but for
precise orbit determination the ocean tides must also
be taken into account (see § 3.3.4.2).

At any point on the surface of the earth, the
potential due to either the moon or the sun is given
by,

$$U_p = \frac{G\,M_j}{|\underline{r} - \underline{r}_j|} = \frac{G\,M_j}{\rho} \qquad (3.87)$$

where   $M_j$     :  mass of the moon or sun,

$\underline{r}$       :  position vector of point P,

$\underline{r}_j$      :  position vector of the centre of

mass, $P_j$, of the moon or sun,

$|\underline{r} - \underline{r}_j|$  :  distance, $\rho$, from the point P to $P_j$

(centre of mass of the sun or moon)

The distance, $\rho$, may be calculated using the cosine
rule (see fig 3.X), as given by,

$$\rho^2 = r^2 + r_j{}^2 - 2\,r\,r_j\,\cos z \qquad (3.88)$$

where   $r = |\underline{r}|$   :  distance of point P from the

geocentre,
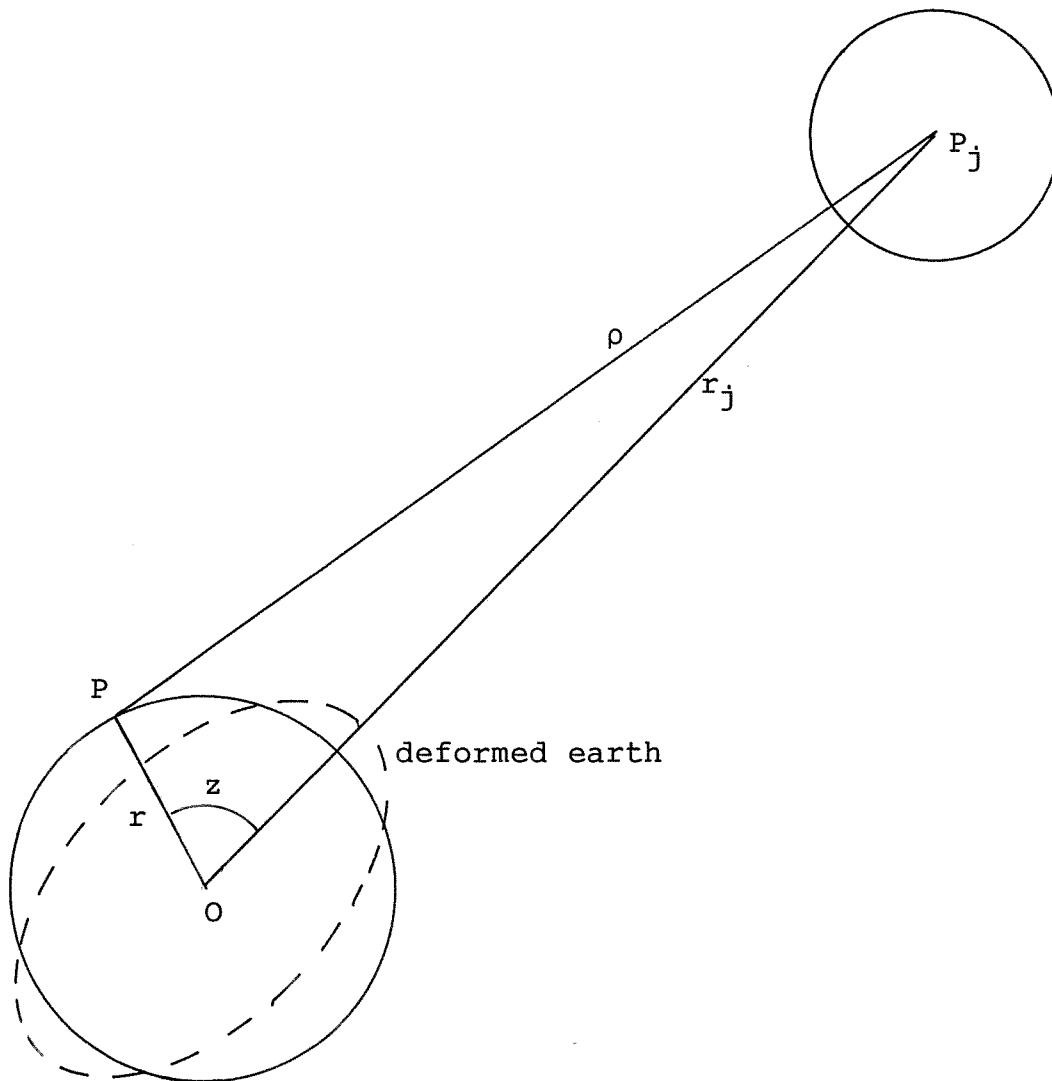
Fig 3.X Earth tides

$r_j = |r_j|$ : distance from the geocentre to the centre of mass of the moon or sun.

z : the angle $POP_j$, in fig 3.X. This angle may be approximated to the zenith at the point of the moon or sun.

By substituting equation (3.88) into equation (3.87) the potential at P is given by,

$$U_p = \frac{G\ M_j}{(r^2 + r_j^2 - 2\ r\ r_j\ \cos z)^{\frac{1}{2}}} \qquad (3.89)$$

This may be expanded, using the binomial expansion, and the infinite series expressed in terms of Legendre polynomials to give,

$$U_p = \frac{G\ M_j}{r_j} \sum_{n=0}^{\infty} \left( \frac{r}{r_j} \right)^n P_n (\cos z) \qquad (3.90)$$

where $P_n (\cos z)$ : Legendre function, as defined in equation (3.65)

The first term of this series, when n=0, is constant and results in no force. Similarly the second term (n=1) produces a constant force, which is independent of both r and z, and so does not produce any tidal variations. The contribution of higher order terms decreases rapidly, due to the ratio of $r/r_j$, which for the moon is of the order of 1/60 and for the sun 1/23000. Consequently, the only significant effect is due to the second harmonic (when n=2), which results in the tide rising potential, $U_T$, as given by,

$$U_T = \frac{G \, M_j \, r^2}{r_j^{\,3}} \, P_2 \, (\cos z) \qquad (3.91)$$

As the Legendre function may be written as,

$$P_2 \, (\cos z) = \tfrac{1}{2} \, (3 \cos^2 z - 1) \qquad (3.92)$$

then equation (3.91) may be re-written as,

$$U_T = \frac{G \, M_j \, r^2}{2r_j^{\,3}} \, (3 \cos^2 z - 1) \qquad (3.93)$$

This potential causes the earth to deform as shown in fig 3.X, with a bulge towards, and away from, the particular body, and a narrowing perpendicualr to that direction. This deformation of the earth leads to an additional potential due to the tidal bulge (Agrotis, 1984) as given by,

$$U = k_2 \, \frac{G \, M_j \, a^5}{r^3 \, r_j^{\,3}} \, P_2 \, (\cos z) \qquad (3.94)$$

where  a  :  earth equatorial radius,

  r  :  distance from the geocentre to the satellite,

  $k_2$  :  love number, nominally 0.3 (Baker, 1984)

By substituting the Lengendre function, as given in equation (3.92), and with,

$$\cos z = \frac{\underline{r} \cdot \underline{r_j}}{r \, r_j} \qquad (3.95)$$

the potential at the satellite due to the tidal bulge, equation (3.94), may be written as,

$$U = k_2 \ \frac{G \ M_j \ a^5}{2 \ r^3 \ r_j{}^3} \left[ \ \frac{3 \ (\underline{r} \cdot \underline{r}_j)^2 - 1}{r^2 \ r_j{}^2} \ \right] \quad (3.96)$$

where $\underline{r}$ : satellite position vector in the inertial frame,

$\underline{r}_j$ : position vector of the moon or sun in the inertial frame, obtained from the planetary ephemeris DE200/LE200, as discussed in § 3.3.3.

The acceleration (in the inertial frame) of the satellite resulting from the tidal effect of the moon or sun (on the earth) is given by evaluating the gradient of the respective potential U, leading to,

$$\ddot{\underline{r}} = k_2 \ \frac{G \ M_j \ a^5}{2 \ r^5 \ r_j{}^3} \left( \ \frac{-15 \ (\underline{r} \cdot \underline{r}_j)^2}{r^2 \ r_j{}^2} \ \underline{r} + \quad (3.97) \right.$$

$$\left. + \ \frac{6 \ (\underline{r} \cdot \underline{r}_j)}{r \ r_j} \ \underline{r}_j + 3 \ \underline{r} \ \right)$$

The body tide love number $k_2$ (Baker, 1984), which gives the change of the potential of the earth due to the tidal potential, is nominally constant with a value of 0.3. However, $k_2$ is not constant but varies according to the periods of the various tides. Any model, such as the Wahr model (Wahr, 1979), which accounts for the frequency dependence of the love numbers, is most efficiently evaluated using a two step procedure. A frequency independent love number ($k_2 = 0.3$) is used during the first stage to evaluate the acceleration of the satellite due to the the change

in potential from equation (3.97). The effect of the
frequency dependent love numbers is accounted for by
computing corrections $\Delta \bar{C}_n^m$ and $\Delta \bar{S}_n^m$ to the normalized
spherical harmonic coefficients, as the second stage.
The corrections are given in the MERIT Standards
(Melbourne, 1983) as,

$$\Delta \bar{C}_n^m - i\Delta \bar{S}_n^m = A_M \sum_{s(n,m)} \delta k_s \ H_s \left. \begin{pmatrix} 1 \\ -i \end{pmatrix} \right. \begin{matrix} n+m \text{ even} \\ n+m \text{ odd} \end{matrix} \ e^{i\theta} \quad (3.98)$$

which may be expressed as,

$$\Delta \bar{C}_n^m = A_M \sum_{s(n,m)} \delta k_s \ H_s \left. \begin{pmatrix} \cos \theta_s \\ \sin \theta_s \end{pmatrix} \right. \begin{matrix} n+m \text{ even} \\ n+m \text{ odd} \end{matrix} \quad (3.99)$$

and

$$\Delta \bar{S}_n^m = A_M \sum_{s(n,m)} \delta k_s \ H_s \left. \begin{pmatrix} -\sin \theta_s \\ \cos \theta_s \end{pmatrix} \right. \begin{matrix} n+m \text{ even} \\ n+m \text{ odd} \end{matrix} \quad (3.100)$$

where

$$A_M = \frac{(-1)^m}{a \ \sqrt{(4\pi \ (2 - \delta_{om}))}} \quad (3.101)$$

with $\delta_{om}$ : Kronecker delta,

$a$ : earth equatorial radius,

$\delta k_s$ : difference between the Wahr model (Wahr,
1979) value for k at frequency s and the
nominal value of $k_2 = 0.3$, in the sense
$k_s - k_2$,

$H_s$ : amplitude (in metres) of the tide with
frequency s, taken from Cartwright and
Taylor (1971),

and

$$\theta_s = \underline{n} \cdot \underline{\beta} = \sum_{i=1}^{6} n_i \ \beta_i \quad (3.102)$$

with $\underline{\beta}$ : vector of Doodson variables ($\tau$, s, h, p,
N', $p_1$),

$\underset{\sim}{n}$ : vector of integer multiples ($n_1$, $n_2$, $n_3$, $n_4$, $n_5$, $n_6$) of the Doodson variables (Melbourne, 1983).

The Doodson variables are related to the fundamental arguments of the nuataion series (see § 3.2.4) by,

$$
\left.
\begin{aligned}
s &= F + \Omega && : \text{moon's mean longitude,} \\[4pt]
h &= s - D && : \text{sun's mean longitude,} \\[4pt]
p &= s - \ell && : \text{longitude of the moon's.} \\
& && \quad\text{mean perigee,} \\[4pt]
P_1 &= s - D - \ell' && : \text{longitude of the sun's} \\
& && \quad\text{mean perigee,} \\[4pt]
N' &= -\Omega && : \text{negative longitude of} \\
& && \quad\text{moon's mean node,} \\[4pt]
\tau &= \theta_g + \pi - s && : \text{time angle in lunar days,} \\
& && \quad\text{from lower transit.}
\end{aligned}
\right\} \quad (3.103)
$$

where $\theta_g$ is Greenwich Mean Siderael Time (GMST).

The MERIT Standards (Melbourne, 1983) recommend the use of six diurnal tides, leading to corrections to the $\bar{C}_2^1$ and $\bar{S}_2^1$ terms, and two semi-diurnal tides correcting the $\bar{C}_2^2$ and $\bar{S}_2^2$ . This recommendation is based on a cut-off amplitude of $9 \times 10^{-2}$ for the product $A_M \, \delta k_s \, H_s$ in equations (3.98) to (3.100) and a nominal value of the $k_2$ love number of 0.3.

Solid earth tides result in a deformation of the earth's surface, which not only changes the potential field at the satellite but also changes the coordinates

of the tracking stations. This effect can lead to movements of up to 32cm and 15cm for lunar and solar tides, respectively. Clearly, this does not affect the force model of the satellite, but the effect on the tracking station coordinates must be accounted for during the analysis process. As with the change in potential, the variations of station coordinates are most effectively evaluated using a two step procedure (Melbourne, 1983). The first step uses frequency independent love and shida numbers ($h_2$ and $\ell_2$) and the vector displacement (inertial frame) of a tracking station, P, due to lunar or solar solid earth tides is given by (Martin et al, 1980),

$$\Delta \underline{r}_p = \frac{M_j \ a^4}{M \ r_j^{\ 3}} \left[ 3\ell_2 \ \frac{(\underline{r}_p \cdot \underline{r}_j)}{r_p \ r_j} \ \frac{\underline{r}_j}{r_j} + \right. \tag{3.104}$$

$$\left. + \left[ \frac{3 \ (h_2 - \ell_2)}{2} \ \frac{(\underline{r}_p \cdot \underline{r}_j)^2}{(r_p \ r_j)^2} - \frac{h_2}{2} \right] \frac{\underline{r}_p}{r_p} \right]$$

where  $\underline{r}_p$  : inertial frame coordinates of station P,

     $\underline{r}_j$  : coordinates of moon or sun (inertial),

     $r_p$  : distance from geocentre to station P,

     $r_j$  : distance from geocentre to moon or sun,

     M  : mass of the earth,

     $M_j$  : mass of moon or sun,

     $h_2$  : nominal second degree love number,

     $\ell_2$  : nominal second degree shida number.

The MERIT Standards recommend nominal values of $h_2$ and $\ell_2$ of 0.6090 and 0.0852, respectively. With these

values, and a cut-off amplitude of 0.005m in the radial
displacement, only one component (radial) needs to be
corrected for the frequency dependence of the love
numbers, in the second step. The correction is for $K_1$
frequency where $h_2$ from Whar's theory is 0.5203 (Whar,
1979). The change in radial component may be expressed
as a change in the height of the station, as given by,

$$\Delta h = -0.0253 \sin \phi \cos \phi \sin (GMST + \lambda) \qquad (3.105)$$

where $\phi$, $\lambda$, h : geocentric earth fixed spheroidal
coordinates of the tracking station,

$\Delta h$ : correction to station height.

This effect is a maximum at a latitude of $45^0$ where
the amplitude is 0.013m (Melbourne, 1983). Solid earth
tides also introduce variations in the rate of rotation
of the earth as discussed in Chapter 4.


### 3.3.4.2 Ocean Tides

The attractions of the moon and sun on the
earth leads to a tide rising potential as given by
equation (3.91). As the surface of the oceans is an
equipotential surface (except for the effects of
temperature, pressure, salinity and currents), this
tide rising potential causes the level of the oceans to
fluctuate with time. Consequently, the oceans apply a
variable load on the body of the earth, which responds
by deforming. Clearly, as with the tides of the solid
earth, this deformation results in a change in the

potential, at the satellite, due to the earth and a corresponding change in the acceleration of the satellite. The effect of ocean tides is most efficiently implemented as corrections to the normalized spherical harmonic coefficients of the geopotential model, which may be expressed as (Eanes et al, 1983 and Melbourne, 1983),

$$\Delta \bar{C}_n^m = F_n^m \sum_{s(n,m)} ( (C_{snm}^+ + C_{snm}^-) \cos \theta_s + \qquad (3.106)$$

$$+ (S_{snm}^+ + S_{snm}^-) \sin \theta_s )$$

$$\Delta \bar{S}_n^m = F_n^m \sum_{s(n,m)} ( (S_{snm}^+ - S_{snm}^-) \cos \theta_s - \qquad (3.107)$$

$$- (C_{snm}^+ - C_{snm}^-) \sin \theta_s )$$

where
$$F_n^m = \frac{4 \pi a^2 \rho_w}{M N_n^m} \cdot \frac{(1 + k_n')}{(2n + 1)} \qquad (3.108)$$

and $N_n^m$   : normalizing factor, equation (3.78),

$a$     : equatorial earth radius,

$M$     : mass of the earth,

$\rho_w$    : density of sea water,

$\theta_s$    : argument of the tide constituent, s, as given by equation (3.102),

$k_n'$    : load deformation coefficients,

$C_{snm}^{\pm}, S_{snm}^{\pm}$ : ocean tide coefficients for the tide s, where $C_{snm}^+$ and $S_{snm}^+$ denote prograde waves and $C_{snm}^-$ and $S_{snm}^-$ denote retrograde waves.

The values of the ocean tide coefficients are given in
the MERIT Standards for the Schwiderski ocean tide
model (Schwiderski, 1980), together with the associated
load deformation coefficients. Long period
perturbations are only produced when the degree, n, is
greater than 1, but the effect decreases rapidly and so
the correction is only evaluated for tides up to degree
6. Terms for the long period tides (order m=0) $S_{sa}$, $M_f$,
and $M_m$, for the diurnal tides (m=1) K1, O1, P1 and Q1,
and for the semi-diurnal tides (m=2) $M_2$, $S_2$, $N_2$ and $K_2$,
are given for degree n=2 to 6.

As discussed previously in § 3.3.4.1, a tracking
station on the earth's surface may be displaced by up
to 40cm due to the effects of solid earth tides.
Similarly, the ocean tidal loading also has an effect
on the coordinates of a tracking station, however the
effect is much less. Typically, the change in the
height of a station may be of the order of 1cm,
however, in certain coastal sites this may increase to
around 10cm. Clearly, if this is the case, the effect
of ocean tidal loading on the tracking station
coordinates must be corrected during the analysis
procedure. For this purpose the MERIT Standards
(Melbourne, 1983) give the necessary coefficients,
evaluated for 25 laser ranging and VLBI sites
(Goad,1980).

### 3.3.5 <u>Solar Radiation Pressure</u>

The intensity of solar radiation, emitted by the sun, varies inversely with distance away from the sun. As a result the radiation pressure acting on a satellite orbiting the earth is given by,

$$P_s = \frac{I_o}{c} \left( \frac{A_u}{|r - r_j|} \right)^2 \qquad (3.109)$$

where $A_u$ : astronomical unit $(1.4959787 \times 10^{11} m)$, the distance equivalent to the semi-major axis of the earth's orbit,

$r$ : inertial frame satellite position vector,

$r_j$ : position vector of the sun, in the inertial frame (obtained from the planetary ephemeris DE200/LE200),

$I_o$ : intensity of solar radiation at one astronomical unit $(I_o = 1367.2 \ Wm^{-2})$

$c$ : speed of light in a vacuum.

This solar radiation pressure results in an acceleration of the satellite in a direction away from the sun, which in the inertial reference frame is given by the vector,

$$\ddot{r} = C_R \frac{I_o}{c} \left( \frac{A_u}{|r - r_j|} \right)^2 \left( \frac{A}{m} \right) \frac{r - r_j}{|r - r_j|} \qquad (3.110)$$

where $A$ : cross sectional area of satellite $(m^2)$,

$m$ : mass of the satellite (kg),

$C_R$ : radiation pressure reflectance coefficent.

The precise modelling of radiation pressure is, for many satellites, a complex process, for a number of reasons. The reflectivity of the outer surface and the shape of the satellite are both important. A fraction of the incident radiation is absorbed (raising the temperature of the spacecraft) and the remainder is reflected, either diffusely of specularly. Clearly, this reflected radiation also imparts a force on the satellite in the opposite direction to that of the incident radiation. The effects of solar radiation pressure are minimised if the area-to-mass ratio of a satellite is kept small, for example, LAGEOS and STARLETTE are both very small dense satellites. However in order to study the effects of solar radiation pressure the most effective type of satellite would be very large and light, such as a balloon satellite. Furthermore, it is preferable to have a constant area-to-mass ratio, to ensure that the solar radiation force does not depend on the orientation of the satellite. This may only be achieved by spherical satellite (such as LAGEOS and STARLETTE). Finally, there are unpredictable variations in the intensity of the sun's radiation due to changes in the solar activity.

The uncertainty in the model, introduced by these various effects, is accounted for by including a reflectance coefficient $C_R$ in equation (3.110). Due to the effect of the reflected radiation this parameter is

typically greater than 1 (for LAGEOS it is approximately 1.14) and may be determined as a unknown in the least squares solution. A further complication arises when the satellite passes into the earth's shadow, which completely cuts off the solar radiation pressure (when the satellite is in the umbra). However, as the satellite passes through the penumbra, there is a gradual decrease in the radiation pressure and a corresponding decrease in the resulting acceleration. To ensure precise modelling of the effects of solar radiation pressure it is necessary to introduce a 'shadow test' to determine when the satellite goes into the earth's shadow, and to cut-off the radiation pressure model accordingly (Agrotis, 1984).

In addition to the main effect of 'direct' solar radiation on a satellite albedo radiation, reflected back from the surface of the earth, also has a similar effect. This, however, decreases according to the inverse square law as the altitude increases, but at an altitude of 800km it may still account for around 10% of the direct effect. In contrast to direct radiation pressure, the modelling of albedo is both complex and time consuming. The first difficulty arises because the albedo is variable depending on the position of the satellite and on the unpredictable temporal changes of the reflective properties of the earth. Consequently, the effect needs to be re-computed at every step of the orbit integration. Secondly, the evaluation involves a

numerical integration over the entire surface of the earth visible from the satellite to determine the components of the total albedo flux. Clearly, this process is computationally very time consuming and accordingly various procedures have been proposed to simplify the modelling of albedo. (Anselmo, 1983).

### 3.3.6 Other Forces

This section will discuss some of the forces which may act on a satellite, but have not been described in any of the previous sections. The modelling of empirical accelerations which may be included to account for any deficiencies in any of the force models, is also discussed. For the LAGEOS satellite the effects of these additional forces are generally considered negligible (or not applicable). However, an empirical along track acceleration is typically modelled.

Although the effects of atmospheric drag are not applicable for LAGEOS, because of its high altitude, for many lower satellites the effects are very significant. The inertial frame acceleration of the satellite due to air drag is given by,

$$\ddot{\underline{r}} = \frac{-1}{2} C_D \left( \frac{A}{m} \right) \rho_a \, \dot{v}_r \, v_r \qquad (3.111)$$

where   $C_D$   :   satellite drag coefficient,

   $A$   :   cross sectional area of satellite,

m : mass of satellite,

$\rho_a$ : air density at satellite,

$\underset{\sim}{v}_r$ : velocity vector of the satellite (inertial frame) with respect to the atmosphere.

The inertial frame velocity vector, $\underset{\sim}{v}_r$, is evaluated from the rate of rotation of the atmosphere (assumed to be the same as the rate of rotation of the earth) and the satellite true-of-date coordinates, by,

$$\underset{\sim}{v}_r = Q^T N^T (\underset{\sim}{\omega} \times \underset{\sim}{r}_T) \qquad (3.112)$$

where Q : precession matrix (see § 3.2.4),

N : nutation matrix (see § 3.2.4),

$\underset{\sim}{\omega}$ : rotation rate vector of the earth (true-of-date),

$\underset{\sim}{r}_T$ : true-of-date coordinates of satellite.

The air density at the satellite, $\rho_a$, is obtained from a model, such as that of Jacchia (1971), which is valid for altitudes of less than 2000km. There are, however, no such models for altitudes greater than 2000km, but the effects of atmospheric drag at these altitudes is very small. As with solar radiation pressure (see § 3.3.5) air drag depends on the area-to-mass ratio (A/m) and so the effects are minimised for a small dense satellite (such as STARLETTE). A further complication arises with non-spherical satellites as the drag is not constant and varies according on the

orientation of the satellite. The drag coefficient $C_D$, in equation (3.111), may be included as an unknown in the least squares solution and so account for deficiencies in the atmospheric drag model.

For satellites which are occasionally manoeuvered it is necessary to include the effects of the thrust forces. These manoeuvres are used, especially for low flying satellites, to maintain a specific orbit configuration. They are however, generally predictable and are modelled as along track, across track, and radial accelerations. Small perturbations may also result from charged or neutral partical drag (Afonso et al, 1985).

These small accelerations may be accounted for by the empirical modelling of forces in specific directions; these take the general form,

$$\ddot{\underline{r}} = C \, \hat{\underline{n}} \qquad (3.113)$$

where  C  :  constant coefficient,

$\hat{\underline{n}}$  :  unit vector in the required direction

i.e. along track, across track.

For the LAGEOS satellite an along track empirical acceleration is modelled and the coefficient $C_T$ is determined as an unknown in the least squares solution. For an along track acceleration equation (3.113) gives the resulting (inertial frame) acceleration of the satellite, by

$$\ddot{r} = C_T \frac{\dot{r}}{\dot{r}}$$

<div align="right">(3.114)</div>

where $\dot{r}$ : inertial frame velocity vector of the satellite (with magnitude $\dot{r}$).

Over the lifetime of the LAGEOS satellite the mean value of $C_T$ has been found to be $-3.1 \times 10^{-12}$ (Melbourne, 1983).

## 3.4 ORBIT INTEGRATION AND ADJUSTMENT BY LEAST SQUARES

### 3.4.1 Numerical Integration of the Equations of Motion

As previously mentioned in § 3.3 the resultant acceleration of the satellite is given by summing all the individual accelerations due to the forces acting on the satellite. Clearly, it may not be necessary to include the effects of all the forces described in § 3.3, if certain forces are considered negligible. As the subsequent numerical integration must be performed in an inertial reference frame, the resultant acceleration vector (and consequently its components) must be evaluated in the same inertial frame. Orbit determination consists of integrating the satellites equations of motion in order to compute its position and velocity vectors as a function of time. The equations of motion are $2^{nd}$ order differential equations, which are functions of position, velocity and time, as given by,

$$\ddot{r} = f( \dot{r}, r, t )  \qquad (3.115)$$

where $\ddot{r}$ : resultant inertial frame acceleration vector,

$\dot{r}$ : satellite velocity vector, inertial frame,

$r$ : satellite position vector, inertial frame,

$t$ : time, usually UTC (see § 3.2.3).

By assuming initial position and velocity vectors at some starting epoch, $t_0$, the position and velocity at

another epoch, t, are given by,

$$\dot{r}(t) = \dot{r}(t_0) + \int_{t_0}^{t} \ddot{r} \, dt \qquad (3.116)$$

$$r(t) = r(t_0) + \int_{t_0}^{t} \dot{r} \, dt \qquad (3.117)$$

where

$r(t), \dot{r}(t)$ : position and velocity vectors at t,

$r(t_0), \dot{r}(t_0)$ : position and velocity vectors at $t_0$.

Initially, the satellite state vectors, $\dot{r}_0$ and $r_0$, need not be known precisely, as they may be improved by determining small corrections to them as unknowns in the least squares solution (following the intoduction of the range observations). Since the advent of high speed computers, it has been possible to carry out the integrations of equations (3.116) and (3.117) numerically. In practice, this is carried out with a 'step length' between the integrations, resulting in a satellite ephemeris consisting of position and velocity vectors at discrete epochs. Subsequently the position (and velocity) of the satellite at any specific epoch may be computed by interpolation between the discrete values. Typical interpolation formulae are discussed in Appendix D.

There are two distinct types of numerical integration procedures which are suitable for the evaluation of equations (3.116) and (3.117). These are 'single-step' methods and 'iterative (or multi-step)' methods. In practice, both methods are used, however,

because of the low accuarcy of single-step methods
their use is usually limited to providing sufficient
initial steps to enable a more precise multi-step
method to take over.

The single-step methods, using only the $i^{th}$
value of the integral, obtain the $(i+1)^{th}$ value in a
'single-step'. This value is subsequently used to
evaluate the $(i+2)^{th}$ value of the integral, and so on
until the ephemeris is generated after succesive
applications of the method. As an example, equation
(3.116) for the $(i+1)^{th}$ value may be written as,

$$\underline{r}(t_i + h) = \underline{r}(t_i) + \int_{ti}^{ti+h} \underline{\dot{r}} \, dt \qquad (3.118)$$

where
$$\underline{r}(t_i) = \underline{r}(t_0 + ih) \qquad (3.119)$$

and    h  :  integration step size.

There are a number of different single-step methods
which are suitable for this application, however a
common choice is a Runge-Kutta procedure (Spencer et
al, 1977). These methods evaluate the function (in
this case $\underline{\ddot{r}}$ or $\underline{\dot{r}}$) at several intermediate points
within the step interval in order to determine the next
value. The $4^{th}$ order Runge-Kutta is widely used (with
an error per step of the order of $h^5$) and applied to
equation (3.118) may be expressed as,

$$\underline{r}_{i+1} = \underline{r}_i + \frac{1}{6} ( \underline{k}_1 + 2\underline{k}_2 + 2\underline{k}_3 + \underline{k}_4 ) \qquad (3.120)$$

where
$$\underline{r}_{i+1} = \underline{r}(t_i + h) \qquad (3.121)$$

$$\underline{r}_i = \underline{r}(t_i) \qquad (3.122)$$

and
$$\dot{\underset{\sim}{r}} = f(t, \underset{\sim}{r})$$
(3.123)

$$\underset{\sim}{k}_1 = h\ f(t_i, \underset{\sim}{r}_i)$$
(3.124)

$$\underset{\sim}{k}_2 = h\ f(t_i + \tfrac{1}{2}h, \underset{\sim}{r}_i + \tfrac{1}{2}\underset{\sim}{k}_1)$$
(3.125)

$$\underset{\sim}{k}_3 = h\ f(t_i + \tfrac{1}{2}h, \underset{\sim}{r}_i + \tfrac{1}{2}\underset{\sim}{k}_2)$$
(3.126)

$$\underset{\sim}{k}_4 = h\ f(t_i + h, \underset{\sim}{r}_i + \underset{\sim}{k}_3)$$
(3.127)

A detailed description of the application of the Runge-Kutta method to orbit determination is given in Agrotis (1984). A disadvantage of the Runge-Kutta methods is that there is no simple formula for evaluating the error associated with each step. However, it is possible to obtain a theoretical estimate of the cumulative error, which is proportional to $h^n$, where n is the order of the method. If $s_i$ is the true value of one element of $r_i$ (i.e. x, y or z), and the value of $s_i$ obtained after i integration steps of size h is $s_{i1}$, then,

$$s_i = s_{i1} - A\ h^n$$
(3.128)

where A is a constant. If $s_{i2}$ is another corresponding value of $s_i$, computed after $\tfrac{i}{2}$ integrations, with step size 2h, then similary,

$$s_i = s_{i2} - A(2h)^n$$
(3.129)

and so combining (3.128) and (3.129) an estimate of the cumulative error, $\varepsilon$, is given by,

$$\varepsilon = A\ h^n = \frac{s_{i2} - s_{i1}}{2^n - 1}$$
(3.130)

which for a 4$^{th}$ order formula becomes,

$$\epsilon = \frac{1}{15} (s_{i2} - s_{i1})$$
(3.131)

Consequently, in order to obtain an estimate of the error, the integration must be repeated with half the original step length. In order to maintain a sufficient level of accuracy it is necessary to use very short step lengths (for example, 15 seconds in the case of LAGEOS orbit integration) for Runge-Kutta methods. Furthermore, each integration step involves the evaluation of the four functions of (3.124) to (3.127), which may be computationally time consuming. Consequently, Runge-Kutta methods are only used, in orbit determination, to compute sufficient values, starting from the initial velocity and position vectors, to allow a multi-step iterative procedure to take over.

Although there are numerous iterative methods of numerical integration, predictor-corrector schemes are the most common (Spencer et al, 1977). These make use of previously computed values, of which there would be n+1 in the case of an n$^{th}$ order scheme, to predict the next value. This value is then used with the previous n values in order to evaluate the corrected value. If the difference between the predicted and corrected values exceeds some pre-set limit then the 'corrector' may be re-applied, using the most recent estimate of the corrected value instead of the predicted value. Clearly, in order that a predictor-corrector may start

the first n+1 values must be known. If this is not the case then a single-step method must be used to compute the necessary values from the initial starting values.

The Adams-Bashforth formulae are derived using the Newton backward difference formula to approximate the function being integrated (Spencer et al, 1977). Rather than considering the entire vectors, as in equations (3.117) to (3.127), it is convenient to refer to just one element $s_i$ of $\underset{\sim}{r}_i$ (i.e. x, y or z), to illustrate the Adams-Bashforth formulae. The predicted value $s^*_{i+1}$, for the $(i+1)^{th}$ value of s is given by,

$$s^*_{i+1} = s_i + h(f_i + \frac{1}{2}\nabla f_i + \frac{5}{12}\nabla^2 f_i + \frac{3}{8}\nabla^3 f_i + ..) \quad (3.132)$$

where $f_i = f(t_i, s_i)$ as in equation (3.123), $\quad$ (3.133)

and

$$\nabla f_i = f_i - f_{i-1} = f(t_i, s_i) - f(t_{i-1}, s_{i-1}) \quad (3.134)$$

$$\nabla^2 f_i = \nabla f_i - \nabla f_{i-1} = f_i - 2f_{i-1} + f_{i-2} \quad (3.135)$$

$$\nabla^3 f_i = \nabla^2 f_i - \nabla^2 f_{i-1} \quad ..... \text{ etc} \quad (3.136)$$

and the predicted value of $f_{i+1}$ is given by,

$$f^*_{i+1} = f(t_{i+1}, s^*_{i+1}) \quad (3.137)$$

The corrected value, $s^{**}_{i+1}$, of the $(i+1)^{th}$ value is then given by,

$$s^{**}_{i+1} = s_i + h (f^*_{i+1} - \frac{1}{2}\nabla f^*_{i+1} - \frac{1}{12}\nabla^2 f^*_{i+1} - \quad (3.138)$$
$$- \frac{1}{24}\nabla^3 f^*_{i+1} - ... )$$

In practice, these formulae, (3.132) to (3.138), are

truncated to some order n, the order of the last backward difference included ($\nabla^n f_i$). Consequently, to evaluate the differences for the $(i+1)^{th}$ step the previous n+1 values, $s_{i-n}$ to $s_i$ must be known. The error, $\varepsilon^{**}$, involved in truncating the formulae after the $n^{th}$ backward difference (Agrotis, 1984) is given by,

$$\varepsilon^{**} = \frac{c_{n+1}}{b_{n+1} - c_{n+1}} (s_{i+1}^{**} - s_{i+1}^{*}) \qquad (3.139)$$

where $b_{n+1}$ and $c_{n+1}$ are the coefficients of the $(n+1)^{th}$ backward differences from the predictor (3.132) and the corrector (3.138) formulae, respectively.

Clearly, the error may be estimated at each step from the difference between the predicted and corrected values. A disadvantage with the Adams-Bashforth method is that the step size, h, cannot be altered, for example if the error is too great. The integration step length must, therefore, be chosen carefully so as to provide the required accuracy without excessive computations. Experience has shown (Ashkenazi, Agrotis and Moore, 1984) that for LAGEOS orbit determination a step length of 120 seconds is suitable. Full details of the application of the Adams-Bashforth predictor-corrector method are given in Agrotis (1984).

### 3.4.2 Introduction to Least Squares Adjustment

The aim of the analysis of laser range

observations is to determine a series of unknown parameters, such as the coordinates of the tracking stations and polar motion components. The observed ranges must, however, be functions of these unknown parameters, such that,

$$r_i = f_i(x_1, x_2, \ldots x_k) \qquad (3.140)$$

where $r_i$    : $i^{th}$ observed satellite range,

$x_1, x_2, \ldots x_k$ : unknown parameters (k unknowns).

If approximate values of the unknowns are assumed then it is possible to obtain a computed value of the observed range,

$$r_{ic} = f_i(x_{1c}, x_{2c}, \ldots x_{kc}) \qquad (3.141)$$

The true values of the unknowns, $\bar{x}_j$, differs from the approximate value, $x_{jc}$, by a small correction $\Delta x_j$, such that,

$$\bar{x}_j = x_{jc} + \Delta x_j \qquad (3.142)$$

and the true value of the range observation will be given by,

$$\bar{r}_i = f_i(x_{1c} + \Delta x_1, x_{2c} + \Delta x_2, \ldots x_{kc} + \Delta x_k) \qquad (3.143)$$

By taking a Taylor series expansion of this equation and assuming second and higher order terms are negligible, it may be re-wriiten as,

$$\bar{r}_i = r_{ic} + \frac{\partial r_{ic}}{\partial x_1} \Delta x_1 + \frac{\partial r_{ic}}{\partial x_2} \Delta x_2 + \ldots + \frac{\partial r_{ic}}{\partial x_k} \Delta x_k \qquad (3.144)$$

where $\dfrac{\partial r_{ic}}{\partial x_j} = \dfrac{\partial f_i}{\partial x_j}(x_{1c}, x_{2c}, \ldots x_{kc}) \qquad (3.145)$

However, due to random errors in the range measurement
(as previously discussed in § 2.3) the observed range,
$r_{io}$, may differ from the true range, $\bar{r}_i$, by a small
residual error, $v_i$, such that,

$$\bar{r}_i = r_{io} + v_i \qquad (3.146)$$

So, by combining equations (3.144) and (3.146) the
'observation equation' of an observed range
measurement, linearised about the approximate values,
is given by,

$$\frac{\partial r_{ic}}{\partial x_1} \Delta x_1 + \frac{\partial r_{ic}}{\partial x_2} \Delta x_2 + \ldots + \frac{\partial r_{ic}}{\partial x_k} \Delta x_k = r_{io} - r_{ic} + v_i \qquad (3.147)$$

Given a set of n observed ranges an observation
equation of the form of equation (3.147) may be set up
for each range. The resulting set of observation
equations may be conveniently expressed in matrix form
as,

$$A \underset{\sim}{x} = \underset{\sim}{b} + \underset{\sim}{v} \qquad (3.148)$$

where  A :  (n × k) matrix of the observation equation
               coefficients (the partial derivatives in
               equation (3.147)),

       $\underset{\sim}{x}$ :  (n × 1) vector of the unknown corrections
               ($\Delta x$) to the approximate values ($x_{ic}$),

       $\underset{\sim}{b}$ :  (n × 1) vector of the observed ($r_{io}$) minus
               computed ($r_{ic}$) range observations,

       $\underset{\sim}{v}$ :  (n × 1) vector of the residuals, $v_i$.

If the observations (in this case range measurements)

are of differing accuracies then the observation
equations may be 'weighted' before solution. Weighting
of observation equations requires a knowledge of the
'a priori' covariance matrix (see § 3.4.5) which if the
observations are correlated will comprise both diagonal
and off-diagonal elements. However, it is usual to
assume that the observations are uncorrelated,
resulting in a diagonal covariance matrix. The diagonal
elements of this matrix are the reciprocals of the
squares of the standard errors of the individual
observations. The weighted observation equations may be
obtained from equation (3.148) as,

$$W^{\frac{1}{2}} A \underset{\sim}{x} = W^{\frac{1}{2}} \underset{\sim}{b} + W^{\frac{1}{2}} \underset{\sim}{v} \qquad (3.149)$$

where

$$W^{\frac{1}{2}} = \begin{bmatrix} \dfrac{1}{\sigma_1} & 0 & . & . & . & 0 \\ 0 & \dfrac{1}{\sigma_2} & . & . & . & 0 \\ . & . & & & & . \\ . & . & & & & . \\ . & . & & & & . \\ 0 & 0 & . & . & . & \dfrac{1}{\sigma_n} \end{bmatrix} \qquad (3.150)$$

and $\sigma_i$ : a priori standard error of the $i^{th}$
observation.

By ensuring the units of the standard errors are
consistent with those of the observations, weighting
also converts all the terms of the observation
equations into dimensionless quantities. Consequently,
observations of different types may be mixed in a

single solution (i.e. position observations may be included with the ranges). It is also possible, by assigning very large weights (low standard errors), to hold certain quantities, such as the coordinates of a tracking station, fixed in the solution.

Provided the residuals may be assumed to be random and normally distributed then the 'least squares' method leads to the most probable solution of equation (3.149). The least squares solution is that which minimises the sum-of-the-squares of the weighted residuals, i.e.,

$$\underset{\sim}{v}^{\tau} \, w \, \underset{\sim}{v} \; \rightarrow \; \text{minimum} \tag{3.151}$$

As shown in Appendix E the values of the unknowns which satisfy (3.151) are given by,

$$(A^{\tau} \, W \, A) \, \underset{\sim}{x} \; = \; A^{\tau} \, W \, \underset{\sim}{b} \tag{3.152}$$

These are known as the 'normal equations' and may be expressed, in matrix form, as,

$$N \, \underset{\sim}{x} \; = \; \underset{\sim}{d} \tag{3.153}$$

where  N  :  (k × k) normal equation coefficient matrix

$\underset{\sim}{d}$  :  (k × 1) right hand side vector of the normal equations ($A^{\tau} \, W \, \underset{\sim}{b}$).

The solution of the normal equations, which gives the vector of unknowns $\underset{\sim}{x}$, may be carried out by a number of methods (Ashkenazi, 1967 and 1969). As the normal equations are positive-definite and symmetrical (see Appendix E), a suitable method of solution is

Choleski's method of symmetric decomposition. The normal equation coefficient matrix N is decomposed symmetrically into $L\ L^T$, to give,

$$N\ =\ L\ L^T \qquad (3.154)$$

where L is a lower triangular matrix. Consequently, the normal equations may be written as,

$$L\ L^T\ \underset{\sim}{x}\ =\ \underset{\sim}{d} \qquad (3.155)$$

or
$$L\ \underset{\sim}{f}\ =\ \underset{\sim}{d} \qquad (3.156)$$

where
$$\underset{\sim}{f}\ =\ L^T\ \underset{\sim}{x} \qquad (3.157)$$

The solution is obtained in two stages; firstly a 'forward substitution', equation (3.156), to obtain the vector $\underset{\sim}{f}$, and secondly a back substitution, equation (3.157), to obtain $\underset{\sim}{x}$, the vector of unknowns.

The vector of unknowns consists of the small corrections $\Delta x_1$, $\Delta x_2$, . . $\Delta x_k$, to the initial approximate estimates of the unknown parameters. Improved estimates of these unknowns are obtained by adding (see equation (3.141)) the corrections to the initial values. If the corrections are within the limits of the linearisation then these will be the 'final' values of the unknowns, otherwise the process may be repeated with the new estimates replacing the original approximate values. Furthermore, the vector of unknowns may also be substituted into equation (3.148) to obtain the vector of residuals $\underset{\sim}{v}$. The computation of the covariance matrix of the unknowns and the analysis of the residuals are discussed in § 3.4.5.

## 3.4.3 Observation Equations

The generalised least squares observation equation for a range measurement, linearised about the approximate values is given by equation (3.147). For the dynamical analysis of laser ranging observations this equation, for an individual range measurement, may be expressed as,

$$\sum_{j=1}^{6} \frac{\partial r}{\partial r_{0j}} \Delta r_{0j} + \sum_{j=1}^{np} \frac{\partial r}{\partial p_j} \Delta p_j + \sum_{j=1}^{ne} \frac{\partial r}{\partial e_j} \Delta e_j + \quad (3.158)$$

$$+ \sum_{j=1}^{3} \frac{\partial r}{\partial R_{sj}} \Delta R_{sj} = (r_{io} - r_{ic}) + v_i$$

where

$r_{0j}$  : a component of the initial position and velocity vectors (inertial frame), $\underset{\sim}{r}_0$ and $\dot{\underset{\sim}{r}}_0$,

$p_j$  : any force model unknown (i.e. $C_R$, $C_T$, $C_D$, GM etc, as given in § 3.3 ),

$n_p$  : number of force model unknowns in the solution,

$e_j$  : an earth rotation parameter $x_p$, $y_p$, or UT1-UTC (see § 3.2.5 and Chapter 4),

$n_e$  : number of earth rotation parameter unknowns in the solution,

$R_{sj}$  : a component of the earth fixed position vector, $\underset{\sim}{R}_s$, of stations (tracking station coordinates),

$r_{io}$, $r_{ic}$ : observed and computed values the $i^{th}$ range,

$v_i$ : least squares residual,

and the range, r, between the satellite and the tracking station, s, is given by,

$$r = ((x - x_s)^2 + (y - y_s)^2 + (z - z_s)^2)^{\frac{1}{2}} \quad (3.159)$$

or by,

$$r = ((X - X_s)^2 + (Y - Y_s)^2 + (Z - Z_s)^2)^{\frac{1}{2}} \quad (3.160)$$

where

x, y, z : $\underset{\sim}{r}$, inertial frame coordinates of the satellite,

$x_s$, $y_s$, $z_s$ : $\underset{\sim}{r}_s$, inertial frame coordinates of the tracking station,

X, Y, Z : $\underset{\sim}{R}$, earth fixed coordinates of the satellite,

$X_s$, $Y_s$, $Z_s$ : $\underset{\sim}{R}_s$, earth fixed coordinates of the tracking station,

Clearly, the range between the tracking station and the satellite is independent of the reference system, and so may be evaluated by either (3.159) or (3.160). The coordinates of the satellite and tracking station (because of the effects of solid earth and ocean tides) must be computed at the epoch of each observation, which for Satellite Laser Ranging is, generally, the epoch of reflection of the laser pulse at the satellite.

The observation equation (3.158) is a general form, and the choice of unknowns in the solution will dictate the particular terms of the equation. In order to constrain certain unknowns to pre-determined or arbitrary values it is possible to introduce additional 'observation equations' with suitably high weights, of the form,

$$\Delta u = (u_o - u_c) + v \qquad (3.161)$$

where   $u$   :   any unknown parameter in (3.158),

$u_o$, $u_c$ :   observed and computed values of the unknown, these would normally both be equal to the required value of the unknown.

For example, to fix the longitude of one of the tracking stations (as is indeed necessary when processing laser ranging observations) then an 'observation' of the from of (3.161) is introduced, as given by,

$$\Delta \lambda_s = (\lambda_{so} - \lambda_{sc}) + v \qquad (3.162)$$

where $\lambda_s$ is the earth fixed longitude of tracking station s. However, $\Delta \lambda_s$ is not one of the unknown cartesian tracking station coordinates in equation (3.158), but $\lambda_s$ is related to $X_s$ and $Y_s$ by equation (3.25) as,

$$\lambda_s = \tan^{-1} \left( \frac{Y_s}{X_s} \right) \qquad (3.163)$$

The observation equation (3.162) may be written in terms of $\Delta X_s$ and $\Delta Y_s$ as,

$$\frac{\partial \lambda_s}{\partial X_s} \Delta X_s + \frac{\partial \lambda_s}{\partial Y_s} \Delta Y_s = (\lambda_{so} - \lambda_{sc}) + v \qquad (3.164)$$

where
$$\frac{\partial \lambda_s}{\partial X_s} = \frac{-Y_s}{X_s^2 + Y_s^2} \qquad (3.165)$$

and
$$\frac{\partial \lambda_s}{\partial Y_s} = \frac{X_s}{X_s^2 + Y_s^2} \qquad (3.166)$$

The longitude of station s may then be fixed assigning a sufficiently high weight (low standard error) to the 'observation equation'.

To form the observation equations it is first necessary to evaluate the various partial derivative coefficients of equation (3.158). The coefficients of the tracking station coordinates are the simplest to compute and are derived from the differentiation of equation (3.160) to give,

$$\frac{\partial r}{\partial R_{sj}} = \frac{R_{sj} - R_j}{r} \qquad (3.167)$$

where $R_{sj}$ : $X_s$, $Y_s$, $Z_s$ - a component of the earth fixed tracking station coordinate vector,

$R_j$ : X, Y, Z - the corresponding component of the earth fixed satellite coordinate vector.

For an earth rotation parameter, the partials may be expanded to give,

$$\frac{\partial r}{\partial e_i} = \frac{\partial r}{\partial X_s}\frac{\partial X_s}{\partial e_i} + \frac{\partial r}{\partial Y_s}\frac{\partial Y_s}{\partial e_i} + \frac{\partial r}{\partial Z_s}\frac{\partial Z_s}{\partial e_i} \qquad (3.168)$$

The partials of range with respect to a coordinate component may be evaluated using equation (3.167), the remaining partials may be expressed in vector form as,

$$\frac{\partial \underset{\sim}{R}_s}{\partial e_i} = \left( \frac{\partial X_s}{\partial e_i} , \frac{\partial Y_s}{\partial e_i} , \frac{\partial Z_s}{\partial e_i} \right) \qquad (3.169)$$

However, as the earth fixed coordinates of tracking station s are related to the corresponding inertial frame coordinates by equation (3.34), i.e.

$$\underset{\sim}{R}_s = P \, E \, N \, Q \, \underset{\sim}{r}_s$$

then
$$\frac{\partial \underset{\sim}{R}_s}{\partial e_i} = \frac{\partial}{\partial e_i} ( P \, E \, N \, Q \, \underset{\sim}{r}_s ) \qquad (3.170)$$

which for the components of polar motion, $x_p$, $y_p$, may be written as,

$$\frac{\partial \underset{\sim}{R}_s}{\partial x_p} = \frac{\partial P}{\partial x_p} ( E \, N \, Q \, \underset{\sim}{r}_s ) \qquad (3.171)$$

$$\frac{\partial \underset{\sim}{R}_s}{\partial y_p} = \frac{\partial P}{\partial y_p} ( E \, N \, Q \, \underset{\sim}{r}_s ) \qquad (3.172)$$

As a change in universal time, $\Delta$UT1, is related to a change in Greenwich Apparent Sidereal Time, $\Delta$GAST, by equation (3.39), observation equations may be formed in terms of $\Delta$GAST in order to determine $\Delta$(UT1-UTC). The coefficient from equation (3.170) is given by,

$$\frac{\partial \underset{\sim}{R}_s}{\partial \text{GAST}} = P \, \frac{\partial E}{\partial \text{GAST}} \, N \, Q \, \underset{\sim}{r}_s \qquad (3.173)$$

The coefficients for the satellite state vector unknowns and the force model unknowns are given by,

$$\frac{\partial r}{\partial r_{0i}} = \frac{\partial r}{\partial x}\frac{\partial x}{\partial r_{0i}} + \frac{\partial r}{\partial y}\frac{\partial y}{\partial r_{0i}} + \frac{\partial r}{\partial z}\frac{\partial z}{\partial r_{0i}} \qquad (3.174)$$

and

$$\frac{\partial r}{\partial p_i} = \frac{\partial r}{\partial x}\frac{\partial x}{\partial p_i} + \frac{\partial r}{\partial y}\frac{\partial y}{\partial p_i} + \frac{\partial r}{\partial z}\frac{\partial z}{\partial p_i} \qquad (3.175)$$

The partials $\frac{\partial r}{\partial x}$, $\frac{\partial r}{\partial y}$ and $\frac{\partial r}{\partial z}$ may be simply evaluated by differentiating equation (3.159), for example,

$$\frac{\partial r}{\partial r_j} = \frac{r_j - r_{sj}}{r} \qquad (3.176)$$

where $r_j$, $r_{sj}$ : corresponding components of the inertial frame position vector of the satellite and the station , s.

However, the partials of the satellite position vector with respect to the components of the initial state vector and with respect to the force model unknowns must be evaluated by numerical integration of the acceleration partials. These are integrated once, to give the velocity partials and twice to give the position partials as a function of time. The partial derivatives with respect to the state vector components (and similarly for the the force model unknowns) are given by,

$$\frac{\partial \dot{r}_j}{\partial r_{0i}} = \left(\frac{\partial \dot{r}_j}{\partial r_{0i}}\right)_{t_0} + \int_{t_0}^{t} \frac{\partial \ddot{r}_j}{\partial r_{0i}}\, dt \qquad (3.177)$$

and

$$\frac{\partial r_j}{\partial r_{0i}} = \left( \frac{\partial r_j}{\partial r_{0i}} \right)_{t_0} + \int_{t_0}^{t} \frac{\partial \dot{r}_j}{\partial r_{0i}} \, dt \qquad (3.178)$$

where $\ddot{r}_j$, $\dot{r}_j$ : components of the inertial frame acceleration and velocity vectors (at time t), $\ddot{\underset{\sim}{r}}$ and $\dot{\underset{\sim}{r}}$.

The acceleration partials, with respect to the state vector unknowns are given by,

$$\frac{\partial \ddot{r}_j}{\partial r_{0i}} = \frac{\partial \ddot{r}_j}{\partial x} \frac{\partial x}{\partial r_{0i}} + \frac{\partial \ddot{r}_j}{\partial y} \frac{\partial y}{\partial r_{0i}} + \frac{\partial \ddot{r}_j}{\partial z} \frac{\partial z}{\partial r_{0i}} + \qquad (3.179)$$

$$+ \frac{\partial \ddot{r}_j}{\partial \dot{x}} \frac{\partial \dot{x}}{\partial r_{0i}} + \frac{\partial \ddot{r}_j}{\partial \dot{y}} \frac{\partial \dot{y}}{\partial r_{0i}} + \frac{\partial \ddot{r}_j}{\partial \dot{z}} \frac{\partial \dot{z}}{\partial r_{0i}}$$

and with respect to the force model unknowns

$$\frac{\partial \ddot{r}_j}{\partial p_i} = \frac{\partial \ddot{r}_j}{\partial x} \frac{\partial x}{\partial p_i} + \frac{\partial \ddot{r}_j}{\partial y} \frac{\partial y}{\partial p_i} + \frac{\partial \ddot{r}_j}{\partial z} \frac{\partial z}{\partial p_i} + \qquad (3.180)$$

$$+ \frac{\partial \ddot{r}_j}{\partial \dot{x}} \frac{\partial \dot{x}}{\partial p_i} + \frac{\partial \ddot{r}_j}{\partial \dot{y}} \frac{\partial \dot{y}}{\partial p_i} + \frac{\partial \ddot{r}_j}{\partial \dot{z}} \frac{\partial \dot{z}}{\partial p_i} + \frac{\partial \ddot{r}_{jpi}}{\partial p_i}$$

where $\dfrac{\partial \ddot{r}_{jpi}}{\partial p_i}$ : obtained by direct differentiation of the force model component containing the parameter, $p_i$. For example, for the reflectance coefficient $C_R$, $\dfrac{\partial \ddot{r}_{jCR}}{\partial C_R}$ would be obtained by differentiation of equation (3.110).

The partial derivatives $\dfrac{\partial \ddot{r}_j}{\partial x}$, $\dfrac{\partial \ddot{r}_j}{\partial \dot{x}}$ etc, may be evaluated as the sum of the individual partial derivatives, obtained by differentiation of all the components of

the force model in turn. However, as least squares provides only a first order correction, the only significant contribution to the acceleration partials is due to the geopotential field of the earth and the effect of all the other force model components may be neglected. The acceleration partials for the acceleration of the satellite due to the earth's gravity field are derived in Agrotis (1984), together with a discussion on the effects of neglecting other forces.

The integration is carried out using the numerical procedures described in § 3.4.1. For the integration to start initial values of $\dfrac{\partial r_j}{\partial r_{0i}}$ at the starting epoch $t_0$ must be provided as given by,

$$\left( \frac{\partial r_j}{\partial r_{0i}} \right)_{t_0} = 1 \quad \text{when } i = j \tag{3.181}$$

and

$$\left( \frac{\partial r_j}{\partial r_{0i}} \right)_{t_0} = 0 \quad \text{when } i \neq j \tag{3.182}$$

for example, from equation (3.181),

$$\left( \frac{\partial x}{\partial x_0} \right)_{t_0} = \frac{\partial x_0}{\partial x_0} = 1 \tag{3.183}$$

and

$$\left( \frac{\partial y}{\partial x_0} \right)_{t_0} = \frac{\partial y_0}{\partial x_0} = 0 \tag{3.184}$$

Similarly, initial values of the velocity partials must also be given, such that,

$$\left( \frac{\partial \dot{r}_j}{\partial \dot{r}_{0i}} \right)_{t_0} = 1 \quad \text{when } i = j \qquad (3.185)$$

and

$$\left( \frac{\partial \dot{r}_j}{\partial \dot{r}_{0i}} \right)_{t_0} = 0 \quad \text{when } i \neq j \qquad (3.186)$$

where

$\dot{r}_{0i}$ : a component of the initial velocity vector $\dot{\underset{\sim}{r}}_0$.

Finally for any force model unknowns,

$$\left( \frac{\partial r_j}{\partial p_i} \right)_{t_0} = 0 \quad \text{for all } i \text{ and } j \qquad (3.187)$$

As the satellite ephemeris is required to a higher accuracy than the partials, satisfactory accuracy is maintained by choosing the step length of this numerical integration to be the same as for the determination of the ephemeris (see § 3.4). A step length of 120 seconds has been found to be suitable for LAGEOS (Ashkenazi, Agrotis and Moore, 1984).

### 3.4.4 Least Squares Adjustment Minimum Requirements

The least squares adjustment of the orbital starting elements and the tracking station coordinates using laser ranging measurements constitutes a 3-dimensional network adjustment. As with all 3-D networks the normal equations, as given by equation (3.152), are singular with seven degrees of freedom. Consequently, in order to carry out a solution seven constraints must be imposed, such that three locate the origin of the coordinate system, three orientate the

axes and one determines the scale of the network. If all these constraints are not provided the normal equations will be rank deficient by the number of constraints not specified.

In the dynamical analysis of laser ranging observations (or indeed, any orbit determination process with other satellite observations) the three origin conditions are satisfied by the model of the earth's gravity field. If the gravity field is represented by the spherical harmonic expansion, as in equation (3.64), then the coefficients $C_1^0$, $C_1^1$ and $S_1^1$ represent the first moments of mass of the earth about the origin of the coordinate reference system. By setting these coefficients to zero, in the expansion, then by implication the origin is located at the mass centre of the earth.

The orientation of the axes is partly satisfied by the adopted values of the polar motion components $x_p$ and $y_p$. These specify the direction of the Z-axis of the earth fixed coordinate system with respect to the instantaneous spin axis of the earth. However, there is still a deficiency in orientation, because the coordinate axes are free to rotate about this Z-axis. This freedom is constrained by fixing the longitude of one of the tracking stations, by introducing an 'observation equation' such as equation (3.164) before forming the normal equations. Clearly this provides a reference meridian for the tracking station solution

and the adoption of different values will introduce a systematic bias in the tracking station coordinates.

Both the speed of light, c, and the geocentric gravitational constant, GM, provide a constraint on the scale of the network and so the two values must be compatible with one another. Any discrepancy between the two adopted values may be accounted for by (for example) fixing the speed of light to the conventional value and solving for GM in the least squares solution.

Clearly, in order to carry out a solution for tracking station coordinates, the six orbital starting elements and a number of force model parameters, the only additional constraint required is the fixing of the longitude of one of the tracking stations. However, if polar motion components ($x_p$ and $y_p$) are also being determined, two additional degrees of freedom are added, because of the release of the orientation of the Z-axis. This may be remedied by fixing the latitudes of two of the tracking stations in addition to the one fixed longitude. Typically, the positions of a number of tracking stations would be fixed, their coordinates having been determined previously using published values of the polar motion components (for example, BIH circular D).

As discussed in § 3.4.3, UT1-UTC may not be determined directly as an unknown from the least squares solution, however GAST may be determined, and

is related to UT1-UTC by a simple expression, equation (3.39). Furthermore, it was seen in § 3.1 that the satellite coordinates are generated (by the numerical integration procedure) in the inertial reference frame and are transformed to the earth fixed frame by the rotation matrices of equation (3.34), of which the matrix E is a function of GAST. Consequently, it is not possible to simultaneously determine absolute values of UT1-UTC and the satellite initial state vector, because this would allow the orbit to be free to rotate. Therefore when determining values of UT1-UTC (i.e. GAST) it is necessary to either hold the components of the initial state vector fixed (to some pre-determined values), or if determining a number of values of UT1-UTC at different epochs, to hold one value fixed at some reference epoch.

The procedures for determining earth rotation parameters ($x_p$, $y_p$ and UT1-UTC) are discussed in more detail in Chapter 4.


### 3.4.5 Residual and Error Analysis

This section is concerned with the 'accuracy' of the observations and the determined parameters, and the detection of 'poor' observations. The term 'accuracy' is rather a vague description, and it is preferable to divide 'accuracy' into four components and discuss 'precision', 'reliability', 'systematic biases' and 'repeatablility'. The precision of a quantity is

defined by its a posteriori standard error, determined from the covariance matrix of the unknowns (these quantities are discussed later in this section). However, precision does not take into account systematic biases in the results or gross errors in the observations. Systematic biases do not affect the internal consistancy of the solution and so may only be detected through comparison with other (external) 'correct' solutions. The reliability of a 3-dimensional network represents the ability of a network to detect gross errors in the observations. With laser ranging data sets this is rarely a problem as there are usually many ranges to the satellite from each tracking station. The final 'accuracy' criteria is repeatabilty, which represents the ability of a network to reproduce the same results with different sets of data. The precision of the determined quantities and the reliability of the observations are considered in the remainder of this section.

Following the solution of the least squares normal equations (3.153), the vector of unknowns, $\underset{\sim}{x}$, may be substituted into equation (3.148) to determine the vector of least squares residuals $\underset{\sim}{v}$, as,

$$\underset{\sim}{v} = A \underset{\sim}{x} - \underset{\sim}{b} \qquad (3.188)$$

From these residuals two statistics may be evaluated. Firstly by considering only the range residuals, the root-mean-square range residual may be computed from,

$$\sigma_R = \left( \frac{v^T v}{n_R} \right)^{\frac{1}{2}} \tag{3.189}$$

where  $n_R$  :  number of range observations,

$\sigma_R$  :  root-mean-square range residual.

The 'rms' residual provides an indication of the mean precision of the range measurements and also the level of agreement between the computed orbit and the orbit implied by the observed ranges. Secondly, the mean square error of an observation of unit weight, denoted by $\sigma_0^2$ may be evaluated from (Ashkenazi, 1970),

$$\sigma_0^2 = \frac{v^T W v}{n - k} \tag{3.190}$$

where  W  :  the 'weight' matrix, as defined by equation (3.150),

n  :  total number of observations,

k  :  number of unknowns.

If the weights applied to the observations were 'on average' estimated correctly then 'sigma zero squared', $\sigma_0^2$ should equal unity. However, if they were not then the original weight matrix may be corrected using,

$$W_{(unbiased)} = \frac{1}{\sigma_0^2} W_{(estimated)} \tag{3.191}$$

The residuals may be used to detect gross errors in the observations. If a residual is large when compared with its corresponding standard error then the observation may be suspected to be in error. The rejection criteria, and the determination of the

standard error of a residual are considered later in this section.

The covariance matrix of the unknowns gives an indication of the strength of the three dimensional network and estimates of the a posteriori (after adjustment) precisions of the unknowns and observed quantities. The covariance matrix, $\sigma_{xx}$ is defined as,

$$\sigma_{xx} = \begin{pmatrix} \sigma^2_{x_1} & \sigma_{x_1 x_2} & \cdot & \cdot & \cdot & \sigma_{x_1 x_k} \\ \sigma_{x_2 x_1} & \sigma^2_{x_2} & \cdot & \cdot & \cdot & \sigma_{x_2 x_k} \\ \cdot & \cdot & & & & \cdot \\ \cdot & \cdot & & & & \cdot \\ \cdot & \cdot & & & & \cdot \\ \sigma_{x_k x_1} & \sigma_{x_k x_2} & \cdot & \cdot & \cdot & \sigma^2_{x_k} \end{pmatrix} \qquad (3.192)$$

where $\sigma^2_{x_i}$ : variance of the $i^{th}$ unknown, $x_i$,

$\sigma_{x_i x_j}$ : covariance of a pair of unknowns $x_i$, $x_j$

It can be shown (Ashkenazi, 1970) that this matrix is given by,

$$\sigma_{xx} = \sigma^2_0 N^{-1} = \sigma^2_0 (A^T W A)^{-1} \qquad (3.193)$$

The covariance matrix can be used to determine the standard errors of any quantity in the adjustment, whether an observation, an unknown, or neither. The standard errors of the unknown quantities, such as the cartesian coordinates of the tracking stations, are merely the respective diagonal elements of the matrix. For quantities derived from unknowns, such as the distances (baselines) between the tracking stations or

indeed the computed ranges, it is necessary to use Gauss' propagation of error theorems. These state that if a scalar quantity, y, is a linear function of the unknowns, as given by,

$$y = \underset{\sim}{f}^{\tau} \cdot \underset{\sim}{x} \tag{3.194}$$

where

$$\underset{\sim}{f}^{\tau} = (f_1, f_2, f_3, \ldots f_k) \tag{3.195}$$

then

$$\sigma_y^2 = \underset{\sim}{f}^{\tau} \sigma_{xx} \underset{\sim}{f} \tag{3.196}$$

For example, the variance of a baseline $L_{ij}$ between two stations $s_i$ ans $s_j$ is given by,

$$\sigma_{L_{ij}}^2 = \underset{\sim}{g}^{\tau} \sigma_{xx_{ij}} \underset{\sim}{g} \tag{3.197}$$

$$\underset{\sim}{g}^{\tau} = \left( \frac{X_i - X_j}{L}, \frac{Y_i - Y_j}{L}, \frac{Z_i - Z_j}{L}, \right. \tag{3.198}$$

$$\left. \frac{X_j - X_i}{L}, \frac{Y_j - Y_i}{L}, \frac{Z_j - Z_i}{L} \right)$$

with

$$L^2 = (X_i - X_j)^2 + (Y_i - Y_j)^2 + (Z_i - Z_j)^2 \tag{3.199}$$

and $\sigma_{xx_{ij}}$ : (6 × 6) matrix, the corresponding section of the covariance matrix of the unknowns,

$X_i, Y_i, Z_i$ : earth fixed coordinates of station i,

$X_j, Y_j, Z_j$ : earth fixed coordinates of station j,

Similarly, for the $i^{th}$ observation (range measurement) the a posteriori variance is given by,

$$\sigma_r^2 \text{ (a posteriori)} = A_i^{\tau} \sigma_{xx} A_i \tag{3.200}$$

where $A_i$ : coefficients of the $i^{th}$ observation

equation, i.e. the $i^{th}$ row of the

A matrix, see equation (3.148),

$\sigma_{xx}$ : the full covariance matrix as defined by

equation (3.193).

The reliability of an observation, that is the ability the network to detect a gross error in that observation, may be assessed (Crane, 1980) by the ratio of the a posteriori standard error to the 'unbiased' a priori standard error, as given by equation (3.191). A totally unreliable observation would result in a ratio of unity and a decrease in the ratio implies an increased reliability.

As discussed previously, reliable observations containing gross errors will result in corresponding large residuals. However, the significance of these must be assessed by comparing them with the standard error of the residuals. If the ratio of $v_i/\sigma_{vi}$ is assumed to be normally distributed then it is possible to assess the probability that the observation contains a gross error. For example, only 5% of the observations should have an absolute value of $v_i/\sigma_{vi}$ of greater than 2.0 and only 1% greater than 2.5. The standard error of a residual, $\sigma_{vi}$, may be computed (Crane, 1980) using,

$$\sigma^2_{vi} = \sigma^2_{ri} \text{ (a priori)} - \sigma^2_{ri} \text{ (a posteriori)} \quad (3.201)$$

If the observation is, however, reliable then the

a posteriori standard error will be small compared to the a priori value and the standard error of the residual may be approximated to be equal to the unbiased a priori standard error of the observation.

When processing laser ranging observations, the problem of local reliability in the network rarely arises, as typically many observations contribute to the unknown parameters. However, although the data is filtered before input to the analysis stage, the ability to detect spurious observations is invaluable. It is also beneficial to compute the a posteriori standard errors of the observations, and more importantly of the unknowns, to assess the precision of the solution. These estimates of the precision are, however, frequently over optimistic as they only represent the 'internal' precision of the adjustment. Only by comparing the results of the adjustment with externally obtained values, for example tracking station coordinates computed by another analysis centre or derived from a different observation technique (such as VLBI), is it possible to assess the 'external' or 'absolute' precision of the unknowns.

CHAPTER   FOUR

DETERMINATION OF EARTH ROTATION PARAMETERS

## 4.1 INTRODUCTION

Although it is often convenient to think of the earth as rotating around a fixed pole at a fixed rate, this is not the case, and in fact the axis is not fixed nor is the rate of rotation constant. The importance of the study and monitoring of these variations has been recognised for many years, and indeed, they were predicted several centuries before the phenomena were observed.

The instantaneous orientation of the earth with respect to a fixed celestial reference system is described by four principal effects; precession, nutation, polar motion and variations in the rate of rotation. As discussed in § 3.2.4, the effects of precession and nutation may be simply evaluated from available models. However, in order to formulate these models the constants and coefficients must be determined from observations, because of our currently inadequate knowledge of the internal structure of the earth. This thesis, however, is not concerned with the development of models for precession and nutation, but with the determination of the direction of the earth's axis of rotation, with respect to the surface of the earth (the polar motion), and the variations of the rate of rotation of the earth about this axis. Over recent years the term, 'earth rotation parameters' or ERP, has been commonly used to collectively refer to the two components of polar motion and the variations

in the rotation rate. This term is also used throughout
this thesis, in preference to the alternative, 'earth
orientation parameters'

The instantaneous axis of rotation of the earth
is not fixed with respect to the body of the earth, but
moves periodically, anti-clockwise, around a roughly
circular path about a mean position. This simplified
description describes, approximately, the effect known
as the 'polar motion'. With no observational data
Euler, in 1765, predicted the existence of polar motion
and by assuming the earth was a rigid body concluded
that it must have a principal period of 300 days.
However, because of the elasticity of the earth, this
period is in fact of the order of 428 days (around 14
months), the 'Chandler Period'. This motion, which is
generally known as the 'Chandler Wobble', is a result
of a slight offset between the axis of rotation of the
earth and the axis of maximum inertia, and has an
amplitude of between 0.08 and 0.18 seconds of arc
(around 2.4 to 5.4 metres on the surface of the earth).
In addition, there is also a similar, approximately
circular, seasonal motion with a period of one year and
an amplitude of between 0.06 and 0.10 arc seconds
(Bomford, 1980). Polar motion values determined over
several years indicate there may also be a long term
drift of the mean orientation of the axis of rotation.

The motion of the pole is described by two small
angles $x_p$ and $y_p$, between the instantaneous axis of

rotation and the mean axis of rotation of the earth, and in the direction of the Greenwich meridian and the $90^0$ west meridian (respectively). The reference direction, fixed with respect to the body of the earth, is known as the Conventional International Origin (CIO), which is defined as the average direction of the rotation axis during the years 1900 - 1905. The CIO was originally defined by the adopted latitudes of the five observatories of the International Latitude Service (ILS, see § 4.2). Polar motion cannot be predicted accurately, because the geophysical phenomena which excite the motion are not fully understood, and so must be determined by observations. The two components of polar motion, published by the BIH (see § 4.2), over the past five years are plotted in fig 4.I.

Traditionally, the basic unit of time was defined by tne diurnal rotation of the earth, which was assumed to be uniform despite the suspicion of variations in the rate. The length of day was determined from observations of the transits of stars across the meridians of a number of astronomical observatories. As clocks became more precise, through pendulums, quartz crystal oscillators and eventually atomic frequency standards (which have stabilities of the order of a few parts in $10^{13}$), the complex variations in the length of day became apparent. These fluctuations may be classified as seasonal, irregular variations and a secular decrease in the rate of
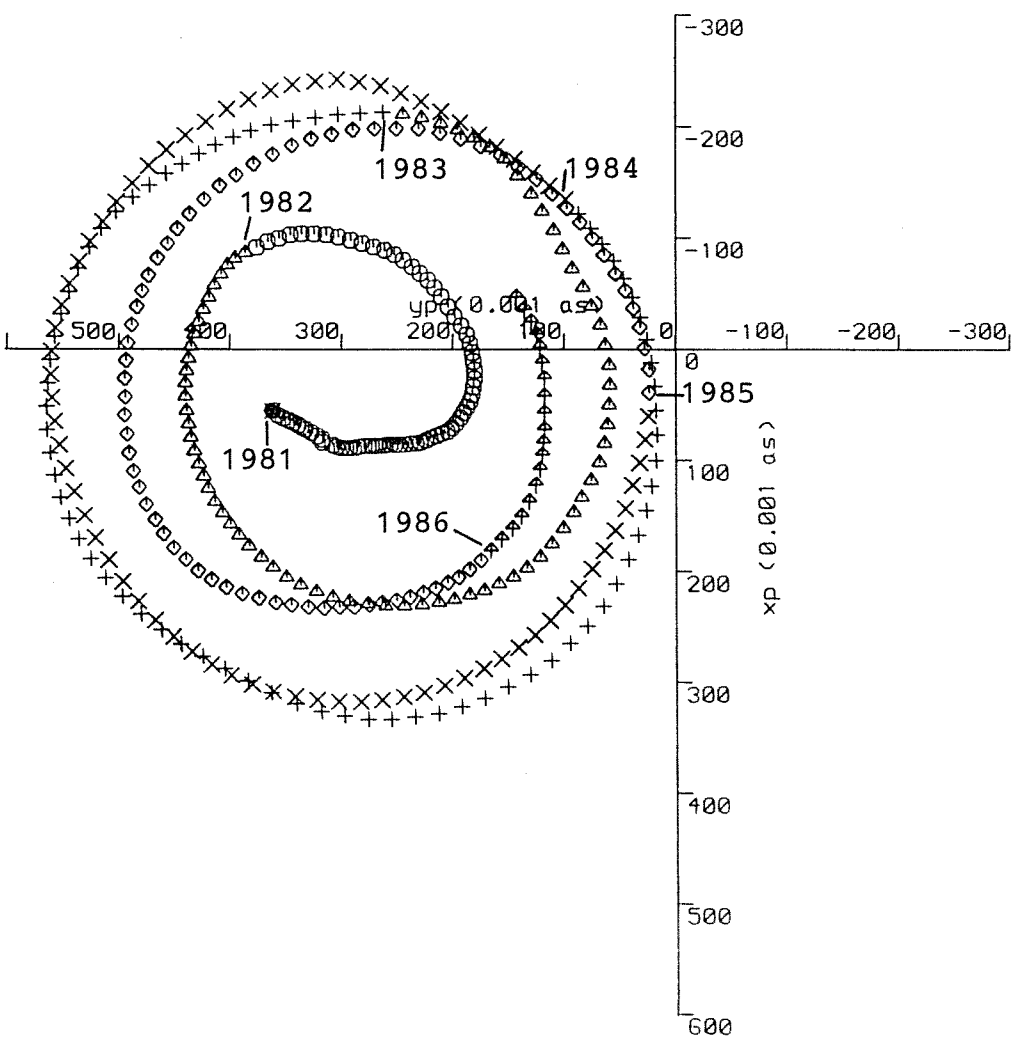
Fig 4.I BIH polar motion

rotation. Around 20 years ago atomic clocks took over the role of defining the basic unit of time, however the variations in the rotation of the earth are still monitored for scientific research and other applications. The secular decrease in the rate of rotation, of about 5ms per year, is generally attributed to the tidal forces of the earth-moon system (Mueller, 1969). At shorter periods, irregular fluctuations in the length of day show a high correlation with changes in the angular momentum of the atmosphere (Lambeck and Cazenave, 1973).

In order to determine the variations in the rate of rotation of the earth, it is necessary to compare a time scale derived from astronomical observations, and so dependent on the earth's rotation, with an atomic based time scale. The time scales UT1, UTC and TAI are defined in § 3.2.3 and clearly the difference, UT1-UTC and UT1-TAI reveal fluctuations in the rotation rate. The excess length of day, D, may also be used to express the variations, and is defined as the difference between the actual length of day and a standard length of day of 86400.0 SI seconds.

An accurate knowledge of the orientation of the earth with respect to a fixed celestial reference system (inertial frame) has applications in geodesy, navigation, astrometry and in geophysics. Geodetic positioning by astronomical or satellite techniques requires a knowledge of the orientation of the earth at

the instant of observation, with respect to the reference system used for the stars or the satellite orbit. Clearly, different applications have different positioning requirements and corresponding requirements for the precision of the earth rotation parameters. For example, for many navigation purposes the effects of polar motion may be neglected and a knowledge of Universal Time (UT) is only required to the nearest second. However, for precise, centimetre level, geodetic positioning for earthquake research or tectonic plate studies, earth rotation parameters of a very high precision (a few milli-arc-seconds for polar motion and around 0.1 milli-seconds in Universal Time) are required. Recent developments of the techniques of Satellite Laser Ranging and Very Long Baseline Interferometry are resulting in these high levels of precision of positioning, and also the precise earth rotation parameters required for the reduction of the data.

The geophysical community is also interested in the variations of the orientation of the earth because many of the short and long period effects are excited by geophysical forces that may not be measured directly. For example, changes in the mass distribution of the earth due to earthquakes and the melting of the polar ice and glaciers, and the coupling between the atmosphere and the earth (and also between the core and the mantle), all have an effect on the earth rotation parameters.

## 4.2    INTERNATIONAL MONITORING SERVICES

The first international cooperating service formed specifically  to monitor earth rotation parameters was the International Latitude Service (ILS). This was established in 1899 by the International Astronomical Union and the International Geodetic Association. As the name suggests, the ILS was set up to monitor polar motion by determining the astronomical latitudes of five optical observatories around the world. There observatories were all close to the $38^0$ $8'$ N parallel at Mizusawa (Japan), Kitah (USSR), Carloforte (Italy), Gaithersburg (USA) and Ukiah (USA). The latitudes of these stations defined the Conventional International Origin (IUGG, 1967). The ILS was succeeded  by the International Polar Motion Service (IPMS) which since 1962 has been based in Japan and regularly publishes values of polar motion. The five observatories of the ILS are used in conjunction with observations from about fifty other optical observatories around the world. An assortment of photo zenith tubes, zenith telescopes, astrolabes and meridian transit telescopes contribute data to the IPMS.

In 1912 the Bureau Intrnational de l'Heure (BIH) was established at the Paris Observatory, to provide an international time scale based on the rotation of the earth. The aim was to produce a unified time system which would be related to the time signals broadcast by

observatories through published offsets. Currently the BIH is responsible for the maintenance of the international atomic and universal time scales. Although the principal role of the BIH is the determination of universal time, polar motion values are also derived during the reduction of the observations . In 1979, astrometric observations were made with 80 instruments at 60 observatories around the world, many of which are common with those used by the IPMS (Feissel, 1980).

The origin of the BIH polar motion values was made to agree with the CIO in 1968. From 1973 onwards, the polar motion series derived from the Doppler tracking of the Transit satellites has been combined with the optical astrometric values in the BIH published polar motion series. It subsequently became evident from the Doppler values that systematic biases, resulting from the classical astrometric techniques, were included in the 1968 BIH system. This was also apparent when polar motion values derived from laser ranging measurements to the moon were introduced. As a result, the 1979 BIH system was introduced which, by using a number of years of Doppler observations, removed the systematic effects of the classical optical methods. In recent years, in addition to the Doppler measurements, earth rotation parameters derived from Satellite and Lunar Laser Ranging and Very Long Baseline Interferometry have also been introduced, and

are becoming increasingly dominant over the published
BIH values.

The earth rotation parameters determined by the
BIH are published monthly, with a delay of about two
months, in the BIH circular D. The complete annual
series is also published in the BIH Annual Report for
the respective year. In addition to these 'delayed'
values the BIH also provides a Rapid Service on a
weekly basis which is published in the Earth
Orientation Bulletin (Series 7 Time Service
Publication) of the United States Naval Observatory.
This latter publication also reproduces earth rotation
parameters derived at the USNO and at other
establishments from astrometric, Doppler and laser
ranging observations.

The history and operation of the earth rotation
and polar motion monitoring services is outlined by
Guinot (1978), and further details of the analysis
procedures and publications of the IPMS and BIH are
given by Wilkins (1980a).

4.3   EARTH ROTATION PARAMETERS FROM LASER RANGING

4.3.1 <u>Basic</u> <u>Principles</u>

The traditional astrometric method of determining earth rotation parametes involves the measurement of the variations of latitude and Universal Time at a number of observatories around the world. The variations are determined with respect to a set of fixed positions for a catalogue of stars. Clearly, each station may only detect the component of polar motion along the meridian passing through the observatory. However, by combining observations from a number of well distributed sites the earth rotation parameters may be obtained.

The application of satellite techniques may be considered an analogous situation with the satellite in orbit replacing the stars. A complication arises in that, the tracking systems used to orientate the earth with respect to the orbit must also be used, in turn, to establish the orbit of the satellite. The early experiments to determine earth rotation parameters from a single laser ranging station (Kolenkiewicz et al, 1977) approached this problem by first establishing a reference orbit from a long period of data (say, one month). The movements of the tracking station (and hence the earth rotation parameters, variation in latitude and length of day) were subsequently obtained by comparison of short period orbits (say, 12 hours) with the reference orbit. However, the drawback of this

approach was the requirement for very precise modelling of the perturbing forces on the satellite during the computation of the long reference orbit. Any errors would subsequemtly appear as apparent variations of the tracking station coordinates.

The approach adopted by the majority of analysts of Satellite Laser Ranging observations is to use a network of tracking stations, in preference to a single station. Consider a situation in which the coordinates of a number of tracking stations, in an earth fixed reference system, are well known and a satellite is tracked during two different periods. If the tracking stations are common to both periods of observations then it is possible to simultaneously determine the satellite's orbit and the (average) coordinates of the point about which the network of tracking stations rotated between the two periods. This method of determining the pole position does not require a very long precise orbit to be computed and shorter orbits (with a corresponding increase in accuracy) may be used. A network approach has been used by the US Department of Defense to routinely derive polar motion components from satellite Doppler (Transit) tracking data since the early 1970's (Anderle, 1973).

As previously shown in § 3.4.3, corrections to provisional polar motion and earth rotation (GAST and hence UT1-UTC) may be included as unknowns in the least squares dynamical analysis of laser ranging data (the

process described in Chapter 3). Although the simple example, of the network approach, given above may suggest it is necessary to fix the coordinates of all the tracking stations, this is not strictly true when analysing laser ranging data and the minimum constraints actually required are given in § 3.4.4. There are, however, several different ways of satisfying these constraints. As a result a number of different analysis procedures for the determination of earth rotation parameters have been implemented by the various laser ranging analysis centres. The procedure developed and adopted at Nottingham is discussed in the following section.

## 4.3.2 Analysis Procedure

As previously discussed (in § 3.4.4), when processing laser ranging observations by the dynamical method it is not possible to simultaneously determine, as unknowns in a solution, the coordinates of all the tracking stations and the two polar motion components, without applying additional constraints. Because of the 'release' of the polar motion components two degrees of freedom are introduced which must be satisfied. By holding the latitudes (in addition to the one fixed longitude, see § 3.4.4) of two of the tracking stations fixed to previously known (and precise) values, the coordinates of all the other tracking stations and the two polar motion components may be determined.

Alternatively, if a solution is to include a number of pairs of polar motion values at a number of different epochs, then by fixing a pair of values at just one epoch all the remaining polar motion values and all the tracking station coordinates may be determined.

A similar situation arises when determining GAST (in order to obtain UT1-UTC, see § 3.4.3), however in this case, GAST and the satellite initial state vector may not be simultaneously determined. If the orbit is expressed in terms of Keplerian orbital elements, rather than the usual cartesian representation (Ashkenazi and Moore, 1986), then by fixing the longitude of the ascending node, to some pre-determined value, the necessary constraint would be applied. However, it is not possible to uniquely distinguish a particular cartesian orbital element in the same way. As a result it is necessary to fix all the elements of the initial satellite state vector to some previously derived values. An alternative method would be, as with the polar motion components, to solve for a number of GAST values at different epochs in a single solution, and satisfy the constraint by holding one value fixed at some reference epoch. Thus allowing the satellite orbit to be released and allowing the initial state vector and the other GAST values to be determined.

It would be clearly preferable to adopt this latter alternative for both polar motion and UT1-UTC (i.e. GAST), as this would allow the satellite state

vector, the tracking station coordinates and a number
of polar motion and UT1-UTC values (at different
epochs) to be simultaneously determined. The only
necessary constraints would be the fixing of the
longitude of one of the tracking stations, and UT1-UTC
and one pair of polar motion values at some reference
epoch. However, the current SODAPOP software package
(see Chapter 5), developed at Nottingham, is not
capable of determining more than one set of earth
rotation parameters in a single solution. Consequently,
a two-stage data processing procedure for determining
earth rotation parameters was adopted. Details of the
data sets processed by this method and the models and
unknowns of the particular solutions are given in
Chapter 6.

Initially, a one month period of laser ranging
data is processed in order to establish a stable
reference orbit and a set of tracking station
coordinates. The necessary constraints are provided by
fixing the longitude of one of the tracking stations
and adopting preliminary values of polar motion and
earth rotation. Typically, these may be taken from
published values, such as the BIH circular D series.
The solution is repeated, iteratively, a number of
times until all the unknown parameters have converged
to the required levels.

Having established the reference orbit and
coordinates of the tracking stations these are then

held fixed for the subsequent stage of the analysis. The one month set of data is split into a number of consecutive short data sets, each spanning a period (for example) of one to five days. The short data sets are processed independently in order to determine the mean earth rotation parameters during the particular period. The resulting series of polar motion and UT1-UTC values may be subsequently used in lieu of the adopted preliminary values, and the first stage of the process repeated to obtain a new reference orbit and coordinate set. If required, or necessary, a revised set of earth rotation parameters may also be obtained, by repeating the second stage. Indeed, the whole computational cycle may be repeated any number of times, although in practice (see, § 6.2.3) this has not been found to be necessary.

### 4.3.3 Post-Processing and Smoothing

The analysis of laser ranging data, to determine earth rotation parameters, results in three series of values at discrete epochs. As polar motion (i.e. $x_p$ and $y_p$) and earth rotation (i.e. UT1-UTC) are time varying quantities then any derived values must be assigned a corresponding epoch. At Nottingham this is calculated as the mean apoch of all the range observations included in the period of data processed,

$$t_{mean} = \frac{1}{n} \sum_{i=1}^{n} t_i \qquad (4.1)$$

where $t_{mean}$ : mean epoch assigned to the earth

    rotation parameters, derived from the

    period of data

  $t_i$  : epoch of the $i^{th}$ range observation

  n   : number of range observations.

The resulting 'raw' time series may be smoothed to remove any high frequency noise and so allow interpolation of the earth rotation parameters to other epochs, as required. The raw values computed or received by the BIH are smoothed using Vondrak's algorithm, in order to produce the continuous smooth series of earth rotation parameters published in the BIH circular D. A comparative discussion of this, and other suitable, methods of smoothing may be found in Feissel and Lewandowski (1984).

The aim at Nottingham was to maintain the raw values and so to avoid any smoothing if at all possible. However, in order to compare the derived earth rotation parameters with those determined at other analysis centres they must first be interpolated to the same epochs. As the BIH circular D values are published for 0.0 hrs UT at 5 day intervals, these epochs were adopted as convenient nominal reference epochs, at which any comparisons would be made. Details of the results of the processing of laser ranging data are given in Chapter 6, however, for the purposes of this discussion it is convenient to mention that the earth rotation parameters were determined at roughly

1 and 5 day intervals. In order to 'transfer' these values to the nominal BIH epochs two different interpolation schemes were used.

For the daily values (of $x_p$, $y_p$, and UT1-UTC) the interpolation consists of a least squares fit of a quadratic function (see Appendix C) to each set of five consecutive values which span either side of the BIH epochs (i.e. the five values whose corresponding epochs are closest to the reference epoch). The daily values are input to the interpolation procedure and are attributed with a priori weights, obtained from the covariance matrices of the individual solutions (see § 3.4.5). This allows the estimation of an a posteriori standard error for the interpolated value, which is obtained by evaluating the quadratic function at the respective BIH epoch.

The raw earth rotation parameters resulting from the 5 day solutions are reduced to the BIH nominal epochs by linear interpolation between the pair of values either side of a particular BIH epoch. Standard errors for the resulting parameters are evaluated by differentiation of the interpolation formula and application of the 'Gaussian propagation of error' theorems (Ashkenazi, 1970). No further smoothing was applied to either series of earth rotation parameters.

Because of the high correlation between the satellite orbital parameters and UT1-UTC (see § 3.4.4) they may not be determined simultaneously, and a

reference value of UT1-UTC must be used. Consequently,
the only truly estimable measure of the rate of
rotation of the earth is the rate of change of UT1-UTC.
This rate of change is usually expressed as the change
in UT1-UTC over a day, which is equivalent to the
excess length of day, D. Having obtained values of
UT1-UTC (from the 1-day or 5-day solutions) at the BIH
epochs, $t_i$, $t_{i-1}$, and $t_{i+1}$, the excess length of day at
epochs $t_i$ - 2.5 days and $t_i$ + 2.5 days may be
evaluated

$$D_{i-2.5} = \frac{(UT1-UTC)_i - (UT1-UTC)_{i-1}}{5} \quad (4.2)$$

$$D_{i+2.5} = \frac{(UT1-UTC)_{i+1} - (UT1-UTC)_i}{5} \quad (4.3)$$

The standard errors of these values may be
calculated from the a posteriori standard errors of the
UT1-UTC values. The excess length of day at epoch $t_i$
($D_i$) may be evaluated as the weighted mean of $D_{i-2.5}$
and $D_{i+2.5}$, i.e.

$$D_i = \frac{W_{i-2.5}D_{i-2.5} + W_{i+2.5}D_{i+2.5}}{W_{i-2.5} + W_{i+2.5}} \quad (4.4)$$

where
$$W_{i\pm2.5} = \frac{1}{\sigma^2_{i\pm2.5}} \quad (4.5)$$

and, $\sigma_{i-2.5}$ and $\sigma_{i+2.5}$ are the standard errors of the
two intermediate values of the excess length of day,
$D_{i-2.5}$ and $D_{i+2.5}$. The standard errors of $D_i$ may also
be calculated from these two values.

4.4   PROJECT MERIT

4.4.1 <u>General</u> <u>Description</u>

The scientific importance of the  study of the
rotation and orientation of the earth  has been
recognised for many years (see § 4.1). However, over
recent years the existing classical astrometric methods
of determining earth rotation parameters could no
longer provide the resolution which was becoming
increasingly necessary. With the advent of several new
space techniques, notably, Transit Doppler, Very Long
Baseline Interferometry and Lunar and Satellite Laser
Ranging, it was clearly demonstrated (McCarthy and
Pilkington, 1978) that a far higher resolution was
achievable. A special working group was formed in 1978,
during the IAU Symposium on 'Time and the Earth's
Rotation', to encourage the further development of
these new technniques with the aim of promoting the
development of a new international service to monitor
polar motion and Universal Time, to succeed the
existing monitoring services (see § 4.2). After
subsequent meetings the working group proposed a
special campaign of observation and analysis and ,in
1979, was officially recognised by both the
International Astronomical Union (IAU) and the
International Union of Geodesy and Geophysics (IUGG)
and became the IAU/IUGG Joint Working group on the
Rotation of the Earth (Wilkins, 1980b).

This 'special programme of international collaboration to Monitor Earth Rotation and Intercompare the Techniques of observation and analysis' (Wilkins, 1980a) adopted the title (and acronym) of Project MERIT. The main objectives of the project were, firstly, to encourage the development of the new techniques of determining polar motion and variations in the rate of rotation, and secondly, to obtain precise data from which the causes and effects of the variations may be assessed. The final aim was to ultimately make recommendations to the International Unions (IAU/IUGG) with regard to the future of the international monitoring services of earth rotation.

It was recognised that the aims of the project would be best achieved by the organisation of an international observational campaign, with the participation of both the classical and the new techniques. Such a campaign would allow a comparative assessment of the relative merits of the various techniques and produce sufficient data to also allow a reliable assessment of the accuracies of the results. However, because of the organisational complexity of such a large international campaign it was decided (Wilkins, 1980a) to first conduct a 'Short Campaign' to allow the arrangements to be refined before the subsequent 'Main Campaign' (see § 4.4.2). As the Global Positioning System (Ashkenazi and Moore, 1986) was not fully operational during the two campaigns, six

observational techniques contributed data, namely,
classical optical astrometry, very long baseline and
connected element radio interferometry, satellite and
lunar laser ranging, and Transit Doppler. A review of
the observational techniques is given by Wilkins
(1980a).

The advancements of these space geodetic
techniques also led to the formation of the IAG/IAU
Joint Working Group on the Establishment and
Maintenance of Conventional Terrestrial Reference
System, COTES (Mueller et al, 1982). The aims of the
working group were to investigate and make
recommendations with regard to the re-definition of the
terrestrial and celestial coordinate reference systems,
exploiting the new observational techniques. It was
agreed (Wilkins and Feissel, 1982) that it would be of
mutual benefit to both working groups if Project MERIT
was organised so as to contribute, whenever possible,
to the re-definition of the reference systems. In order
to establish the differences between the reference
frames particular to certain techniques, two methods
were identified by the working groups (Feissel and
Wilson, 1983). Firstly, by determining the coordinates
of the stations by two or more observational
techniques, simultaneously, i.e. colocation, and
secondly, by determining any diurnal differences
between the earth rotation parameters determined by the
different techiniques. As a result, an 'intensive

campaign' was proposed, to take place during the Main MERIT Campaign. During this period all the participating stations would be asked to observe as frequently as possible and the colocation of different techniques (with the particular aid of mobile systems) would be encouraged. Furthermore, it was also decided to determine the coordinates, by Transit Doppler, of all the observational stations contributing data to the Main MERIT Campaign.

In order to simplify the comparison of the results obtained by the different techniques, or by different analysis centres for the same technique, a sub-committee was formed with the task of producing a series of standard models, procedures and constants for use by all the participants of Project MERIT. The resulting MERIT Standards (Melbourne, 1983) have since been used, not just for Project MERIT but, extensively for the analysis of space geodetic observations.

### 4.4.2 Organistion, Campaigns and Analysis

Within the working group on 'the Rotation of the Earth' a steering committee was formed to oversee the organisation of Project MERIT. The officers, steering committee and members of the working group, including the principal coordinators for each observational technique, are given by Wilkins (1984). The transmission of data and the collection of results was controlled by an 'Operational Center' for each

technique and a single, overall, 'Coordinating Center' (at the BIH) which gathered all the results and published then in the MERIT Monthly Circulars and the final report of the campaign (Feissel, 1986). The Operational Centers distributed the observational data to the Analysis Centers, and computed 'rapid' earth rotation parameters on a weekly basis and reported these to the Coordinating Center. The analysis of the full data sets was carried out by a number of Analysis Centers for each technique. Although the Designated Analysis Centers (DAC) were expected to provide a complete series of earth rotation parameters for the total duration of the Main Campaign, in compliance with the MERIT Standards, the Associate Analysis Centers (AAC) were only expected to provide a partial analysis of the data. During and after the Main Campaign, the Geodesy Group of the University of Nottingham contributed to Project MERIT as an Associate Analysis Center for both Satellite Laser Ranging and Very Long Baseline Interferometry.

As previously oultlined, Project MERIT centered around two observational campaigns. The Short Campaign was held for three months between August and October of 1980, with the aim of testing and developing the organisation required during the Main Campaign. Although only two techniques (Transit Doppler and Optical Astrometry) had regularly determined earth rotation parameters before the Short Campaign,

six observational techinques participated during the three months. Details of the contribution of the various techniques during the Short Campaign are given in fig 4.II, which is reproduced from Table 1 of the MERIT/COTES Joint Summary Report (Wilkins and Mueller, 1985). The results of the Short Campaign were presented at the IAU Sympossium No 63 (Calame, 1982), and the campaign was reviewed at the first MERit Workshop (Wilkins and Feissel, 1982).

The duration of the Main Campaign was chosen to be sufficiently long to allow the principal periodic terms of the polar motion (and the variations in the rate of rotation) to be determined. A period of 14 months, roughly the Chandler period of the polar motion, was selected from the $1^{st}$ of September 1983 to the $31^{st}$ of October 1984. Clearly, the objectives of the Main Campaign of Project MERIT were very similar to the overall aims of the project (see § 4.4.1). The major difference between the observations of the Short and Main Campaigns was the increased precision of the results due to the development of the new techniques that had taken place during the intervening period. The participation of the various techniques to the Main Campaign are outlined in fig 4.III, which is reproduced from Table 2 of the MERIT/COTES Joint Summary Report (Wilkins and Mueller, 1985).

During a three month period, from April to June of 1984, of the Main Campaign the Intensive Campaign

| Observational Technique | Number of observing stations | Number of operational centres | Number of analysis centres |
|---|---|---|---|
| Optical astrometry | 85 | 1 | 2 |
| Doppler tracking of satellites | 31 | 2 | 2 |
| Satellite laser ranging | 31 | 2 | 6 |
| Lunar laser ranging | 3 | 1 | 4 |
| Connected element radio interferometry | 2 | 2 | - |
| Very long baseline radio interferometry | 9 | 1 | 3 |

Fig 4.II Participation in the MERIT Short Campaign (1980)

| Observational Technique | Number of observing stations | Number of operational centres | Number of analysis centres |
|---|---|---|---|
| Optical astrometry | 61 | 2 | 3 |
| Doppler tracking of satellites | 203 | 2 | 3 |
| Satellite laser ranging | 27 | 4 | 8 |
| Lunar laser ranging | 3 | 1 | 3 |
| Connected element radio interferometry | 1 | 1 | 1 |
| Very long baseline radio interferometry | 8 | 2 | 5 |

Fig 4.III Participation in the MERIT Main Campaign (1983/4)

was held. The aim of this campaign was to detect any diurnal differences in the earth rotation parameters derived by the various techniques, due to differences in the reference systems. A further aim was to determine whether any very short term variations could be detected by the new techniques. Consequently, all the participating observatories were requested to observe as frequently as possible, and the colocation of mobile SLR anf VLBI facilities with permanent stations was encouraged. Although there was a slight increase in the activities in optical astrometry, Satellite Laser Ranging and Very Long Baseline Interferometry, there were fewer colocations than had been hoped for (Wilkins and Mueller, 1985).

Following the main campaign a period of about nine months was dedicated to the processing of the observational data by the Dedicated and Associate Analaysis Centers. The preliminary results of Project MERIT were reported to the International Conference on Earth Rotation and the Terrestrial Reference Frame and the $3^{rd}$ MERIT Workshop, both in 1985, and are presented in the proceedings of the conference (Mueller, 1985) and summary of the results of Project MERIT (Feissel, 1986).

### 4.4.3 Satellite Laser Ranging and Project MERIT

Of the new observational techniques which promoted the establishment of Project MERIT, it was

generally recognised that both Satellite Laser Ranging and VLBI had already demonstrated very high potential accuracies, and would probably form the basis of any future earth rotation monitoring service. Consequently, a considerable effort was made by the laser ranging community, both before and after the Main Campaign, to complete the construction and testing of new and upgraded tracking stations, in order to produce a well distributed (global) network of precise ranging systems (Schutz, 1983a). During the Main Campaign laser range observations, to LAGEOS, were reported from a total of 38 tracking stations. Details of the participating stations are presented in fig 2.II and their locations are graphically illustrated in fig 2.III.

Three different satellites, namely LAGEOS, STARLETTE and GEOS-III, were tracked during the Short MERIT Campaign (Aardoom, 1982). However, at the second MERIT Workshop (Schutz, 1984) the Satellite Laser Ranging Group recommended that only LAGEOS and STARLETTE should be tracked during the Main Campaign, with LAGEOS the primary target.

The observational data was reported from the tracking stations to the Data Collection Centers in two formats (and quantities). The 'quick look' data, which is a sample of the full data set (say, 50-60 observed ranges per good LAGEOS pass), was reported once a week and processed by the Operational Center of Satellite Laser Ranging (at the Center for Space Research of the
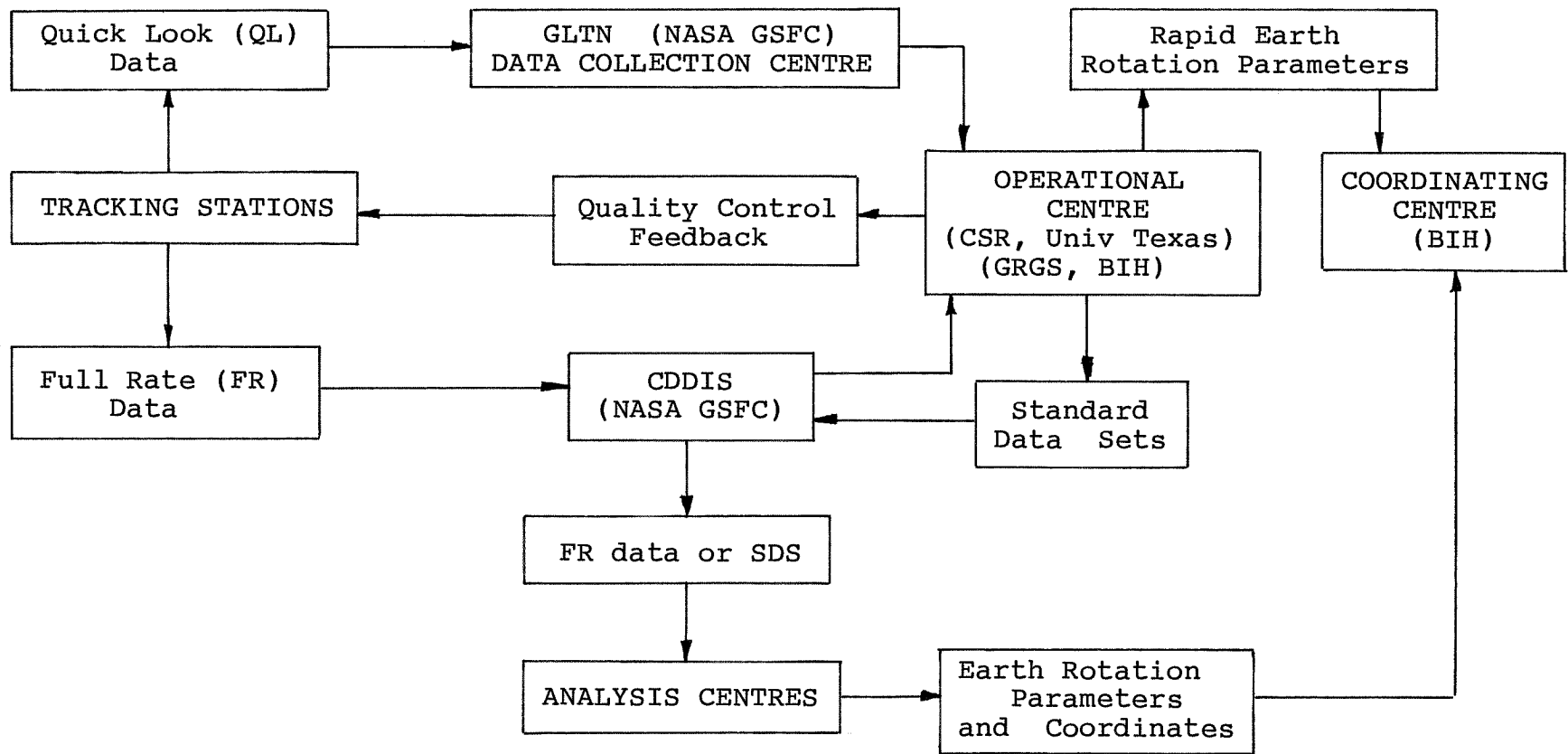
Fig 4.IV Flow of MERIT Satellite Laser Ranging Data

University of Texas at Austin), to produce a rapid determination of the earth rotation parameters. In comparison, the 'full rate' data, the complete set of observed ranges (after initial filtering at the tracking stations), was reported to the Crustal Dynamics Data Imformation System (of NASA) some time after the observations. Considering the rate at which data is accumulated from $3^{rd}$ generation laser ranging facilities (see § 2.4.1.1), the full rate data was compressed to produce 'normal point' ranges by the Operational Center. However, the major purpose of the creation of the Standard Data Sets was to produce sets of data compatible with both the MERIT Standards and the supplementary Satellite Laser Ranging Data Analysis Standards (Schutz, 1983b), to facilitate the inter-comparison of the derived earth rotation parameters. The resulting monthly Standard Data Sets and the Full Rate data were subsequently made available to the various Designated and Associate Analysis Centers (for Satellite Laser Ranging).

This apparently complex flow of laser ranging data and the resulting earth rotation parameters between the participants of Project MERIT is summarised in fig 4.IV. Further details of the data sets and formats may also be found in the Satellite Laser Ranging Procedures Guide for Project MERIT (Schutz, 1983b).

CHAPTER  FIVE

UNIVERSITY OF NOTTINGHAM SATELLITE LASER

RANGING ANALYSIS SOFTWARE

## 5.1 INTRODUCTION

A Satellite Orbit Determination and Analysis Package Of Programs, with the acronym SODAPOP, has been developed at Nottingham in order to process Satellite Laser Ranging data. Currently, a number of routines and models are specifically tailored for laser range measurements to the LAGEOS satellite. However, because of the 'modular' approach adopted during the writing of the software package, it may be easily modified to enable the analysis of laser range observations to different satellites (such as STARLETTE) or indeed different types of data altogether.

The package consists principally of two programs, ORBIT, an orbit integration program and SOAP, the Satellite Orbit Analysis Program, which performs the least squares adjustment and error analysis. Whearas ORBIT is a 'general' orbit integration program, with only specific models tailored to suit LAGEOS, SOAP is designed specifically for the analysis of Satellite Laser Ranging observations. Despite the high level of compatability between the two programs their independence is maintained to allow for future development. The remainder of the package consists of ancillary service programs to pre-process raw laser ranging data and post-process the residuals and products. The efficiency of both ORBIT and SOAP is improved by the CHEBPOL program discussed in § 5.2.2. The interaction between the various programs of the SODAPOP suite is illustrated in fig 5.I.
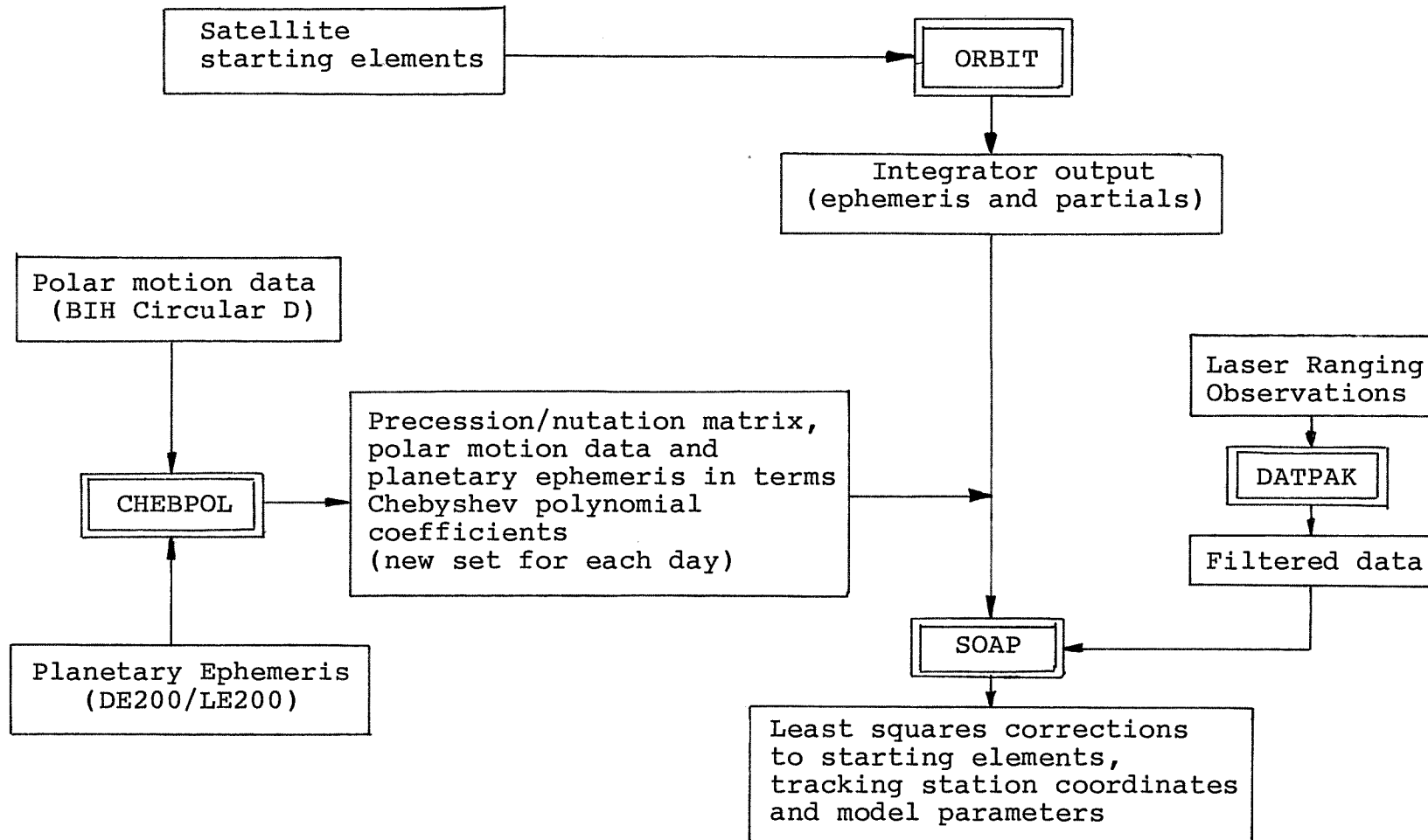
Fig 5.I <u>SODAPOP - Satellite Orbit Determination and Analysis Package of Programs</u>

The package has been developed by the author, and by Dr. L. G. Agrotis during his research period at Nottingham (Agrotis, 1984), on ICL 2900 series computers. The ORBIT and CHEBPOL programs were originally written by Dr. Agrotis and ORBIT has required little modification since. However, CHEBPOL has been upgraded (to increase it's flexibility) by the author. The first 'prototype' version of SOAP was written jointly by the author and Dr. Agrotis, however, since then all later versions have been developed by the author. All the remaining service programs for the pre-processing of data and the plotting (and processing) of residuals and results have also been developed by the author, with the exception of the TRANSFORM program (see § 3.2.1.5). This program was taken from the University of Nottingham Doppler Adjustment Package (UNDAP), and was originally written by Dr. R. M. Sykes (Sykes, 1979).

The orbit integration program, ORBIT, is based on the principles of orbit determination described in Chapter 3. Starting with an initial satellite state vector and a model of the forces acting on the satellite it computes, using numerical integration procedures, the satellite ephemeris (§ 3.4.1) and the observation equation partial derivatives (§ 3.4.3). The ephemeris and partials computed by ORBIT are subsequently used by SOAP which takes the pre-processed laser range observations and performs a least squares adjustment (§ 3.4.2) and error analysis (§ 3.4.5).

Both ORBIT and SOAP need to evaluate the large

nutation series (§ 3.2.4) and the precession equations

at each integration step or observation epoch

(respectively). These time consuming computations are

avoided by the program CHEBPOL, which derives, for each

day, a set of Chebyshev polynomial interpolation

coefficients for the precession and nutation matrices.

The interpolation formulae may be used by ORBIT and

SOAP to efficiently evaluate the relevant matrices as

required. CHEBPOL also computes interpolation formulae

for the nutation in longitude (§ 3.2.4), the planetary

coordinates (§ 3.3.3) and the earth rotation

parameters, $x_p$, $y_p$, and UT1-UTC (§ 3.2.5).

The data pre-processing package consists of a

series of programs to filter, compress and sort the

laser range measurements and produce data in a suitable

format for the analysis program SOAP. The principal

programs of the SODAPOP suite are discussed, in detail,

in the remainder of this Chapter, which is concluded in

§ 5.5 with details of the testing and validation of the

software and a description of the operational use of

the package.

## 5.2    ANCILLARY PROGRAMS

### 5.2.1   Data Pre-processing Programs

#### 5.2.1.1 General Description

The requirements for, and method of, pre-processing laser ranging observations were discussed in § 2.4.1. Two pre-processing strategies were outlined; a simple polynomial technique and a method based on the residuals from a computed orbit. The SODAPOP suite currently allows either approach to pre-processing to be adopted. However, despite the complexity of the second method, its use is recommended whenever possible (this method is not suitable if no satellite state vector is available).

The raw laser range data is distributed to the analysis centres on magnetic tapes in the modified Seasat Decimal (SSD) format (Schutz, 1983b). The (MERIT) data consists of one file for each calender month, sorted into chronological order. When pre-processing the observations it is convenient to handle the ranges from one station at a time. Consequently, there are a number of programs common to both pre-processing packages which either sort the observations according to their tracking station or combine the individual pre-processed data sets to give a single data file. The program 'NUMB' scans the complete file of raw observations and outputs the station identification numbers for which data was found together with the number of ranges observed at each

station. For a specified tracking station number (as obtained from NUMB) the program 'READ' will read all the observed ranges for that station from the magnetic tape and store them in a disc file. Following the pre-processing of the 'subsets' of observations the 'SORT' program combines the individual files and sorts the observations into chronological order, resulting in a single data file ready for input to the analysis program, SOAP.

The 'RESPLOT' program is also used by both pre-processing packages. This is a general plotting program to produce graphical representations of the residuals from the filtering procedures and also of the least squares residuals from SOAP.

## 5.2.1.2   Pre-Processing Package, DATPAK-1

This package of programs was written to pre-process laser ranging data by the polynomial method discussed in § 2.4.1.4. The general outline of DATPAK-1 and the flow of data through the package are illustrated in fig 5.II. The two principal programs of the package, FILTER and NORMAL, have not been previously discussed. The FILTER program takes the observed ranges from one station and splits the data into individual passes over the station. A break in the data of more than 30 minutes is used to detect the end of one pass and the start of the next. An $n^{th}$ order polynomial is fitted by least squares to each pass and
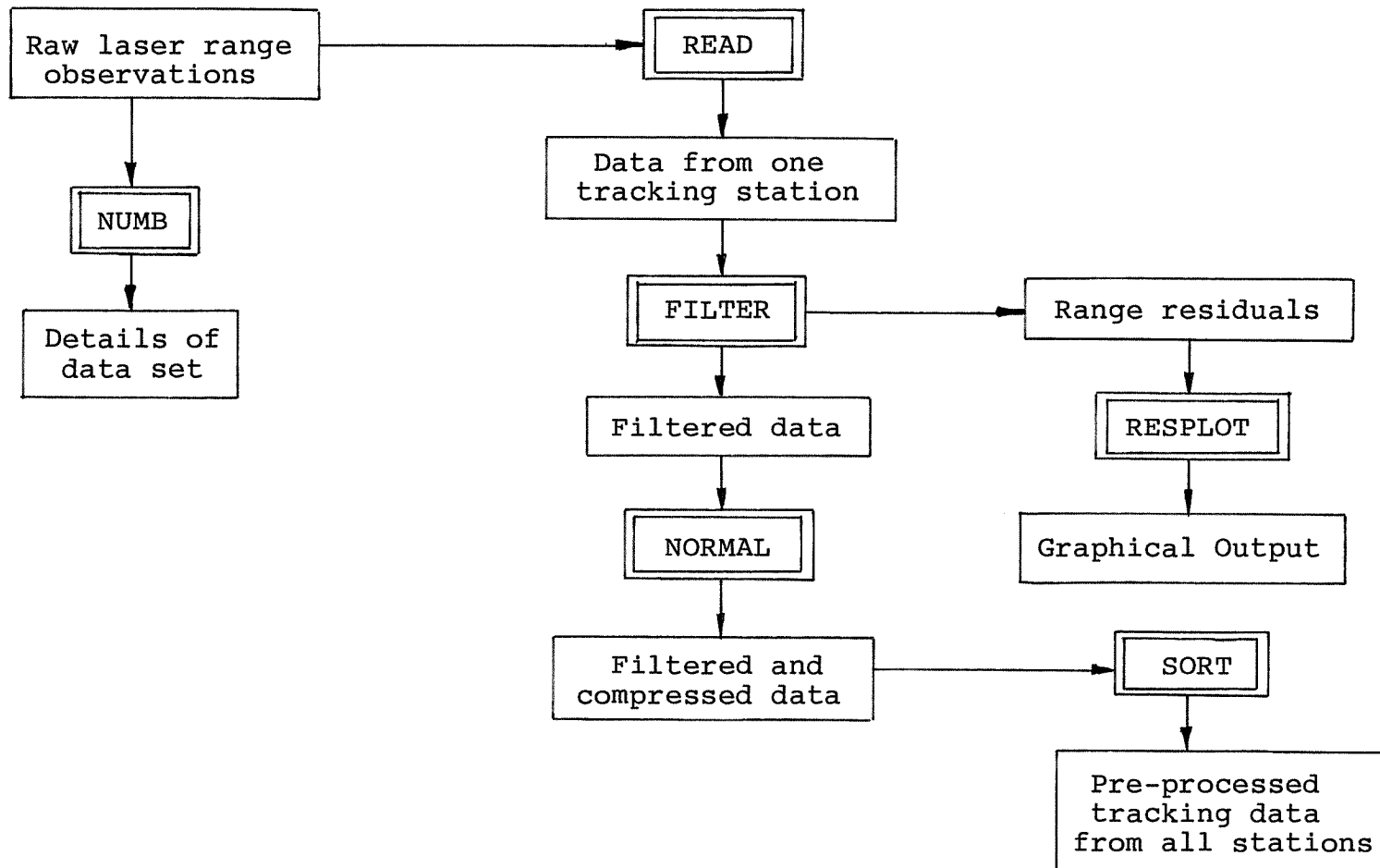
Fig 5.II Data Pre-Processing Package : DATPAK-1

any ranges with large residuals (say, > 2σ) are
rejected, as described in § 2.4.1.4. The input to the
program consists of the raw ranges from one station and
a control file which informs the program of the order
of the polynomial, the rejection criterion to be used,
and the number of times the filter is to be repeated.
The program outputs the filtered observations and the
residuals which may be subsequently graphically output
using the RESPLOT program.

The file of filtered observations forms the
input to the data compression program, NORMAL. This
program splits the data, from one tracking station,
into short periods, typically 3 minutes, and computes
one 'normal point' range for each period. The procedure
used by NORMAL to generate the normal points is
described in § 2.4.1.4. An additional input file allows
the order of the polynomial to be modified and also the
period of data, to be compressed into each normal
point, to be specified. The normal point ranges are
output from the procedure in Seasat Decimal format,
with the relevant parameters set to indicate the
observations are normal points and not raw ranges
(Schutz, 1983b). Similar sets of normal points from the
other tracking stations are combined and the
observations sorted into chronological order by the
SORT program.

This package of pre-processing programs was
initially tested, and subsequently used, with mainly

$2^{nd}$ generation laser ranging data, observed during 1980. Experience showed that a $10^{th}$ order polynomial and a rejection level of $2\sigma$ was, generally, a suitable combination for filtering. Normal point ranges were obtained for each minute of data using a $7^{th}$ order polynomial. The subsequent processing of the observations which were pre-processed using this package is described in § 6.1.

For the reasons outlined in § 2.4.1.4 the pre-processing procedure used by this package was found to have several limitations, especially with high repetition rate $3^{rd}$ generation laser ranging data. Consequently, a completely different approach to pre-processing was adopted, and has since made the first version effectively redundant.

### 5.2.1.3 Pre-processing Package, DATPAK-2

The theoretical considerations on which the programs of this package are based are described in § 2.4.1.5. Basically, the satellite orbit is not represented by a polynomial fitted to the ranges, as with DATPAK-1, but by a 'computed' orbit generated by the ORBIT program (see § 5.3) which is fitted to a sample of the raw range observations using the SOAP program (see § 5.4). The structure of the DATPAK-2 package, and the necessary inclusion of major programs from the SODAPOP suite, is illustrated in fig 5.III. The programs ORBIT, SOAP, SORT and RESPLOT are not used
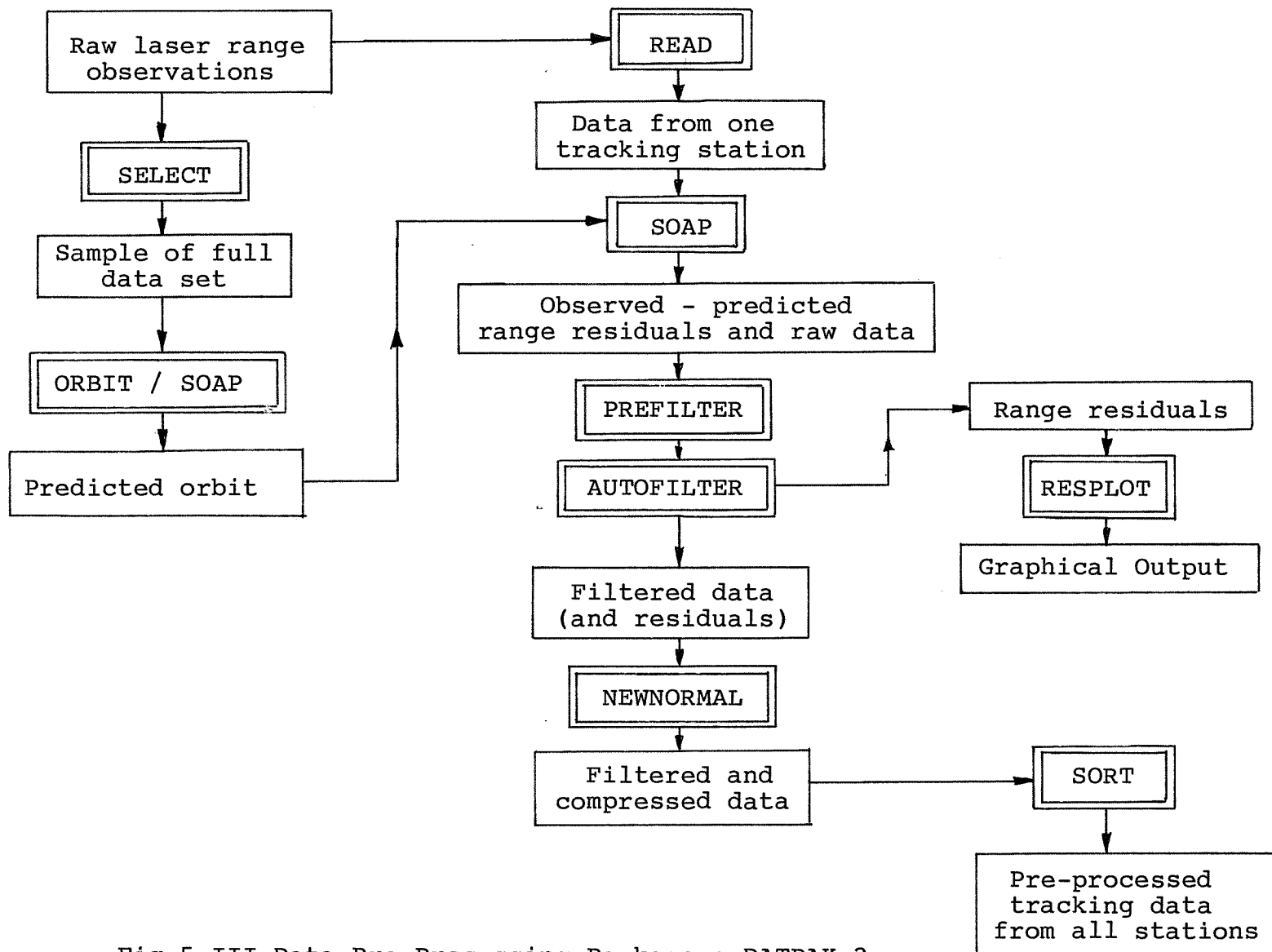
Fig 5.III <u>Data Pre-Processing Package : DATPAK-2</u>

exclusively by DATPAK-2 and are described elsewhere in this Chapter, while the other programs, namely, SELECT, PREFILTER, AUTOFILTER, and NORMAL-2, are outlined in this section.

If the orbit of the satellite is known, from previous data sets (for example), then this may usually be extrapolated to span the period of data to be pre-processed. Otherwise, it is necessary to determine the orbit by using a sample of the range observations from the data set. It is important to note that any 'trends' remaining in the 'computed' orbit may be removed at a later stage and so a 'precise' orbit is not required. A sample of the full data set is used simply to increase the efficiency of the process and ideally normal point ranges would be used, however, these are not (usually) available at this stage of the pre-processing. The SELECT program scans a raw data file and selects one observation every 3 minutes (for example) and neglects all the other observations.

The SOAP program is operated in a mode (see, § 5.4) which, for every observed range, computes and outputs the 'observed - computed' range residual. The PRE-FILTER program appends these residuals to the corresponding data record in the file of raw observations, in a non-standard extended SSD format. The filtering of noisy or bad observations from the data set is carried out by the AUTOFILTER program by the method described in § 2.4.1.5. This program

operates automatically and the only input required is the data file, for one station, as prepared by PRE-FILTER. Any 'trends' introduced into the distribution of the residuals, which are typically linear or quadratic, are removed by fitting a low order polynomial (by least squares) to the residuals from each pass. Observations are rejected with residuals greater than twice or three times the root-mean-square residual. The order of the polynomial, the choice of rejection criteria and the number of times the filter is repeated are all controlled by the program itself. This ensures a minimum of intervention is required from the operator and automatically optimises the procedure to suit the data. The output from AUTOFILTER is in the same format as the input, but the rejected observations are removed from the data file. Residuals are also output in a format suitable for graphical plotting by the RESPLOT program.

The NORMAL-2 program splits the data into short 'bins' and generates a normal point range for each 'bin' by the standard procedure, described in § 2.4.1.3. This involves the averaging of the residuals output from AUTOFILTER. The input consists of the filtered data file and the period of data (in seconds) to be compressed into each normal point. The only output is the compressed and filtered data from one tracking station, which may be subsequently combined with other such files using the SORT program.

DATPAK-2 has been tested and used with 3$^{rd}$ generation laser ranging observations and has repeatedly demonstrated its ability to pre-process such data more efficiently and reliably than DATPAK-1. Clearly, this approach does require the generation of a computed orbit, however, this need only be determined once for each set of data, even though the filtering and compression of the data is carried out one tracking station at a time.

## 5.2.2 CHEBPOL Chebyshev Polynomial Program

The computation of the nutation matrix (see, § 3.2.4) at a specific epoch involves the evaluation of the 108 terms of the nutation series. For a dynamical analysis of laser ranging data this computation must be performed for every observation epoch (in SOAP) and for every numerical integration step (in ORBIT). Clearly, this is a time consuming and inefficient approach. The CHEBPOL program enables SOAP and ORBIT to compute the nutation matrix without having to evaluate the long series, by previously deriving a number of Chebyshev interpolation coefficients for the elements of the matrix B, where

$$B = Q^T N^T \qquad\qquad (5.1)$$

and, Q and N are the precession and nutation matrices defined in § 3.2.4. Consequently, to compute this precession/nutation matrix at a particular epoch SOAP

and ORBIT simply need to evaluate the Chebyshev
interpolation formulae with the coefficients output
from CHEBPOL.

Together with the 9 elements of the B matrix (as
defined in equation (5.1)) CHEBPOL also outputs the
Chebyshev polynomial coefficients for the nutation in
longitude, $\Delta\psi$ (see equation (3.53)) and the geocentric
inertial frame coordinates of the moon, sun and planets
(Venus, Mars, Jupiter and Saturn). The nutation in
longitude is required by both SOAP and ORBIT in order
to convert from GMST to GAST, when computing the earth
rotation matrix (equation (3.61)). Both programs also
require the planetary coordinates, when evaluating the
the third body gravitational effects, the solar
radiation pressure, and tidal corrections (see § 3.33,
§ 3.35, § 3.34, respectively). CHEBPOL also provides
daily linear interpolation coefficients for the earth
rotation parameters ($x_p$, $y_p$ and UT1-UTC) which are
obtained from 5-day values (typically, BIH circular D)
input to the program.

The current version of the CHEBPOL program
computes and outputs daily polynomial coefficients for
40 days. The starting day number (and year) are
specified as input to the program. CHEBPOL also
requires input of the earth rotation parameters at
5-day intervals. In order to cover the 40 day period,
9 sets of earth rotation parameters must be provided,
the first of which must coincide with the specified

starting epoch. The only remaining inputs required are the heliocentric inertial frame coordinates of the moon and planets. These are provided by the planetary ephemeris DE200/LE200 (see § 3.3.3) which covers the period 1979 to 2006. Rather than inputing the complete ephemeris file it is often more efficient to extract the relevant portion of the ephemeris and input this to CHEBPOL.

The output from CHEBPOL consists of a set of Chebyshev polynomial (and linear interpolation) coefficients for 0.0hrs UT of each day of the specified 40 day period. These coefficients enable the required values to be evaluated at any epoch within the period.

The Chebyshev representation of a function is discussed in Appendix D. In CHEBPOL a particular set of coefficients is valid for 24 hours and the variable is UTC time since 0.0hrs of that day. The coefficients of a $10^{th}$ order polynomial are evaluated for each function, however, the full series is truncated and only the first five coefficients $a_0$-$a_4$ are output. Consequently, a particular value of a function $f(t)$ within the corresponding interval is given by

$$f(t_{UTC}) = \sum_{k=0}^{4} a_k \cos k\theta \qquad (5.2)$$

where $\qquad \theta = \cos^{-1} \left( \dfrac{t_{UTC} - 12^h.0}{24^h.0} \right) \qquad (5.3)$

A total of 140 coefficients are output for each day, which enable the coordinates of the moon, sun and

planets to be evaluated as well as the 9 elements of the B matrix (equation (5.1)) and the nutation in longitude $\Delta\psi$. To compute the coefficients the functions must be evaluated at 11 data points within each one day interval (see Appendix D). However, the planetary and lunar coordinates are given as discrete values at 0.0hrs TDB of each day, and so they are interpolated to the required epochs using the Everett formulae, with up to $4^{th}$ order central differences (see Appendix D). These coordinates are, however, given in terms of Astronomical Units and in a heliocentric reference frame and so must first be converted to metres (1AU = $1.4959787 \times 10^{11}$m) and to the geocentric inertial frame (see § 3.3.3).

For each day CHEBPOL also evaluates and outputs two linear interpolation coefficients $C_0$ and $C_1$, for each of $x_p$, $y_p$, and UT1-UTC. The earth rotation parameters at any epoch $t_{UTC}$, during the particular day, is given (for example) by

$$x_p = C_0 + C_1 t_{UTC} \qquad (5.4)$$

The coefficients are obtained by linear interpolation between the earth rotation parameters, at 5-day intervals, input to the program.

5.3    SATELLITE ORBIT INTEGRATION PROGRAM - ORBIT

5.3.1 General Description

The SODAPOP suite divides the analysis of laser
range observations into two distinct tasks, firstly,
the determination of the satellites orbit and secondly
the least squares adjustment. The ORBIT program carries
out the numerical integration, in the inertial frame,
of the satellite acceleration vector $\ddot{r}$ and the
acceleration partial derivatives (see § 3.4). This
results in the inertial frame position and velocity
vectors of the satellite at intervals of UTC, specified
by the integration step size. For the integration to
start it is necessary to assign initial approximate
position and velocity vectors (and also inital values
for the position and velocity partial derivatives), at
some starting epoch. As previously described in § 3.4.1
there are several suitable methods of numerical
intergration, those implemented by ORBIT are :

(i)   a $4^{th}$ order Runge-Kutta single step
      procedure (the starting procedure)

(ii)  a $9^{th}$ order Adams-Bashforth predictor-
      corrector multi step method.

The Runge-Kutta procedure is used to start the
integration from the initial vectors. As shown in
§ 3.4.1, the limited efficiency and low accuracy of a
single step method restrict its use to just providing
sufficient data points (in this case 8, in addition to

the starting vectors) to enable the predictor-corrector
scheme to operate. In order to achieve the necessary
accuracy it is usual to use a substantially smaller
integration step length for a single step method than
for a multi step method. Experience with ORBIT has
shown (Ashkenazi, Agrotis and Moore, 1984) that
suitable step lengths, for LAGEOS, are 15 seconds for
the starting procedure and 120 seconds for the
predictor-corrector. However, these values are input to
the program (see § 5.3.2) and so may be varied as
appropriate. With the current step lengths, the Runge-
Kutta starting procedure must operate for a total of 64
integration steps before the predictor-corrector may
take over.

In order to monitor the truncation error of the
Adams-Bashforth procedure, the error is evaluated at
each integration step, using equation (3.139), for each
component of the state vector. If this value exceeds
$1 \mu m$ then a message is output and the corrector is
repeated.

The force model (see § 3.3) currently installed
in ORBIT is particularly suited to LAGEOS and wherever
possible has been kept in close agreement with the
models and constants recommended by the MERIT Standards
(Melbourne, 1983). The constituents of the force model
are as follows.

(i)    The GEM-10 or GEM-L2 geopotential model,
complete to degree and order 20. The MERIT

recommended constraints on $c_2^1$ and $s_2^1$ terms of GEM-L2 are applied, however they were not applied during the processing of LAGEOS laser range data discussed in Chapter 6.

(ii) The third body attractions of the sun and moon and the planets (Venus, Mars, Jupiter and Saturn).

(iii) Lunar and Solar solid earth tides, the Whar model (see § 3.3.4.1).

(iv) Ocean tides, Schwiderski model (see § 3.3.4.2).

(v) Solar radiation pressure (see § 3.3.5).

(vi) Along track acceleration (see § 3.3.6).

At the altitude of LAGEOS ($\simeq$ 6000km) there is no need for an atmospheric drag model (see § 3.3.6). However, for lower satellites, such as STARLETTE at an altitude of around 800km, drag is a very significant effect and must be accounted for in the force model.

The solar radiation pressure model of ORBIT also includes the facility to test whether the satellite is in the area of shadow cast by the earth, and cut off the effect of the model accordingly. However, this approach introduces sudden changes in the force model, which can lead to very large truncation errors. Clearly, it would be preferable to slowly decrease, or increase, the effect of solar radiation pressure as the

satellite passes into (or out of) the area of shadow. As only a simple cut-off model is, currently, available in ORBIT this 'shadow test' is not generally used.

As previously discussed, in § 3.4, several of the forces may be neglected when evaluating the acceleration partial derivatives, without significantly affecting the results. In ORBIT only the effects of the geopotential (all 20×20 terms) and the third body attractions are included. Although the effects of ocean tides are insigificant, the contributions are included because the coefficiennts of the geopotential model are corrected for earth tides before the acceleration partials are evaluated. In addition to the position and velocity partials ORBIT may also output partials for the along track acceleration coefficient $C_T$, the solar radiation pressure coefficient $C_R$, the geocentric gravitational constant GM and up to 12 normalized spherical harmonic coefficients, $\bar{C}_n^m$ or $\bar{S}_n^m$, of the geopotential model.

ORBIT may be operated in two modes which differ only by the starting procedure. The first, and usual, mode operates as described previously in that the orbit integration is started from initial approximate state vectors using the Runge-Kutta procedure until the predictor-corrector takes over for the remainder of the arc. The second mode allows an existing orbit to be continued to produce a new orbit, by-passing the single step starting procedure. To enable this, at the end of

an arc ORBIT outputs the last nine position and velocity vectors (and the position and velocity partials) to a file. When operating in the second mode, ORBIT reads in these values and treats them as the previous nine steps of the orbit integration and continues directly with the predictor-corrector procedure. This approach allows very long orbital arcs, say one month long, to be split into a number of smaller and more manageable orbit computations, which when combined give the complete orbit.

The efficiency of the ORBIT program is increased by using the files of Chebyshev polynomial coefficients generated by CHEBPOL (as described in § 5.2.2). A new set of coefficients is produced for each day, and so at each integration step ORBIT checks the current date and when this changes a new set of coefficients is read from the data file to replace the existing coefficients. If required daily values of the earth rotation parameters ($x_p$, $y_p$ and UT1-UTC) may be input to ORBIT and used in preference to the values read from the CHEBPOL file. This allows the values to be updated, for example as unknowns in a least squares solution, without the need to generate a complete new file of Chebyshev polynomial coefficients.

A full and detailed description of the operation of ORBIT, including a simplified flow chart of the program is given by Agrotis (1984).

5.3.2 <u>Program Input and Output</u>

The operation of the ORBIT program is controlled
by a number of input parameters. In addition, ORBIT
also requires input of other data, such as the file of
Chebyshev polynomial coefficients, from a number of
serial and random access computer files. The particular
details of the file handling are not included (however,
details are given by Agrotis (1984)), but the required
input is comprised as follows.

(i)     Various 'flags' which control the operation of
        the program.

        (a) Input mode of starting elements. Modes 1
            and 2 specify whether the input starting
            elements are given in the earth fixed or
            inertial reference frames. Mode 3 denotes
            that ORBIT is to continue an existing
            orbit and so the 9 previous position and
            velocity vectors (and partials) are
            required. In this mode ORBIT by-passes
            the starting procedure.

        (b) Flags to indicate whether partials are
            required for a particular force model
            parameter (i.e. $C_T$, $C_R$ or GM).

        (c) Shadow Test. This flag indicates whether
            or not the solar radiation pressure is
            cut off when the satellite passes through
            the earth's shadow.

(d) Input source of earth rotation parameters. These daily values may be input from two sources and either fixed throughout the day or interpolated. The options are; input from the CHEBPOL file and either linearly interpolated to the particular epoch or fixed throughout the day, or input from a separate file and fixed throughout the day.

(ii)    Epoch of starting elements. The UTC time, $t_0$, corresponding to the orbit starting elements given as year, day number, and time in hours minutes and seconds.

(iii)   Satellite state vector in the appropriate reference frame (according to mode 1 or 2).

(iv)    The position and velocity vectors (and partials) for the last nine steps of a previous orbit, if operating in mode 3.

(v)     The integration step size of both the starting procedure and the predictor-corrector scheme, and the total number of integration steps.

(vi)    The earth's angular velocity. Although always required as an input parameter, this value is only used from atmospheric drag models.

(vii)   Cross sectional area and mass of satellite. These values are required for both the solar radiation pressure and atnospheric drag models.

(viii)  The values of the solar radiation pressure
coefficient, $C_R$, the along track acceleration,
coefficient $C_T$, and the geocentric constant of
gravitation, GM.

(ix)  The degree and order of the normalized
spherical harmonic coefficients for which
partials are required.

(x)  The Chebyshev polynomial coefficients, from
the CHEBPOL file.

(xi)  The Schwiderski ocean tide model coefficients
and load numbers $k_n'$ (see § 3.3.4.2).

The output from ORBIT consists of various levels of
printed output which give the user details of the
status and modes of operation of the program. In
addition ORBIT also outputs to six computer files as
follows.

(i)  Inertial frame ephemeris. This file consists
of the inertial frame position and velocity
vectors of the satellite, time tagged, at even
intervals of UTC. The interval is determined by
the step length set for the predictor-corrector
procedure, typically (for LAGEOS) 120 seconds.

(ii)  Earth fixed ephemeris. Identical to file (i)
except that the position and velocity vectors
are given in the earth fixed reference frame.

(iii)  Position partial derivatives, at intervals
corresponding to the ephemeris.

(iv)   Velocity partial derivatives, as (iii).

(v)    File containing the last 9 records of the
       inertial frame ephemeris file , corresponding
       to the last 9 integration steps.

(vi)   File containing the last 9 records of the file
       of position partials (iii) and the velocity
       partials (iv), corresponding to the last 9
       integration steps.

If ORBIT is to be used, subsequently, in mode 3, to
continue the orbit integration, then the last two files
contain the necessary state vectors and partials. When
processing laser range observations to satellites the
least squares analysis program, SOAP, requires the
first and third of these files (ie the inertial frame
ephemeris annd the position partials). The remaining
two files are not used at present, but may be required
for different  satellite tracking/positioning systems.

5.4    SATELLITE ORBIT ANALYSIS PROGRAM - SOAP

5.4.1 General Description

The Satellite Orbit Analysis Program, SOAP, is
the second principal program of the SODAPOP suite and
carries out the least squares analysis of satellite
laser range observations, following the principles
described in § 3.4. The analysis procedure involves the
formation of an 'observation equation' for each
observed range using the approximate coordinates of the
tracking stations and a predicted satellite ephemeris.
These equations are then combined and solved for the
most probable values of corrections to the approximate
parameters by the process of least squares. The
predicted (computed) orbit is obtained by numerical
integration, using the ORBIT program. Together with the
least squares solution, SOAP also performs a
statistical error analysis giving the least squares
residuals and the a posteriori precision (from the
covariance matrix) of the unknowns and the observations
(see § 3.4.5). Similar to ORBIT, SOAP is currently
'tailored' for the analysis of LAGEOS laser ranging
observations, however, wherever possible extensions to
enable the analysis of STARLETTE data have been
included.

The present version of the software may include
any of the following as unknowns in the least squares
solution.

(i)   Initial satellite position and velocity vectors.

(ii)  Tracking station coordinates.

(iii) Earth rotation parameters ($x_p$, $y_p$ and UT1-UTC).

(iv)  Gravity field normalized spherical harmonic coefficients.

(v)   Geocentric gravitational constant, GM.

(vi)  Solar radiation pressure reflectance coefficient, $C_R$.

(vii) Along track acceleration coefficient (for LAGEOS), $C_T$.

The program may be operated in 3 different modes, which are designed to optimise the efficiency of the package when dealing with short or long periods of data. The particular mode is selected by the operator as an input parameter, as described in § 5.4.2. When the program is operating in mode 1, the laser range data is read in, the observation equations are formed and the least squares solution and error analysis is performed. This is, therefore, the usual mode of operation and could, theoretically, be used for all the processing of laser ranging observations. However, when dealing with longer periods of data, say one month, it is necessary to generate, using the ORBIT program, the satellite's ephemeris and the partial derivatives over this period. This is a very time consuming task, and

results in a number of very large and unmanageable computer files. Consequently the facility is included in ORBIT, as described in § 5.3.1, to split a long orbital arc into a series of consecutive shorter arcs. Given one of these sections of the complete orbit, SOAP, when operated in mode 2, will read in the corresponding batch of data and form and store the observation equations. After repeating this procedure for all the remaining portions of the orbit (and data set) the resulting observation equations may be read back into the SOAP program, when operating in mode 3, and the least squares solution performed. Clearly, modes 2 and 3 correspond, approximately, to the first and second halves of mode 1, the division occurring directly after the formation of the observation equations.

The laser range data is read into SOAP in Modified Seasat Decimal (SSD) format (Schutz, 1983b), regardless of whether the observations are 'full rate' or compressed into 'normal points' (see § 2.4.1.3). The data is stored in chronological order with each record of data corresponding to one range observation (or normal point). The data records consist of the range measurement (one-way), the UTC epoch of observation, the identity of the tracking station, metereological data, and pre-processing flags and information. It was recommended (Schutz, 1983b) that the data from the MERIT main campaign should not have the atmospheric

refraction and centre-of-mass corrections applied, however, as SOAP reads in each observation data record it checks the relevant flags and removes any corrections that have been incorrectly applied. The program reads in one observation at a time and for each range forms the observation equation, and adds the contribution of that equation to the normal equations, before reading in the next range observation.

The Chebyshev polynomial coefficients generated by CHEBPOL are used by SOAP, in order to compute the rotation matrices between the inertial and earth fixed reference frames and to evaluate the solar and lunar coordinates at a particular epoch. The latter are required in order to correct the tracking station coordinates for the effect of lunar and solar solid earth tides (see § 3.3.4.1). A new set of coefficients is read from the CHEBPOL file, if the date of the observations changes

The epoch of a range observation is defined by SOAP to be the UTC time at which the laser pulse hits, and is reflected by, the satellite. Clearly, this epoch is not observable as the satellites are generally remote and passive, and so the only observable epochs are the time of firing and time of return of the laser pulse. As the one way range may be approximated, to sufficient accuarcy, to half the total time of flight, the time of observation may be defined as the mid epoch between the times of firing and return of the pulse.

Indeed, the data transmitted in the SSD format is time tagged in this way. However, any errors in the range measurement will also corrupt the epoch of observation. To avoid this problem an independent iterative method of determining the epoch of observation is adopted by SOAP. Firstly, the time of firing, $t_f$, of the laser is computed from,

$$t_f = t_o - \frac{r^o}{c} \qquad (5.5)$$

where   $t_o$  :  time of observation (from data record)

        $r^o$  :  observed one-way range

        $c$  :  speed of light, in a vacuum.

As a first approximation it is assumed, obviously incorrectly, that the time of observation is equal to the time of firing. The position vector (inertial frame) of the satellite is obtained at this epoch from the ephemeris by means of Everett interpolation (using up to 8$^{th}$ order central differences, see Appendix D). After rotating the tracking station coordinates into the inertial frame, using equation (3.35), it is possible to compute the range, $r_1$, between the station and the satellite, using equation (3.159). This range leads to a second approximation of the epoch of observation,

$$t_2 = t_f + \frac{r_1}{c} \qquad (5.6)$$

The process may then be repeated with this time of obsrvation, $t_2$, used to determine a updated inertial

frame position vector of the satellite and corresponding range $r_2$, leading to a new epoch of observation, $t_3$, from an equation similar to equation (5.6). The iteration continues until the difference between two successive values of the time of observation is below some preset value. Once the epoch of observation is obtained the process is reversed in order to find the 'computed' time of return, $t_r$, of the laser pulse to the tracking station. The 'computed' two-way range may be then be calculated from,

$$r^c = c \ (t_r - t_f) \tag{5.7}$$

Two corrections are applied to the observed ranges by SOAP to account for errors in the measurement model. Firstly, the centre-of-mass corection (see § 2.3.3.2) and secondly, a correction for the effects of atmospheric refraction (see § 2.3.3.1). For spherical satellites, such as LAGEOS and STARLETTE, the centre-of-mass correction is simply a constant value (24cm and 7.5 cm, respectively) which is added to the observed range. For tropospheric refraction the Marini-Murray model (Marini and Murray, 1973) is recommended by the MERIT Standards, and is accordingly adopted by SOAP. The model requires the surface pressure, temperature and relative humidity at the tracking station, and the true elevation angle of the satellite at the epoch of observation. The first three values are available from the observational data record, whearas the latter is calculated from the satellite and tracking

station coordinates (see Appendix B).

For each range measurement an observation equation of the form of equation (3.158) is formed. The coefficients of the equation, the partial derivatives, are evaluated as outlined in § 3.4.3. The partials for the satellite state vector and force model parameters are obtained from the file of partial derivatives generated by ORBIT. As the partials are produced at even intervals of UTC, corresponding to the integration step length, they must be interpolated (using Everett formulae, with up to $4^{th}$ central differences) to the observation epoch. The laser range measurements are treated, by SOAP, as two-way ranges and so the observed ranges and the observation equation coefficients must be multiplied by a factor of two.

At present, no weighting is applied to the range observation equations which implies a default weighting of one metre for all the observations. In order to hold various quantities fixed during a solution, such as the longitude of a tracking station, it is possible to introduce additional observations of the form of equations (3.161) and (3.162), with suitably high weights. In addition to fixing the longitude of any tracking station, it is also posible to hold fixed the satellite starting elements and the coordinates of the tracking stations.

From the observations equations the normal equations are formed, as given by equation (3.152) and

these are subsequently solved by Choleski's method of triangular decomposition (equations (3.154) to (3.157)) for the unknown parameters. The full covariance matrix (equation (3.193)) is also evaluated and the a posteriori standard errors of the observed ranges and the unknown parameters are computed and output. The least squares residuals, with corresponding reliability and error analysis, are also output from the program, and may be output graphically using the RESPLOT program of the SODAPOP suite.

### 5.4.2 Program Input and Output

The mode and operation of SOAP are controlled by values input from a serial computer file. In addition, input is also required from a minimum of four other serial (and random) access computer files. These provide the laser range observations, the satellite ephemeris, the partial derivatives and the Chebyshev polynomial coefficients. Concise details of the file handling are not included in this section, but the required input may be summarised as follows.

(i) Program mode. This parameter may take three values, as described in § 5.4.1.

(ii) Input of earth rotation parameters. The available options are similar to those in ORBIT. The earth rotation parameters may be either input from the CHEBPOL file or from a separate file. If input from the CHEBPOL

file they may be either linearly
interpolated or fixed throughout the day.
If, however, they are input from a separate
file then only the latter option is
available.

(iii)   Number of tracking stations.

(iv)   Details of the reference ellipsoid on which
the coordinates of the tracking stations are
given. The required parameters are the
semi-major axis and the flattening of the
ellipsoid.

(v)   Approximate coordinates, latitude,
longitude and height, of each tracking
station.

(vi)   Number of tracking stations to be held
fixed in the solution, and the
identification number of each station to be
fixed.

(vii)   Number of tracking stations whose longitude
is to be fixed in the solution, and the
identification number of each station.

(viii)   Orbit fixed flag. This flag indicates
whether the orbit starting elements are to
be fixed or solved for during the solution.

(ix)   Earth rotation parameter flags. These
indicate whether polar motion ($x_p$ and $y_p$)

and/or UT1-UTC are to be solved for as
unknowns.

(x)     Flags to indicate which force model
        parameters are to be determined as unknowns.
        These may include the geocentric
        gravitational constant GM, the along track
        acceleration coefficient $C_T$, the solar
        radiation pressure reflectance coefficient
        $C_R$ and normalized spherical harmonic
        coefficients $\bar{C}_n^m$ and $\bar{S}_n^m$. Clearly, SOAP may
        only determine those parameters for which
        partials have been previously generated by
        ORBIT.

(xi)    Approximate values of the force model
        unknowns which are included in the
        solution.

(xii)   The epoch corresponding to the initial
        satellite state vector used by ORBIT, input
        as year,day number and UTC time in hours,
        minutes and seconds.

(xiii)  The inertial frame satellite state vector.

(xiv)   The integration step size, in seconds, of
        the predictor-corrector scheme of the ORBIT
        program. This corresponds to the interval
        between successive records in the ephemeris
        and partials files generated by ORBIT and
        used by SOAP.

(xv)      The satellite ephemeris file (inertial
          frame) produced by ORBIT.

(xvi)     The file of (inertial frame) position
          partial derivatives, with respect to the
          starting elements and the force model
          unknowns (also from ORBIT).

(xvii)    Laser range observations file. If the
          program is operating in modes 1 or 2 then
          the range observations are required.
          In mode 3 the file(s) should contain the
          observation equations previously created by
          SOAP in mode 2.

The output from SOAP is principally in the form
of a computer printout, which gives details of the
particular solution and the data set, and the results
of the adjustment. If required the output may also
include the residual and error analysis of each range
measurement. The least squares range residuals may also
be output to a computer file in a format suitable for
the graph plotting program RESPLOT. However, when SOAP
is operating in mode 2, no solution is performed and so
the the only outputs are a printout giving details of
the data set and a file of the observation equations.

## 5.5 VALIDATION AND OPERATION OF SODAPOP

### 5.5.1 <u>Software</u> <u>Validation</u>

As with any computer program, a very important stage of the development of the SODAPOP suite was the process of checking whether the various programs perform the required tasks correctly and to sufficient accuracy. Certain tests may be performed 'in house' but at some stage the products of the programs must be compared with corresponding results from a totally independent source. In this particular context, these 'products' are the coordinates and parameters resulting from the analysis of the same set of laser ranging data by both SODAPOP and another orbit determination package. The suite has been tested using several different sets of LAGEOS laser ranging data, and the resulting tracking station coordinates (and other parameters) compared with external values. The results of these tests and the subsequent processing of other data sets are presented in Chapter 6.

At various stages of the development of the programs internal checks have also been carried out. In order to verify the validity of using Chebyshev polynomials to evaluate the precession and nutation matrices, in both SOAP and ORBIT, the ORBIT program was initially developed using the exact evaluation of the complete series and formulae. When the later version of ORBIT was subsequently developed, to include the Chebyshev polynomial representation in preference to

the exact evaluation, the corresponding ephemerides generated by the two programs were compared and no sigificant differences were detected (Agrotis, 1984).

The precision of the orbit integration was checked by first generating one orbital ephemeris and then repeating the procedure after halving the integration step length. An ephemeris produced by ORBIT was also compared with a corresponding ephemeris generated by the ORBIT program of the SATAN package developed independently at the Royal Greenwich Observatory by Dr. A. T. Sinclair and Mr. G. M. Appleby (Sinclair and Appleby, 1986). The results of this comparison are presented by Agrotis (1984).

The operation of SOAP in modes 2 and 3 was checked by first running the program in mode 1 and processing a sample of laser ranging data. This data set was then split into two separate files and observation equations for these two data subsets were produced by SOAP operating in mode 2. The combined solution was performed, using SOAP in mode 3, and the results of the two solutions compared. Clearly, the two solutions should produce identical results and this was indeed verified.

It was also important to check the operation of the pre-processing software to ensure no biases or errors were introduced into the resulting data set. Initially, a set of filtered observations and the corresponding set of normal points were processed

separately, in order to demonstrate the effects of using normal points. There were no significant differences between the two solutions, however there was a considerable saving of both time and storage when normal point ranges were used. Similarly, the results of a solution carried out using normal points generated by DATPAK-2 was also compared with a solution performed using the normal points of the MERIT Standard Data Sets. These were produced by the Centre for Space Research of the University of Texas (Schutz, 1983b), from the same raw laser ranging observations. Again, there was a very close agreement between the two solutions.

The process of refinement and validation of the SODAPOP suite is still continuing, as more data sets are processed. This has allowed more extensive, and significant, comparisons to be made with results produced by other analysis centres and with comparable results produced by different techniques (such as Very Long Baseline Interferometry).

## 5.5.2 Operation of SODAPOP

Previously in this Chapter, the programs of SODAPOP have been discussed separately and with only limited reference to the other programs of the package. Although each program may be operated in several different modes, even greater flexibility is introduced by operating the programs in various combinations. The

aim of this section is to bring together all the programs of the package, and describe typical operational configuations of combinations of the programs. For example, the pre-processing package DATPAK-2 currently uses virtually every program of the SODAPOP suite, including the two main programs ORBIT and SOAP. The combination of the programs used by DATPAK-2 is illustrated in fig 5.III, and the details of the operational modes of the programs are discussed in § 5.2.1.3.

Variations in the operation of SOAP and ORBIT arise for two main reasons. Firstly, when processing long periods of data (say, longer than one month) it is necessary to use a different approach to that used when processing, say, 5 days of laser ranging data. Secondly, particular procedures must be adopted when determining earth rotation parameters, to avoid ill-conditioning of the normal equations (see § 3.4.4). The procedure adopted at Nottingham for the determination of earth rotation parameters is discussed in § 4.3.2.

The analysis of a short period of data, (say 5-days), to obtain the coordinates of the tracking stations and the orbital starting elements may be considered as a standard mode of solution. The ephemeris and partials may be generated in a single computation, without the need to divide the orbit into smaller and more manageable sections. The least squares solution may also be completed in a single execution of

the program. In contrast, the analysis of longer
periods of data (for example, one month) requires a
totally different approach. Although possible, it is
not currently practical to store the ephemeris and
partial derivatives for a complete month (or longer)
and the generation of such an orbit in a single program
execution is exceedingly time consuming. Consequently,
the ephemeris and data are handled more efficiently by
considering short (say, 5-days) periods at a time and
combining these to give the complete one month
solution. An operation of the two programs (SOAP and
ORBIT) may be as follows.

(i)     The one month set of tracking data is
        divided into a number of smaller (5-day)
        subsets.

(ii)    From the orbital initial starting elements
        the ephemeris and partial derivatives are
        generated for the first 5-day period. The
        observation equations are formed from the
        corresponding tracking data.

(iii)   The orbit integration is continued for a
        further 5 days (replacing the existing
        ephemeris and partials files) and the
        observation equations form for this 5 day
        period.

(iv)    Stage (iii) is repeated for the remainder
        of the sections of the long arc.

(v)    All the observation equation are read back
into SOAP (operating in mode 3) and the
least squares solution is performed. No
ephemeris or partials files are required
during this last stage.

Although this process is manageable, it is not
particularly efficient and a more elegant approach is
afforded by the use of Helmert blocking of the normal
equations (Cross, 1983). The SODAPOP package is
currently being modified to enable the analysis of very
long periods (for example, over one year) of laser
ranging observations, by adopting the Helmert-Wolf
procedures (Hill, Moore and Ashkenazi, 1986). However,
a discussion of the principles or applications of this
technique is beyond the scope of this thesis.

CHAPTER  SIX

DATA PROCESSING AND THE RESULTS

OF THE ANALYSIS

## 6.1 MERIT SHORT CAMPAIGN DATA[*]

### 6.1.1 <u>Introduction</u>

The initial development versions of the SODAPOP package (as described in Chapter 5) were tested using two short periods (four days each) of LAGEOS laser ranging data, observed in 1980. The aim of the analysis was not only to test and validate the software but also to ascertain the precision with which unknown parameters, such as tracking station coordinates, could be determined. As outlined in § 5.1 the package was developed jointly by the author and Dr. L. G. Agotis, and similarly the initial processing was also carried out jointly. However, the principal interest of Dr. Agrotis was to assess the effects of the various parameters of the force model and to test the suitability of different geopotential models. Consequently, the results of these particular tests will not be included in this thesis, but are presented in detail in Agrotis (1984). Details of the pre-processing of the data and the solutions performed in

---

[*] Although the title of of this section may imply the processed data was observed during the Short MERIT campaign, this is not strictly true for the second of the two periods of data considered. However, the intention is to convey the approximate period during which the observations were made.

order to recover the coordinates of the tracking
stations and the earth rotation parameters are given in
the following sections, with reference where
appropriate to the thesis of Dr. Agrotis.

With a view to the later processing of
observations from the Main MERIT Campaign, a further
aim of the initial trials was to develop and test
suitable analysis procedures for the determination of
earth rotation parameters. As a result, the package was
modified so as to enable longer periods of data to be
processed, and was tested using a fourteen day data set
from December 1980. The results of this latter solution
are presented in § 6.1.5.

## 6.1.2 Data Sets and Pre-Processing

Two 4-day periods of LAGEOS laser ranging data,
observed during 1980, have been processed using the
SODAPOP package. The aim of the analysis was,
principally, to test the software package and to asses
the capabilities of the orbit determination procedure
(see § 6.1.1). The data sets were observed between
September $2^{nd}$ and $5^{th}$ 1980, and December $2^{nd}$ and $5^{th}$
1980, and were provided to the University of Nottingham
by the Royal Greenwich Observatory, which in turn
received the data from the NASA Goddard Space Flight
Center (GSFC). At the time of the observations the
contributing tracking stations were generally $2^{nd}$
generation facilities (see § 2.2.2), i.e. with a

single shot range accuarcy of about 10 - 20cm and a firing repetition rate of around 1 pulse per second. However, several first generation systems were still operational. The details of the tracking stations which contributed data during the two periods are given in fig. 6.I, together with their nominal coordinates which are taken from the GSFC SL5 geodetic parameter solution (Christodoulidis et al, 1982). It is noticeable that all of the tracking stations are operated by the Goddard Laser Tracking Network (see § 2.2.2) and consequently the majority are located around the American continent (particularly in California). The global locations of the tracking stations are also shown on the world map of fig. 6.II.

The data was received as 'full rate' raw range observations and so required pre-processing before the main analysis stage. Although referred to as 'raw' data a number of corrections had been applied to the data (either at the tracking stations or the data distribution centre) before release to analysts. The observed ranges were generally corrected for the effects of atmospheric refraction (using the Marini and Murray model, see § 2.3.3.1), the satellite centre-of-mass correction (see § 2.3.3.2) and other instrument errors particular to each tracking station. However, in order to ensure a standard form of data, and a unified modelling of errors, the effects of any corrections applied to the data (for atmospheric refraction and

| ID No. | System | Location | Nominal Tracking Station Coordinates latitude (deg min sec) | longitude (deg min sec) | height (m) | Data Sets (1980) |
|--------|--------|----------|------------------------|----------------------|-----------|------------------|
| 7063 | STALAS | Greenbelt | 39 1 13.3581 | 283 10 19.8002 | 15.252 | Sept/Dec |
| 7090 | MOBLAS-5 | Yarragadee | -29 2 47.4115 | 115 20 48.1106 | 237.411 | Sept/Dec |
| 7091 | MOBLAS-7 | Haystack | 42 37 21.6820 | 288 30 44.3452 | 88.353 | Sept |
| 7096 | MOBLAS-6 | Am. Samoa | -14 20 7.5191 | 189 16 30.3563 | 45.142 | Sept |
| 7114 | MOBLAS-2 | Owens Val. | 37 13 57.2091 | 241 42 22.2214 | 1174.590 | Dec |
| 7115 | MOBLAS-3 | Goldstone | 35 14 53.8977 | 243 12 28.9542 | 1035.159 | Sept/Dec |
| 7120 | MOBLAS-1 | Haleakala | 20 42 27.3907 | 203 34 38.1072 | 3064.181 | Sept/Dec |
| 7896 | TLRS-1 | Pasadena | 34 12 20.0227 | 241 49 39.7243 | 437.894 | Dec |
| 7907 | ARELAS | Arequipa | -16 27 56.7010 | 288 30 24.6028 | 2485.156 | Sept/Dec |
| 7943 | ORRLAS | Orroral Val | -35 37 29.7593 | 148 57 17.1341 | 941.858 | Sept/Dec |
| 7929 | NATLAS | Natal | -5 55 40.1238 | 324 50 7.2367 | 32.245 | Sept |

$$a_e = 6378144.11m \qquad\qquad 1/f = 298.255$$

Fig 6.I Details of Tracking Stations (1980) and Nominal Coordinates
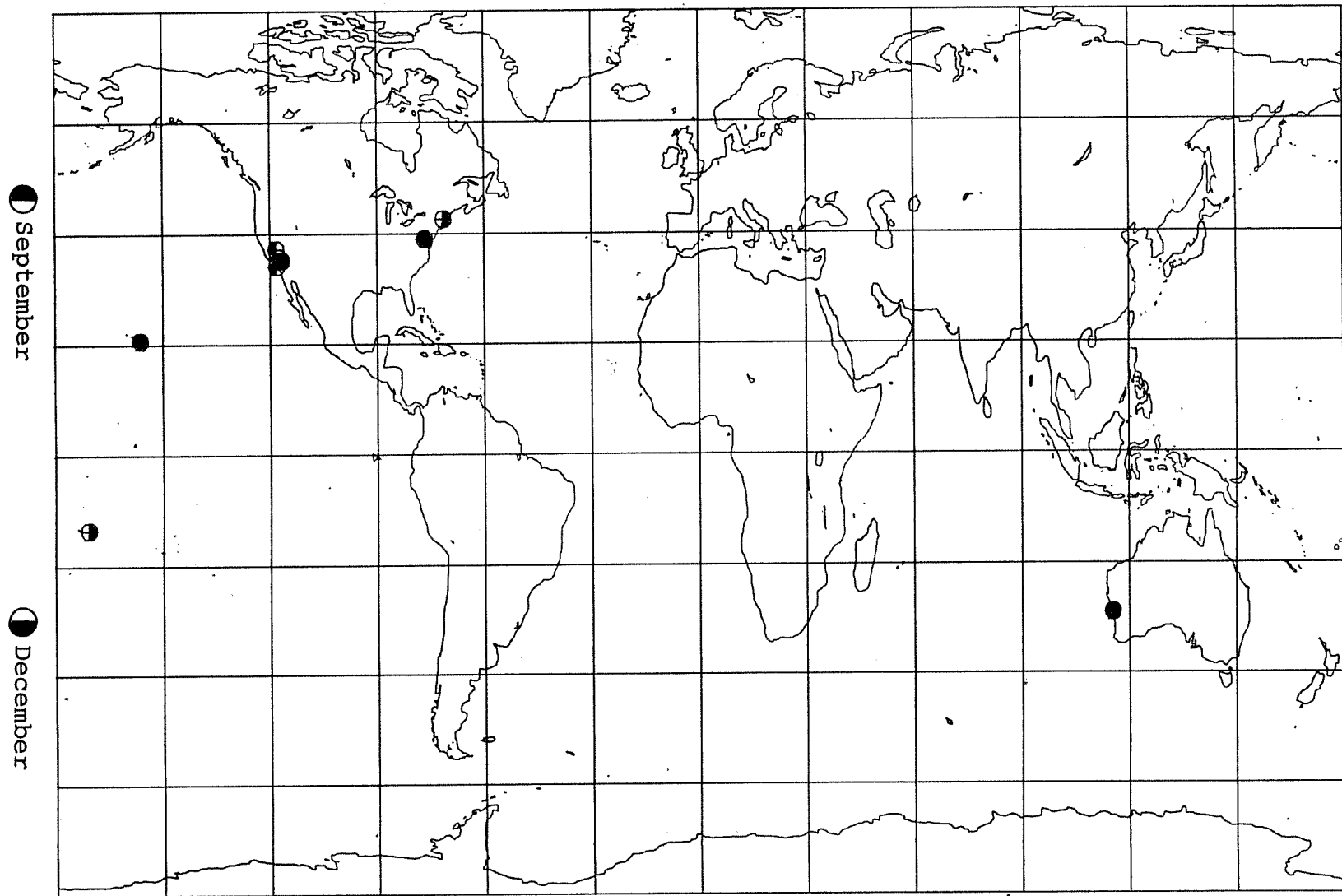
Fig 6.II <u>Location of Tracking Stations (1980)</u>

|  | September<br>2 - 5, 1980 | December<br>2 - 5, 1980 | December<br>2 - 15, 1980 |
|---|---|---|---|
| No. of Tracking Stations | 6 | 6 | 6 |
| No. of Raw Range Observations | 28271 | 13498 | – |
| No. of Normal Point Ranges | 645 | 356 | 1019 |
| Ratio | 40:1 | 38:1 | – |

Fig 6.III <u>Specifications of Data Sets (1980)</u>

centre-of-mass) were removed before pre-processing and
the subsequent analysis. As outlined in § 5.5.1
corrections of these effects are evaluated using
standard models by the SOAP program and applied to each
range observation (or normal point range) during the
analysis phase. The table in fig 6.III outlines the
general specifications of the two periods of data.
Clearly, for the process of obtaining an initial
evaluation and validation of the software and
procedure, the number of raw range observations far
exceeded the requirements and was unmanageable. For
this reason the data sets were 'compressed' by means of
normal points (see § 2.4.1.3) after any spurious
observations (and passes) had been filtered out. The
pre-processing was carried out using the DATPAK-1
software (as described in § 5.2.2) which was operated
such that the data was filtered up to a maximum of four
time (using a $10^{th}$ order polynomial) and normal point
ranges were produced for each minute of data. This
procedure resulted in approximately a 40:1 reduction in
the quantity of data.

The coverage of the ranges of the four day
periods was far from ideal and the data sets were
dominated by observations from station 7090 (Yarragadee
in Australia). However, considering the objectives of
the analysis, as outlined in the previous section, it
was decided that the data was suitable.

6.1.3 <u>Solutions</u> <u>for</u> <u>Tracking</u> <u>Station</u> <u>Coordinates</u>

The two LAGEOS data sets, from September and December 1980, were each processed twice with the aim of obtaining the coordinates of the tracking stations and consequently the inter-station baselines. The same 'model' was used in both solutions with the exception of the polar motion components. In the first solutions (for both data sets) the polar motion values adopted were linearly interpolated from the BIH Circular D published values. Subsequently, polar motion components were determined from the same tracking data (as described in § 6.1.4) and these new polar motion values were used to re-adjust the tracking station coordinates in the final processing of the data. During the latter solution the 'derived' polar motion components replaced the BIH circular D values, and were fixed throughout the four day periods. The resulting coordinate sets are presented later in this section together with comparisons with independently obtained corresponding coordinates of the tracking stations.

The solution vector comprised the cartesian earth fixed coordinates of all the contributing tracking stations, the six elements of the initial satellite state vector (inertial frame) and the coefficients of the along track acceleration, $C_T$, and of the solar radiation pressure model, $C_R$. A number of tests had been previously performed in order to determine the effects of releasing different parameters

of the force model as unknowns of the solution vector
(Agrotis, 1984). The suitability of different
geopotential models was investigated (Agrotis, 1984 and
Ashkenazi, Agrotis and Moore, 1984) and as a result the
GEM-L2 geopotential model (see § 3.3.2) was adopted.
Scale was provided by the adopted speed of light
($2.99792458 \times 10^8$ $ms^{-1}$) and the compatible value of the
geocentric gravitational constant, ($3986000.448 \times 10^{-14}$
$m^3 s^{-2}$) which was fixed during the solutions. The earth
rotation parameters used are discussed above, with the
exception of the UT1-UTC values which were linearly
interpolated from the BIH Circular D values. As
outlined in § 3.4.4, the only additional constraint
required was satisfied by fixing the longitude of one
of the tracking stations. Accordingly, the longitude of
STALAS (station 7063, see fig 6.I) was restrained to
the GSFC SL5 value of $283^0$ 10' 19.8" (Christodoulidis
et al, 1982). A spheroid of semi major axis 6378144.11m
and a flattening of 298.255 was used for all the
geodetic coordinates (i.e. $\phi$, $\lambda$, h).

As only 4-day periods of data were processed, no
special 'long arc' techniques, as described in § 5.6.2,
were necessary and so the analysis procedure consisted
of the determination of the satellite orbit (by a
single execution of the ORBIT program) followed by the
least squares adjustment, using the SOAP program. This
procedure was repeated, iteratively, a number of times
until the corrections to the unknowns were considered

negligible. The a posteriori standard errors of all the unknown parameters (see § 3.4.5) were also evaluated by the analysis program (SOAP).

The root-mean-square range residuals (as defined in § 3.4.5) from all the least squares solutions were of the order of 10cm. This parameter gives an indication of not only the precision (on average) of the range measurements but also the precision of the computed orbit. As the 'raw' range data had an accuracy of around 10 - 20cm, a high level of agreement between the computed orbit and that implied by the range measurements may be inferred.

As mentioned previously, the data sets were processed twice, with different polar motion values, and accordingly the results of the two analyses will be presented and discussed separately. The final coordinates of the tracking stations, obtained using the BIH Circular D values of polar motion, are presented in fig G.I and fig G.II of Appendix G, for September and December respectively. These are geocentric earth fixed coordinates and are tabulated in both cartesian and geodetic representations. The internal standard errors, evaluated from the covariance matrix, of the coordinates are also included.

The internal standard errors of the station coordinate determinations for the September data set are of the order of 5cm, with the exception of station 7096. In this particular case one of the component

standard errors is in excess of one metre, however, this is attributable to the fact that only one pass of observations from this station was included in the data set. As there were fewer observations, and consequently a slightly worse coverage, in the December data set, there is a noticeable increase of the internal standard errors of the tracking station coordinates, to around 10 - 20cm. However, there appears to be no particular station which is determined significantly better (or worse) than any other. These standard errors do not, however, give a true indication of the repeatability or the 'external' accuracy of the station coordinates. For this purpose, it is necessary to compare the derived coordinates with compatable values determined independently.

The differences between the cartesian coordinates of the tracking stations obtained from the September and December 1980 solutions, and the differences between these and the coordinates of the GSFC SL5.1 solution (Christodoulidis et al, 1982) are presented in fig G.III. Similarly the differences in geodetic coordinates ($\phi$, $\lambda$, h) are tabulated in fig G.IV. To give an indication of the average difference between the coordinate sets the root-mean-square differences are evaluated and included at the bottom of the respective figures. From these it can be seen that the cartesian components are repeatable, and in agreement with the SL5.1 solution, to better than 80cm (on average). Similarly, the

geodetic coordinates are in agreement to better than 90cm. However, it is noticeable that all the differences in station heights are significantly lower than the differences in longitude or latitude. In particular the heights of the stations common to both the September and December solutions are repeatable to around 6cm. The largest differences are of the latitudes of the tracking stations and these may be attributed to errors in the adopted BIH polar motion values. Consequently, the second stage of the processing involved the determination of the earth rotation parameters during the two periods, and is discussed in the following section (§ 6.1.4).

In addition to the coordinates of the tracking stations the inter-station baselines were also evaluated and those common to all three solutions (Sept 80, Dec 80 and GSFC SL5) are presented in fig G.V, together with the differences between the baseline lengths and the root-mean-square differences. It is noticeable that the baselines from the different solutions are in agreement to around 20cm (on average), which compares with the average differences of tracking station coordinates of around 80cm. This improvement may be attributed to the fact that any small errors in the orientation of the network of tracking stations should not effect the baseline lengths. Furthermore, it also supports the hypothesis that the large coordinate differences were due to errors in the polar motion values.

Following the determination of the polar motion components during the two periods (see § 6.1.4) the solutions outlined above were repeated. The unknown parameters and the model were the same as previously, except that the new polar motion values replaced the corresponding BIH Circular D values and were fixed throughout the 4 day periods. The cartesian and geodetic earth fixed coordinates of the tracking stations re-determined from the September and December data sets are tabulated in fig G.VI and fig G.VII, respectively. The internal standard errors of these coordinates were not significantly different from those obtained from the previous solutions (see fig G.I and fig G.II).

The coordinate differences between the revised September and December solutions and the GSFC SL5 solution are given in fig G.VIII (for X, Y, Z) and fig G.IX (for $\phi$, $\lambda$, h). Comparing these figures with those for the coordinate differences using the BIH polar motion values (fig G.III and fig G.IV) it can be seen that there was a very significant improvement. As would be expected the differences in latitude showed the greatest improvement, the average difference decreasing from around 80cm to 20cm. However, the improvement of the longitude and height differences was not significant. The September coordinate solution, with the exception of station 7096 (due to the limited coverage and large standard errors), was generally in

agreement with the SL5 solution to better than 20cm.
The agreement between the December solution and SL5 was
slightly worse (better than 45cm), however this may be
attributed to fewer observations and more restricted
coverage (see fig 6.III).

The revised baselines between the tracking
stations and the differences in baseline lengths
between the September, December and SL5 solutions are
given in fig G.X. Comparing this table with the values
tabulated in fig G.V, it can be seen that the adoption
of different polar motion components has had a
negligible effect on the lengths of the baselines.
However, the differences of station coordinates are now
of the same order as the differences of the baselines.
These average differences (in fig G.VIII and fig G.IX)
give a better indication of the 'true' accuracy of the
station coordinates than the internal standard errors
given in fig G.I. Considering the short duration of the
data sets these results encouraged the subsequent
analysis of longer periods of data (see § 6.1.5).

## 6.1.4 Solutions for Polar Motion

The large differences of the latitudes of the
tracking stations (see fig G.IV), between the September
and December solutions and the SL5 solution, were
attributed to errors in the adopted polar motion
components. These values were taken from the BIH
Circular D and linearly interpolated to the epochs of

the observations. In order to aleviate this problem new polar motion values were determined from the same laser ranging data sets. The general methods of determining the polar motion components from laser ranging observations are described in § 4.3, however in this particular case the analysis procedure was as follows.

As previously explained, it is not possible to simultaneously determine polar motion and the latitudes of all the tracking stations, and the minimum requirement requires that either one pair of polar motion values are fixed or the latitudes of two of the tracking stations are fixed. With only four day data sets the former solution is not viable and so the latitudes of at least two of the tracking stations must be constrained. Consequently, during the first stage of the analysis the coordinates of all the tracking stations were held fixed to the GSFC SL5.1 values (Christodoulidis et al, 1982). The polar motion components and the satellite initial state vector (and the two force model coefficients) were then determined from the September data set. One value of $x_p$ and one of $y_p$ were obtained for the four day period and assigned an epoch equivalent to the mean epoch of all the observations during the period. With these polar motion values fixed, and the tracking station coordinates released, the solution to compute the coordinates of the tracking stations was performed (for the September

data), resulting in the values tabulated in fig G.VI.
In order to compute the polar motion components for the
December period of data, the coordinates of the four
common stations were fixed to the final September
values and the remaining two values fixed to the SL5
values. Finally, the coordinates of the tracking
stations were recomputed using the December data set
and the derived polar motion components.

The polar motion values determined from the
September and December four day data sets are tabulated
in fig G.XI, together with the corresponding, five day
average, values from the BIH Circular D and those
determined by the Goddard Space Flight Center (GSFC
GEM-L2) during the computation of the GEM-L2
geopotential model (Lerch et al, 1982). All the values
are given in units of milli-arc-seconds (0.001 seconds
of arc), where 1 mas is approximately equivalent to 3cm
on the earth's surface. The Nottingham values were
determined with an internal precision of the order of
1 mas, compared with approximately 3 mas for the 'GSFC
GEM-L2' values.

From fig G.XI it can be seen that for both the
September and December epochs there is a close
agreement between the Nottingham and GSFC values,
however both these solutions differ, considerably, from
the BIH circular D values. During this period the
smoothed BIH polar motion was derived, principally,
from Classical Astrometric and Transit Doppler

observations, with very little (or no) contribution from laser ranging. Because of the dependence of the derived components on the adopted tracking station coordinates, independent absolute values of polar motion may not be obtained. However, the change of the component between the epochs may be determined. The final column of fig G.XI gives the difference between the December and September polar motion components and again a close agreement may be seen between the Nottingham and GSFC differences.

The possibility of determining UT1-UTC, and changes of this parameter (often expressed as changes in the length of day, LOD) were also investigated. Because of the short periods of data being processed errors in UT1-UTC did not significantly effect the tracking station coordinates. Consequently, the results of the investigation are not included in this thesis, but are discussed in detail in Agrotis (1984).

### 6.1.5 Analysis of Fourteen Day Data Set

Following the successful analysis of the two 4-day data sets the software package was modified so as to enable longer orbits to be generated and consequently longer periods of data to be processed. The analysis procedures adopted for the SODAPOP package are discussed in § 5.6.2. In summary, the method consists of dividing the long orbit into a series of smaller, more manageable, consecutive arcs, for example

each with a duration of 5 days. The range observation
equations are formed, separately, for each short period
and then combined to give the final solution. In order
to test this major modification to the software a data
set consisting of 14 days of LAGEOS range data observed
between the $2^{nd}$ and $15^{th}$ of December 1980 was
processed. This period of data included the four days
of data from December 1980 which was processed
previously. The specifications of the data are given if
fig 6.III and as with the previous analysis the raw
data was filtered and compressed into 1 minute normal
points. The pre-processing resulted in a total of 1019
normal points from 6 tracking stations (see fig 6.I and
fig 6.II). The data was divided into three consecutive
four day periods and a final two day period, and a
single solution was performed to determine the tracking
station coordinates, the initial sateliite state vector
and the two coefficients of the force model ($C_T$ and
$C_R$). As before the earth rotation parameters were
interpolated between the BIH circular D values and all
other components of the model were mainatained as
described in § 6.1.3.

For both the fou day solutions the
root-mean-square range residual (one-way) was of the
order of 10cm, however because of the increased orbital
errors introduced by the 14 day integration (a total of
10080 predictor-corrector 2 minute integration steps)
the rms residual in this case was of the order of 13cm.

The resulting earth fixed tracking station coordinates are tabulated in fig G.XII. Both the geodetic and cartesian representations are given together with the corresponding internal standard errors. These coordinates are compared with the corresponding coordinates from both the four day December 1980 (BIH polar motion) solution and the GSFC SL5.1 solutions, in fig G.XIII and fig G.XIV. It is noticeable that there is a close agreement between the two Nottingham December solutions, with the mean differences all better than 30cm. This result is not suprising considering the same model and earth rotation parameters were used, however it does serve to verify the adopted analytical principles. The intercomparison with the SL5.1 solution again reveals a close agreement between the heights (an average difference of 12cm) and longitudes (25cm) and a poor agreement between the latitudes (56cm). This, as previously, may be attributed to errors in the adopted polar moion components.

Clearly, differences between the latitues may be reduced by determining a set of polar motion values from the same data set. However, an alternative approach was adopted, which entailed the determination of systematic rotational biases (about the X and Y axes of the earth fixed system) between the derived coordinates and those of the GSFC SL5.1 solution. These small rotations correspond to the systematic biases in

the coordinates introduced by the systematic errors in the polar motion components. The principles of this procedure are discussed in § 3.2.1.5, and the biases between the two coordinate sets were determined using the TRANSFORM program (see § 5.1).

After the removal of the effects of the two rotations ($\alpha_x$ = -0.016 arc seconds and $\alpha_y$ = -0.012 arc seconds) the resulting coordinates (D80/14b) are compared with the SL5.1 solution in the final column of fig G.XIII and fig G.XIV. As would be expected the modelling of the systematic rotations, introduced by the polar motion components, has removed the large differences between the latitudes of the two solutions.

As described previously (in § 6.1.3) the baselines between the tracking stations are insensitive to small errors in the polar motion components. Consequently, there is a very good agreement between the baseline lengths resulting from the December fourteen day solution and both the December four day solution and the GSFC SL5.1 solution. A selection of the baselines, corresponding to those tabulated in fig G.V, are presented in fig G.XV. In addition the baseline lengths are compared with the other solutions and the differences are also tabulated along with the root-mean-square differences.

6.2    MERIT MAIN CAMPAIGN DATA

6.2.1  Introduction

As previously mentioned in § 4.4.2 the Geodesy Research Group of the Univeristy of Nottingham contributed to Project MERIT as an Associate Analysis Centre for both Satellite Laser Ranging and Very Long Baseline Interferometry. This section is concerned with the results obtained from the processing of a subset of the MERIT LAGEOS laser ranging data. With Project MERIT in mind the aim of the analysis was to derive a series of earth rotation parameters over the period considered and compare this with other independently obtained series. In addition the aim was to also determine a reliable set of coordinates of the tracking stations. The suitability of determining these station coordinates and earth rotation parameters from different periods of data was also investigated.

The SODAPOP suite of programs (see Chapter 5) was used to process and analyse the LAGEOS laser ranging data collected during the first four months (September to December 1983, inclusive) of the Main MERIT Campaign. On recognising that the pre-processing of the full rate 'raw' data would have presented a considerable, time consuming, task it was decided that the MERIT Standard Data Sets (as described in § 4.4.3) would be processed, in preference to the full rate data.

The specifcations of the data sets, and the procedures and models adopted, are detailed in the following sections. In addition the results of the processing and comparisons with corresponding results from other analysis centres are also presented.

## 6.2.2 Data Set Specifications

The four 1 month Standard Data Sets of LAAGEOS laser ranging data, observed during the period September to December 1983, were received at Nottingham on Magnetic tapes from the Royal Greenwich Observatory. The RGO previously received the data through the MERIT communications network illustrated in fig 4.IV. The selection of the first four months, in preference to any of the later months of the campaign, was dictated by the availability of the data sets, at the time. Clearly, the observations taken at the start of the campaign became generally available before any of the later observations. The time constraint of the research project restricted the analysis to the first four months.

During these four months a total of over 1.1 million raw range observations were received at the Data Collection Centre, from 23 stations around the world. The pre-processing, consisting of filtering and data compression, of this raw data resulted in the total of 11091 'normal point' observations, from 19 stations, of the Standard Data Sets.

This pre-processing was performed at the Center for Space Research (CSR) of the University of Texas at Austin, the MERIT Operational Centre for Satellite Laser Ranging. The normal points were generated by the method described in § 2.4.1.3, each representing a 3 minute period of raw data.

As the raw range measurements were observed at so many sites there was a large variation of the estimated a priori standard errors of the raw ranges, from between 2 and 20cm ($2^{nd}$ and $3^{rd}$ generation instumentation). During the data compression standard errors of the resulting normal point ranges were evaluated, and these ranged between 0.1 and 10cm (schutz, 1983b). The details of the tracking stations are given in fig 6.IV and their approximate locations are illustrated in fig 6.V. The stations separated in the second half of fig 6.IV contributed observations to the full rate data sets but these were not included in the Standard Data Sets.

Before the formation of the normal point ranges the full rate data (or 'Quick Look' data) was converted, at the CSR, into a standard format. This consisted of correcting all the various time tags to UTC(BIH) and removing any corrections applied to the data for atmospheric refraction and satellite centre-of-mass. The ranges are scaled by the standard speed of light (299792458 $ms^{-1}$) and any other anomalies corrected. This extensive pre-processing stage

| ID No. | System | Location |
|--------|--------|----------|
| 1181 | POTSDM | ZIPE, Potsdam, GDR |
| 7086 | MLRS | Ft. Davis, Texas |
| 7090 | MOBLAS-5 | Yarragadee, Australia |
| 7105 | MOBLAS-7 | GSFC, Greenbelt, Md |
| 7109 | MOBLAS-8 | Quincy, Ca |
| 7110 | MOBLAS-4 | Monument Peak, Ca |
| 7112 | MOBLAS-2 | Platteville, Co |
| 7121 | MOBLAS-1 | Huanhine, French Pol. |
| 7122 | MOBLAS-6 | Mazatlan, Mexico |
| 7210 | HOLLAS | Haleakala, Maui, Hawaii |
| 7805 | METFIN | Metsahovi, Finland |
| 7831 | HELWAN | HIAG and TUP, Helwan, Egypt |
| 7833 | KOOTWK | Kootwijk Obs., Netherlands |
| 7834 | WETZEL | IfAG, Wetzell, FRG |
| 7838 | SHO | Simosato Hydrographic Obs., Japan |
| 7839 | GRAZ | Obs. Graz-Lustbuehel, Austria |
| 7840 | RGO | Royal Greenwich Obs., UK |
| 7907 | ARELAS | Arequipa, Peru |
| 7939 | MATERA | PSN, Matera, Italy |
| | | |
| 1837 | SIMIEZ | Simiez, Crimea, USSR |
| 7062 | TLRS-2 | Otay Mountain, Ca |
| 7220 | TLRS-1 | Monument Peak, Ca |
| 7837 | CHILAS | Shanghai, China |

Fig 6.IV Details of Tracking Stations (1983)

| Standard Data Set | Sept | Dec | Nov | Dec | Total |
|-------------------|------|-----|-----|-----|-------|
| No. of Stations | 14 | 18 | 18 | 16 | 19 |
| No. of Raw Ranges | 240202 | 315462 | 284971 | 179223 | 1019858 |
| No. of N.P. Ranges | 2388 | 3532 | 2771 | 2400 | 11091 |
| Nottingham Solns. | | | | | |
| No. of Stations | 14 | 17 | 16 | 18 | 18 |
| No. of N.P. Ranges | 2387 | 3528 | 3762 | 2379 | 11056 |

Fig 6.VI Specifications of Data Sets (1983)
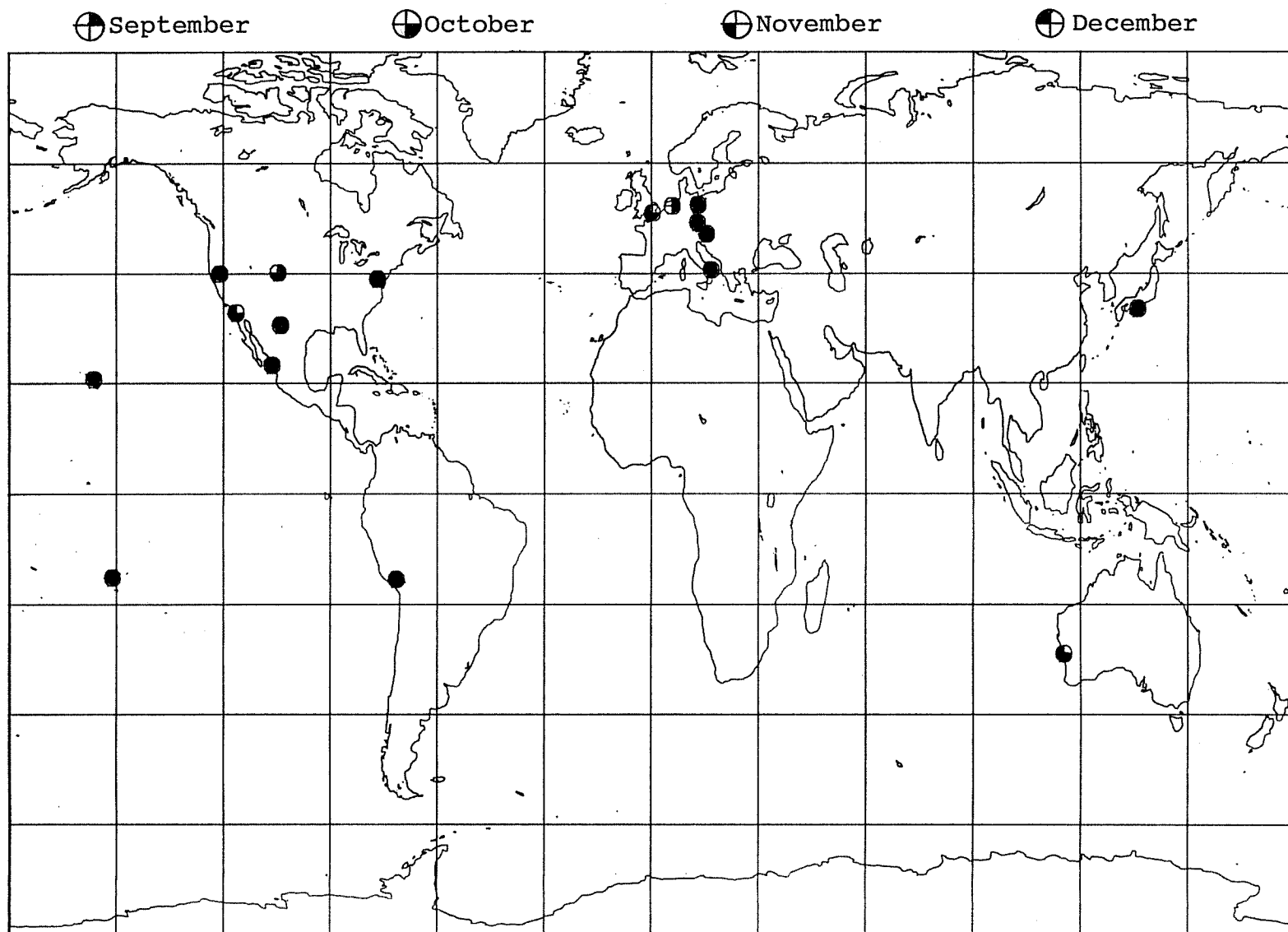
Fig 6.V Locations of Tracking Stations (1983)

simplifies the subsequent analysis and also ensures a unified set of observations.

On receipt of the data at Nottingham it was initially scanned and a number of whole data sets from certain stations were rejected. This editing was based on an assessment of whether there was a sufficient quantity of data for a coordinate solution for that station. The observations from Helwan (7831) were rejected from both the October (4 ranges) and November (6 ranges) data sets. In addition the 3 ranges from Metsahovi (7805) were also rejected from the November set. The entire data set from Platteville (7112) was similarly rejected from the December set (9 ranges). Because of an anomaly of the SOAP program any ranges with observation epochs within the first 10 minutes of an orbit must also be rejected. This situation arises because of the interpolation algorithm used for the satellite ephemeris, which requires the satellite state vector to be known for the preceding 5 integration steps (2 minutes each). As a result a number of other ranges were also edited from the data sets. The total number of stations and normal point ranges of the Standard Data Sets and the corresponding numbers used in the monthly solutions are given in fig 6.VI.

### 6.2.3 Analysis Procedure and Models

The basic principles of the procedure adopted for the processing of laser ranging data are outlined in § 4.3.2.

In summary, the four monthly sets of observations were processed separately and the processing of each month was carried out in two distinct stages. The first stage consisted of establishing a stable reference orbit and set of tracking station coordinates using all the observations from the particular month. This required the generation of a 30 (or 31) day orbit which was performed using the method outlined in § 5.6.2. For this purpose the complete orbit (and corresponding range data) was divided into six consecutive 5 day periods (with an additional day for October and December). The unknowns in the least squares solution included the initial satellite state vector, the coordinates of all the tracking stations, and the coefficients of the solar radiation pressure ($C_R$) and the along track acceleration ($C_T$) models. The geocentric gravitational constant, GM, was also determined from the September and October data sets. During this first stage, the earth rotation parameters were interpolated between the BIH circular D values. As described previously the only additional constraint required to enable a solution was the fixing of the longitude of one of the tracking stations. In this case the longitude of station 7210 (see fig 6.IV) was held fixed at the value given in the CSR 8112.2 LAGEOS Station coordinate solution. Despite the variation of the a priori standard errors of the range data (see § 6.2.2) no weighting was applied to the observations

This results in a default weighting of 1 metre for all the range observations.

The one month data sets were then divided into 1-day and 5-day subsets, for the second stage of the processing. A separate solution was performed for each subset of range observations, in order to determine UT1-UTC and the two components of polar motion, $x_p$ and $y_p$. During the second stage the initial satellite state vector, the cartesian coordinates of the tracking stations and the coefficients $C_T$ and $C_R$ (and GM) were all held fixed at the values determined from the first stage of the analysis.

This process resulted in two series of earth rotation parameters at roughly 1 and 5 day intervals, for each month. An epoch was assigned to each set of earth rotation parameters calculated as the mean of all the observations epochs of the particular data subsets. Finally, the new earth rotation parameters were interpolated to the nominal BIH epochs (0.0hrs UT, at 5-day intervals). By adopting these values, in replacement of the BIH Circular D values, the first stage of the procedure was repeated in order to re-establish the satellite orbit and the tracking station coordinates.

Throughout the processing the same models and parameters were used, so as to ensure a uniformity between the solutions. The models were configured so as

to be in close agreement, wherever possible, with the MERIT standards. The detailed specifications of the parameters, constants and models adopted are given in fig 6.VII. There are two notable deviations from the recommendations of the MERIT Standards. Firstly, the $c_2^1$ and $s_2^1$ harmonic coefficients of the geopotential model were not modified, as recommended, but maintained at the GEM-L2 values. The modification was overlooked during the processing of the first month of data (September 1983) and so for consistency was not applied before the later solutions. Secondly, the displacements of the tracking stations due to ocean tidal loading were neglected, as they were not considered to be significant compared to the observational accuracies. Only the effects of direct solar radiation pressure were modelled, and so the effects of Albedo radiation were neglected. The 'shadow' test of the solar radiation pressure model was not operated, however the reflectance coefficient was included as an unknown parameter.

## 6.2.4 Solutions for Tracking Station Coordinates

As described in the previous section the coordinates of the tracking stations were determined twice for each monnth of LAGEOS laser range data. The models and unknowns in the solutions were identical except for the earth rotation parameters. The initial solutions used the BIH circular D series while the

| | |
|---|---|
| Geopotential Model | GEM-L2 - 20×20, with $C_2^1$ and $S_2^1$ not modified as recommended by the MERIT Standards. |
| GM | $3.98600448×10^{14}$ $m^3s^{-2}$ |
| Velocity of Light, c | $2.99792458×10^8$ $ms^{-1}$ |
| Third Body Attractions | sun, moon and Planets : Venus, Mars, Saturn, Jupiter. |
| Solid Earth Tides | Appendix 5, MERIT Standards (Wahr model), frequency dependent Love numbers, Gravitational effect on satellite and station displacements modelled. |
| Ocean Tides | Appendix 6, MERIT Standards (Schwiderski model), station displacements not modelled. |
| Solar Radiation Pressure | Direct radiation (no Albedo), reflectance coefficient $C_R$ is an adjusted parameter, no earth shadow cut-off. |
| LAGEOS Along Track Acceleration | $C_T$ is an adjusted parameter |
| Refraction Correction | Marini-Murray model |
| Centre-of-mass Corrn. | 0.240m (for LAGEOS) |
| Nutation | IAU 1980 |
| Precession | IAU 1976 |
| Spheroid | $a_e$ = 6378137.0m, 1/f = 298.255 |

Fig 6.VII <u>Adopted Constants and Models</u>

second solutions used the series of earth rotation parameters derived at Nottingham (from the same data sets). The coordinates determined from both sets of solutions are presented in this section.

In addition to the tracking station coordinates the remaining unknowns in the solutions were the initial satellite state vector and the two force model coefficients $C_T$ and $C_R$. The parameters and models used during the processing are given in § 6.2.3. The rms (root-mean-square) range residual of all the solutions was of the order of 20 - 25cm. As described in § 6.1.3, this value indicates the mean accuarcy of the tracking data (over short arcs) and the accuarcy of the orbit determination (over longer arcs). However, this parameter must be viewed with caution because simply by including more unknown parameters in the solution the residuals, and consequently the rms residual, tend to become smaller.

The sets of tracking station coordinates resulting from the four 1 month solutions, using BIH earth rotation parameters, are presented in fig H.I, fig H.II, fig H.III and fig H.IV (of Appendix H) for the September, October, November and December data sets, respectively. The geodetic ($\phi$, $\lambda$, h) coordinate representation is given, expressed with respect to a spheroid with a semi major axis of 6378137.0m and flattening of 298.255. In addition the internal standard errors of the various components,

derived from the respective covariance matrices, are
also given (in units of metres). It is notable that the
standard errors of a number of stations of the
September 1983 solution are considerably larger than
those of all the other stations. In particular three
stations, 1181, 7834 and 7838 (see fig 6.IV) have
standard errors of the coordinate components of greater
than 30cm, while those of the remaining stations are of
the order of 5 - 15cm. However, these large values may
be attributed to the limited number of LAGEOS passes
tracked by the stations during September (2 passes for
1181 and 3 each for 7834 and 7838). Other variations of
the standard errors may be approximately correlated
with the estimated a priori standard errors of the
range observations (Schutz, 1983b).

Although the internal standard errors may give
an indication of which station coordinates are poorly
determined, they do not give a 'true' estimate of the
accuracy of the derived coordinate set. As previously
described the repeatability of the solutions (from one
month to the next) and the external comparison with
other independent coordinate sets give a more realistic
estimate of the 'true' accuracy.

The four sets of coordinates were compared,
individually, with the LAGEOS station coordinate
solution 8112.2 (LSC 8112) of the Center for Space
Research (CSR) of the University of Texas at Austin.
Because of the large number of tracking stations common

to the coordinate sets it is not practical to present all the difference of the coordinate components and baselines. Consequently, only the root-mean-square (rms) differences of the cartesian and geodetic coordinates and the rms differences of the baseline lengths are given in fig H.V. The Nottingham solutions are identified in the figure by a four character code (i.e. SEPB) of which the first three characters indicate the particular month of the data and the final character differentiates between coordinate sets obtained using BIH (B) earth rotation parameters and those using the Nottingham (N) values.

The LSC 8112 coordinates were determined from approximately five years of LAGEOS tracking data, and this set was selected in prefernce to the GSFC SL5.1 set (Christodoulidis et al, 1982) because the latter offered fewer stations in common with the Nottingham coordinate sets. However, it has been since shown that the LSC 8112 coordinates may contain systematic biases, notably a 0.7m offset of the origin in the direction of the Z-axis (Tapley et al, 1985). Consequently, the selection of these coordinates as a reference set may now be questioned, however at the time they were considered to be the most suitable.

From fig H.V it can be seen that the rms differences of all the coordinate components are of the order of 20 - 50cm. as with the previous coordinate solutions (see § 6.1.3) the best agreement was between

the heights (above the reference ellipsoid) of the tracking stations and the worst between the latitudes, with the latter possibly atributabe to errors in the adopted polar motion series. A seven parameter least squares adjustment of each monthly set of coordinates to the the LSC 8112 coordinates was performed as described in § 3.2.1.5. These seven parameters included the rigid body translations of the implied origin ($\delta x$, $\delta y$, and $\delta z$), three rotations about the orthogonal axes ($\alpha_x$, $\alpha_y$, and $\alpha_z$) and a scale parameter (c). The transformation parmeters determined between the coordinate sets are tabulated in fig H.VI. It is notable that the largest (and most significant) translations for each month are along the Z-axis, however this may be due to the systematic errors of the LSC 8112 coordinates. The scale difference of around $3.0 \times 10^{-8}$ between the September, October and November coordinates and LSC 8112 may be due to the adopted GM value (see § 3.4.4). The LSC 8112 coordinates were determined using a fixed value of $3.98600440 \times 10^{14}$ $m^3 s^{-2}$ whereas the value of GM was determined as an unknown parameter (see fig H.X) from the September, October and November data sets. The December solution, however, adopted the MERIT recommended value of GM and consequently only a very small scale difference was determined between the two coordinate sets.

After the removal of these bias parameters from the Nottingham coordinate sets the comparisons with

LSC 8112 coordinates were repeated and the resulting rms differences are tabulated in fig H.VII. The sets of coordinates are identified by the same codes used in fig H.V, however, a subscript is added to indicate that the biases with respect to the University of Texas solution have been removed. The rms differences of the coordinate components (both cartesian and geodetic) are all less than 40cm, with a mean of around 28cm. The rms differences of the baseline lengths, after the removal of the scale bias, are of the order of 45cm.

In order to test the repeatability of the monthly coordinate solutions the sets of coordinates were inter-compared, both before and after the removal of the transformation parameters from LSC 8112. The resulting rms differences of the geodetic and cartesian coordinates and the baseline lengths are given in fig H.VIII. The corresponding rms differences after the removal of the transformation parameters are similarly tabulated in fig H.IX. As would be expected the agreement between the Nottingham solutions is better than the agreement with the LSC 8112 coordinates. From fig H.IX it can be seen that the rms differences of the coordinate components and the baseline lengths are of the order of 20cm and 30cm respectively. These monthly variations were, however, larger than anticipated and required further investigation (see Chapter 7).

For the second stage of the processing of the data (see § 6.2.3) the coordinates of the tracking

stations given in figures H.I to H.IV were held fixed,
and the resulting earth rotation parameters are
discussed in § 6.2.5. Following the interpolation of
these new values to the same epochs as the BIH
Circular D values, they replaced the latter in the one
month coordinate solutions. The analysis outlined
previously was repeated for each month of laser ranging
data and the resulting coordinates of the tracking
stations are tabulated, together with their internal
standard errrors, in figures H.XI to H.XIV.

The root-mean-square range residuals from the
various solutions reduced from around 25cm to 20cm when
the Nottingham earth rotation parameters were adopted.
There was also a corresponding reduction of the
internal standard errors of the coordinates of the
tracking stations. As described previously, each
monthly set of coordinates was compared both with the
LSC 8112 coordinates and with those from the other
monthly solutions. The rms differences of the
coordinates and the baseline lengths between the
Nottingham solutions and LSC 8112 are given in
fig H.XV. The codes used to identify the particular
solution are similar to those described previously,
except that the last character is now 'N' (rather than
'B') to indicate that the Nottingham earth rotation
parameters were used. In comparison with fig H.V the
introduction of the new earth rotation parameter series
had very little effect on the tracking station

coordinates, and no consistent reduction (or increase) of a particular component (such as latitude) is evident.

The transformation parameters between the Nottingham solutions and LSC 8112 were re-determined and are tabulated in fig H.XVI. Except for the September values all the remaining transformation parameters are similar to those determined previously (see fig H.VI). After the removal of these bias parameters from the Nottingham coordinates they were again compared with LSC 8112, and the rms differences of the baseline lengths and cartesian and geodetic coordinates are given in fig H.XVII. Following the replacement of the BIH earth rotation parameters with the Nottingham derived values an improvement of the agreement between the resulting sets of coordinates and the LSC 8112 coordinates had been expected. However, in practice, there was a slight degradation of the agreement, as may be seen by comparing fig H.XVII with fig H.VII. This may indicate that either the method of determining earth rotation parameters was not producing a representative and accurate series (see § 6.2.5) or the differences are due to some other effect not accounted for in the analytical model.

Finally, the monthly coordinate sets were inter-compared, both before and after the removal of the transformation parameters of fig H.XVI. The resulting rms differences of the coordinates and baseline lengths

are tabulated in fig H.XVIII and fig H.XIX. In
comparison with fig H.VIII and fig H.IX, the adoption
of the new series of earth roataion parameters does not
appear to have significantly increased or decreased the
level of agreement between the individual monthly
coordinate solutions.

### 6.2.5 Solutions for Earth Rotation Parameters

The procedure adopted for the determination of
earth rotation parameters is described, in principle,
in §4.3.2 and in detail, for the particular solutions
performed, in § 6.2.3. The analyses resulted in two 4
month series for each of the unknown earth rotation
parameters ($x_p$, $y_p$ and UT1-UTC) at roughly one and five
day intervals. An epoch was assigned to each set of
values and as described in § 4.3.3. post-processing
procedures were used to interpolate (and compress in
the case of the daily series) the 'raw' values to the
same epochs as the BIH Circular D series. From the
resultng UT1-UTC values, corresponding values of the
excess length of day, D, were also evaluated, using the
principles outlined in § 4.3.3. Estimates of the
a posteriori standard errors of all the derived
parameters were also obtained.

The earth rotation parameters detemined over the
four month period and the correspponding standard
errors are given in fig J.I and fig J.II (of
Appendix J) for the values resulting from the 1-day

(UNOTT.1) and 5-day (UNOTT.5) solutions. The internal standard errors of all the components of the UNOTT.5 series are very consistent, with those of the polar motion components varying between 0.0012 and 0.0026 arc seconds and the excess length of day between 0.0 and 0.3 milli-seconds of time. However, the corresponding standard errors of the UNOTT.1 series are far less consistent, with occasional very large values. These variations may be attributed, to some extenet, to the interpolation process, which required the fitting of a quadratic function to five of the daily values. Principally, however, the variations are a result of only using a single day of tracking data to determine each 'raw' value.

In order to assess the accuracy and reliability of the two series of earth rotation parameters, they were compared with three corresponding series derived independently at other institutions. These comprised the smoothed series published by the BIH in their Circular D, and two series determined by the Centre for Space Research of the University of Texas. The BIH values were determined from a combination of results derived by different observational techniques (see § 4.2), whereas the CSR values were derived from only LAGEOS laser range 'Quick Look' data. The two CSR solutions were determined using the LPM 81.12 and LPM 84.02 systems (Schutz, 1983b)and will be referred to as CSR 81.12 and CSR 84.02 during the remainder of this section.

The tables of the differences between these 5 different series of earth rotation parameters are given in fig J.III, fig J.IV, fig J.V and fig J>VI for $x_p$, $y_p$, UT1-UTC and excess length of day D, respectively. The values are given for 0.0 hours UT on the day numbers of 1983 tabulated in the first column of the figures. As previously, the root-mean-square differences were also evaluated and are given at the bottom of the respective columns.

From these figures it can be seen that the agreement between the two Nottingham series was of the order of 4 - 8 mas (milli-arc-seconds) for the polar motion components. In comparison, however, the agreement between either of the Nottingham series and the BIH valus was of the order of 8 - 10 mas ad with the CSR values, 11 - 16 mas. These comparisons also indicated the existence of large systematic differences between portions of the series and the external values. In particular, a systematic difference, of the order of -17 mas,may be seen between UNOTT.1 and BIH series during the period (day numbers) 274 to 300. This period corresponds to the October data set and indicates that monthly discontinuities have been introduced to the Nottingham UNOTT.1 and UNOTT.5 series. Similar large differences also exist between the Notingham and CSR series, however, there are no systematic differences between the two Nottingham solutions.

The differences between the Nottingham UT1-UTC series and the BIH series are given in fig J.V and show an agreement between the sets of Nottingham values of the order of 0.7 ms (milli-seconds of time). This compares with an rms difference between either of these and the BIH values of the order of 1.0 ms. Rather than considering the 'absolute' values of UT1-UTC, fig J.VI gives the differences between the changes of UT1-UTC, expressed as the excess length of day, D. Because this latter series does not depend on the absolute values of UT1-UTC, it is largely free from any systematic differences introduced during the solutions. Consequently, the agreement the between different series is improved, resulting in rms differences of the order of 0.1 to 0.2 ms. Furthermore there is no indication of any systematic differences between these values.

In order to assess the 'true' level of agreement between the different series of earth rotation parameters, any systematic differences between the Nottigham vaues and the corresponding BIH values were determined (by least squares) and removed from the Nottingham values. Discrete monthly sets of range data were used during the determination of the Nottingham earth rotation parameters and so the series were first divided into the corresponding monthly sections and a set of bias parameters were determined for each month. The resulting systematic differences are presented in

fig J.VII and fig J.VIII, for UNOTT.1 and UNOTT.5. It
is notable that similar differences were detected for
both the UNOTT.1 and UNOTT.5 series, indicating that
the differences had not been introduced during the
determination of the earth rotation parameters, but
during the initial computation of the reference orbit
and tracking station coordinates.

The effects of these systematic differences were
removed from the UNOTT.1 and UNOTT.5 series and
resulted in UNOTT.1b and UNOTT.5b as given in fig J.IX
and fig J.X, respectively. The differences between
these two Nottingham series and the BIH Circular D
values were re-computed and are tabulated in fig J.XI,
fig J.XII, fig J.XIII and fig J.XIV for $x_p$, $y_p$, UT1-UTC
and D, respectively. The agreements between the two
sets of Nottingham values of $x_p$ and $y_p$ are of the order
of 5 mas and 7 mas, which are not significantly
different from the agreements before the removal of the
biases. However, the agreement between the Nottingham
values of $x_p$ and $y_p$ and those of the BIH are now of the
order of 4 mas and 6 mas respectively (as compared to
around 8 - 10 mas previously). Similarly, the agreement
of the UT1-UTC series has also improved to around 0.9
ms. However, as would be expected, the differences
between the various series of the excess length of day
(fig J.XIV) shows no significant changes from those of
fig J.VI.

This level of agreement between the Nottingham earth rotation parameters and those determined independently is of a similar order to the agreement between the CSR 81.12, CSR 84.02 and BIH (smoothed) values. However, this agreement, particularly with the University of Texas LAGEOS derived values, is slightly worse than anticipated, and again may be principally a result of the analytical procedures adopted, rather than the particular models (as these were in accordance with the MERIT recommendations).

In conclusion, the Nottingham values of $x_p$, $y_p$ and the excess length of day, resulting from the 1-day and 5-day solutions (UNOTT.1 and UNOTT.5), are illustrated graphically together with the BIH Circular D values in figures J.XV to J.XXII. The corresponding values after the removal of the systematic differences of figures J.VII and J.VIII are similarly illustrated in figures J.XXIII to J.XXX. Because of the range of the UT1-UTC values determined during the four month period it is not possible to present a representative illustration, however the values of the excess length of day are illustrated in the figures.

CHAPTER   SEVEN

CONCLUSIONS  AND  SUGGESTIONS  FOR

FURTHER  WORK

7.1    CONCLUSIONS

1.    A suite of computer programs, known as SODAPOP
      (Satellite Orbit Determination and Analysis
      Package Of Programs), has been developed in order
      to process Satellite Laser Ranging observations
      to the LAGEOS satellite. The programs are
      structured so as to enable, after slight
      modifications, the extension of the package to
      include different satellites and different types
      of tracking data.

2.    The constants, models and procedures adopted
      during the development of the software were,
      wherever possible, in accordance with the
      recommendations of the Committee for Project
      MERIT Standards (Melbourne, 1983).

3.    The programs were tested and validated by
      processing two short 4-day periods of LAGEOS
      laser range data from September and December
      1980.

4.    The earth fixed coordinates of the tracking
      stations were determined from each data set,
      using earth rotation parameters as published by
      the BIH, with an internal precision of between 5
      and 20 cm. The agreement between the two sets of
      coordinates, and each with the GSFC SL5.1
      coordinates, was better than 90 cm. The baseline
      lengths agreed to better than 40 cm.

5. Using the two 4-day periods of LAGEOS data the two components of polar motion ($x_p$ and $y_p$) were determined. Although these values differed from the BIH values by about 1m they agreed with the 'GEM-L2' values to better than 20cm.

6. The coordinates of the tracking stations were re-computed using the derived polar motion values and the resulting coordinates agreed with the SL5.1 coordinates to better than 40cm.

7. To test a modification of the software, to enable the processing of long periods of data (say one month), a 14-day data set from December 1980 was processed. The agreement between the resulting tracking station coordinates and GSFC SL5.1 was of the order of 30 - 50cm. After the modelling of systematic rotations about the X and Y axes, the agreement of the coordinates was of the order of 20 - 30cm.

8. Following the testing of the various programs, SODAPOP was used to process LAGEOS laser range data observed during the first four months (September to December, 1983) of the Main MERIT Campaign, with the aim of determining the coordinates of the tracking stations and the earth rotation parameters.

9. In order to reduce the necessary work load, pre-processed 'compressed' data, prepared at the

University of Texas was processed in preference to the 'full rate' data sets.

10. Using each month of data, the earth fixed coordinates of the tracking stations were determined, twice. Firstly, with the BIH Circular D earth rotation parameters and secondly with the Nottingham derived values.

11. The coordinates agreed with the University of Texas 8112.2 coordinate set to better than 60cm. They were also repeatable, between the monthly solutions, to around 50cm.

12. Seven parameter transformations were modelled between the monthly coordinate solutions and 8112.2. After the removal of the transformation parameters the agreement was better than 40cm, and the repeatability was around 20 - 30cm.

13. Two series of earth rotation parameters were determined, for the four month period. The first series was derived from 'raw' values determined from daily batches of range data, whereas the values of the second series were determined from 5-day periods of data.

14. The agreement between the two series and with other independent series was of the order of 8mas for $x_p$ and $y_p$ and better than 0.2ms for the excess length of day.

15. After the removal of systematic differences between the Nottingham and BIH series the agreement was of the order of 3 - 7mas for $x_p$ and $y_p$.

16. The use of the Nottingham series (UNOTT.1) of earth rotation parameters in replacement of the BIH Circular D smoothed values, in the monthly coordinate solutions, degraded the agreement between the derived coordinates and the 8112.2 coordinate set.

17. The analytical procedure adopted for the determination of earth rotation parameters is not considered to be a completely satisfactory method. Several limitations and restrictions of the method became evident and in particular the requirement to hold the orbit fixed was considered to be an inappropriate approach.

18. The ability of the dynamical analysis of Satellite Laser Ranging data to determine earth rotation parameters, and the dependence of the resulting series on the adopted analytical procedure, have been demonstrated.

7.2   SUGGESTIONS FOR FURTHER WORK

1.   The SODAPOP software should be modified so as to enable the determination of a number of polar motion and earth rotation (UT1-UTC) values in a single solution. In addition it should be possible to hold any pair of polar motion components (or the latitudes of two tracking stations) and UT1-UTC fixed to any pre-determined (or standard) initial values. These two modifications would enable a single stage analysis procedure to be adopted, only requiring the additional constraint of the two components of polar motion (or two latitudes) and UT1-UTC at a particular reference epoch during the period of data.

2.   Methods of efficiently extending the period of data that may be processed in a single solution should be investigated. The method of storng the observation equations described in this thesis soon becomes inefficient and methods such as Helmert blocking may be more appropriate. Such an approach would also, for example, enable the processing of all the data from the Main MERIT Campaign in a single solution, resulting in a single, continuous, earth rotation parameter series.

3.  The analysis of the Main MERIT Campaign data should be continued, by whatever method, so as to enable a more detailed evaluation of the resulting coordinates and earth rotation parameters.

4.  The methods of post-processing of the earth rotation parameters also requires further investigation and the merits of the various approaches evaluated.

5.  Because of the variation of the estimated a priori standard errors of the current laser range data, the weighting of range observation equations in the least squares solution should be investigated. This should include the determination of representative standard errors of 'normal point' compressed range data.

6.  The SODAPOP package should be modified so as to enable the analysis of laser range data to, initially, STARLETTE and other satellites. This would require, for example, the inclusion of a model for air drag to be added to the current force model of the ORBIT program.

7.  The effects of 'tuning' the geopotential coefficients of the gravity field should be investigated, paricularly for low altitude satellites, such as STARLETTE. Clearly, the determination of geopotential coefficients would

require the analysis of long periods of data and so would be dependent on the fulfillment of other suggestions for further work.

8. The variations of the individual coordinate components of the monthly coordinate solutions, with repsect to an average coordinate set, should be further investigated.

Note. During the interval between the end of the research period and the completion of this thesis, research including a number of these suggestions for further work has been started at the University of Nottingham.

# APPENDIX A

# ROTATION MATRICES

APPENDIX A

ROTATION MATRICES

For a right handed orthogonal coordinate system a rotation about the $i^{th}$ axis, through an anticlockwise angle $\theta$ (when viewed from the positive end of the axis towards the origin) may be expressed by a rotation matrix $R_i(\theta)$, (Krakiwsky and Wells, 1971) where,

$$R_1(\theta) = \begin{pmatrix} 1 & 0 & 0 \\ 0 & \cos\theta & \sin\theta \\ 0 & -\sin\theta & \cos\theta \end{pmatrix} \quad (A.1)$$

$$R_2(\theta) = \begin{pmatrix} \cos\theta & 0 & -\sin\theta \\ 0 & 1 & 0 \\ \sin\theta & 0 & \cos\theta \end{pmatrix} \quad (A.2)$$

$$R_3(\theta) = \begin{pmatrix} \cos\theta & \sin\theta & 0 \\ -\sin\theta & \cos\theta & 0 \\ 0 & 0 & 1 \end{pmatrix} \quad (A.3)$$

The order of the execution of a number of rotations (expressed as a product of the matrices) must be strictly adhered to as the rotation matrices do not commute.

APPENDIX B

COMPUTATION OF SATELLITE

ELEVATION ANGLE

APPENDIX B

COMPUTATION OF SATELLITE ELEVATION ANGLE
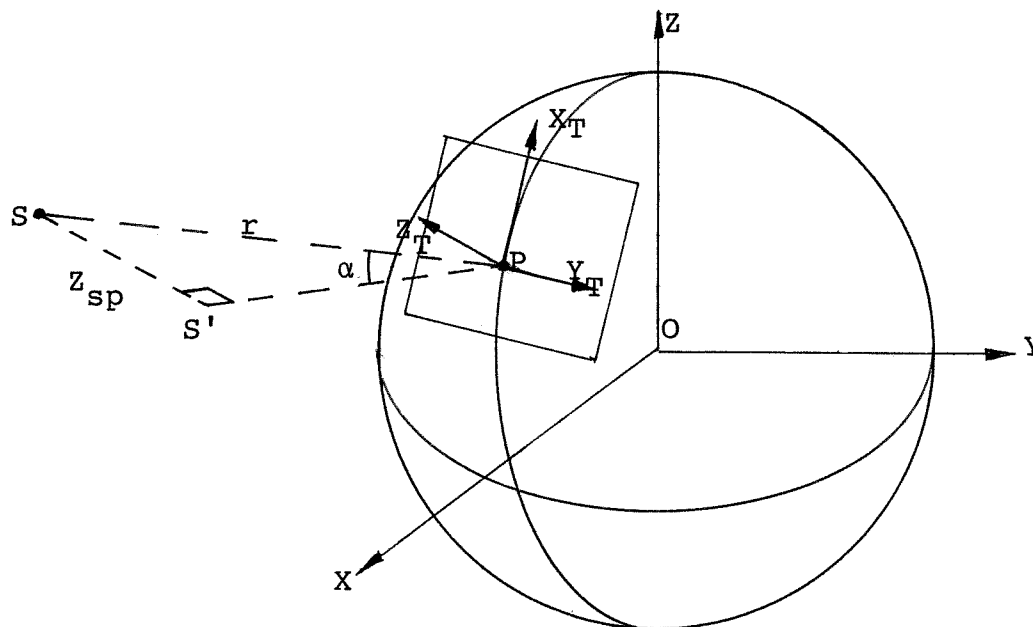


Fig B.I Satellite Elevation Angle

In fig B.I point P represents the tracking station on the earth's surface and point S the satellite. The geocentric earth fixed coordinate axes are X, Y and Z and the local topocentric axes at point P are $X_T$, $Y_T$ and $Z_T$ (see § 3.2.1.4). Line S'P lies in the plane of the $X_T$ and $Y_T$ axes, and line SS' is parallel to the $Z_T$-axis.

The elevation angle of a satellite is the angle between the local horizontal plane and the line between the tracking station and the satellite (Marini and Murray, 1973), and is given by,

$$\alpha_{sp} = \sin^{-1} (Z_{sp} / r) \qquad (B.1)$$

where $\alpha_{sp}$ : elevation angle of satellite, S, at

point p,

$Z_{sp}$ : zenith height of the satellite, S, above the horizontal plane through P,

r : computed range between S and P, as given by equation (3.160).

The zenith height of the satellite above the horizontal plane is the $Z_T$ component of the local topocentric coordinates of the satellite. This may be evaluated by converting the earth fixed coordinates of the satellite into the local topocentric system, using equation (3.29). However, as only the $Z_T$ component is required, equation (3.29) may be simplified to give,

$$Z_{sp} = (X_s - X_p) \cos \phi \cos \lambda + (Y_s - Y_p) \cos \phi \sin \lambda$$
$$+ (Z_s - Z_p) \sin \phi \qquad \text{(B.2)}$$

where $X_s$, $Y_s$, $Z_s$ : earth fixed coordinates of the satellite,

$X_p$, $Y_p$, $Z_p$ : earth fixed coordinates of the tracking station,

$\phi$, $\lambda$ : geodetic latitude and longitude of the tracking station.

APPENDIX C

FITTING OF POLYNOMIALS

BY LEAST SQUARES

APPENDIX C

FITTING OF POLYNOMIALS BY LEAST SQUARES

The example discussed in this Appendix is concerned with the fitting of an $n^{th}$ order polynomial to a set of k range observations. However, the principles may be generalised and used with any form of data or time series. From equation (2.13) the polynomial representation of the range may take the form,

$$a_o + a_1(t_i - t_0) + a_2(t_i - t_0)^2 + . .$$
$$. . + a_n(t_i - t_0)^n = r_{t_i} + v_i \qquad (C.1)$$

where $a_0, , a_n$   :   polynomial coefficients,

$(t_i - t_0)$  :   time interval since reference epoch, $t_0$,

$v_i$       :   least squares residual,

$r_{t_i}$     :   observed range at epoch $t_i$,

Given a series of k range observations, where k is greater than n, an equation such as (C.1) may be set up for each range and expressed in matrix form by,

$$T \cdot \underset{\sim}{a} = \underset{\sim}{r} + \underset{\sim}{v} \qquad (C.2)$$

where

$$T = \begin{pmatrix} 1 & (t_1 - t_0) & (t_1 - t_0)^2 & . . . & (t_1 - t_0)^n \\ 1 & (t_2 - t_0) & (t_2 - t_0)^2 & . . . & (t_2 - t_0)^n \\ . & . & . & & . \\ . & . & . & & . \\ 1 & (t_k - t_0) & (t_k - t_0)^2 & . . . & (t_k - t_0)^n \end{pmatrix} \qquad (C.3)$$

and $\underline{a}$ : vector of unknown coefficients $a_0$ to $a_n$,

$\underline{r}$ : vector of observed ranges $r_1$ to $r_k$,

$\underline{v}$ : vector of least squares residuals.

The least squares normal equations (see Appendix E) may be formed from equation (C.2) and these solved for the unknown coefficients $a_0$ to $a_n$. A suitable method of solution of the normal equations would be Choleski's method of symmetric decomposition (see § 3.4.2). Following the solution, the residuals may be obtained, if required (for example, for the filtering of raw data), by back substitution using equation (C.2).

APPENDIX D

INTERPOLATION FORMULAE

APPENDIX D

INTERPOLATION FORMULAE

D.1  Chebyshev Polynomials

A function $f(t)$ may be represented over an interval $t_0$ to $t_0 + \Delta t$, in terms of Chebyshev polynomials, as,

$$f(t_i) = \sum_{k=1}^{n} a_k \cos k\,\theta \qquad (D.1)$$

where  $\theta = \cos^{-1}\left( \dfrac{(t_i - t_0) - \dfrac{\Delta t}{2}}{\Delta t} \right) \qquad (D.2)$

and n is the order of the polynomial.

The coefficients $a_k$ are computed by evaluating the function at n+1 specific data points, $f(t_j)$ where (from equation D.2),

$$t_j = \Delta t \cos \theta_j + \frac{\Delta t}{2} + t_0 \qquad (D.3)$$

and  $\theta_j = \left( \dfrac{2j + 1}{n + 1} \right) \dfrac{\pi}{2}$  for $j = 0, 1, - - n$  (D.4)

The Chebyshev polynomial coefficients are given by,

$$a_0 = \frac{1}{n + 1} \sum_{j=0}^{n} f(t_j) \qquad (D.5)$$

$$a_k = \frac{2}{n + 1} \sum_{j=0}^{n} f(t_j) \cos k\theta_j \qquad (D.6)$$

Although n+1 coefficeints may be computed, when the function is evaluated at some epoch within the interval a truncated series of m terms may be used ( $m < n$ ).

## D.2   Everett Interpolation

Given a function $f(t)$ which is known at discrete data points $t_i$, at constant intervals $\Delta t$, then the function may be interpolated within the interval $t_i$ to $t_{i+1}$ by using the Everett central difference formula,

$$f(t) = E_0 \; f(t_i) + E_2 \; \delta^2 f(t_i) + E_4 \; \delta^4 f(t_i) + \; .. \quad (D.7)$$
$$+ \; F_0 \; f(t_{i+1}) + F_2 \; \delta^2 f(t_{i+1}) + F_4 \; \delta^4 f(t_{i+1}) + \; ..$$

where   $E_0 = 1 - u$ $\qquad\qquad\qquad$ (D.8)

$\qquad E_1 = u(1 - u)(2 - u)/3!$ $\qquad\qquad$ (D.9)

$\qquad E_2 = (-1 - u)u(1 - u)(2 - u)(3 - u)/5!$ $\quad$ (D.10)

$\qquad F_0 = u$ $\qquad\qquad\qquad\qquad$ (D.11)

$\qquad F_2 = u(u^2 - 1)/3!$ $\qquad\qquad\qquad$ (D.12)

$\qquad F_4 = u(u^2 - 1)(u^2 - 4)/5!$ $\qquad\qquad$ (D.13)

with

$$u = \frac{t - t_i}{\Delta t} \qquad (D.14)$$

and the term $\delta^n f(t_j)$ is the $n^{th}$ central difference of $f(t_j)$ as defined by,

$$\delta^2 f(t_j) = f(t_{j-1}) - 2f(t_j) + f(t_{j+1}) \qquad (D.15)$$

$$\delta^4 f(t_j) = f(t_{j-2}) - 4f(_{j-1}) + 6f(t_j) - \qquad (D.16)$$
$$- 4f(t_{j+1}) + f(t_{j+2})$$

The series is, in practice, truncated after the $n^{th}$ central difference (n must be an even integer) which implies that n+2 discrete data points must be known, evenly distributed about the particular epoch. The terms above are sufficient to the $4^{th}$ central

difference, in order to extend this to include the $8^{th}$ central difference additional terms would be required, as follows,

$$E_6 = (u + 2) E_4 (u - 4) \frac{3! \ 5!}{7!} \qquad (D.17)$$

$$E_8 = (u + 3) E_6 (u - 5) \frac{3! \ 5! \ 7!}{9!} \qquad (D.18)$$

$$F_6 = (u + 3) F_4 (u - 3) \frac{3! \ 5!}{7!} \qquad (D.19)$$

$$F_8 = (u + 4) F_6 (u - 4) \frac{3! \ 5! \ 7!}{9!} \qquad (D.20)$$

and the central differences,

$$\delta^6 f(t_j) = f(t_{j-3}) - 6f(t_{j-2}) + 15f(t_{j-1}) - \qquad (D.21)$$
$$- 20f(t_j) + 15f(t_{j+1}) - 6f(t_{j+2}) +$$
$$+ f(t_{J+3})$$

$$\delta^8 f(t_j) = f(t_{j-4}) - 8f(t_{j-3}) + 28f(t_{j-2}) - \qquad (D.22)$$
$$- 56f(t_{j-1}) + 70f(t_j) - 56f(t_{j+1}) +$$
$$+ 28f(t_{j+2}) - 8f(t_{j+3}) + f(t_{j+4})$$

APPENDIX E

LEAST SQUARES NORMAL EQUATIONS

APPENDIX E

LEAST SQUARES NORMAL EQUATIONS

E.1   Derivation of the Normal Equations

In order to obtain the most probable values of a vector of unknowns $\underline{x}$ from a given set of observations then the required values of $\underline{x}$ are those which minimise the sum of the squares of the residuals, i.e.

$$\underline{v}^T W \underline{v} = \text{minimum} \tag{E.1}$$

which gives

$$\frac{\partial (\underline{v}^T W \underline{v})}{\partial \underline{x}} = 0 \tag{E.2}$$

Given a set of observation equations, expressed in matrix form by,

$$A \underline{x} = \underline{b} + \underline{v} \tag{E.3}$$

which may be weighted to give,

$$W^{\frac{1}{2}} A \underline{x} = W^{\frac{1}{2}} \underline{b} + W^{\frac{1}{2}} \underline{v} \tag{E.4}$$

or

$$W^{\frac{1}{2}} \underline{v} = W^{\frac{1}{2}} A \underline{x} - W^{\frac{1}{2}} \underline{b} \tag{E.5}$$

then squaring this gives,

$$\underline{v}^T W \underline{v} = (W^{\frac{1}{2}} A \underline{x} - W^{\frac{1}{2}} \underline{b})^T \cdot (W^{\frac{1}{2}} A \underline{x} - W^{\frac{1}{2}} \underline{b}) \tag{E.6}$$

$$= \underline{x}^T A^T W A \underline{x} - \underline{x}^T A^T W \underline{b} - \underline{b}^T W A \underline{x} + \underline{b}^T W \underline{b} \tag{E.7}$$

Differentiating this with respect to x gives,

$$\frac{\partial (\underline{v}^T W \underline{v})}{\partial \underline{x}} = 2A^T W A \underline{x} - A^T W \underline{b} - A^T W \underline{b} \tag{E.8}$$

and so for a minimum,

$$2A^T W A \underline{x} - 2A^T W \underline{b} = 0 \tag{E.9}$$

which gives the matrix form of the normal equations as,

$$A^T W A \underline{x} = A^T W \underline{b} \tag{E.10}$$

## E.2 Symmetric Properties of the Normal Equations

The normal equation matrix, N, is given by,

$$N = A^T W A \qquad (E.11)$$

and so the transpose is given by,

$$N^T = (A^T W A)^T = A^T W^T A \qquad (E.12)$$

However, as W is a symmetric matrix then,

$$N^T = A^T W A = N \qquad (E.13)$$

## E.3 Positive Definite Property of Normal Equations

If the quadratic form of a symmetric matrix A is always positive for any real non-zero vector y, then the matrix A is said to be 'positive definite'. The normal equation matrix, N, is given by equation (E.11) and so for any vector $\underline{y} = [y_1, y_2, - - y_n]^T$, the quadratic form is,

$$\underline{y}^T N \underline{y} = \underline{y}^T.(A^T W A).\underline{y} \qquad (E.14)$$
$$= \underline{y}^T.(A^T W^{\frac{1}{2}}.W^{\frac{1}{2}} A).\underline{y}$$
$$= \underline{y}^T.(W^{\frac{1}{2}} A)^T.(W^{\frac{1}{2}} A).y$$

and so $\underline{y}^T N \underline{y} = (W^{\frac{1}{2}} A \underline{y})^T.(W^{\frac{1}{2}} A \underline{y}) > 0 \qquad (E.15)$

Clearly, the above result must be true since the sum of the squares of $(W^{\frac{1}{2}} A \underline{y})$ must always be positive.

Because the normal equation matrix, N, is positive definite, then by implication all the diagonal elements of N must be positive. For example, as,

$$\underline{y}^T N \underline{y} > 0 \qquad (E.16)$$

and choosing the real non-zero vector,

$$\underline{y} = [\ 1,\ 0,\ 0,\ -\ -\ 0\ ]^{\mathrm{T}} \qquad\qquad (E.17)$$

then the first element on the diagonal, $d_1$, must be positive. Similarly by choosing other suitable vectors for $\underline{y}$ it can be shown that all the other diagonal elements are positive.

Without these properties it would be impossible to solve the normal equations by Choleski's method of triangular decomposition (see § 3.4.2). This is because the method involves the computation of the square roots of the elements on the leading diagonal of the normal equation coefficient matrix. Clearly, non of these elements must be less than, or equal to, zero.

APPENDIX F

SATELLITE ACCELERATION DUE TO

THE EARTH'S ATTRACTION

APPENDIX F

SATELLITE ACCELERATION DUE TO THE EARTH'S ATTRACTION

From equation (3.74) a component, $\ddot{R}_i$, of the acceleration vector $\ddot{R}$ of the satellite due to the earth's attraction is given by,

$$\ddot{R}_i = \frac{\partial U}{\partial R_i} = \frac{\partial U}{\partial R_p} \frac{\partial R_p}{\partial R_i} + \frac{\partial U}{\partial \lambda_p} \frac{\partial \lambda_p}{\partial R_i} + \frac{\partial U}{\partial \phi_p} \frac{\partial \phi_p}{\partial R_i} \qquad (F.1)$$

where $R_i$ : component (X, Y, Z) of the earth fixed coordinates of the satellite,

$\ddot{R}_i$ : corresponding component ($\ddot{X}$, $\ddot{Y}$, $\ddot{Z}$) of the satellite acceleration vector.

The partials of the potential U with respect to the spherical polar coordinates, $R_p$, $\phi_p$, and $\lambda_p$, are evaluated by differentiating the expansion of the geopotential, as given in equation (3.64), to give,

$$\frac{\partial U}{\partial R_p} = \frac{-GM}{R_p^2} \left( 1 + \sum_{n=2}^{\infty} \sum_{m=0}^{n} \left( \frac{a}{R_p} \right)^n (n + 1) P_n^m \right. \qquad (F.2)$$
$$\left. \times (C_n^m \cos m\lambda_p + S_n^m \sin m\lambda_p) \right)$$

$$\frac{\partial U}{\partial \lambda_p} = \frac{GM}{R_p} \left( \sum_{n=2}^{\infty} \sum_{m=0}^{n} \left( \frac{a}{R_p} \right)^n m\, P_n^m \right. \qquad (F.3)$$
$$\left. \times (C_n^m \cos m\lambda_p - S_n^m \sin m\lambda_p) \right)$$

$$\frac{\partial U}{\partial \phi_p} = \frac{GM}{R_p} \left( \sum_{n=2}^{\infty} \sum_{m=0}^{n} \left( \frac{a}{R_p} \right)^n ( P_n^{m+1} - m \tan \phi_p\, P_n^m ) \right.$$
$$\left. \times (C_n^m \cos m\lambda_p\, S_n^m \sin m\lambda_p) \right) \qquad (F.4)$$

and the partial derivatives of the spherical polar coordinate components with respect to the components of

the cartesian coordinate vector are obtained by differentiating equations (3.6), (3.7) and (3.8), to give,

$$\frac{\partial R_p}{\partial X} = \frac{X}{R_p} \quad , \quad \frac{\partial \lambda_p}{\partial X} = \frac{-Y}{(X^2 + Y^2)} \quad , \quad \frac{\partial \phi_p}{\partial X} = \frac{- Z\ X}{(X^2 + Y^2)^{\frac{1}{2}}\ R_p^2} \quad (F.5)$$

$$\frac{\partial R_p}{\partial Y} = \frac{Y}{R_p} \quad , \quad \frac{\partial \lambda_p}{\partial Y} = \frac{X}{(X^2 + Y^2)} \quad , \quad \frac{\partial \phi_p}{\partial Y} = \frac{- Z\ Y}{(X^2 + Y^2)^{\frac{1}{2}}\ R_p^2} \quad (F.6)$$

$$\frac{\partial R_p}{\partial Z} = \frac{Z}{R_p} \quad , \quad \frac{\partial \lambda_p}{\partial Z} = 0 \quad , \quad \frac{\partial \phi_p}{\partial Z} = \frac{(1 - Z^2 / R_p^2)}{(X^2 + Y^2)^{\frac{1}{2}}} \quad (F.7)$$

APPENDIX G

TABLES OF RESULTS (SHORT MERIT DATA)

| Station | Latitude (deg min sec) | | | Longitude (deg min sec) | | | Height (m) | Standard Errors (cm) | | |
|---|---|---|---|---|---|---|---|---|---|---|
| | | | | | | | | $\sigma_\phi$ | $\sigma_\lambda$ | $\sigma_h$ |
| 7063 | 39 | 1 | 13.39497 | 283 | 10 | 19.80020 | 15.332 | 0.050 | 0.012 | 0.044 |
| 7090 | -29 | 2 | 47.43349 | 115 | 20 | 48.10653 | 237.521 | 0.047 | 0.056 | 0.041 |
| 7091 | 42 | 37 | 21.71790 | 288 | 30 | 44.34828 | 88.383 | 0.037 | 0.058 | 0.037 |
| 7096 | -14 | 20 | 7.51619 | 189 | 16 | 30.37933 | 45.522 | 0.622 | 1.135 | 0.258 |
| 7115 | 35 | 14 | 53.93166 | 243 | 12 | 28.94113 | 1035.369 | 0.051 | 0.058 | 0.051 |
| 7120 | 20 | 42 | 27.41463 | 203 | 44 | 38.08404 | 3064.291 | 0.049 | 0.074 | 0.043 |

$$a_e = 6378144.11\,m \qquad\qquad 1/f = 298.255$$

| Station | X (m) | Y (m) | Z (m) | Standard Errors (cm) | | |
|---|---|---|---|---|---|---|
| | | | | $\sigma_X$ | $\sigma_Y$ | $\sigma_Z$ |
| 7063 | 1130711.924 | -4831370.633 | 3994089.653 | 0.010 | 0.030 | 0.060 |
| 7090 | -2389003.531 | 5043333.515 | -3078527.390 | 0.060 | 0.030 | 0.050 |
| 7091 | 1492451.379 | -4457281.917 | 4296818.401 | 0.060 | 0.030 | 0.040 |
| 7096 | -6100049.853 | -996200.161 | -1568977.200 | 0.100 | 1.150 | 0.640 |
| 7115 | -2350866.197 | -4655547.058 | 3661000.634 | 0.060 | 0.050 | 0.050 |
| 7120 | -5466003.132 | -2404405.758 | 2242230.145 | 0.030 | 0.080 | 0.050 |

Fig G.I Tracking Station Coordinates - Sept 1980 (BIH Polar Motion)

| Station | Latitude (deg min sec) | | | Longitude (deg min sec) | | | Height (m) | Standard Errors (cm) $\sigma_\phi$ | $\sigma_\lambda$ | $\sigma_h$ |
|---|---|---|---|---|---|---|---|---|---|---|
| 7063 | 39 | 1 | 13.38650 | 283 | 10 | 19.80020 | 15.352 | 0.096 | 0.040 | 0.104 |
| 7090 | -29 | 2 | 47.43252 | 115 | 20 | 48.10357 | 237.451 | 0.093 | 0.182 | 0.099 |
| 7114 | 37 | 13 | 57.20716 | 241 | 42 | 22.20028 | 1174.560 | 0.080 | 0.102 | 0.080 |
| 7115 | 35 | 14 | 53.89673 | 243 | 12 | 28.94113 | 1035.439 | 0.152 | 0.153 | 0.199 |
| 7120 | 20 | 42 | 27.37679 | 203 | 44 | 38.11135 | 3064.241 | 0.088 | 0.121 | 0.078 |
| 7896 | 34 | 12 | 20.03078 | 241 | 49 | 39.71218 | 438.024 | 0.086 | 0.094 | 0.082 |

$$a_e = 6378144.11m \qquad 1/f = 298.255$$

| Station | X (m) | Y (m) | Z (m) | Standard Errors (cm) $\sigma_X$ | $\sigma_Y$ | $\sigma_Z$ |
|---|---|---|---|---|---|---|
| 7063 | 1130711.965 | -4831370.808 | 3994089.462 | 0.030 | 0.120 | 0.080 |
| 7090 | -2389003.438 | 5043333.507 | -3078527.330 | 0.200 | 0.060 | 0.090 |
| 7114 | -2410427.211 | -4477803.643 | 3838688.512 | 0.110 | 0.070 | 0.080 |
| 7115 | -2350866.503 | -4655547.664 | 3661000.795 | 0.110 | 0.260 | 0.080 |
| 7120 | -5466003.148 | -2404406.629 | 2242230.038 | 0.060 | 0.130 | 0.090 |
| 7896 | -2493215.745 | -4655230.002 | 3565577.465 | 0.100 | 0.070 | 0.090 |

Fig G.II <u>Tracking Station Coordinates - Dec 1980 (BIH Polar Motion)</u>

| Tracking Station | Dec 80 - Sept 80 | | | GSFC SL5 - Sept 80 | | | GSFC SL5 - Dec 80 | | |
|---|---|---|---|---|---|---|---|---|---|
| | $\Delta X$ (m) | $\Delta Y$ (m) | $\Delta Z$ (m) | $\Delta X$ (m) | $\Delta Y$ (m) | $\Delta Z$ (m) | $\Delta X$ (m) | $\Delta Y$ (m) | $\Delta Z$ (m) |
| 7063 | 0.04 | -0.18 | -0.19 | 0.15 | -0.64 | -0.93 | 0.11 | -0.46 | -0.74 |
| 7090 | 0.09 | -0.01 | 0.06 | -0.20 | 0.16 | 0.65 | -0.29 | 0.17 | 0.59 |
| 7091 | - | - | - | 0.16 | -0.71 | -0.84 | - | - | - |
| 7096 | - | - | - | 0.27 | 0.74 | 0.01 | - | - | - |
| 7114 | - | - | - | - | - | - | 0.46 | -0.24 | 0.07 |
| 7115 | -0.31 | -0.61 | -0.84 | 0.10 | -0.54 | -0.98 | 0.41 | 0.07 | -0.14 |
| 7120 | -0.02 | -0.87 | -1.11 | 0.13 | -0.68 | -0.73 | 0.14 | 0.19 | 0.38 |
| 7896 | - | - | - | - | - | - | 0.26 | -0.18 | -0.28 |
| RMS Difference | 0.16 | 0.54 | 0.70 | 0.18 | 0.61 | 0.76 | 0.31 | 0.25 | 0.14 |

Fig G.III <u>Comparison of Tracking Station Coordinates (BIH Polar Motion)</u>

| Tracking Station | Dec 80 - Sept 80 | | | GSFC SL5 - Sept 80 | | | GSFC SL5 - Dec 80 | | |
|---|---|---|---|---|---|---|---|---|---|
| | $\Delta\phi$ (m) | $\Delta\lambda$ (m) | $\Delta h$ (m) | $\Delta\phi$ (m) | $\Delta\lambda$ (m) | $\Delta h$ (m) | $\Delta\phi$ (m) | $\Delta\lambda$ (m) | $\Delta h$ (m) |
| 7063 | -0.26 | 0.00 | 0.02 | -1.14 | 0.00 | -0.08 | -0.88 | 0.00 | -0.10 |
| 7090 | 0.03 | -0.08 | -0.07 | 0.68 | 0.11 | -0.11 | 0.65 | 0.19 | -0.04 |
| 7091 | - | - | - | -1.11 | -0.07 | -0.03 | - | - | - |
| 7096 | - | - | - | -0.09 | -0.69 | -0.38 | - | - | - |
| 7114 | - | - | - | - | - | - | 0.06 | 0.52 | 0.03 |
| 7115 | -1.08 | 0.00 | 0.07 | -1.05 | 0.33 | -0.21 | 0.03 | 0.33 | -0.28 |
| 7120 | -1.17 | 0.79 | -0.05 | -0.74 | 0.67 | -0.11 | 0.43 | -0.12 | -0.06 |
| 7896 | - | - | - | - | - | - | -0.25 | 0.31 | -0.13 |
| RMS Difference | 0.81 | 0.40 | 0.06 | 0.88 | 0.42 | 0.19 | 0.49 | 0.30 | 0.14 |

$$a_e = 6378144.11m \qquad 1/f = 298.255$$

Fig G.IV Comparison of Geodetic Station Coordinates (BIH Polar Motion)

| Inter-Station Baseline | Nominal Length of Baseline (m) | Sept 80 (m) | Dec 80 (m) | GSFC SL5 (m) | Dec 80 – Sept 80 (m) | SL5 – Sept 80 (m) | SL5 – Dec 80 (m) |
|---|---|---|---|---|---|---|---|
| 7063 – 7090 | 12645951 | .55 | .53 | .39 | -0.02 | -0.17 | -0.14 |
| 7063 – 7115 | 3501892 | .12 | .51 | .18 | 0.38 | 0.06 | -0.33 |
| 7063 – 7120 | 7244019 | .59 | .63 | .54 | 0.04 | -0.04 | -0.08 |
| 7090 – 7115 | 11810629 | .82 | .80 | .47 | -0.02 | -0.35 | -0.33 |
| 7090 – 7120 | 9656459 | .37 | .43 | .16 | 0.06 | -0.21 | -0.27 |
| 7115 – 7120 | 4096904 | .32 | .04 | .13 | -0.27 | -0.18 | 0.09 |
| RMS Difference | | | | | 0.20 | 0.20 | 0.23 |

Fig G.V Comparison of Baseline Lengths (BIH Polar Motion)

| Station | Latitude (deg min sec) | | | Longitude (deg min sec) | | | Height (m) |
|---|---|---|---|---|---|---|---|
| 7063 | 39 | 1 | 13.36198 | 283 | 10 | 19.80020 | 15.332 |
| 7090 | -29 | 2 | 47.40568 | 115 | 20 | 48.10764 | 237.521 |
| 7091 | 42 | 37 | 21.68685 | 288 | 30 | 44.34300 | 88.383 |
| 7096 | -14 | 20 | 7.53107 | 189 | 16 | 30.38434 | 45.532 |
| 7115 | 35 | 14 | 53.89576 | 243 | 12 | 28.96014 | 1035.379 |
| 7120 | 20 | 42 | 27.39167 | 203 | 44 | 38.10789 | 3064.291 |

$$a_e = 6378144.11m \qquad 1/f = 298.255$$

| Station | X (m) | Y (m) | Z (m) |
|---|---|---|---|
| 7063 | 1130712.070 | -4831371.257 | 3994088.862 |
| 7090 | -2389003.736 | 5043333.878 | -3078526.641 |
| 7091 | 1492451.471 | -4457282.570 | 4296817.696 |
| 7096 | -6100049.727 | -996200.292 | -1568977.646 |
| 7115 | -2350866.059 | -4655547.852 | 3660999.736 |
| 7120 | -5466003.083 | -2404406.491 | 2242229.484 |

Fig G.VI Tracking Station Coordinates - Sept 1980 (Nottm Polar Motion)

| Station | Latitude (deg min sec) | | | Longitude (deg min sec) | | | Height (m) |
|---|---|---|---|---|---|---|---|
| 7063 | 39 | 1 | 13.36101 | 283 | 10 | 19.80020 | 15.342 |
| 7090 | -29 | 2 | 47.40342 | 115 | 20 | 48.09469 | 237.441 |
| 7114 | 37 | 13 | 57.20296 | 241 | 42 | 22.20637 | 1174.550 |
| 7115 | 35 | 14 | 53.89059 | 243 | 12 | 28.94628 | 1035.439 |
| 7120 | 20 | 42 | 27.39361 | 203 | 44 | 38.10409 | 3064.261 |
| 7896 | 34 | 12 | 20.02755 | 241 | 49 | 39.71609 | 438.024 |

$$a_e = 6378144.11\text{m} \qquad 1/f = 298.255$$

| Station | X (m) | Y (m) | Z (m) |
|---|---|---|---|
| 7063 | 1130712.076 | -4831371.283 | 3994088.845 |
| 7090 | -2389003.404 | 5043333.995 | -3078526.541 |
| 7114 | -2410427.113 | -4477803.776 | 3838688.403 |
| 7115 | -2350866.436 | -4655547.820 | 3660999.641 |
| 7120 | -5466003.082 | -2404406.370 | 2242229.530 |
| 7896 | -2493215.683 | -4655230.099 | 3565577.383 |

Fig G.VII Tracking Station Coordinates - Dec 1980 (Nottm Polar Motion)

| Tracking Station | Dec 80 – Sept 80 | | | GSFC SL5 – Sept 80 | | | GSFC SL5 – Dec 80 | | |
|---|---|---|---|---|---|---|---|---|---|
| | $\Delta X$ (m) | $\Delta Y$ (m) | $\Delta Z$ (m) | $\Delta X$ (m) | $\Delta Y$ (m) | $\Delta Z$ (m) | $\Delta X$ (m) | $\Delta Y$ (m) | $\Delta Z$ (m) |
| 7063 | 0.01 | -0.03 | -0.02 | 0.00 | -0.01 | -0.14 | 0.00 | 0.01 | -0.13 |
| 7090 | 0.33 | 0.12 | 0.10 | 0.01 | -0.20 | -0.10 | -0.33 | -0.32 | 0.20 |
| 7091 | – | – | – | 0.07 | -0.06 | -0.13 | – | – | – |
| 7096 | – | – | – | 0.15 | 0.88 | 0.45 | – | – | – |
| 7114 | – | – | – | – | – | – | 0.37 | -0.10 | 0.17 |
| 7115 | -0.38 | 0.03 | -0.10 | -0.04 | 0.26 | -0.08 | 0.34 | 0.23 | 0.02 |
| 7120 | 0.00 | 0.12 | 0.05 | 0.08 | 0.06 | -0.07 | 0.08 | -0.07 | -0.11 |
| 7896 | – | – | – | – | – | – | 0.20 | -0.08 | -0.20 |
| RMS Difference | 0.25 | 0.09 | 0.07 | 0.08 | 0.38 | 0.21 | 0.26 | 0.17 | 0.15 |

Fig G.VIII <u>Comparison of Cartesian Tracking Station Coordinates (Nottm Polar Motion)</u>

| Tracking Station | Dec 80 - Sept 80 | | | GSFC SL5 - Sept 80 | | | GSFC SL5 - Dec 80 | | |
|---|---|---|---|---|---|---|---|---|---|
| | $\Delta\phi$ (m) | $\Delta\lambda$ (m) | $\Delta h$ (m) | $\Delta\phi$ (m) | $\Delta\lambda$ (m) | $\Delta h$ (m) | $\Delta\phi$ (m) | $\Delta\lambda$ (m) | $\Delta h$ (m) |
| 7063 | -0.03 | 0.00 | 0.01 | -0.12 | 0.00 | -0.08 | -0.09 | 0.00 | -0.09 |
| 7090 | 0.07 | -0.35 | -0.08 | -0.18 | 0.08 | -0.11 | -0.25 | 0.43 | -0.03 |
| 7091 | - | - | - | -0.15 | 0.05 | -0.03 | - | - | - |
| 7096 | - | - | - | 0.37 | -0.84 | -0.39 | - | - | - |
| 7114 | - | - | - | - | - | - | 0.19 | 0.37 | 0.04 |
| 7115 | -0.16 | -0.35 | 0.06 | 0.06 | -0.15 | -0.22 | 0.22 | 0.20 | -0.28 |
| 7120 | 0.06 | -0.11 | -0.03 | -0.03 | -0.02 | -0.11 | -0.09 | 0.09 | -0.08 |
| 7896 | - | - | - | - | - | - | -0.15 | 0.21 | -0.13 |
| RMS Difference | 0.09 | 0.25 | 0.05 | 0.19 | 0.35 | 0.20 | 0.18 | 0.26 | 0.14 |

$$a_e = 6378144.11m \qquad 1/f = 298.255$$

Fig G.IX Comparison of Geodetic Station Coordinates (Nottm Polar Motion)

| Inter-Station Baseline | Nominal Length of Baseline (m) | Sept 80 (m) | Dec 80 (m) | GSFC SL5 (m) | Dec 80 - Sept 80 (m) | SL5 - Sept 80 (m) | SL5 - Dec 80 (m) |
|---|---|---|---|---|---|---|---|
| 7063 - 7090 | 12645951 | .56 | .52 | .39 | -0.04 | -0.17 | -0.13 |
| 7063 - 7115 | 3501892 | .13 | .52 | .18 | 0.39 | 0.05 | -0.34 |
| 7063 - 7120 | 7244019 | .61 | .65 | .54 | 0.04 | -0.06 | -0.10 |
| 7090 - 7115 | 11810629 | .83 | .79 | .47 | -0.04 | -0.36 | -0.32 |
| 7090 - 7120 | 9656459 | .36 | .43 | .16 | 0.07 | -0.20 | -0.27 |
| 7115 - 7120 | 4096904 | .33 | .05 | .13 | -0.29 | -0.20 | 0.08 |
| RMS Difference | | | | | 0.20 | 0.20 | 0.23 |

Fig G.X Comparison of Baseline Lengths (Nottm Polar Motion)

| Polar Motion Series | Sept 80 $2^{nd} - 5^{th}$ | | Dec 80 $2^{nd} - 5^{th}$ | | Dec - Sept | |
|---|---|---|---|---|---|---|
| | $x_p$ (mas) | $y_p$ (mas) | $x_p$ (mas) | $y_p$ (mas) | $\Delta x_p$ (mas) | $\Delta y_p$ (mas) |
| Nottingham | -25 | 354 | 49 | 396 | 74 | 42 |
| GSFC GEM-L2 | -26 | 343 | 45 | 378 | 71 | 35 |
| BIH Circular D | -17 | 317 | 19 | 378 | 36 | 61 |

Fig G.XI Polar Motion Values (and Comparisons)

| Station | Latitude (deg min sec) | | | Longitude (deg min sec) | | | Height (m) | Standard Errors (cm) $\sigma_\phi$ | $\sigma_\lambda$ | $\sigma_h$ |
|---|---|---|---|---|---|---|---|---|---|---|
| 7063 | 39 | 1 | 13.38897 | 283 | 10 | 19.80020 | 15.300 | 0.096 | 0.047 | 0.113 |
| 7090 | -29 | 2 | 47.43525 | 115 | 20 | 48.12231 | 237.525 | 0.048 | 0.116 | 0.068 |
| 7114 | 37 | 13 | 57.21448 | 241 | 42 | 22.21275 | 1174.651 | 0.061 | 0.106 | 0.072 |
| 7115 | 35 | 14 | 53.90848 | 243 | 12 | 28.94180 | 1035.148 | 0.068 | 0.116 | 0.088 |
| 7120 | 20 | 42 | 27.37480 | 203 | 44 | 38.12006 | 3064.374 | 0.052 | 0.133 | 0.080 |
| 7896 | 34 | 12 | 20.02753 | 241 | 49 | 39.72218 | 438.074 | 0.052 | 0.104 | 0.067 |

$$a_e = 6378144.11\,m \qquad 1/f = 298.255$$

| Station | X (m) | Y (m) | Z (m) | Standard Errors (cm) $\sigma_X$ | $\sigma_Y$ | $\sigma_Z$ |
|---|---|---|---|---|---|---|
| 7063 | 1130711.945 | -4831370.722 | 3994089.448 | 0.034 | 0.144 | 0.049 |
| 7090 | -2389003.907 | 5043333.312 | -3078527.439 | 0.125 | 0.059 | 0.036 |
| 7114 | -2410426.910 | -4477803.732 | 3838688.746 | 0.114 | 0.073 | 0.043 |
| 7115 | -2350866.286 | -4655547.273 | 3660999.923 | 0.120 | 0.100 | 0.039 |
| 7120 | -5466003.180 | -2404406.918 | 2242229.028 | 0.067 | 0.142 | 0.046 |
| 7896 | -2493215.565 | -4655230.209 | 3565577.410 | 0.113 | 0.064 | 0.035 |

Fig G.XII Tracking Station Coordinates - Dec 80/14 (BIH Polar Motion)

| Tracking Station | Dec 80/14 - Dec 80 | | | Dec 80/14 - SL5.1 | | | Dec 80/14b - SL5.1 | | |
|---|---|---|---|---|---|---|---|---|---|
| | ΔX (m) | ΔY (m) | ΔZ (m) | ΔX (m) | ΔY (m) | ΔZ (m) | ΔX (m) | ΔY (m) | ΔZ (m) |
| 7063 | -0.02 | 0.09 | 0.03 | 0.13 | -0.55 | -0.77 | -0.10 | -0.23 | -0.32 |
| 7090 | -0.47 | -0.20 | -0.11 | 0.18 | 0.37 | 0.69 | 0.36 | 0.12 | 0.16 |
| 7114 | 0.30 | -0.09 | 0.23 | 0.16 | -0.15 | -0.17 | -0.06 | 0.15 | 0.04 |
| 7115 | 0.22 | 0.39 | 0.13 | 0.19 | -0.32 | -0.26 | -0.02 | -0.03 | -0.04 |
| 7120 | -0.03 | -0.29 | -0.01 | 0.17 | 0.48 | 0.39 | 0.04 | 0.66 | 0.26 |
| 7896 | 0.18 | -0.21 | -0.05 | 0.08 | 0.03 | -0.22 | -0.13 | 0.31 | 0.00 |
| RMS Difference | 0.26 | 0.24 | 0.12 | 0.16 | 0.36 | 0.48 | 0.16 | 0.32 | 0.18 |

Fig G.XIII Comparison of Cartesian Tracking Station Coordinates (BIH Polar Motion)

| Tracking Station | Dec 80/14 - Dec 80 | | | Dec 80/14 - SL5.1 | | | Dec 80/14b - SL5.1 | | |
|---|---|---|---|---|---|---|---|---|---|
| | $\Delta\phi$ (m) | $\Delta\lambda$ (m) | $\Delta h$ (m) | $\Delta\phi$ (m) | $\Delta\lambda$ (m) | $\Delta h$ (m) | $\Delta\phi$ (m) | $\Delta\lambda$ (m) | $\Delta h$ (m) |
| 7063 | 0.08 | 0.00 | -0.05 | -0.95 | 0.00 | -0.05 | -0.38 | -0.15 | -0.05 |
| 7090 | -0.08 | 0.51 | 0.07 | 0.73 | -0.32 | -0.11 | 0.12 | -0.37 | -0.11 |
| 7114 | 0.23 | 0.31 | 0.09 | -0.17 | 0.21 | -0.06 | 0.10 | -0.13 | -0.06 |
| 7115 | 0.36 | 0.02 | -0.29 | -0.33 | 0.31 | 0.01 | -0.05 | -0.01 | 0.01 |
| 7120 | -0.06 | 0.25 | 0.13 | 0.49 | -0.37 | -0.19 | 0.35 | -0.59 | -0.19 |
| 7896 | -0.10 | 0.26 | -0.05 | -0.15 | 0.05 | -0.18 | 0.12 | -0.26 | -0.18 |
| RMS Difference | 0.19 | 0.28 | 0.14 | 0.56 | 0.25 | 0.12 | 0.23 | 0.31 | 0.12 |

$$a_e = 6378144.11m \qquad 1/f = 298.555$$

Fig G.XIV Comparison of Geodetic Tracking Station Coordinates (BIH Polar Motion)

| Inter-Station Baseline | Nominal Length of Baseline (m) | Dec 80/14 (m) | Dec 80 (m) | GSFC SL5 (m) | Dec 80/14 - Dec 80 (m) | Dec 80/14 - SL5.1 (m) |
|---|---|---|---|---|---|---|
| 7063 - 7090 | 12645951 | .56 | .53 | .39 | -0.02 | -0.12 |
| 7063 - 7115 | 3501892 | .28 | .51 | .18 | -0.23 | -0.10 |
| 7063 - 7120 | 7244019 | .52 | .63 | .54 | -0.11 | 0.02 |
| 7090 - 7115 | 11810629 | .46 | .80 | .47 | -0.34 | 0.02 |
| 7090 - 7120 | 9656459 | .42 | .43 | .16 | -0.01 | -0.26 |
| 7115 - 7120 | 4096904 | -.09 | .04 | .13 | -0.14 | 0.23 |
| RMS Difference | | | | | 0.18 | 0.16 |

Fig G.XV Comparison of Baseline Lengths (BIH Polar Motion)

# APPENDIX H

## TABLES OF TRACKING STATION

## COORDINATES (MAIN MERIT DATA)

| Station | Latitude (deg min sec) | | | Longitude (deg min sec) | | | Height (m) | Standard Errors (cm) $\sigma_\phi$ | $\sigma_\lambda$ | $\sigma_h$ |
|---|---|---|---|---|---|---|---|---|---|---|
| 1181 | 52 | 22 | 48.91793 | 13 | 3 | 54.81372 | 147.793 | 0.332 | 0.506 | 0.315 |
| 7086 | 30 | 40 | 37.14004 | 255 | 59 | 2.64204 | 1963.294 | 0.073 | 0.085 | 0.065 |
| 7105 | 39 | 1 | 14.17014 | 283 | 10 | 20.10885 | 22.114 | 0.062 | 0.064 | 0.059 |
| 7109 | 39 | 58 | 30.01472 | 239 | 3 | 18.89282 | 1109.282 | 0.051 | 0.041 | 0.048 |
| 7112 | 40 | 10 | 58.01280 | 255 | 16 | 26.29400 | 1504.745 | 0.094 | 0.131 | 0.087 |
| 7121 | -16 | 44 | 0.67736 | 208 | 57 | 31.74290 | 46.730 | 0.087 | 0.084 | 0.088 |
| 7122 | 23 | 20 | 34.25524 | 253 | 32 | 27.09491 | 33.893 | 0.091 | 0.086 | 0.101 |
| 7210 | 20 | 42 | 26.00928 | 203 | 44 | 38.53700 | 3068.204 | 0.067 | 0.023 | 0.043 |
| 7833 | 52 | 10 | 42.22071 | 5 | 48 | 35.09235 | 93.280 | 0.214 | 0.487 | 0.252 |
| 7834 | 49 | 8 | 41.74915 | 12 | 52 | 40.92621 | 661.183 | 0.134 | 0.175 | 0.140 |
| 7838 | 33 | 34 | 39.69575 | 135 | 56 | 13.12745 | 101.500 | 0.260 | 0.324 | 0.303 |
| 7839 | 47 | 4 | 1.66464 | 15 | 29 | 35.85413 | 539.410 | 0.095 | 0.113 | 0.097 |
| 7907 | -16 | 27 | 56.69380 | 288 | 30 | 24.54455 | 2492.148 | 0.058 | 0.044 | 0.049 |
| 7939 | 40 | 38 | 55.77123 | 16 | 42 | 16.63624 | 535.816 | 0.065 | 0.059 | 0.063 |

$$a_e = 6378137.0m \qquad 1/f = 298.255$$

Fig H.I Tracking Station Coordinates - Sept 1983 (BIH ERP)

| Station | Latitude (deg min sec) | | | Longitude (deg min sec) | | | Height (m) | Standard Errors (cm) | | |
|---|---|---|---|---|---|---|---|---|---|---|
| | | | | | | | | $\sigma_\phi$ | $\sigma_\lambda$ | $\sigma_h$ |
| 1181 | 52 | 22 | 48.94059 | 13 | 3 | 54.81116 | 147.599 | 0.123 | 0.136 | 0.127 |
| 7086 | 30 | 40 | 37.10692 | 255 | 59 | 2.64397 | 1963.244 | 0.132 | 0.156 | 0.144 |
| 7090 | -29 | 2 | 47.44543 | 115 | 20 | 48.00050 | 244.440 | 0.096 | 0.110 | 0.100 |
| 7105 | 39 | 1 | 14.15753 | 283 | 10 | 20.09640 | 22.054 | 0.058 | 0.044 | 0.052 |
| 7109 | 39 | 58 | 29.99603 | 239 | 3 | 18.87163 | 1109.198 | 0.062 | 0.047 | 0.057 |
| 7110 | 32 | 53 | 30.22846 | 243 | 34 | 38.18315 | 1841.792 | 0.063 | 0.042 | 0.051 |
| 7112 | 40 | 10 | 57.99108 | 255 | 16 | 26.26928 | 1504.609 | 0.067 | 0.059 | 0.063 |
| 7121 | -16 | 44 | 0.70257 | 208 | 57 | 31.72664 | 47.148 | 0.078 | 0.060 | 0.056 |
| 7122 | 23 | 20 | 34.23236 | 253 | 32 | 27.08522 | 33.794 | 0.073 | 0.048 | 0.051 |
| 7210 | 20 | 42 | 25.96808 | 203 | 44 | 38.53700 | 3068.189 | 0.075 | 0.019 | 0.041 |
| 7833 | 52 | 10 | 42.24039 | 5 | 48 | 35.09183 | 92.962 | 0.087 | 0.112 | 0.089 |
| 7834 | 49 | 8 | 41.76975 | 12 | 52 | 40.93064 | 660.929 | 0.062 | 0.064 | 0.066 |
| 7838 | 33 | 34 | 39.68082 | 135 | 56 | 13.13113 | 101.127 | 0.070 | 0.052 | 0.061 |
| 7839 | 47 | 4 | 1.68013 | 15 | 29 | 35.87935 | 539.133 | 0.062 | 0.057 | 0.065 |
| 7840 | 50 | 52 | 2.56398 | 0 | 20 | 9.80761 | 75.062 | 0.058 | 0.062 | 0.064 |
| 7907 | -16 | 27 | 56.69379 | 288 | 30 | 24.53935 | 2492.213 | 0.061 | 0.044 | 0.043 |
| 7939 | 40 | 38 | 55.77701 | 16 | 42 | 16.65735 | 535.828 | 0.060 | 0.047 | 0.058 |

$a_e$ = 6378137.0m        1/f = 298.255

Fig H.II Tracking Station Coordinates - Oct 1983 (BIH ERP)

| Station | Latitude (deg min sec) | | | Longitude (deg min sec) | | | Height (m) | Standard Errors (cm) $\sigma_\phi$ $\sigma_\lambda$ $\sigma_h$ | | |
|---|---|---|---|---|---|---|---|---|---|---|
| 1181 | 52 | 22 | 48.90982 | 13 | 3 | 54.81162 | 147.981 | 0.121 | 0.108 | 0.121 |
| 7086 | 30 | 40 | 37.12666 | 255 | 59 | 2.62956 | 1963.006 | 0.085 | 0.063 | 0.070 |
| 7090 | -29 | 2 | 47.43464 | 115 | 20 | 48.04716 | 244.656 | 0.075 | 0.062 | 0.063 |
| 7105 | 39 | 1 | 14.15888 | 283 | 10 | 20.09738 | 21.976 | 0.074 | 0.062 | 0.067 |
| 7109 | 39 | 58 | 29.98912 | 239 | 3 | 18.88648 | 1109.296 | 0.150 | 0.130 | 0.140 |
| 7110 | 32 | 53 | 30.23708 | 243 | 34 | 38.19525 | 1841.837 | 0.095 | 0.089 | 0.082 |
| 7112 | 40 | 10 | 57.98556 | 255 | 16 | 26.28672 | 1504.731 | 0.083 | 0.072 | 0.079 |
| 7121 | -16 | 44 | 0.70218 | 208 | 57 | 31.72715 | 47.262 | 0.112 | 0.098 | 0.083 |
| 7122 | 23 | 20 | 34.23434 | 253 | 32 | 27.09699 | 33.890 | 0.093 | 0.068 | 0.070 |
| 7210 | 20 | 42 | 25.98343 | 203 | 44 | 38.53700 | 3068.024 | 0.092 | 0.024 | 0.050 |
| 7834 | 49 | 8 | 41.74967 | 12 | 52 | 40.92670 | 660.930 | 0.074 | 0.064 | 0.078 |
| 7838 | 33 | 34 | 39.69420 | 135 | 56 | 13.13286 | 101.096 | 0.086 | 0.066 | 0.076 |
| 7839 | 47 | 4 | 1.65317 | 15 | 29 | 35.87337 | 539.126 | 0.081 | 0.085 | 0.082 |
| 7840 | 50 | 52 | 2.54328 | 0 | 20 | 9.82478 | 74.971 | 0.082 | 0.104 | 0.085 |
| 7907 | -16 | 27 | 56.70952 | 288 | 30 | 24.53902 | 2492.279 | 0.083 | 0.053 | 0.052 |
| 7939 | 40 | 38 | 55.76412 | 16 | 42 | 16.64210 | 535.376 | 0.081 | 0.061 | 0.078 |

$$a_e = 6378137.0m \qquad 1/f = 298.255$$

Fig H.III Tracking Station Coordinates - Nov 1983 (BIH ERP)

| Station | Latitude (deg min sec) | | | Longitude (deg min sec) | | | Height (m) | Standard Errors (cm) $\sigma_\phi$ | $\sigma_\lambda$ | $\sigma_h$ |
|---|---|---|---|---|---|---|---|---|---|---|
| 1181 | 52 | 22 | 48.92229 | 13 | 3 | 54.80469 | 147.936 | 0.124 | 0.121 | 0.115 |
| 7086 | 30 | 40 | 37.13856 | 255 | 59 | 2.64787 | 1963.257 | 0.086 | 0.065 | 0.071 |
| 7090 | -29 | 2 | 47.42871 | 115 | 20 | 48.05817 | 244.458 | 0.077 | 0.064 | 0.066 |
| 7105 | 39 | 1 | 14.16357 | 283 | 10 | 20.10862 | 22.268 | 0.084 | 0.072 | 0.083 |
| 7109 | 39 | 58 | 29.99310 | 239 | 3 | 18.90302 | 1109.457 | 0.116 | 0.122 | 0.123 |
| 7110 | 32 | 53 | 30.24747 | 243 | 34 | 38.20592 | 1842.149 | 0.098 | 0.080 | 0.101 |
| 7121 | -16 | 44 | 0.68206 | 208 | 57 | 31.72317 | 47.640 | 0.105 | 0.066 | 0.061 |
| 7122 | 23 | 20 | 34.25566 | 253 | 32 | 27.09517 | 34.113 | 0.098 | 0.061 | 0.074 |
| 7210 | 20 | 42 | 25.99901 | 203 | 44 | 38.53700 | 3068.350 | 0.090 | 0.017 | 0.042 |
| 7834 | 49 | 8 | 41.75907 | 12 | 52 | 40.94343 | 661.143 | 0.081 | 0.079 | 0.083 |
| 7838 | 33 | 34 | 39.70227 | 135 | 56 | 13.13852 | 101.405 | 0.081 | 0.048 | 0.064 |
| 7839 | 47 | 4 | 1.66480 | 15 | 29 | 35.87824 | 539.318 | 0.084 | 0.076 | 0.084 |
| 7840 | 50 | 52 | 2.54170 | 0 | 20 | 9.83580 | 74.315 | 0.071 | 0.068 | 0.076 |
| 7907 | -16 | 27 | 56.70202 | 288 | 30 | 24.54998 | 2492.486 | 0.090 | 0.050 | 0.045 |
| 7939 | 40 | 38 | 55.77024 | 16 | 42 | 16.64300 | 535.938 | 0.071 | 0.057 | 0.067 |

$$a_e = 6378137.0m \qquad 1/f = 298.255$$

Fig H.IV <u>Tracking Station Coordinates - Dec 1983 (BIH ERP)</u>

| Coordinate Solutions | Root-Mean-Square (RMS) Differences | | | | | | |
|---|---|---|---|---|---|---|---|
| | X (m) | Y (m) | Z (m) | φ (m) | λ (m) | h (m) | Baseline Length (m) |
| SEPB - LSC 8112 | 0.35 | 0.32 | 0.49 | 0.49 | 0.35 | 0.34 | 0.57 |
| OCTB - LSC 8112 | 0.56 | 0.41 | 0.49 | 0.54 | 0.60 | 0.27 | 0.51 |
| NOVB - LSC 8112 | 0.34 | 0.38 | 0.44 | 0.53 | 0.38 | 0.19 | 0.43 |
| DECB - LSC 8112 | 0.29 | 0.39 | 0.53 | 0.56 | 0.36 | 0.28 | 0.43 |

fig H.V Coordinate Comparison (BIH ERP)

| Coordinate Solutions From    To | Transformation Parameters | | | | | | |
|---|---|---|---|---|---|---|---|
| | $\partial x$ (m) | $\partial y$ (m) | $\partial z$ (m) | $\alpha x$ (sec) | $\alpha y$ (sec) | $\alpha z$ (sec) | c (ppm) |
| SEPB - LSC 8112 | -0.076 | 0.116 | -0.444 | 0.004 | 0.007 | -0.009 | 0.038 |
| OCTB - LSC 8112 | -0.085 | -0.043 | -0.174 | 0.013 | -0.015 | -0.014 | 0.031 |
| NOVB - LSC 8112 | 0.050 | -0.017 | -0.055 | 0.016 | 0.006 | -0.009 | 0.020 |
| DECB - LSC 8112 | 0.133 | 0.014 | -0.390 | 0.014 | 0.010 | -0.004 | 0.006 |

fig H.VI Transformation Parameters

| Coordinate Solutions | Root-Mean-Square (RMS) Differences | | | | | | |
|---|---|---|---|---|---|---|---|
| | X (m) | Y (m) | Z (m) | φ (m) | λ (m) | h (m) | Baseline Length (m) |
| $\mathrm{SEPB}_u$ - LSC 8112 | 0.31 | 0.20 | 0.33 | 0.37 | 0.20 | 0.26 | 0.49 |
| $\mathrm{OCTB}_u$ - LSC 8112 | 0.30 | 0.30 | 0.32 | 0.34 | 0.35 | 0.28 | 0.44 |
| $\mathrm{NOVB}_u$ - LSC 8112 | 0.27 | 0.23 | 0.30 | 0.39 | 0.21 | 0.15 | 0.40 |
| $\mathrm{DECB}_u$ - LSC 8112 | 0.24 | 0.29 | 0.35 | 0.39 | 0.26 | 0.20 | 0.42 |

fig H.VII Coordinate Comparison - Biases Removed (BIH ERP)

| Coordinate Solutions | Root-Mean-Square (RMS) Differences | | | | | | |
|---|---|---|---|---|---|---|---|
| | X (m) | Y (m) | Z (m) | $\phi$ (m) | $\lambda$ (m) | h (m) | Baseline Length (m) |
| SEPB - OCTB | 0.47 | 0.25 | 0.58 | 0.67 | 0.33 | 0.21 | 0.35 |
| SEPB - NOVB | 0.26 | 0.25 | 0.53 | 0.53 | 0.23 | 0.27 | 0.38 |
| SEPB - DECB | 0.34 | 0.30 | 0.24 | 0.28 | 0.29 | 0.32 | 0.49 |
| OCTB - NOVB | 0.49 | 0.25 | 0.35 | 0.49 | 0.39 | 0.18 | 0.39 |
| OCTB - DECB | 0.59 | 0.30 | 0.48 | 0.55 | 0.54 | 0.27 | 0.43 |
| NOVB - DECB | 0.27 | 0.17 | 0.40 | 0.35 | 0.23 | 0.29 | 0.29 |

fig H.VIII <u>Monthly Coordinate Inter-comparison (BIH ERP)</u>

| Coordinate Solutions | Root-Mean-Square (RMS) Differences | | | | | | |
|---|---|---|---|---|---|---|---|
| | X (m) | Y (m) | Z (m) | $\phi$ (m) | $\lambda$ (m) | h (m) | Baseline Length (m) |
| $SEPB_u - OCTB_u$ | 0.22 | 0.26 | 0.15 | 0.19 | 0.26 | 0.19 | 0.31 |
| $SEPB^u - OCTB^u$ | 0.20 | 0.22 | 0.20 | 0.20 | 0.19 | 0.24 | 0.34 |
| $SEPB^u - OCTB^u$ | 0.26 | 0.24 | 0.20 | 0.20 | 0.25 | 0.25 | 0.36 |
| $SEPB^u - OCTB^u$ | 0.29 | 0.21 | 0.15 | 0.22 | 0.25 | 0.19 | 0.33 |
| $SEPB^u - OCTB^u$ | 0.25 | 0.27 | 0.21 | 0.23 | 0.33 | 0.13 | 0.36 |
| $SEPB^u_u - OCTB^u_u$ | 0.22 | 0.14 | 0.14 | 0.16 | 0.18 | 0.18 | 0.26 |

fig H.IX <u>Monthly Coordinate Inter-comparison - Biases Removed (BIH ERP)</u>

| Data Set | Along Track Acceleration, $C_T$ | Solar Radiation Pressure, $C_R$ | GM, Geocentric Gravitational Constant |
|---|---|---|---|
| SEPTEMBER | $-0.328\times10^{-11}$ | 1.113 | $3.98600430\times10^{14}$ |
| OCTOBER | $-0.323\times10^{-11}$ | 1.114 | $3.98600428\times10^{14}$ |
| NOVEMBER | $-0.454\times10^{-11}$ | 1.049 | $3.98600429\times10^{14}$ |
| DECEMBER | $-0.554\times10^{-11}$ | 0.980 | $-$ |

fig H.X Coefficients and Constants Determined from Monthly Data Sets

| Station | Latitude (deg min sec) | | | Longitude (deg min sec) | | | Height (m) | Standard Errors (cm) $\sigma_\phi$ | $\sigma_\lambda$ | $\sigma_h$ |
|---|---|---|---|---|---|---|---|---|---|---|
| 1181 | 52 | 22 | 48.91259 | 13 | 3 | 54.83250 | 147.699 | 0.232 | 0.351 | 0.220 |
| 7086 | 30 | 40 | 37.15149 | 255 | 59 | 2.64656 | 1963.266 | 0.050 | 0.059 | 0.045 |
| 7105 | 39 | 1 | 14.18122 | 283 | 10 | 20.11628 | 22.116 | 0.043 | 0.045 | 0.042 |
| 7109 | 39 | 58 | 30.02235 | 239 | 3 | 18.89433 | 1109.367 | 0.036 | 0.029 | 0.034 |
| 7112 | 40 | 10 | 58.02689 | 255 | 16 | 26.28140 | 1504.927 | 0.066 | 0.091 | 0.061 |
| 7121 | -16 | 44 | 0.66575 | 208 | 57 | 31.74358 | 46.964 | 0.061 | 0.059 | 0.061 |
| 7122 | 23 | 20 | 34.27013 | 253 | 32 | 27.09294 | 33.834 | 0.063 | 0.059 | 0.070 |
| 7210 | 20 | 42 | 26.01472 | 203 | 44 | 38.53700 | 3068.202 | 0.046 | 0.016 | 0.030 |
| 7833 | 52 | 10 | 42.21788 | 5 | 48 | 35.12258 | 93.129 | 0.149 | 0.339 | 0.176 |
| 7834 | 49 | 8 | 41.74475 | 12 | 52 | 40.94665 | 661.095 | 0.093 | 0.121 | 0.097 |
| 7838 | 33 | 34 | 39.67366 | 135 | 56 | 13.13017 | 101.755 | 0.181 | 0.225 | 0.210 |
| 7839 | 47 | 4 | 1.65799 | 15 | 29 | 35.87864 | 539.305 | 0.065 | 0.079 | 0.067 |
| 7907 | -16 | 27 | 56.68457 | 288 | 30 | 24.54680 | 2492.208 | 0.040 | 0.030 | 0.033 |
| 7939 | 40 | 38 | 55.76793 | 16 | 42 | 16.64828 | 535.781 | 0.045 | 0.041 | 0.044 |

$$a_e = 6378137.0m \qquad 1/f = 298.255$$

Fig H.XI <u>Tracking Station Coordinates - Sept 1983 (Nottm ERP)</u>

| Station | Latitude (deg min sec) | | | Longitude (deg min sec) | | | Height (m) | Standard Errors (cm) | | |
|---|---|---|---|---|---|---|---|---|---|---|
| | | | | | | | | $\sigma_\phi$ | $\sigma_\lambda$ | $\sigma_h$ |
| 1181 | 52 | 22 | 48.94125 | 13 | 3 | 54.80233 | 147.729 | 0.105 | 0.115 | 0.107 |
| 7086 | 30 | 40 | 37.11246 | 255 | 59 | 2.63009 | 1963.333 | 0.112 | 0.132 | 0.122 |
| 7090 | -29 | 2 | 47.42972 | 115 | 20 | 47.99791 | 244.459 | 0.084 | 0.094 | 0.086 |
| 7105 | 39 | 1 | 14.15755 | 283 | 10 | 20.09023 | 22.185 | 0.049 | 0.037 | 0.044 |
| 7109 | 39 | 58 | 29.99504 | 239 | 3 | 18.87829 | 1109.318 | 0.053 | 0.040 | 0.049 |
| 7110 | 32 | 53 | 30.22718 | 243 | 34 | 38.18189 | 1841.934 | 0.054 | 0.035 | 0.043 |
| 7112 | 40 | 10 | 57.99005 | 255 | 16 | 26.26942 | 1504.746 | 0.057 | 0.060 | 0.054 |
| 7121 | -16 | 44 | 0.69993 | 208 | 57 | 31.72338 | 47.217 | 0.066 | 0.051 | 0.048 |
| 7122 | 23 | 20 | 34.23467 | 253 | 32 | 27.08425 | 33.919 | 0.062 | 0.041 | 0.044 |
| 7210 | 20 | 42 | 25.97277 | 203 | 44 | 38.53700 | 3068.245 | 0.063 | 0.017 | 0.035 |
| 7833 | 52 | 10 | 42.24554 | 5 | 48 | 35.07395 | 93.156 | 0.074 | 0.095 | 0.076 |
| 7834 | 49 | 8 | 41.77449 | 12 | 52 | 40.91683 | 661.109 | 0.052 | 0.054 | 0.056 |
| 7838 | 33 | 34 | 39.69937 | 135 | 56 | 13.13427 | 101.266 | 0.059 | 0.044 | 0.052 |
| 7839 | 47 | 4 | 1.68472 | 15 | 29 | 35.86532 | 539.290 | 0.053 | 0.048 | 0.055 |
| 7840 | 50 | 52 | 2.56574 | 0 | 20 | 9.79274 | 75.228 | 0.050 | 0.053 | 0.054 |
| 7907 | -16 | 27 | 56.69816 | 288 | 30 | 24.54219 | 2492.272 | 0.052 | 0.037 | 0.036 |
| 7939 | 40 | 38 | 55.78291 | 16 | 42 | 16.64779 | 535.949 | 0.053 | 0.040 | 0.049 |

$$a_e = 6378137.0m \qquad 1/f = 298.255$$

Fig H.XII Tracking Station Coordinates - Oct 1983 (Nottm ERP)

| Station | Latitude (deg min sec) | | | Longitude (deg min sec) | | | Height (m) | Standard Errors (cm) | | |
|---|---|---|---|---|---|---|---|---|---|---|
| | | | | | | | | $\sigma_\phi$ | $\sigma_\lambda$ | $\sigma_h$ |
| 1181 | 52 | 22 | 48.90912 | 13 | 3 | 54.81821 | 148.043 | 0.118 | 0.106 | 0.118 |
| 7086 | 30 | 40 | 37.13185 | 255 | 59 | 2.63322 | 1962.984 | 0.082 | 0.062 | 0.068 |
| 7090 | -29 | 2 | 47.43452 | 115 | 20 | 48.04884 | 244.548 | 0.073 | 0.061 | 0.062 |
| 7105 | 39 | 1 | 14.16339 | 283 | 10 | 20.10169 | 22.016 | 0.074 | 0.060 | 0.065 |
| 7109 | 39 | 58 | 29.99641 | 239 | 3 | 18.88424 | 1109.320 | 0.143 | 0.130 | 0.139 |
| 7110 | 32 | 53 | 30.24638 | 243 | 34 | 38.19484 | 1841.856 | 0.093 | 0.087 | 0.080 |
| 7112 | 40 | 10 | 57.99317 | 255 | 16 | 26.28718 | 1504.722 | 0.081 | 0.071 | 0.077 |
| 7121 | -16 | 44 | 0.69458 | 208 | 57 | 31.72571 | 47.161 | 0.110 | 0.096 | 0.081 |
| 7122 | 23 | 20 | 34.24104 | 253 | 32 | 27.10055 | 33.903 | 0.091 | 0.066 | 0.069 |
| 7210 | 20 | 42 | 25.98734 | 203 | 44 | 38.53700 | 3068.032 | 0.090 | 0.023 | 0.049 |
| 7834 | 49 | 8 | 41.75175 | 12 | 52 | 40.93408 | 660.993 | 0.072 | 0.062 | 0.076 |
| 7838 | 33 | 34 | 39.69351 | 135 | 56 | 13.14275 | 101.179 | 0.084 | 0.065 | 0.074 |
| 7839 | 47 | 4 | 1.65664 | 15 | 29 | 35.88199 | 539.200 | 0.079 | 0.083 | 0.080 |
| 7840 | 50 | 52 | 2.54884 | 0 | 20 | 9.83546 | 75.053 | 0.080 | 0.102 | 0.083 |
| 7907 | -16 | 27 | 56.70327 | 288 | 30 | 24.53809 | 2492.235 | 0.081 | 0.052 | 0.051 |
| 7939 | 40 | 38 | 55.76911 | 16 | 42 | 16.64618 | 535.436 | 0.079 | 0.060 | 0.076 |

$$a_e = 6378137.0m \qquad 1/f = 298.255$$

Fig H.XIII <u>Tracking Station Coordinates - Nov 1983 (Nottm ERP)</u>

| Station | Latitude (deg min sec) | | | Longitude (deg min sec) | | | Height (m) | Standard Errors (cm) | | |
|---|---|---|---|---|---|---|---|---|---|---|
| | | | | | | | | $\sigma_\phi$ | $\sigma_\lambda$ | $\sigma_h$ |
| 1181 | 52 | 22 | 48.92229 | 13 | 3 | 54.80469 | 147.936 | 0.124 | 0.121 | 0.115 |
| 7086 | 30 | 40 | 37.13856 | 255 | 59 | 2.64787 | 1963.257 | 0.086 | 0.065 | 0.071 |
| 7090 | -29 | 2 | 47.42871 | 115 | 20 | 48.05817 | 244.458 | 0.077 | 0.064 | 0.066 |
| 7105 | 39 | 1 | 14.16357 | 283 | 10 | 20.10862 | 22.268 | 0.084 | 0.072 | 0.083 |
| 7109 | 39 | 58 | 29.99310 | 239 | 3 | 18.90302 | 1109.457 | 0.116 | 0.122 | 0.123 |
| 7110 | 32 | 53 | 30.24747 | 243 | 34 | 38.20592 | 1842.149 | 0.098 | 0.080 | 0.101 |
| 7121 | -16 | 44 | 0.68206 | 208 | 57 | 31.72317 | 47.640 | 0.105 | 0.066 | 0.061 |
| 7122 | 23 | 20 | 34.25566 | 253 | 32 | 27.09517 | 34.113 | 0.098 | 0.061 | 0.074 |
| 7210 | 20 | 42 | 25.99901 | 203 | 44 | 38.53700 | 3068.350 | 0.090 | 0.017 | 0.042 |
| 7834 | 49 | 8 | 41.75907 | 12 | 52 | 40.94343 | 661.143 | 0.081 | 0.079 | 0.083 |
| 7838 | 33 | 34 | 39.70227 | 135 | 56 | 13.13852 | 101.405 | 0.081 | 0.048 | 0.064 |
| 7839 | 47 | 4 | 1.66480 | 15 | 29 | 35.87824 | 539.318 | 0.084 | 0.076 | 0.084 |
| 7840 | 50 | 52 | 2.54170 | 0 | 20 | 9.83580 | 74.315 | 0.071 | 0.068 | 0.076 |
| 7907 | -16 | 27 | 56.70202 | 288 | 30 | 24.54998 | 2492.486 | 0.090 | 0.050 | 0.045 |
| 7939 | 40 | 38 | 55.77024 | 16 | 42 | 16.64300 | 535.938 | 0.071 | 0.057 | 0.067 |

$$a_e = 6378137.0m \qquad 1/f = 298.255$$

Fig H.IV Tracking Station Coordinates - Dec 1983 (BIH ERP)

| Coordinate Solutions | Root-Mean-Square (RMS) Differences | | | | | | |
|---|---|---|---|---|---|---|---|
| | X (m) | Y (m) | Z (m) | $\phi$ (m) | $\lambda$ (m) | h (m) | Baseline Length (m) |
| SEPN - LSC 8112 | 0.33 | 0.29 | 0.62 | 0.62 | 0.26 | 0.35 | 0.63 |
| OCTN - LSC 8112 | 0.53 | 0.55 | 0.58 | 0.64 | 0.68 | 0.27 | 0.45 |
| NOVN - LSC 8112 | 0.33 | 0.33 | 0.41 | 0.47 | 0.34 | 0.21 | 0.47 |
| DECN - LSC 8112 | 0.30 | 0.36 | 0.54 | 0.56 | 0.35 | 0.29 | 0.41 |

fig H.XV Coordinate Comparison (Nottm ERP)

| Coordinate Solutions From    To | Transformation Parameters | | | | | | |
|---|---|---|---|---|---|---|---|
| | $\partial x$ (m) | $\partial y$ (m) | $\partial z$ (m) | $\alpha x$ (sec) | $\alpha y$ (sec) | $\alpha z$ (sec) | c (ppm) |
| SEPN - LSC 8112 | 0.062 | 0.055 | -0.302 | -0.009 | 0.009 | -0.004 | 0.028 |
| OCTN - LSC 8112 | -0.083 | -0.041 | -0.385 | 0.022 | -0.013 | -0.016 | 0.026 |
| NOVN - LSC 8112 | 0.076 | -0.039 | -0.193 | 0.013 | 0.006 | -0.007 | 0.025 |
| DECN - LSC 8112 | 0.123 | 0.013 | -0.412 | 0.013 | 0.008 | -0.005 | 0.006 |

fig H.XVI Transformation Parameters

| Coordinate Solutions | Root-Mean-Square (RMS) Differences | | | | | | |
|---|---|---|---|---|---|---|---|
| | X (m) | Y (m) | Z (m) | $\phi$ (m) | $\lambda$ (m) | h (m) | Baseline Length (m) |
| $SEPN_u$ - LSC 8112 | 0.34 | 0.27 | 0.44 | 0.47 | 0.24 | 0.32 | 0.59 |
| $OCTN_u$ - LSC 8112 | 0.27 | 0.28 | 0.31 | 0.32 | 0.32 | 0.21 | 0.39 |
| $NOVN_u$ - LSC 8112 | 0.29 | 0.25 | 0.30 | 0.39 | 0.23 | 0.16 | 0.42 |
| $DECN_u$ - LSC 8112 | 0.25 | 0.25 | 0.36 | 0.40 | 0.24 | 0.20 | 0.41 |

fig H.XVII Coordinate Comparison - Biases Removed (Nottm ERP)

| Coordinate Solutions | Root-Mean-Square (RMS) Differences | | | | | | |
|---|---|---|---|---|---|---|---|
| | X (m) | Y (m) | Z (m) | $\phi$ (m) | $\lambda$ (m) | h (m) | Baseline Length (m) |
| SEPN  – OCTN | 0.46 | 0.55 | 0.71 | 0.88 | 0.45 | 0.20 | 0.43 |
| SEPN  – NOVN | 0.26 | 0.37 | 0.54 | 0.59 | 0.27 | 0.27 | 0.42 |
| SEPN  – DECN | 0.30 | 0.36 | 0.42 | 0.51 | 0.24 | 0.27 | 0.43 |
| OCTN  – NOVN | 0.47 | 0.38 | 0.36 | 0.49 | 0.47 | 0.20 | 0.36 |
| OCTN  – DECN | 0.51 | 0.36 | 0.42 | 0.52 | 0.53 | 0.17 | 0.37 |
| NOVN  – DECN | 0.26 | 0.18 | 0.29 | 0.27 | 0.19 | 0.28 | 0.31 |

fig H.XVIII <u>Monthly Coordinate Inter-comparison (Nottm ERP)</u>

| Coordinate Solutions | Root-Mean-Square (RMS) Differences | | | | | | |
|---|---|---|---|---|---|---|---|
| | X (m) | Y (m) | Z (m) | $\phi$ (m) | $\lambda$ (m) | h (m) | Baseline Length (m) |
| $SEPN$ – $OCTN$ | 0.24 | 0.30 | 0.26 | 0.29 | 0.26 | 0.26 | 0.43 |
| $SEPN^{u}$ – $OCTN^{u}$ | 0.23 | 0.28 | 0.29 | 0.26 | 0.25 | 0.29 | 0.43 |
| $SEPN^{u}$ – $OCTN^{u}$ | 0.27 | 0.21 | 0.19 | 0.21 | 0.21 | 0.26 | 0.38 |
| $SEPN^{u}$ – $OCTN^{u}$ | 0.28 | 0.24 | 0.13 | 0.20 | 0.26 | 0.20 | 0.35 |
| $SEPN^{u}$ – $OCTN^{u}$ | 0.21 | 0.26 | 0.17 | 0.19 | 0.30 | 0.11 | 0.32 |
| $SEPN^{u}_{u}$ – $OCTN^{u}_{u}$ | 0.25 | 0.14 | 0.13 | 0.18 | 0.18 | 0.18 | 0.27 |

fig H.XIX <u>Monthly Coordinate Inter-comparison – Biases Removed (Nottm ERP)</u>

APPENDIX J

TABLES OF EARTH ROTATION PARAMETERS

| Epoch<br>Yr Day Time | $x_p$<br>(mas) | $\sigma_{xp}$<br>(mas) | $y_p$<br>(mas) | $\sigma_{yp}$<br>(mas) | UT1-UTC<br>( 0.1ms) | $\sigma_{\Delta UT}$<br>(0.1ms) | D<br>(0.1ms) | $\sigma_D$<br>(0.1ms) |
|---|---|---|---|---|---|---|---|---|
| 83 250 0.0 | 309.6 | 1.0 | 140.7 | 2.6 | 6454.0 | 3.2 | – | – |
| 83 255 0.0 | 294.1 | 2.7 | 129.8 | 5.9 | 6348.8 | 0.8 | 19.88 | 0.4 |
| 83 260 0.0 | 284.6 | 5.8 | 101.5 | 3.4 | 6252.3 | 2.5 | 18.73 | 0.5 |
| 83 265 0.0 | 272.1 | 6.6 | 73.8 | 4.3 | 6161.1 | 3.7 | 19.60 | 0.7 |
| 83 270 0.0 | 248.3 | 2.3 | 67.3 | 4.9 | 6054.0 | 3.6 | 20.00 | 1.1 |
| 83 275 0.0 | 213.6 | 14.8 | 70.8 | 0.9 | 5981.4 | 9.5 | 18.62 | 1.4 |
| 83 280 0.0 | 192.6 | 2.5 | 59.0 | 1.9 | 5868.7 | 2.9 | 24.22 | 1.0 |
| 83 285 0.0 | 170.3 | 1.4 | 48.8 | 3.3 | 5746.6 | 1.7 | 20.39 | 0.4 |
| 83 290 0.0 | 151.2 | 3.7 | 38.6 | 1.0 | 5649.9 | 0.2 | 19.54 | 0.5 |
| 83 295 0.0 | 131.3 | 3.8 | 49.3 | 0.6 | 5545.3 | 4.6 | 22.10 | 0.7 |
| 83 300 0.0 | 111.0 | 5.2 | 35.0 | 0.4 | 5426.9 | 2.7 | 23.30 | 1.0 |
| 83 305 0.0 | 102.0 | 11.2 | 16.7 | 2.4 | 5314.9 | 7.4 | 24.22 | 1.1 |
| 83 310 0.0 | 82.5 | 1.8 | 18.5 | 2.4 | 5185.3 | 1.8 | 25.21 | 0.8 |
| 83 315 0.0 | 55.6 | 3.6 | 12.5 | 3.2 | 5059.8 | 2.6 | 25.27 | 0.5 |
| 83 320 0.0 | 37.4 | 3.4 | 9.0 | 4.9 | 4932.0 | 3.1 | 25.51 | 0.5 |
| 83 325 0.0 | 15.2 | 1.5 | 23.3 | 2.7 | 4804.6 | 1.4 | 24.65 | 0.4 |
| 83 330 0.0 | -18.3 | 2.8 | 44.4 | 20.2 | 4684.3 | 2.5 | 23.44 | 0.9 |
| 83 335 0.0 | -25.9 | 0.3 | 34.0 | 5.2 | 4591.9 | 7.7 | 19.60 | 1.1 |
| 83 340 0.0 | -45.8 | 1.2 | 39.2 | 2.1 | 4488.3 | 2.3 | 20.07 | 0.9 |
| 83 345 0.0 | -64.8 | 2.7 | 40.1 | 3.3 | 4389.1 | 4.0 | 20.71 | 0.6 |
| 83 350 0.0 | -80.8 | 1.9 | 57.4 | 3.9 | 4281.9 | 1.4 | 19.94 | 0.5 |
| 83 355 0.0 | -96.5 | 0.8 | 59.7 | 5.8 | 4185.8 | 2.6 | 21.40 | 0.4 |
| 83 360 0.0 | -106.2 | 4.9 | 84.7 | 3.8 | 4068.8 | 1.1 | 22.90 | 0.4 |
| 83 365 0.0 | -125.4 | 9.7 | 92.0 | 6.4 | 3956.2 | 2.2 | – | – |

Fig J.I <u>Earth Rotation Parameter Series - UNOTT.1</u>

| Epoch Yr Day Time | $x_p$ (mas) | $\sigma_{xp}$ (mas) | $y_p$ (mas) | $\sigma_{yp}$ (mas) | UT1-UTC ( 0.1ms) | $\sigma_{\Delta UT}$ (0.1ms) | D (0.1ms) | $\sigma_D$ (0.1ms) |
|---|---|---|---|---|---|---|---|---|
| 83 250 0.0 | 314.2 | 1.7 | 146.6 | 1.4 | 6453.3 | 1.0 | – | – |
| 83 255 0.0 | 301.6 | 1.4 | 126.5 | 1.2 | 6349.0 | 0.9 | 20.11 | 0.2 |
| 83 260 0.0 | 286.0 | 1.8 | 105.1 | 1.3 | 6252.2 | 1.0 | 19.24 | 0.2 |
| 83 265 0.0 | 265.2 | 2.6 | 81.1 | 2.1 | 6157.1 | 1.5 | 19.72 | 0.3 |
| 83 270 0.0 | 244.5 | 2.1 | 68.6 | 1.9 | 6054.0 | 1.4 | 18.46 | 0.3 |
| 83 275 0.0 | 213.1 | 1.6 | 59.5 | 1.5 | 5969.8 | 1.1 | 18.39 | 0.2 |
| 83 280 0.0 | 186.2 | 1.9 | 56.4 | 1.6 | 5871.3 | 1.2 | 21.49 | 0.2 |
| 83 285 0.0 | 169.8 | 1.6 | 44.1 | 1.4 | 5755.6 | 1.0 | 22.30 | 0.2 |
| 83 290 0.0 | 151.8 | 1.8 | 38.8 | 1.3 | 5647.6 | 1.0 | 21.64 | 0.2 |
| 83 295 0.0 | 129.9 | 2.1 | 43.7 | 1.8 | 5539.2 | 1.3 | 22.10 | 0.2 |
| 83 300 0.0 | 110.4 | 1.7 | 36.1 | 1.4 | 5426.4 | 1.1 | 22.50 | 0.2 |
| 83 305 0.0 | 100.5 | 2.0 | 21.0 | 1.5 | 5314.1 | 1.2 | 24.17 | 0.2 |
| 83 310 0.0 | 83.9 | 1.4 | 15.4 | 1.1 | 5186.5 | 0.8 | 26.21 | 0.2 |
| 83 315 0.0 | 57.8 | 1.5 | 15.0 | 1.2 | 5053.0 | 0.9 | 26.26 | 0.2 |
| 83 320 0.0 | 29.8 | 2.1 | 14.9 | 1.8 | 4925.9 | 1.4 | 25.09 | 0.2 |
| 83 325 0.0 | 5.2 | 1.7 | 22.3 | 1.5 | 4802.3 | 1.1 | 21.95 | 0.3 |
| 83 330 0.0 | -12.6 | 2.2 | 18.6 | 2.2 | 4706.4 | 1.4 | 19.24 | 0.3 |
| 83 335 0.0 | -28.1 | 2.5 | 21.0 | 2.4 | 4609.9 | 1.6 | 21.42 | 0.3 |
| 83 340 0.0 | -45.2 | 1.7 | 39.0 | 1.6 | 4493.9 | 1.1 | 21.74 | 0.2 |
| 83 345 0.0 | -60.0 | 1.6 | 52.1 | 1.4 | 4389.4 | 1.0 | 21.08 | 0.2 |
| 83 350 0.0 | -77.5 | 1.9 | 63.3 | 1.5 | 4283.1 | 1.1 | 21.09 | 0.2 |
| 83 355 0.0 | -98.1 | 2.0 | 67.3 | 1.9 | 4178.7 | 1.3 | 21.24 | 0.3 |
| 83 360 0.0 | -106.9 | 1.7 | 80.9 | 2.0 | 4070.5 | 1.3 | – | – |

Fig J.II Earth Rotation Parameter Series - UNOTT.5

| Day No. 1983 | BIH Circ D | UNOTT.1 - UNOTT.5 | UNOTT.1 - BIH Circ D | UNOTT.1 - CSR 81.12 | UNOTT.1 - CSR 84.02 | UNOTT.5 - BIH Circ D | UNOTT.5 - CSR 81.12 | UNOTT.5 - CSR 84.02 |
|---|---|---|---|---|---|---|---|---|
| 250 | 304.0 | -4.6 | 5.6 | 4.6 | 21.6 | 10.2 | 9.2 | 26.2 |
| 255 | 293.0 | -7.5 | 1.1 | -0.9 | 19.1 | 8.6 | 6.6 | 26.6 |
| 260 | 280.0 | -1.5 | 4.6 | 0.6 | 20.6 | 6.0 | 2.0 | 22.0 |
| 265 | 265.0 | 6.9 | 7.1 | 6.1 | 22.1 | 0.2 | -0.8 | 15.2 |
| 270 | 249.0 | 3.8 | -0.7 | 6.3 | 19.3 | -4.5 | 2.5 | 15.5 |
| 275 | 231.0 | 0.5 | -17.4 | -19.4 | -0.4 | -17.9 | -19.9 | -0.9 |
| 280 | 211.0 | 6.6 | -18.4 | -22.4 | -5.4 | -25.0 | -29.0 | -12.0 |
| 285 | 189.0 | 0.5 | -18.7 | -21.7 | -5.7 | -19.2 | -22.2 | -6.2 |
| 290 | 167.0 | -0.6 | -15.8 | -24.8 | -7.8 | -15.2 | -24.2 | -7.2 |
| 295 | 145.0 | 1.4 | -13.7 | -15.7 | -5.7 | -15.1 | -17.1 | -7.1 |
| 300 | 123.0 | 0.6 | -12.0 | -8.0 | -1.0 | -12.6 | -8.6 | -1.6 |
| 305 | 100.0 | 1.5 | 2.0 | - | 13.0 | 0.5 | - | 11.5 |
| 310 | 77.0 | -1.4 | 5.5 | - | 17.5 | 6.9 | - | 18.9 |
| 315 | 55.0 | -2.3 | 0.6 | - | 9.6 | 2.8 | - | 11.8 |
| 320 | 33.0 | 7.7 | 4.5 | - | 14.5 | -3.3 | - | 6.8 |
| 325 | 12.0 | 10.0 | 3.2 | - | 21.2 | -6.8 | - | 11.2 |
| 330 | -9.0 | -5.8 | -9.3 | - | -1.3 | -3.6 | - | 4.5 |
| 335 | -29.0 | 2.6 | 3.5 | - | 0.5 | 0.9 | - | -2.1 |
| 340 | -47.0 | -0.6 | 1.3 | - | 14.2 | 1.8 | - | 14.8 |
| 345 | -64.0 | -4.7 | -0.8 | - | -5.8 | 4.0 | - | -1.0 |
| 350 | -80.0 | -3.3 | -0.8 | - | 8.2 | 2.5 | - | 11.5 |
| 355 | -95.0 | 1.7 | -1.5 | - | -9.5 | -3.1 | - | -11.1 |
| 360 | -109.0 | 0.7 | 2.8 | - | -8.2 | 2.1 | - | -8.9 |
| 365 | -122.0 | - | -3.4 | - | -14.4 | - | - | - |
| RMS Difference | | 4.3 | 8.8 | 14.7 | 13.2 | 10.1 | 16.0 | 13.2 |

Fig J.III Comparison of $x_p$ components of Polar Motion

| Day No. 1983 | BIH Circ D | UNOTT.1 - UNOTT.5 | UNOTT.1 - BIH Circ D | UNOTT.1 - CSR 81.12 | UNOTT.1 - CSR 84.02 | UNOTT.5 - BIH Circ D | UNOTT.5 - CSR 81.12 | UNOTT.5 - CSR 84.02 |
|---|---|---|---|---|---|---|---|---|
| 250 | 151.0 | -5.8 | -10.3 | -6.3 | -1.3 | -4.4 | -0.4 | 4.6 |
| 255 | 131.0 | 1.3 | -1.2 | 18.8 | 5.8 | -2.5 | 17.5 | 4.5 |
| 260 | 112.0 | -3.6 | -10.5 | 4.5 | -5.5 | -6.9 | 8.1 | -1.9 |
| 265 | 95.0 | -7.3 | -21.2 | -11.2 | -18.2 | -13.9 | -3.9 | -10.9 |
| 270 | 80.0 | -1.2 | -12.7 | -4.7 | -5.7 | -11.4 | -3.4 | -4.4 |
| 275 | 66.0 | 11.3 | 4.9 | 7.9 | 13.8 | -6.5 | -3.5 | 2.5 |
| 280 | 54.0 | 2.6 | 5.0 | 13.0 | 12.0 | 2.4 | 10.4 | 9.4 |
| 285 | 43.0 | 4.7 | 5.8 | 22.8 | 14.8 | 1.1 | 17.1 | 10.1 |
| 290 | 34.0 | -0.2 | 4.6 | 18.6 | 11.6 | 4.8 | 18.8 | 11.8 |
| 295 | 27.0 | 5.5 | 22.3 | 19.3 | 27.3 | 16.7 | 13.7 | 21.8 |
| 300 | 22.0 | -1.0 | 13.1 | 21.1 | 20.1 | 14.1 | 22.1 | 21.1 |
| 305 | 18.0 | -4.3 | -1.3 | - | 6.7 | 3.0 | - | 11.0 |
| 310 | 17.0 | 3.2 | 1.5 | - | 8.5 | -1.7 | - | 5.4 |
| 315 | 18.0 | -2.5 | -5.5 | - | 2.5 | -3.0 | - | 5.0 |
| 320 | 19.0 | -5.9 | -10.0 | - | -3.0 | -4.1 | - | 2.9 |
| 325 | 22.0 | 1.0 | 1.3 | - | 7.3 | 0.3 | - | 6.3 |
| 330 | 26.0 | 25.8 | 18.4 | - | 23.4 | -7.4 | - | -2.4 |
| 335 | 32.0 | 12.9 | 2.0 | - | 8.0 | -11.0 | - | -5.0 |
| 340 | 39.0 | 0.2 | 0.2 | - | 7.2 | 0.0 | - | 7.0 |
| 345 | 47.0 | -11.9 | -6.9 | - | 5.2 | 5.1 | - | 17.1 |
| 350 | 56.0 | -5.9 | 1.4 | - | 14.4 | 7.3 | - | 20.3 |
| 355 | 66.0 | -7.6 | -6.3 | - | 5.7 | 1.3 | - | 13.3 |
| 360 | 76.0 | 3.8 | 8.7 | - | 21.7 | 4.9 | - | 17.9 |
| 365 | 87.0 | - | 5.0 | - | 19.0 | - | - | - |
| RMS Difference | | 7.9 | 9.7 | 14.8 | 13.2 | 7.4 | 12.9 | 11.3 |

Fig J.IV Comparison of $y_p$ components of Polar Motion

| Day No. 1983 | BIH Circ D | UNOTT.1 – UNOTT.5 | UNOTT.1 – BIH Circ D | UNOTT.5 – BIH Circ D |
|---|---|---|---|---|
| 250 | 6442.0 | 0.7 | 12.0 | 11.3 |
| 255 | 6358.0 | -2.2 | -11.2 | -9.0 |
| 260 | 6269.0 | 0.1 | -16.7 | -16.8 |
| 265 | 6173.0 | 4.0 | -11.9 | -15.9 |
| 270 | 6070.0 | 0.0 | -16.0 | -16.0 |
| 275 | 5964.0 | 11.6 | 17.4 | 5.8 |
| 280 | 5859.0 | -2.6 | 9.7 | 12.3 |
| 285 | 5754.0 | -9.0 | -7.4 | 1.6 |
| 290 | 5648.0 | 2.3 | 1.9 | -0.4 |
| 295 | 5537.0 | 6.1 | 8.3 | 2.2 |
| 300 | 5423.0 | 0.5 | 3.9 | 3.4 |
| 305 | 5305.0 | 0.3 | 9.4 | 9.1 |
| 310 | 5183.0 | -1.3 | 2.3 | 3.5 |
| 315 | 5057.0 | 6.7 | 2.8 | -4.0 |
| 320 | 4933.0 | 6.1 | -1.0 | -7.1 |
| 325 | 4815.0 | 2.2 | -10.4 | -12.7 |
| 330 | 4698.0 | -22.1 | -13.7 | 8.4 |
| 335 | 4588.0 | -18.0 | 3.9 | 21.9 |
| 340 | 4485.0 | -5.6 | 3.3 | 8.9 |
| 345 | 4386.0 | -0.4 | 3.1 | 3.4 |
| 350 | 4283.0 | -1.3 | -1.1 | 0.1 |
| 355 | 4179.0 | 7.1 | 6.8 | -0.3 |
| 360 | 4077.0 | -1.7 | -8.2 | -6.5 |
| 365 | 3982.0 | - | -25.8 | - |
| RMS Difference | | 7.4 | 10.6 | 9.8 |

Fig J.V Comparison of UT1-UTC Series

| Day No. 1983 | BIH Circ D | UNOTT.1 – UNOTT.5 | UNOTT.1 – BIH Circ D | UNOTT.1 – CSR 81.12 | UNOTT.1 – CSR 84.02 | UNOTT.5 – BIH Circ D | UNOTT.5 – CSR 81.12 | UNOTT.5 – CSR 84.02 |
|---|---|---|---|---|---|---|---|---|
| 250 | 16.3 | – | – | – | – | – | – | – |
| 255 | 17.3 | -0.3 | 2.6 | 2.0 | 3.9 | 2.8 | 2.2 | 4.1 |
| 260 | 18.5 | -0.5 | 0.2 | 1.1 | 2.2 | 0.7 | 1.6 | 2.7 |
| 265 | 19.9 | -0.1 | -0.3 | 0.3 | 1.0 | -0.2 | 0.4 | 1.1 |
| 270 | 20.9 | 1.5 | -0.9 | 2.6 | 1.0 | -2.4 | 1.1 | -0.5 |
| 275 | 21.1 | 0.2 | -2.5 | -1.9 | -1.4 | -2.7 | -2.1 | -1.6 |
| 280 | 21.0 | 2.7 | 3.2 | 0.7 | 1.7 | 0.5 | -2.0 | -1.0 |
| 285 | 21.1 | -1.9 | -0.7 | -1.0 | -1.8 | 1.2 | 0.9 | 0.1 |
| 290 | 21.6 | -2.9 | -2.1 | -0.3 | -0.5 | 0.0 | 2.3 | 1.6 |
| 295 | 22.4 | 0.0 | -0.3 | -0.9 | 1.3 | -0.3 | -0.9 | 1.3 |
| 300 | 23.2 | 0.8 | 0.1 | 0.5 | 1.2 | -0.7 | -0.3 | 0.4 |
| 305 | 24.5 | 0.1 | -0.3 | – | -0.2 | -0.3 | – | -0.2 |
| 310 | 25.4 | -1.0 | -0.2 | – | -0.4 | 0.8 | – | 0.6 |
| 315 | 25.6 | -1.0 | -0.3 | – | -0.8 | 0.7 | – | 0.2 |
| 320 | 24.9 | 0.4 | 0.6 | – | 2.3 | 0.2 | – | 1.9 |
| 325 | 24.0 | 2.7 | 0.7 | – | 0.3 | -2.1 | – | -2.5 |
| 330 | 22.8 | 4.2 | 0.6 | – | 2.0 | -3.6 | – | -2.2 |
| 335 | 21.2 | -1.8 | -1.6 | – | -3.6 | 0.2 | – | -1.8 |
| 340 | 20.2 | -1.7 | -0.1 | – | -0.7 | 1.5 | – | 0.9 |
| 345 | 20.1 | -0.4 | 0.6 | – | 1.8 | 1.0 | – | 2.2 |
| 350 | 20.4 | -1.2 | -0.5 | – | -1.3 | 0.7 | – | -0.1 |
| 355 | 20.4 | 0.2 | 1.0 | – | -1.4 | 0.8 | – | -1.6 |
| 360 | 19.5 | – | 3.4 | – | 5.8 | – | – | – |
| 365 | 17.8 | – | – | – | – | – | – | – |
| RMS Difference | | 1.5 | 1.4 | 1.3 | 2.0 | 1.4 | 1.5 | 1.6 |

Fig J.VI Comparison of Excess Length of Day (D) Series

| Month 1983 | Period (Day Nos.) | $\Delta x_p$ (mas) | $\Delta y_p$ (mas) | $\Delta$(UT1-UTC) (0.1ms) |
|------------|-------------------|--------------------|--------------------|---------------------------|
| SEPT | 250 - 270 | -3.5 | 11.2 | 8.7 |
| OCT | 275 - 300 | 16.0 | -9.2 | -5.6 |
| NOV | 305 - 330 | -1.1 | -0.7 | 1.8 |
| DEC | 335 - 365 | -0.2 | -0.6 | 2.6 |

Fig J.VII  Systematic Differences between UNOTT.1 and BIH Circular D

| Month 1983 | Period (Day Nos.) | $\Delta x_p$ (mas) | $\Delta y_p$ (mas) | $\Delta$(UT1-UTC) (0.1ms) |
|------------|-------------------|--------------------|--------------------|---------------------------|
| SEPT | 250 - 270 | -3.3 | 9.5 | 5.3 |
| OCT | 275 - 300 | 18.0 | -6.3 | -6.1 |
| NOV | 305 - 330 | 0.2 | 4.9 | -0.9 |
| DEC | 335 - 365 | -1.9 | -3.9 | 0.4 |

Fig J.VIII  Systematic Differences between UNOTT.5 and BIH Circular D

| Epoch Yr Day Time | $x_p$ (mas) | $\sigma_{xp}$ (mas) | $y_p$ (mas) | $\sigma_{yp}$ (mas) | UT1-UTC ( 0.1ms) | $\sigma_{\Delta UT}$ (0.1ms) | D (0.1ms) | $\sigma_D$ (0.1ms) |
|---|---|---|---|---|---|---|---|---|
| 83 250 0.0 | 306.1 | 1.0 | 151.9 | 2.6 | 6462.8 | 3.2 | - | - |
| 83 255 0.0 | 290.6 | 2.7 | 140.9 | 5.9 | 6355.6 | 0.8 | 19.88 | 0.4 |
| 83 260 0.0 | 281.1 | 5.8 | 112.7 | 3.4 | 6261.1 | 2.5 | 18.73 | 0.5 |
| 83 265 0.0 | 268.5 | 6.6 | 84.9 | 4.3 | 6169.9 | 3.7 | 19.60 | 0.7 |
| 83 270 0.0 | 244.8 | 2.3 | 78.5 | 4.9 | 6062.8 | 3.6 | 20.60 | 1.1 |
| 83 275 0.0 | 229.6 | 14.8 | 61.6 | 0.9 | 5975.8 | 9.5 | 20.03 | 1.4 |
| 83 280 0.0 | 208.6 | 2.5 | 49.7 | 1.9 | 5863.1 | 2.9 | 24.22 | 1.0 |
| 83 285 0.0 | 186.3 | 1.4 | 39.5 | 3.3 | 5741.0 | 1.7 | 20.39 | 0.4 |
| 83 290 0.0 | 167.2 | 3.7 | 29.3 | 1.0 | 5644.2 | 0.2 | 19.54 | 0.5 |
| 83 295 0.0 | 147.3 | 3.8 | 40.0 | 0.6 | 5539.6 | 4.6 | 22.10 | 0.7 |
| 83 300 0.0 | 127.0 | 5.2 | 25.8 | 0.4 | 5421.3 | 2.7 | 22.84 | 1.0 |
| 83 305 0.0 | 100.9 | 11.2 | 16.0 | 2.4 | 5316.2 | 7.4 | 23.50 | 1.1 |
| 83 310 0.0 | 81.4 | 1.8 | 17.8 | 2.4 | 5187.1 | 1.8 | 25.21 | 0.8 |
| 83 315 0.0 | 54.5 | 3.6 | 11.8 | 3.2 | 5061.6 | 2.6 | 25.27 | 0.5 |
| 83 320 0.0 | 36.4 | 3.4 | 8.2 | 4.9 | 4933.8 | 3.1 | 25.51 | 0.5 |
| 83 325 0.0 | 14.1 | 1.5 | 23.6 | 2.7 | 4806.4 | 1.4 | 24.65 | 0.4 |
| 83 330 0.0 | -19.4 | 2.8 | 43.6 | 20.2 | 4686.1 | 2.5 | 23.42 | 0.9 |
| 83 335 0.0 | -25.6 | 0.3 | 33.4 | 5.2 | 4594.5 | 7.7 | 19.53 | 1.1 |
| 83 340 0.0 | -45.9 | 1.2 | 38.7 | 2.1 | 4490.9 | 2.3 | 20.07 | 0.9 |
| 83 345 0.0 | -64.9 | 2.7 | 39.6 | 3.3 | 4391.6 | 4.0 | 20.71 | 0.6 |
| 83 350 0.0 | -81.0 | 1.9 | 56.8 | 3.9 | 4284.4 | 1.4 | 19.94 | 0.5 |
| 83 355 0.0 | -96.6 | 0.8 | 59.1 | 5.8 | 4188.4 | 2.6 | 21.40 | 0.4 |
| 83 360 0.0 | -106.4 | 4.9 | 84.1 | 3.8 | 4071.3 | 1.1 | 22.90 | 0.4 |
| 83 365 0.0 | -125.6 | 9.7 | 91.4 | 6.4 | 3958.8 | 2.2 | - | - |

Biases (with respect to BIH Circular D) removed

Fig J.IX <u>Earth Rotation Parameter Series - UNOTT.1b</u>

| Epoch | | | $x_p$ | $\sigma_{xp}$ | $y_p$ | $\sigma_{yp}$ | UT1-UTC | $\sigma_{\Delta UT}$ | D | $\sigma_D$ |
|---|---|---|---|---|---|---|---|---|---|---|
| Yr | Day | Time | (mas) | (mas) | (mas) | (mas) | ( 0.1ms) | (0.1ms) | (0.1ms) | (0.1ms) |
| 83 | 250 | 0.0 | 310.9 | 1.7 | 156.1 | 1.4 | 6458.6 | 1.0 | – | – |
| 83 | 255 | 0.0 | 298.3 | 1.4 | 138.0 | 1.2 | 6354.3 | 0.9 | 20.11 | 0.2 |
| 83 | 260 | 0.0 | 282.8 | 1.8 | 114.6 | 1.3 | 6257.5 | 1.0 | 19.24 | 0.2 |
| 83 | 265 | 0.0 | 261.9 | 2.6 | 90.6 | 2.1 | 6162.4 | 1.5 | 19.72 | 0.3 |
| 83 | 270 | 0.0 | 241.2 | 2.1 | 78.1 | 1.9 | 6059.2 | 1.4 | 19.28 | 0.3 |
| 83 | 275 | 0.0 | 223.1 | 1.6 | 59.1 | 1.5 | 5968.0 | 1.1 | 19.50 | 0.2 |
| 83 | 280 | 0.0 | 204.0 | 1.9 | 50.9 | 1.6 | 5865.2 | 1.2 | 21.90 | 0.2 |
| 83 | 285 | 0.0 | 187.8 | 1.6 | 37.8 | 1.4 | 5749.5 | 1.0 | 22.30 | 0.2 |
| 83 | 290 | 0.0 | 169.8 | 1.8 | 32.5 | 1.3 | 5641.5 | 1.0 | 21.64 | 0.2 |
| 83 | 295 | 0.0 | 147.9 | 2.1 | 37.5 | 1.8 | 5533.1 | 1.3 | 22.10 | 0.2 |
| 83 | 300 | 0.0 | 128.4 | 1.7 | 29.8 | 1.4 | 5420.3 | 1.1 | 22.16 | 0.2 |
| 83 | 305 | 0.0 | 107.1 | 2.0 | 21.9 | 1.5 | 5311.3 | 1.2 | 23.67 | 0.2 |
| 83 | 310 | 0.0 | 84.1 | 1.4 | 20.2 | 1.1 | 5185.6 | 0.8 | 26.06 | 0.2 |
| 83 | 315 | 0.0 | 58.0 | 1.5 | 19.9 | 1.2 | 5052.1 | 0.9 | 26.26 | 0.2 |
| 83 | 320 | 0.0 | 29.9 | 2.1 | 19.8 | 1.8 | 4925.0 | 1.4 | 25.09 | 0.2 |
| 83 | 325 | 0.0 | 5.3 | 1.7 | 27.1 | 1.5 | 4801.4 | 1.1 | 21.95 | 0.3 |
| 83 | 330 | 0.0 | -12.4 | 2.2 | 23.5 | 2.2 | 4705.5 | 1.4 | 19.18 | 0.3 |
| 83 | 335 | 0.0 | -28.9 | 2.5 | 21.7 | 2.4 | 4609.6 | 1.6 | 21.29 | 0.3 |
| 83 | 340 | 0.0 | -45.1 | 1.7 | 35.1 | 1.6 | 4494.3 | 1.1 | 21.69 | 0.2 |
| 83 | 345 | 0.0 | -61.9 | 1.6 | 48.2 | 1.4 | 4389.8 | 1.0 | 21.08 | 0.2 |
| 83 | 350 | 0.0 | -79.4 | 1.9 | 59.4 | 1.5 | 4283.6 | 1.1 | 21.09 | 0.2 |
| 83 | 355 | 0.0 | -100.0 | 2.0 | 63.4 | 1.9 | 4179.2 | 1.3 | 21.24 | 0.3 |
| 83 | 360 | 0.0 | -108.9 | 1.7 | 77.0 | 2.0 | 4070.9 | 1.3 | – | – |

Biases (with respect to BIH Circular D) Removed

Fig J.X Earth Rotation Parameter Series - UNOTT.5b

| Day No. 1983 | BIH Circ D | UNOTT.1 – UNOTT.5 | UNOTT.1 – BIH Circ D | UNOTT.5 – BIH Circ D |
|---|---|---|---|---|
| 250 | 304.0 | -4.8 | 2.1 | 6.7 |
| 255 | 293.0 | -7.7 | -2.4 | 5.3 |
| 260 | 280.0 | -1.7 | 1.0 | 2.8 |
| 265 | 265.0 | 6.7 | 3.5 | -3.1 |
| 270 | 249.0 | 3.6 | -4.2 | -7.8 |
| 275 | 231.0 | 6.5 | -1.4 | -7.9 |
| 280 | 211.0 | 4.6 | -2.4 | -7.0 |
| 285 | 189.0 | -1.5 | -2.7 | -1.2 |
| 290 | 167.0 | -2.6 | 0.2 | 2.8 |
| 295 | 145.0 | -0.6 | 2.3 | 2.9 |
| 300 | 123.0 | -1.4 | 4.0 | 5.4 |
| 305 | 100.0 | -6.1 | 0.9 | 7.1 |
| 310 | 77.0 | -2.6 | 4.4 | 7.1 |
| 315 | 55.0 | -3.5 | -0.5 | 3.0 |
| 320 | 33.0 | 6.5 | 3.4 | -3.1 |
| 325 | 12.0 | 8.8 | 2.1 | -6.7 |
| 330 | -9.0 | -7.0 | -10.4 | -3.4 |
| 335 | -29.0 | 3.3 | 3.4 | 0.1 |
| 340 | -45.0 | 1.1 | 1.1 | -0.1 |
| 345 | -64.0 | -3.0 | -0.9 | 2.1 |
| 350 | -80.0 | -1.5 | -1.0 | 0.6 |
| 355 | -95.0 | 3.4 | -1.6 | -5.0 |
| 360 | -109.0 | 2.4 | 2.6 | 0.2 |
| 365 | -122.0 | – | -3.6 | – |
| RMS Difference | | 4.6 | 3.3 | 4.7 |

Biases (with respect to BIH Circular D) Removed from Nottm series

J.XI  Comparison of  $x_p$  components of Polar Motion

| Day No.<br>1983 | BIH<br>Circ D | UNOTT.1 –<br>UNOTT.5 | UNOTT.1 –<br>BIH Circ D | UNOTT.5 –<br>BIH Circ D |
|---|---|---|---|---|
| 250 | 151.0 | -4.1 | 0.9 | 5.1 |
| 255 | 131.0 | 3.0 | 9.9 | 7.0 |
| 260 | 112.0 | -1.9 | 0.7 | 2.6 |
| 265 | 95.0 | -5.7 | -10.1 | -4.4 |
| 270 | 80.0 | 0.4 | -1.5 | -1.9 |
| 275 | 66.0 | 2.5 | -4.4 | -6.9 |
| 280 | 54.0 | -0.4 | -4.3 | -4.0 |
| 285 | 43.0 | 1.7 | -3.5 | -5.2 |
| 290 | 34.0 | -3.2 | -4.7 | -1.5 |
| 295 | 27.0 | 2.6 | 13.0 | 10.5 |
| 300 | 22.0 | -4.0 | 3.8 | 7.8 |
| 305 | 18.0 | -5.9 | -2.0 | 3.9 |
| 310 | 17.0 | -2.4 | 0.8 | 3.2 |
| 315 | 18.0 | -8.1 | -6.2 | 1.9 |
| 320 | 19.0 | -11.6 | -10.8 | 0.8 |
| 325 | 22.0 | -4.6 | 0.6 | 5.1 |
| 330 | 26.0 | 20.2 | 17.6 | -2.6 |
| 335 | 32.0 | 11.7 | 1.4 | -10.3 |
| 340 | 39.0 | 3.5 | -0.4 | -3.9 |
| 345 | 47.0 | -8.6 | -7.4 | 1.2 |
| 350 | 56.0 | -2.6 | 0.8 | 3.4 |
| 355 | 66.0 | -4.3 | -6.9 | -2.6 |
| 360 | 76.0 | 7.1 | 8.1 | 1.0 |
| 365 | 87.0 | – | 4.4 | – |
| RMS Difference | | 6.8 | 6.8 | 5.0 |

Biases (with respect to BIH Circular D) Removed from Nottm series

J.XII Comparison of $y_p$ components of Polar Motion

| Day No. 1983 | BIH Circ D | UNOTT.1 - UNOTT.5 | UNOTT.1 - BIH Circ D | UNOTT.5 - BIH Circ D |
|---|---|---|---|---|
| 250 | 6442.0 | 4.2 | 20.8 | 16.6 |
| 255 | 6358.0 | 1.3 | -2.5 | -3.7 |
| 260 | 6269.0 | 3.6 | -7.9 | -11.6 |
| 265 | 6173.0 | 7.5 | -3.2 | -10.6 |
| 270 | 6070.0 | 3.5 | -7.3 | -10.8 |
| 275 | 5964.0 | 7.8 | 11.8 | 4.0 |
| 280 | 5859.0 | -2.2 | 4.1 | 6.2 |
| 285 | 5754.0 | -8.5 | -13.0 | -4.5 |
| 290 | 5648.0 | 2.7 | -3.8 | -6.5 |
| 295 | 5537.0 | 6.5 | 2.6 | -3.9 |
| 300 | 5423.0 | 0.9 | -1.7 | -2.7 |
| 305 | 5305.0 | 4.9 | 11.2 | 6.3 |
| 310 | 5183.0 | 1.4 | 4.1 | 2.6 |
| 315 | 5057.0 | 9.4 | 4.6 | -4.9 |
| 320 | 4933.0 | 8.8 | 0.8 | -8.0 |
| 325 | 4815.0 | 4.9 | -8.6 | -13.6 |
| 330 | 4698.0 | -19.4 | -11.9 | 7.5 |
| 335 | 4588.0 | -15.1 | 6.5 | 21.6 |
| 340 | 4485.0 | -3.4 | 5.9 | 9.3 |
| 345 | 4386.0 | 1.8 | 5.6 | 3.9 |
| 350 | 4283.0 | 0.9 | 1.4 | 0.6 |
| 355 | 4179.0 | 9.2 | 9.4 | 0.2 |
| 360 | 4077.0 | 0.5 | -5.7 | -6.1 |
| 365 | 3982.0 | - | -23.2 | - |
| RMS Difference | | 7.3 | 9.3 | 8.8 |

Biases (with respect to BIH Circular D) Removed

Fig J.XIII Comparison of UT1-UTC Series

| Day No. 1983 | BIH Circ D | UNOTT.1 – UNOTT.5 | UNOTT.1 – BIH Circ D | UNOTT.5 – BIH Circ D |
|---|---|---|---|---|
| 250 | 16.3 | – | – | – |
| 255 | 17.3 | -0.2 | 2.6 | 2.8 |
| 260 | 18.5 | -0.5 | 0.2 | 0.7 |
| 265 | 19.9 | -0.1 | -0.3 | -0.2 |
| 270 | 20.9 | 1.3 | -0.3 | -1.6 |
| 275 | 21.1 | 0.5 | -1.1 | -1.6 |
| 280 | 21.0 | 2.3 | 3.2 | 0.9 |
| 285 | 21.1 | -1.9 | -0.7 | 1.2 |
| 290 | 21.6 | -2.1 | -2.1 | 0.0 |
| 295 | 22.4 | 0.0 | -0.3 | -0.3 |
| 300 | 23.2 | 0.7 | -0.4 | -1.0 |
| 305 | 24.5 | -0.2 | -1.0 | -0.8 |
| 310 | 25.4 | -0.8 | -0.2 | 0.7 |
| 315 | 25.6 | -1.0 | -0.3 | 0.7 |
| 320 | 24.9 | 0.4 | 0.6 | 0.2 |
| 325 | 24.0 | 2.7 | 0.7 | -2.1 |
| 330 | 22.8 | -14.2 | 0.6 | -3.6 |
| 335 | 21.2 | -1.8 | -1.7 | 0.1 |
| 340 | 20.2 | -1.6 | -0.1 | 1.5 |
| 345 | 20.1 | -0.4 | 0.6 | 1.0 |
| 350 | 20.4 | -1.1 | -0.5 | 0.7 |
| 355 | 20.4 | 0.2 | 1.0 | 0.8 |
| 360 | 91.5 | – | 3.4 | – |
| 365 | 17.8 | – | – | – |
| RMS Difference | | 1.5 | 1.3 | 1.3 |

Biases (with respect to BIH Circular D) Removed from UT1-UTC values

Fig J.XIV Comparison of Excess Length od Day (D) Series
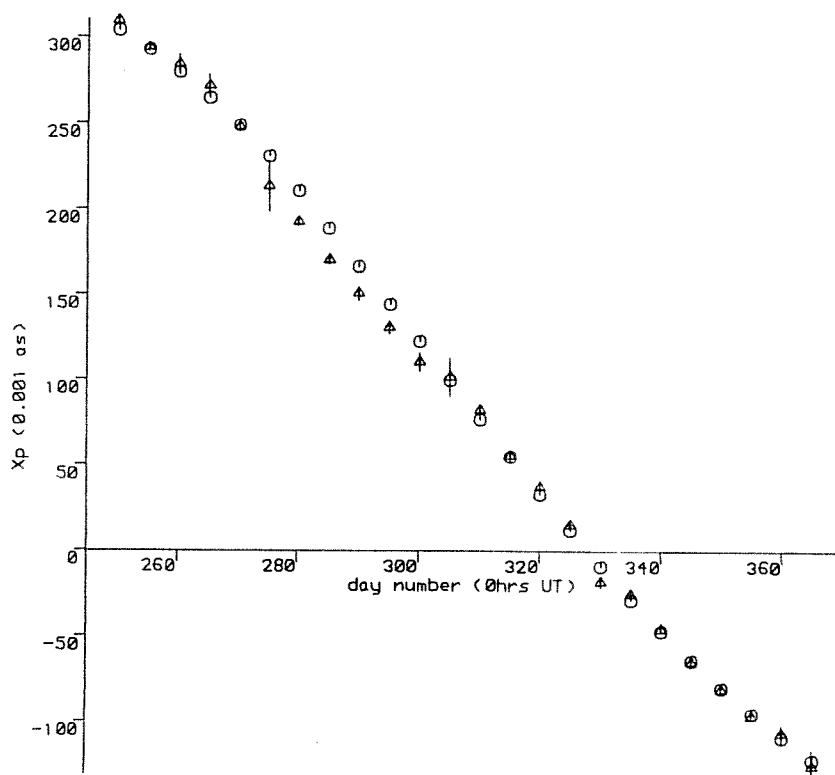
Fig J.XV $x_p$ component of polar motion (UNOTT.1)
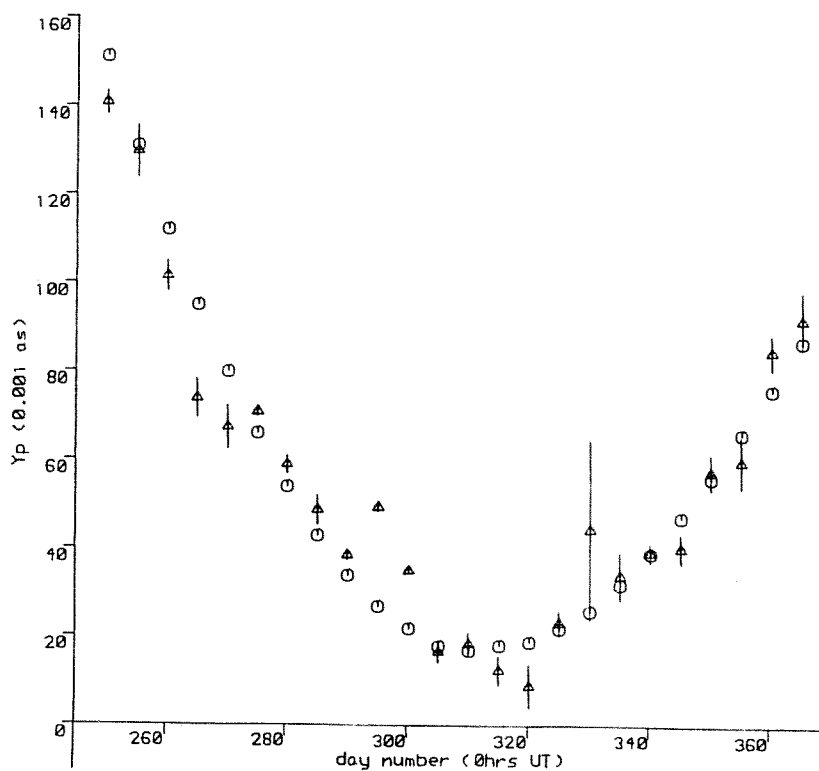
Fig J.XVI $y_p$ component of polar motion (UNOTT.5)
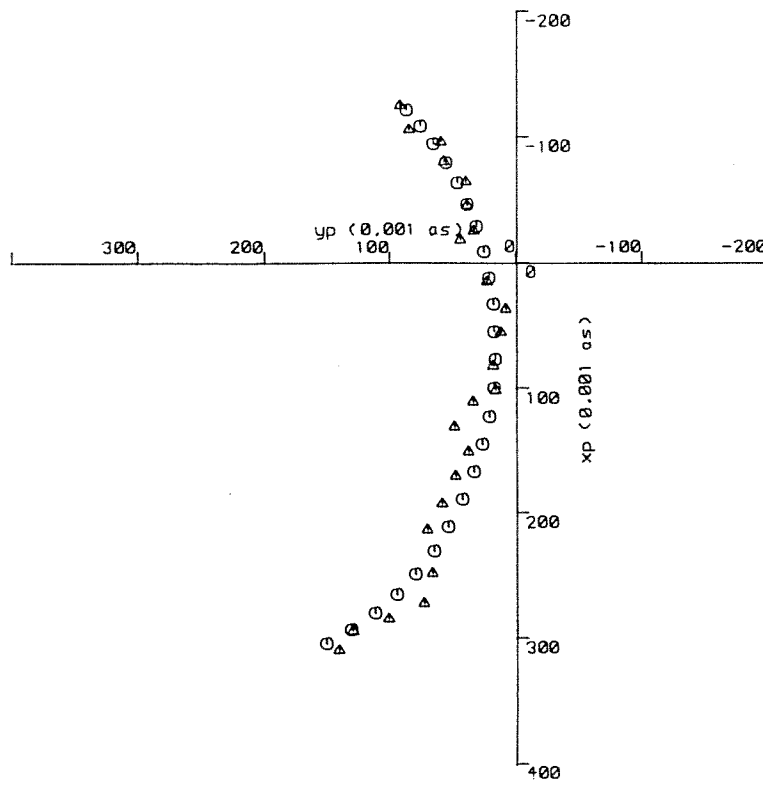
Fig J.XVII <u>Polar motion</u> (UNOTT.1)
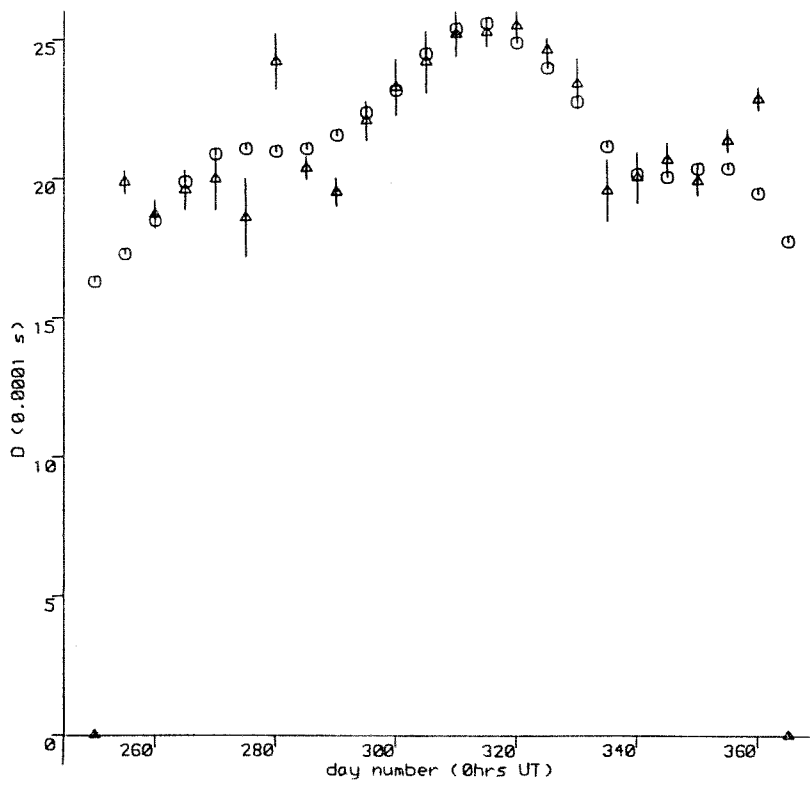


Fig J.XVIII <u>Excess length of day</u> (UNOTT.1)
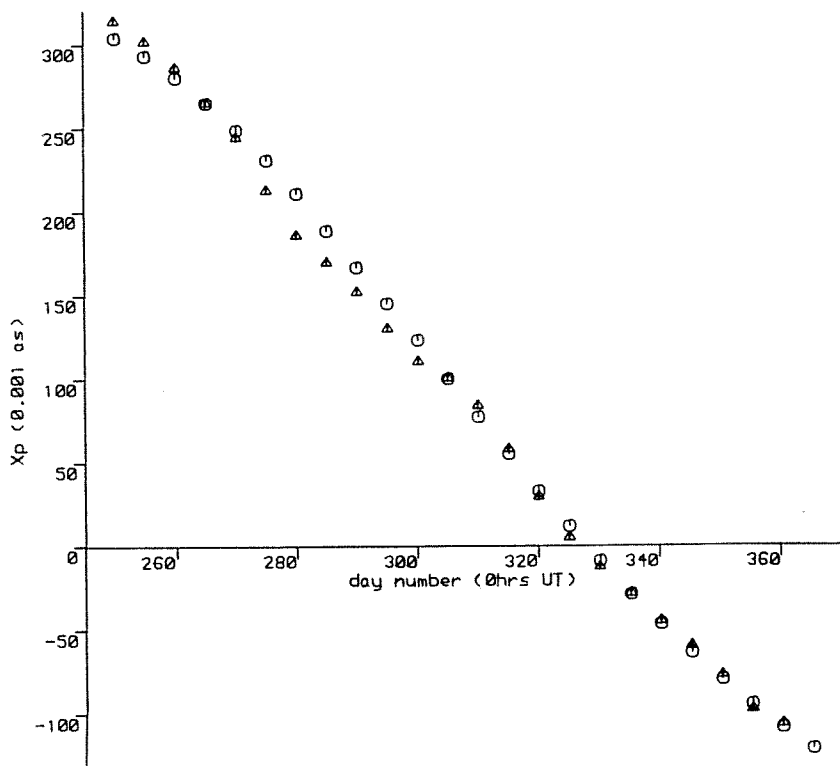
Fig J.XIX $x_p$ component of polar motion (UNOTT.5)
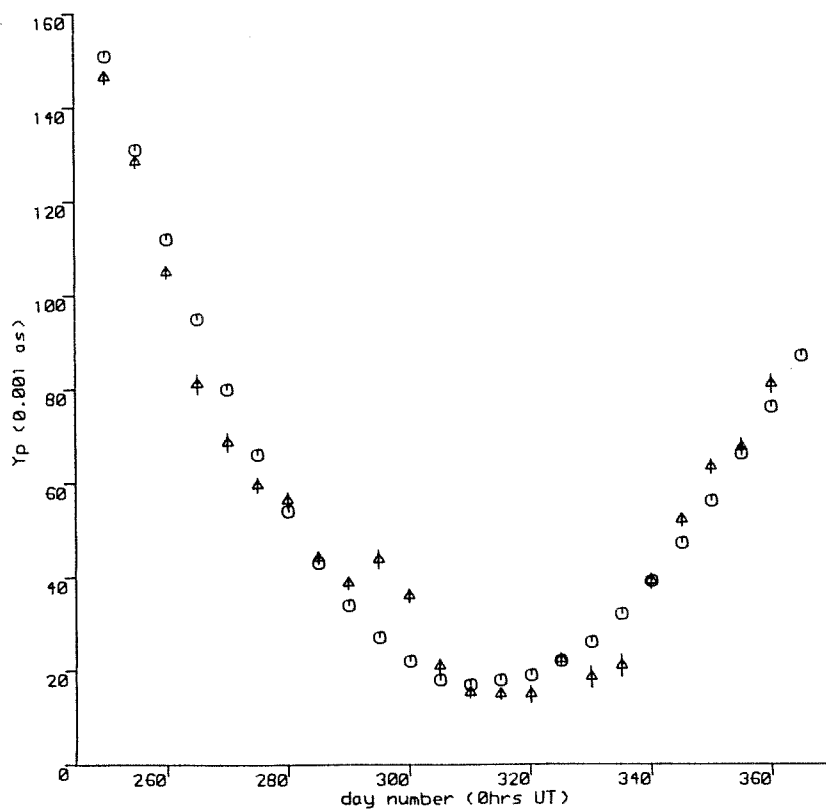


Fig J.XX $y_p$ component of polar motion (UNOTT.5)
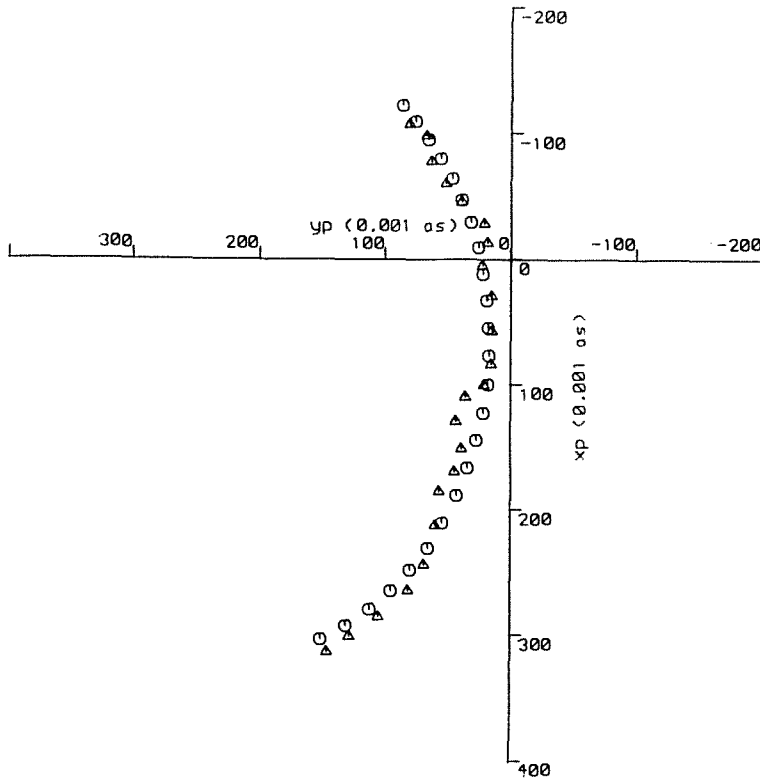
Fig J.XXI Polar motion (UNOTT.5)
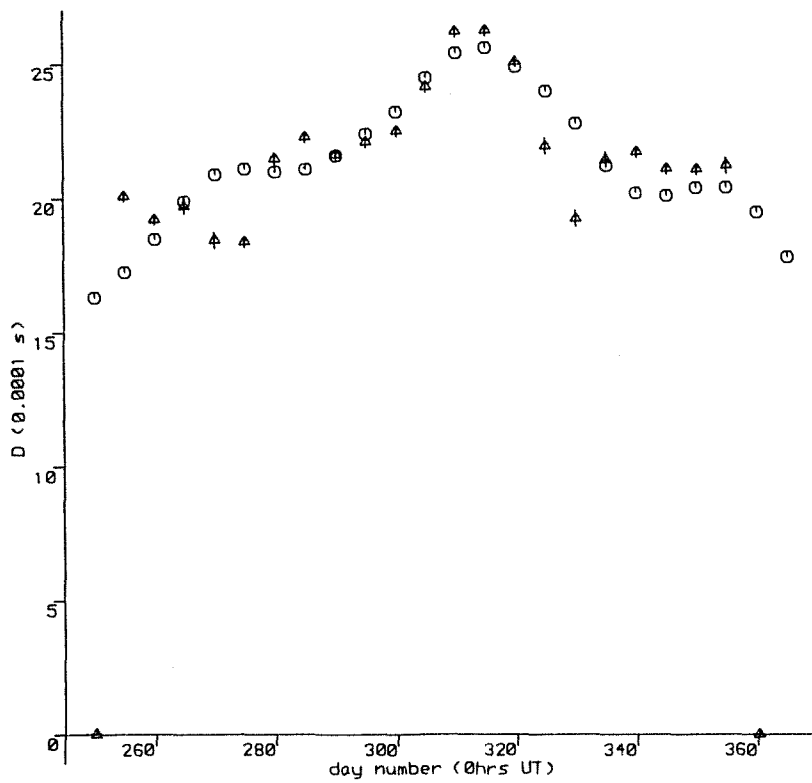


Fig J.XXII Excess length of day (UNOTT.5)
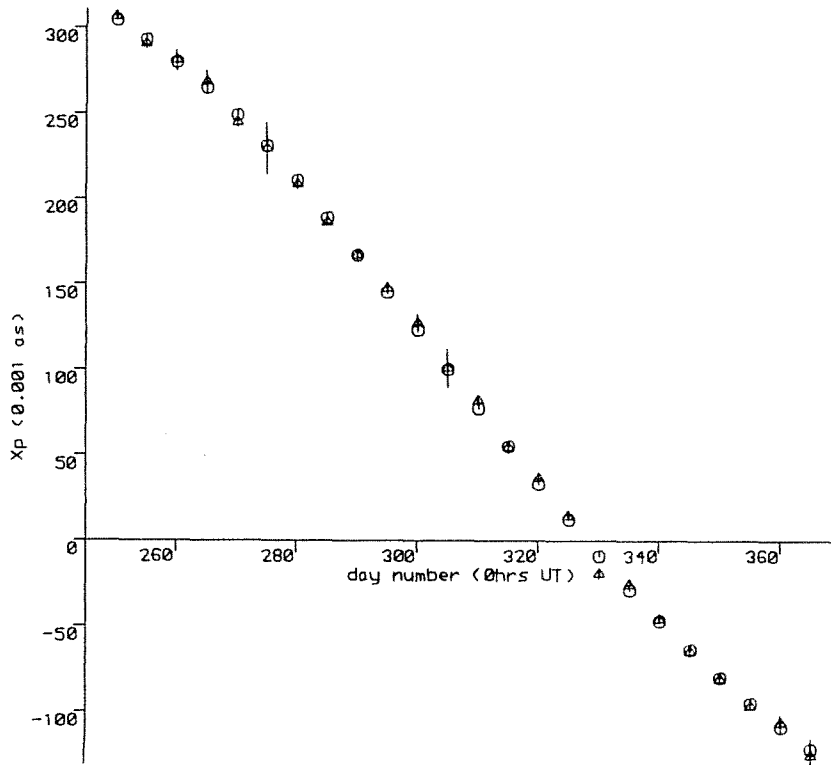
Fig J.XXIII $\underline{x}_p$ component of polar motion (UNOTT.1b)
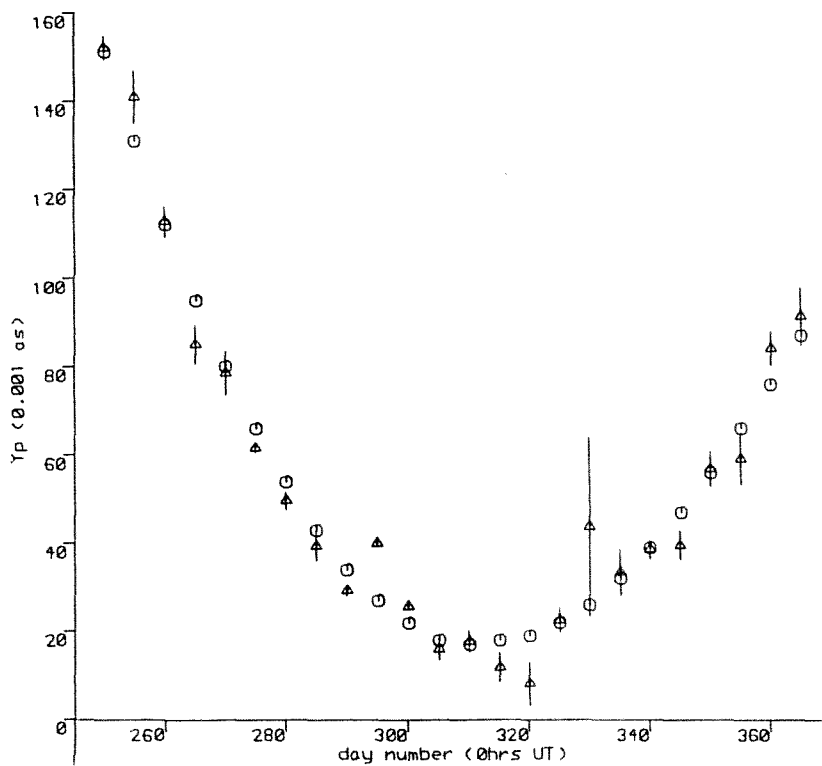
Fig J.XXIV $\underline{y}_p$ component of polar motion (UNOTT.1b)
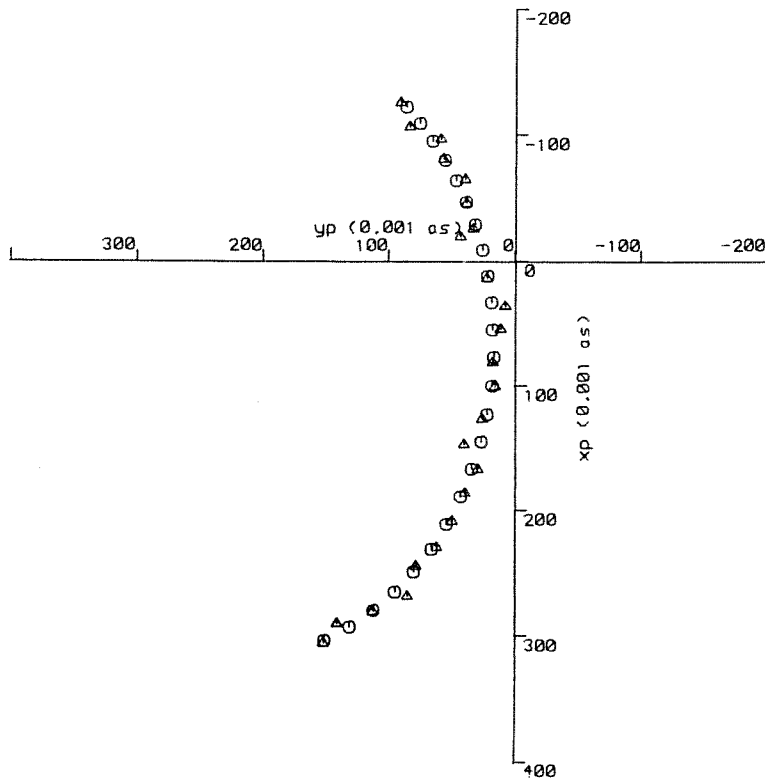
Fig JXXV Polar motion (UNOTT.1b)
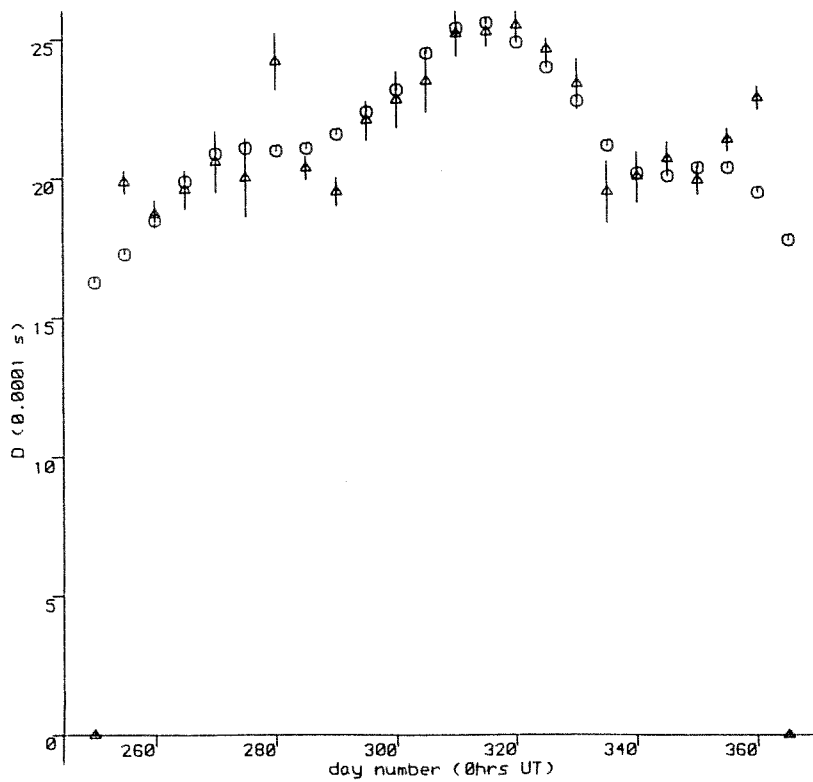


Fig J.XXVI Excess length of day (UNOTT.1b)
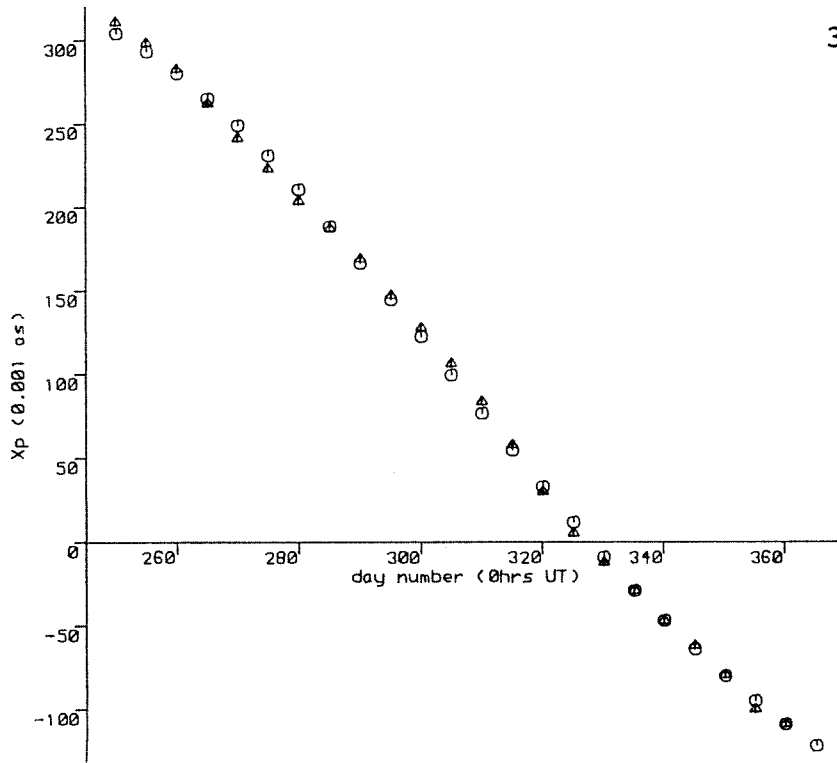
Fig J.XXVII $x_p$ component of polar motion (UNOTT.5b)
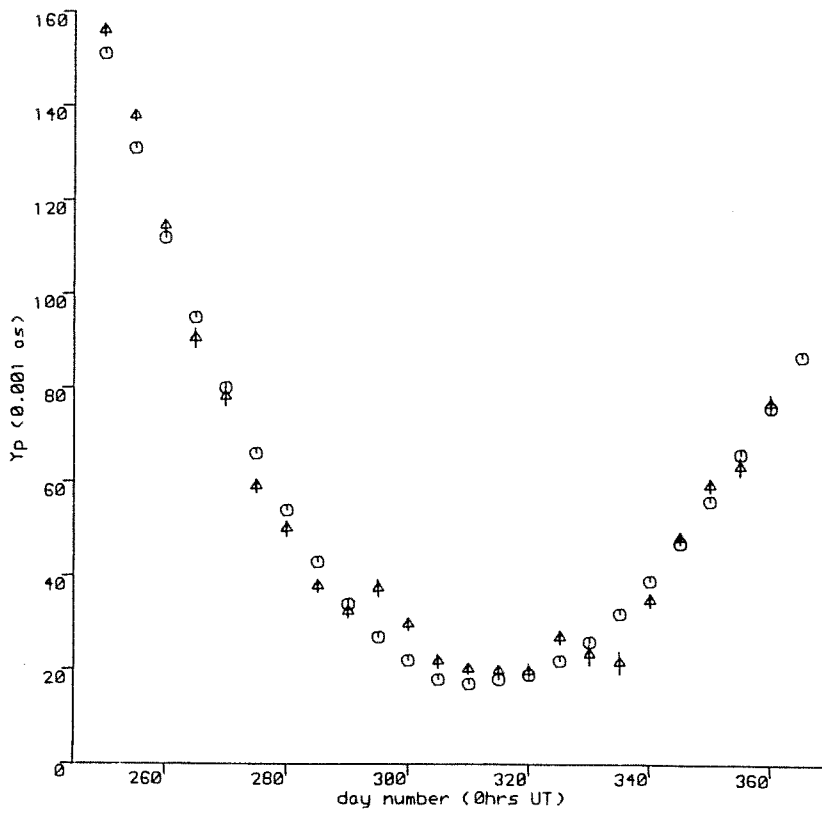


Fig J.XXVIII $y_p$ component of polar motion (UNOTT.5b)
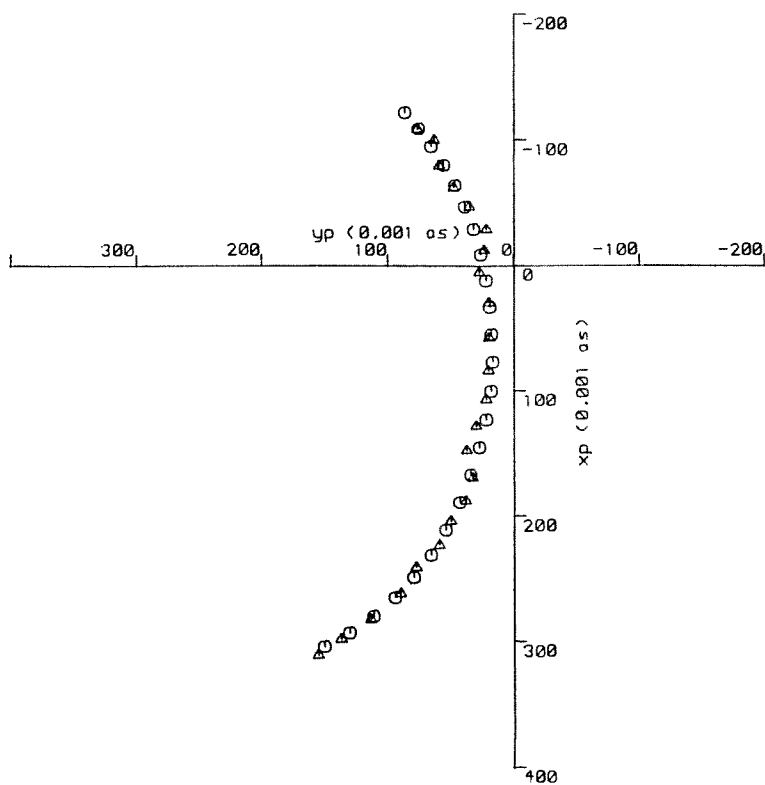
**Fig J.XXX** Polar Motion (UNOTT.5b)
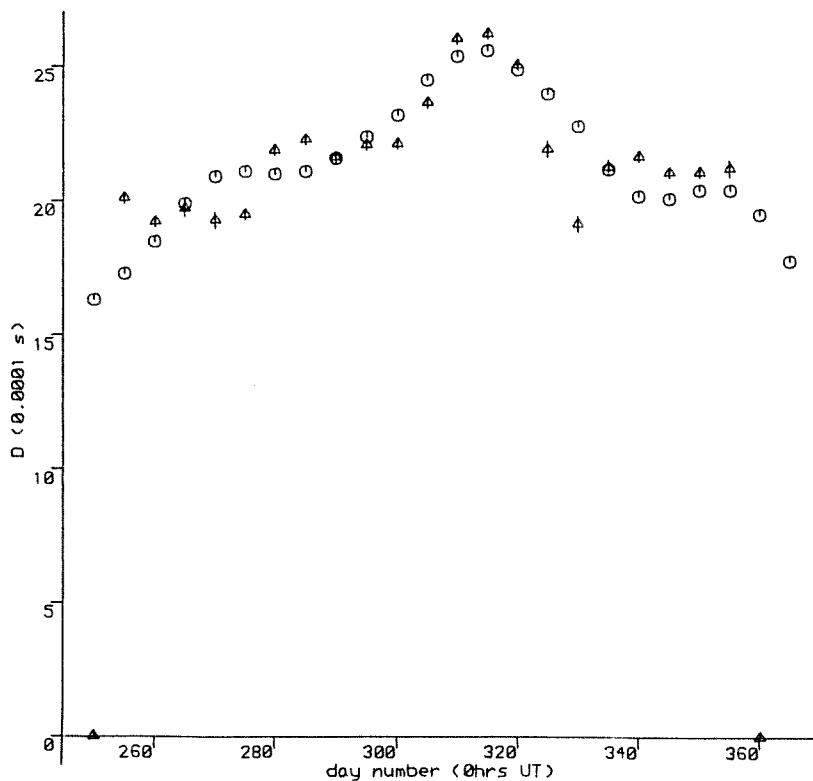


**Fig J.XXXI** Excess length of day (UNOTT.5b)

REFERENCES AND BIBLIOGRAPHY

## REFERENCES AND BIBLIOGRAPHY

Aardoom L, 1978. Earth Rotation and Polar Motion from Laser Ranging to the Moon and Artificial Satellites. Proc. 9th GEOP conference, Dept. of Geodetic Science Report 280, Ohio State University.

Aardoom L, 1982. Coordinators Report : Satellite Laser Ranging. Project MERIT : Report on the Short Campaign (Wilkins and Feissel, 1982).

Abshire J B and Gardner C S, 1985. Atmospheric Refractivity Corrections to Satellite Laser Ranging. Special Geodynamics issue of IEEE Transactions on Geoscience and Remote Sensing.

Afonso G, Barlier F, Berger C, Mignard F and Walch J J, 1985. Reassessment of the Charge and Neutral Drag of LAGEOS and its Geophysical Implications. Journal of Geophys. Res. Vol. 90, B11.

Agrotis L G, 1984. Determination of Satellite Orbits and the Global Positioning System. PhD Thesis, University of Nottingham.

Anderle R J, 1973. Determination of Polar Motion from Satellite Observations. Geophys. Surv. 1.

Anselmo L, Farinella P, Milani A and Nobili A M, 1983. Effects of Earth Reflected Sunlight of the Orbit of the LAGEOS Satellite. Astron. Astrophysics 117.

Arnold D A, 1978. Optical and Infrared Transfer Function of the LAGEOS Retroreflector Array. NASA Grant NGR 09-015-002.

Ashkenazi V, 1967. Solution and Error Analysis of Large Geodetic Networks, Part I, Direct Methods. Survey Review 146 and 147.

Ashkenazi V, 1969. Solution and Error Analysis of Large Geodetic Networks, Part II, Indirect Methods. Survey Review 151 and 152.

Ashkenazi V, 1970. Adjustment of Control Networks for Precise Engineering Surveys. Chartered Surveyor Jan. 1970.

Ashkenazi V, Agrotis L G and Moore T, 1984.
        Determination of Satellite Orbits and the
        Analysis of LAGEOS Laser Range Data.
        Pres. 8th UK Geophysical Assembly,
        University of Newcastle-upon-Tyne.

Ashkenazi V, Gough R J and Sykes R M, 1977.  Satellite
        Doppler Positioning. Prepared for a Seminar
        held at the University of Nottingham, January
        1977.

Ashkenazi V and Moore T, 1985.  Earth Rotation and
        Polar Motion by Laser Ranging to Satellites.
        Pres. 3rd European Union of Geosciences
        Biennial Meeting, Strasburg 1985, and Pres.
        9th UK Geophysical Assembly, University of
        East Anglia.

Ashkenazi V and Moore T, 1986.  The Navigation of
        Navigation Satellites. The Journal of
        Navigation, Vol. 39, No. 3.

Ashkenazi V, Moore T and Howard P D, 1985.  MERIT Data
        Processing at Nottingham. Proc. Int. Conf. on
        Earth Rotation and the Terrestrial Reference
        Frame, Columbus, Ohio.

Baker T F, 1984.  Tidal Deformations of the Earth.
        Sci. Prog. Oxf. 69.

Bomford G, 1980.  Geodesy (4th Edition). Clarendon
        Press Oxford.

Bufton J L, 1978.  Review of Atmospheric Correction
        for Laser Ranging Data. Proc. 3rd Int.
        Workshop on Laser Ranging Instrumentation,
        Lagonissi, Greece.

Bureau International de l'Heure, 1984. Annual Report
        for 1983.

Calame O (ed), 1982.  High Precision Earth Rotation
        and Earth Moon Dynamics : Lunar Distances and
        Related Observations. Proc. IAU colloquim 63,
        Grasse, France.

Cartwright D E and Taylor R J, 1971.  New Computations
        of the Tide Generating Potential. Geophy. J.
        R. Astro. Soc.

Christodoulidis D C and Smith D E, 1983a. Global
        Geotectonics from Satellite Laser Ranging.
        NASA/GSFC Tech. Memorandum 85078.

Christodoulidis D C and Smith D E, 1983b. The Role of
        Satellite Laser Ranging Through the 1990's.
        NASA/GSFC Tech. Memorandum 85104.

Christodoulidis D C, Smith D E, Dunn P J,
        Torrence M H, Knode S and Anders S, 1982.
        The SL5 Geodetic Parameter Recovery Solution.
        Pres. 3rd Int. Symp. on the Use of
        Artificial Satellites for Geodesy and
        Geodynamics, Athens.

Christodoulidis D C and Zerbini S, 1985. LAGEOS II :
        NASA-PSN Mission. CSTG Bull. No. 8.

Crane S A, 1980. Geodetic Control Networks :
        Accuarcy, Reliabilty and Systematic Errors.
        PhD Thesis, University of Nottingham.

Cross P A, 1983. Advanced Least Squares Applied to
        Position Fixing. Working Paper No. 6, Dept.
        of Land Surveying, North East London
        Polytechnic.

Degnan J J, 1985. Satelliite Laser Ranging : Current
        Status and Future Prospects. Special
        Geodynamics issue of IEEE Trans. on
        Geoscience and Remote Sensing.

Eanes R J, Schutz B, Tapley B, 1983. Earth and Ocean
        Tide effects on LAGEOS and STARLETTE. Proc.
        Ninth Int. Symp. on Earth Tides, Stuttgart.

Feissel M, 1980. Determination of the Earth Rotation
        Parameters by the Bureau International de
        l'Heure, 1962 - 1979. Bull. Geod. 54.

Feissel M, 1986. Observational Results on Earth
        Rotation and Reference Frames. Reports on the
        MERIT-COTES Campaign on Earth Rotation and
        Reference Systems, Part III, BIH.

Feissel M and Lewandowski W, 1984. A Comparative
        Analysis of Vondrak and Gaussian Smoothing
        Techniques. Bull. Geod. 58.

Feissel M and Wilson P (eds), 1983. MERIT Campaign:
        Connection of Reference Frames -
        Implementation Plan. BIH.

Fitzmaurice M W, Minott P O, Abshire J B and Rowe H E, 1978. Prelaunch Testing of the Laser Geodynamic Satellite (LAGEOS). Technical Paper No. TP-1062, GSFC, Maryland.

Gaignebet J (ed), 1984. Proc. Fifth Int. Workshop on Laser Ranging Instrumentation, Royal Greenwich Observatory, Herstmonceux.

Gardner C S, 1976. Effects of Horizontal Refractivity Gradients on the Accuarcy of Laser Ranging to Satellites. Radio Science Vol. 11, No. 12.

Goad C C, 1980. Gravimetric Tidal Loading from Integrated Greens Functions. J. Geophys. Res. 85.

Guinot B, 1978. Rotation of the Earth and Polar Motion Services. Proc. 9th GEOP conference. Dept. Geodetic Science Report 280, Ohio State University.

Haskell A, 1983. The ERS-1 Programme of the European Space Agency. ESA Journal Vol. 7, No. 1.

Hill C J, Moore T and Ashkenazi V, 1986. 3-D Coordinates of GINFEST Stations from SLR Observations. Pres. 10th UK Geophysical Assembly, University of Glasgow.

IUGG, 1967. Resolution 19. Bull. Geod. 86.

Jacchia L G, 1971. Revised Static Models for the Thermosphere and Exosphere with Empirical Temperature Profiles. Smithsonian Astrophysical Observatory, Special Report 332.

Kaplan G H (ed), 1981. The IAU Resolutions on Astronomical Constants, Time Scales and the Fundamental Reference Frame. United States Naval Observatory Circular No. 163.

Kolenkiewicz R, Smith D E, Rubincam D P, Dunn P J and Torrence M H, 1977. Polar Motion and Earth Tides from Laser Tracking. Phil. Trans. R. Soc. Lond. A 284.

Krakiwsky E J and Wells D E, 1971. Coordinate Systems in Geodesy. Dept. of Surveying Engineering, University of New Brunswick, Frederiction.

Lambeck K and Cazenave A, 1973. The Earth's Rotation and Atmospheric Circulation - I, Seasonal Variations. Geophysical Journal 32.

Lerch F J, Klosko S M and Patel G B, 1983. A Refined Gravity Model for LAGEOS (GEM-L2). NASA Technical Memorandum 84986.

Lerch F J, Klosko S M, Wagner C A and Patel G B, 1985. On the Accuracy of Recent Goddard Gravity Models. Journal of Geophysical Research Vol. 90, No. B11.

Marini J W and Murray C W, 1973. Correction of Laser Tracking Data for Atmospheric Refraction at Elevation Angles Above 10 Degrees. Doc. X-591-73-351, GSFC, Maryland.

Marsh J G, Lerch F J and Williamson R G, 1985. Precision Geodesy and Geodynamics using STARLETTE Laser Ranging. Journal of Geophysical Research, Vol. 90, No. B11.

Martin T V, Eddy W F, Brenner A, Rosen B and McCarthy J, 1980. GEODYN System Description Manual, Vol 1. NASA Goddard Space Flight Centre, Maryland.

Masters E G, Stolz A and Hirsch B, 1983. On Filtering and Compressing LAGEOS Laser Range Data. Bull. Geod. No. 57.

McCarthy D D and Pilkington J D H (eds), 1979. Time and the Earth's Rotation. Proc. IAU Symp. No. 82, Cadiz.

Melbourne W G (ed), 1983. Project MERIT Standards. USNO Circular No. 167.

Minster J B and Jordan T H, 1978. Present Day Plate Motions. Journal of Geophysical Research 83.

Moore P, 1985. Laser Station Coordinates and Baselines from Long-arc and Short-arc Analyses of STARLETTE. Earth Satellite Research Unit, Aston University.

Moore T, 1983. Orbital Analysis and Satellite Laser Ranging Research at Nottingham. Comptes Rendus 53rd Meeting JLG.

Mueller I I, 1969.  Spherical and Practical Astronomy
        as Applied to Geodesy. Frederick Ungar
        Publishing Co. New York.


Mueller I I, Zhu S-Y and Bock Y, 1982.  Reference
        Frame Requirements for the MERIT Campaign.
        Dept. Geodetic Science Report No. 329. Ohio
        State University.


O'Toole J W, 1976.  CELEST Computer Program for
        Computing Satellite Orbits. NSWC/DL TR-3565,
        Dahlgren, Virginia.


Pavlis E C, 1982.  On the Geodetic Applications of
        Simultaneous Range Differencing to LAGEOS.
        Dept. of Geodetic Science Report NO. 338,
        Ohio State University.


Pavlis E C, 1985.  On the Geodetic Applications of
        Simultaneous Range Differencing to LAGEOS.
        Journal Geophysical Research Vol. 90.
        No. B11.


Pearlman M R, 1984.  Laser System Characterization.
        Proc. 5th Int. Workshop on Laser Ranging
        Instrumentation.


Reigber C, Müller H, Rizos C, Bosch W, Balmino G and
        Moynot B, 1983.  An Improved GRIM3 Earth
        Gravity Model (GRIM3B). Pres. IUGG 18th
        General Assembly, Hamburg.


Reinhart E, Wilson P, Aardoom L and Vermaat E, 1985.
        The WEGENER Mediterranean Laser Tracking
        Project, WEGENER-MEDLAS. CSTG Bull. No. 8.


Rubincam D P, 1984.  Postglacial Rebound Observed by
        LAGEOS and the Effective Viscosity of the
        Lower Mantle. Journal of Geophysical
        Research, Vol. 89.


Schutz B E, 1983a.  Satellite Laser Ranging
        Participants During Project MERIT. Center for
        Space Research, The University of Texas at
        Austin.


Schutz B E, 1983b.  Satellite Laser Ranging Procedures
        Guide for Project MERIT. Center for Space
        Research, The University of Texas at Austin.

Schutz B E, 1983c.  Analysis of LAGEOS Laser Range
        Data, Monthly Circular, Center for Space
        Research, The University of Texas at Austin.

Schutz B E, 1984a.  Coordinators Report: Sateliite
        Laser Ranging. Report of the Second MERIT
        Workshop (Wilkins, 1984).

Schutz B E, 1984b.  Univeristy of Texas LAGEOS Station
        Coordinate Solution 8112.2. Private
        Communication.

Schwiderski E W, 1980.  On Charting Global Ocean
        Tides. Review of Geophysics and Space Physics
        18(1).

Sharman P, 1982.  The UK Satellite Laser Ranging
        Facility. SLR Technical Note No. 1, Royal
        Greenwich Observatory, Herstmonceux.

Sinclair A T, 1982.  The Effects of Atmospheric
        Refraction on Laser Ranging Data. NAO
        Technical Note No. 59, Royal Greenwich
        Observatory.

Sinclair A T, 1985.   The Radial Accuarcy of Orbits
        Determined from SLR Data. SLR Technical Note
        No. 7, Royal Greenwich Observatory.

Sinclair A T and Appleby G M, 1986.   SATAN - Programs
        for the Determination and Analysis of
        Satellite Orbits from SLR Data. SLR Technical
        Note No. 9, Royal Greenwich Observatory.

Smith D E, Christodoulidis D C, Kolenkiewicz R,
        Dunn P J, Klosko S M, Torrence M H, Fricke S
        and Blackwell S, 1985.  A Global Geodetic
        Reference Frame from LAGEOS Ranging
        (SL5.1AP). Journal of Geophysical Research,
        Vol. 90, No. B11.

Smith D E, Kolenkiewicz R, Dunn P J, Torrence M H,
        1979.  Determination of Polar Motion and
        Earth Rotation from Laser Tracking of
        Satellites. Time and the Earth's Rotation.
        Porc. IAU Symp. No. 82.

Spencer A J M, Parker D F, Berry D S, England A H,
        Faulkner T R, Green W A, Holden J T,
        Middleton D and Rogers T G, 1977.
        Engineering Mathematics, Vol. 2. Van Nostrand
        Reinhold.

Sykes R M, 1979.  Translocation and Orbit Relaxation
          Techniques in Satellite Doppler Tracking. PhD
          Thesis, University of Nottingham.


Tapley B D, Schutz B E and Eanes R J, 1982.  A
          Critical Analysis of Satellite Laser Ranging
          Data. Proc. 4th Int. Workshop on Laser
          Ranging Instrumentation, University of
          Texas at Austin.


Tapley B D, Schutz B E and Eanes R J, 1985.  Station
          Coordinates, Baselines and Earth Rotation
          Parameters from LAGEOS Laser Ranging
          1976 - 1984.  Journal of Geophysical
          Research, Vol. 90, No. B11.


Vincenty T, 1979.  The HAVAGO Three Dimensional
          Adjustment Program. NOAA Technical Memorandum
          NOS NGS 17.


Wahr J M, 1979.  The Tidal Motions of a Rotating,
          Elliptical, Elastic and Oceanless Earth. PhD
          Thesis, University of Colorado, Boulder,
          Colorado.


Wahr J M, 1981.  Body Tides of an Elliptical,
          Rotating, Elastic and Oceanless Earth.
          Geophysical Journal of the Royal Astronomical
          Society, Vol. 64.


Wilkins G A (ed), 1980a.  A Review of the Techniques
          to be used during Project MERIT to Monitor
          the Rotation of the Earth. Published jointly
          by the Institut für Angewandte Geodäsie,
          Frankfurt, and the Royal Greenwich
          Observatory, Herstmonceux.


Wilkins G A, 1980b.  Project MERIT. CSTG Bull. No. 1.


Wilkins G A (ed), 1984.  Project MERIT, Report on the
          Second MERIT Workshop and on other activities
          in 1983. Royal Greenwich Observatory.


Wilkins G A and Feissel M (eds), 1982.  Project MERIT:
          Report on the Short Campaign and Grasse
          Workshop with Observations and Results on
          Earth Rotation during 1980 August - October.
          Royal Greenwich Observatory.

Wilkins G A and Mueller I I, 1985.  Joint Summary
        Report of the IAU/IUGG Working Groups on the
        Rotation of the Earth and the Terrestrial
        Reference System. Pres. IAU General Assembly,
        Delhi.


Williamson R G and Marsh J G, 1985.  STARLETTE
        Geodynamics : The Earth's Tidal Response.
        Journal of Geophysical Research, Vol. 90,
        No. B11.


Wintzer C M and de Villiers J N, 1982.  POPSAT, A Tool
        for Earthquake Research. ESA Bull. No. 31.